Université de Montréal

Pétrologie et géochimie isotopique de xénolites mantelliques de la Cordillère Canadienne

Département de Géologie
Faculté des Arts et des Sciences

Anne H. Peslier

Faculté des études supérieures

Thèse de Doctorat

Université de Montréal

Pétrologie et géochimie isotopique de xénolites mantelliques de la Cordillère Canadienne

par

Anne Hélène Peslier

Département de Géologie

Faculté des Arts et des Sciences

Thèse présentée à la Faculté des Etudes Supérieures

en vue de l'obtention du grade de

Philosophiae Doctor (Ph. D.)

en **Géologie**

Novembre 1998

Université de Montréal
Faculté des études supérieures

Cette thèse intitulée:

Pétrologie et géochimie isotopique de xénolite mantelliques
de la Cordillère Canadienne

présentée par:

Anne H. Peslier

a été évaluée par un jury composé des personnes suivantes:

Président-rapporteur:	Jacques G. Martignole
Membre du jury (directeur de recherche):	John N. Ludden
Membre du jury (codirecteur):	Don Francis
Membre du jury:	John Stix
Examinateur externe:	Richard J. Walker
Représentant du doyen de la F.E.S.:	Alain Vincent

Thèse acceptée le: 19 février 1999

Abstract

In this thesis, the mantle lithosphere of the southern Canadian Cordillera was studied via petrological, geochemical and isotopic techniques. Mantle xenoliths were sampled from mid-Tertiary to recent alkali basalt volcanic centers throughout various orogenic belts and accreted tectonic terranes. A particular emphasis was placed on the Re-Os isotopic system, applied to peridotites from the entire Canadian Cordillera.

The dominant type of peridotite among the southern Canadian Cordillera xenoliths is spinel lherzolite, with chemical compositions consistent with residues from up to 15 % extraction of a picritic melt from a pyrolite type source. Rare harzburgites and dunites, on the other hand, require up to 25 and 30% melting respectively. Some of the depleted-lherzolites, harzburgites and dunites, however, are too Fe-rich to be the simple residues of melting and likely result from the interaction of the peridotite with an alkali melt at depth. Metasomatism is expressed by the crystallisation of amphibole and phlogopite at two sites, but is cryptic elsewhere, with variable enrichment in LREE and depletion in Hf, Zr and Ti. A comparison with other peridotites indicates that the Canadian Cordillera xenoliths resemble other continental spinel xenoliths, and some Hawaiian mantle xenoliths. They are, however, different from peridotites found in arc tectonic settings and generally less depleted than abyssal peridotites. Augite-wehrlites and pyroxenites are abundant at two sites close to the American craton and appear to represent veins which cross-cut the lherzolitic lithospheric mantle.

Lherzolites from the entire Canadian Cordillera show a positive correlation of their $^{187}Os/^{188}Os$ with indices of fusion such as Al_2O_3, and heavy rare earth elements (HREE). This likely reflects Re/Os fractionation during various degrees of partial melting of the mantle, followed by a long period of radiogenic ingrowth. The correlation between $^{187}Os/^{188}Os$ and Lu has been used to infer a model age of 1.12 ± 0.26 Ga for the mantle lithosphere beneath the Canadian Cordillera. The same age is found in mantle xenoliths from within individual belts and tectonic terranes of the Canadian Cordillera. A Re-

depletion age in one harzburgite that apparently escapes Os metasomatism, and Hf model ages for two unmetasomatized lherzolites also give similar ages. The sub-continental lithosphere thus appears to have been stabilized in this region about 1.1 Ga, possibly in a continental rifting environment. This age is younger than the 1.9 to 2.3 Ga of the North American cratonic basement, but much older than the depleted-mantle Nd-model ages of the upper-crust tectonic terranes (about 0.5 Ga). Although no crustal rocks of 1.1 Ga exist in the Canadian Cordillera, detrital zircons of this age are widespread in the entire region and may testify to the former existence of a crust of this age (Ross, 1991). This interpretation is also in agreement with recent seismic profiles in the southern Canadian Cordillera (Clowes et al., 1998) showing a lower-crust extending from the craton under most of the orogenic belts, which may represent the crust associated with the 1.1 Ga old lithospheric mantle.

The presence of abundant harzburgites enriched in incompatible trace elements in some northern xenolith sites has been interpreted to result from metasomatism-induced melting linked to the presence of an anomalous high-temperature zone in the mantle at more than 100 km depth beneath these sites (Francis, 1987; Frederiksen et al., 1998; Shi et al., 1998). Harzburgites from both the southern and northern Canadian Cordillera have $^{187}Os/^{188}Os$ ratios correlating with 1/Os and plotting above the regional $^{187}Os/^{188}Os$ vs Lu correlation of the lherzolites. The Os system thus appears to have been disturbed by high $^{187}Os/^{188}Os$ metasomatic agents that scavenged Os from the peridotite. This process apparently occured throughout the entire Canadian Cordillera, but was particularly intense in the northern sites due to the presence of a thermal anomaly in the mantle. In the harzburgite-rich sites, this asthenosphere-lithosphere interaction appears to have reset the Pb-Pb, Rb-Sr (Carignan et al., 1996), Lu-Hf and Sm-Nd isotopic characteristics of the lherzolites as well. The fluids or melts in these northern sites interacted with the peridotite less than 170 Ma ago and may have had EMII isotopic characteristics.

Résumé

Cette thèse constitue une étude pétrologique, géochimique et isotopique de la lithosphère mantellique du Sud de la Cordillère Canadienne. Les xénolites du manteau dont il est question ici proviennent de centres volcaniques de composition alcaline datant de la fin du Tertiaire à la période récente. L'échantillonnage a été effectué dans les diverses ceintures orogéniques et terrains tectoniques accrétés au craton Américain au Jurassique et au Crétacé, et dont est constituée cette chaîne Phanérozoique bordant l'Ouest du continent Nord-Américain. Ainsi, ces xénolites constituent des échantillons d'un manteau lithosphérique situé entre la racine cratonique d'un continent à l'Est et du manteau océanique convectif à l'Ouest. Une grande partie de cette thèse est consacrée au système isotopique Re-Os qui a été appliqué à des péridotites provenant de toute la Cordillère Canadienne, du sud de la Colombie Britannique au Sud, à l'Alaska au Nord.

L'étude pétrologique des xénolites du Sud concerne les sites West Kettle River (KR), Lightning Peak (LP), Lassie Lake (LL), Rayfield River (RR), Big Timothy (BT), Kostal Lake (KL) et Summit Lake (SL). Le type dominant de péridotite que l'on trouve dans cette région est celui des lherzolites à spinelle. Les compositions en éléments majeurs de ces dernières peuvent être expliquées par l'extraction de liquides picritiques, à l'aide de 15% au maximum de fusion partielle d'une source de type pyrolite. Des harzburgites et des dunites sont aussi présentes, bien que beaucoup plus rares que les lherzolites. Elles sont issues du même processus mais avec des degrés de fusion plus importants, environ 25 et jusqu'à 30% respectivement. Cependant, certaines d'entre-elles ainsi que certaines des lherzolites appauvries en éléments majeurs possèdent une composition en Fe trop élevée pour pouvoir être les produits d'une simple fusion. Ainsi, il est probable qu'elles résultent de l'interaction entre la péridotite et un liquide de fusion alcaline, qui a provoqué la dissolution des orthopyroxènes et la cristallisation d'olivine nouvelle. Tous ces processus se sont déroulés entre 30 et 60 km de profondeur (champ de stabilité du spinelle) et les

températures d'équilibration sont comprises entre 900 et 1000°C, sauf au site de SL où elles montent jusqu'à 1070°C.

Le métasomatisme a résulté en la cristallisation de phases hydratées telles que l'amphibole et la phlogopite à LP et KL respectivement. Dans tous les autres sites de xénolites, il est responsable d'enrichissements variables en terres rares légères (LREE) et est caractérisé dans presque toutes les suites par des anomalies négatives en Zr, Hf et Ti par rapport aux terres rares lourdes (HREE). Il est possible que les fluides ou les liquides de fusion qui en sont responsables soient liés à la zone de subduction à l'Ouest.

Une comparaison avec des péridotites d'autres régions du monde a permis de mettre en évidence que les xénolites mantelliques de la Cordillère Canadienne sont semblables aux autres péridotites à spinelle continentales, mais aussi à des xénolites remontées par des basaltes d'île océanique (OIB) d'Hawaii. Cependant, les péridotites trouvées dans des contextes tectoniques d'arc sont plus appauvries et ont des Mg# de spinelle plus élevés. Enfin, les péridotites abyssales ont des compositions globalement plus appauvries que les lherzolites de la Cordillère Canadienne.

Les rapports $^{187}Os/^{188}Os$ de lherzolites provenant de toute la Cordillère Canadienne présentent une corrélation positive avec des indices de fusion tels que l'Al_2O_3 et les HREE. De telles corrélations ont été trouvées dans des massifs orogéniques de péridotites et dans d'autres suites de xénolites à spinelle (Reisberg and Lorand, 1995; Meisel et al., 1996), mais ont des pentes qui diffèrent dans chacune des régions où les péridotites sont situées. Ceci laisse à penser que ces corrélations résultent du fractionnement du rapport Re/Os au cours de la fusion partielle, suivi d'une longue période de croissance radiogénique, propre à chaque partie du monde, et non de processus continus de mélange dans le manteau convectif. D'autre part, un mélange entre un pôle harzburgitique et un liquide basaltique produirait des courbes qui n'ont rien à voir avec cette corrélation. Il est possible d'utiliser cette corrélation pour déterminer des âges modèles du

manteau (Reisberg and Lorand, 1995). Le Lu, dont le comportement dans les processus magmatiques apparaît être très semblable à celui du Re (Meisel et al., 1996; Hauri and Hart, 1997), est pris comme analogue du rapport $^{187}Re/^{188}Os$. Ce dernier, en effet, ne peut pas être utilisé comme dans une méthode classique d'isochrone, car il est généralement perturbé par du métasomatisme postérieur à la fusion. Ainsi, l'intersection de la droite de corrélation $^{187}Os/^{188}Os$ en fonction du Lu avec l'axe des ordonnées permet de calculer le rapport isotopique initial des lherzolites. Celui-ci est projeté sur une courbe d'évolution des rapports isotopiques du manteau primitif au cours du temps afin de calculer un âge modèle, c'est à dire quand la fusion a eu lieu. Cette méthode, appliquée à toutes les lherzolites de la Cordillère Canadienne, permet de calculer un âge modèle de 1.12 ± 0.26 Ga pour la lithosphère mantellique située sous cette région. L'application du même calcul sur un nombre plus restraint de lherzolites, groupées par ceinture orogénique ou par terrain tectonique, donne aussi le même âge. De plus, un calcul de l'âge minimum d'appauvrissement en Re appliqué à la seule harzburgite qui n'a pas vu ses rapports d'$^{187}Os/^{188}Os$ perturbés par du métasomatisme, conclu à 1 Ga. Enfin, des âges modèles Hf sur deux lherzolites non métasomatisées tombent dans le même ordre de grandeur.

Le manteau sous-continental de la Cordillère Canadienne apparaît ainsi s'être stabilisé il y a environ 1 Ga, peut-être dans un contexte de rifting continental. Cet âge est inférieur à celui de la base du craton Nord-Américain adjascent (1.9 à 2.3 Ga), mais est bien supérieur aux âges modèles Nd des terrains tectoniques de la croûte supérieure (environ 0.5 Ga). Bien qu'il n'existe aucune roche âgée de 1 Ga dans toute la Cordillère Canadienne, des zircons détritiques datés à 1 Ga y sont très couramment trouvés, et pourraient être les témoins de l'existence ancienne d'une croûte de cet âge (Ross, 1991). Cette interprétation est en accord avec les résultats des profils sismiques récents réalisés dans le Sud de la Colombie Britannique, et qui semblent montrer la présence d'une croûte inférieure située sous la plupart des terrains tectoniques et en prolongation avec celle du

craton (Clowes et al., 1998). Celle-ci pourrait représenter la croûte associée au manteau lithosphérique de 1 Ga.

L'abondante présence de harzburgites dans certains sites du Nord de la Cordillère, ainsi que l'enrichissement en éléments traces incompatibles de leurs clinopyroxènes, ont été interprétés comme le résultat d'une fusion induite par du métasomatisme (Francis, 1987; Shi et al., 1998). Ce dernier serait à relier à une zone de température anormalement élevée, située à plus de 100 km de profondeur sous ces sites (Frederiksen et al., 1998; Shi et al., 1998). Les rapports $^{187}Os/^{188}Os$ mesurés dans des harzburgites provenant du Sud comme du Nord de la Cordillère Canadienne, sont corrélés avec 1/Os et se placent au dessus de la corrélation régionale en fonction des indices de fusion des lherzolites. Ainsi, le système Os semble avoir été perturbé par des agents métasomatiques aux rapports d'$^{187}Os/^{188}Os$ élevés, et qui ont extrait préférenciellement l'Os de la péridotite. Ce processus s'est déroulé partout dans la Cordillère Canadienne mais a été particulièrement intense dans la région Nord, à l'aplomb de l'anomalie thermique du manteau. Dans les sites de xénolites riches en harzburgites, cette interaction asthénosphère-lithosphère apparaît même avoir perturbé les caractéristiques isotopiques en Pb-Pb, Rb-Sr (Carignan et al., 1996), Lu-Hf et Sm-Nd des lherzolites. En effet, les rapports $^{176}Hf/^{177}Hf$ mesurés dans deux lherzolites d'un de ces sites, sont parmi les plus bas parmi les rares analyses existantes de péridotite pour cet isotope. Les fluides ou liquides de fusion ont interagi à cet endroit avec la péridotite il y a moins de 170 Ma et avaient sans doute des caractéristiques isotopiques de type EMII.

Table des matières

Liste des tableaux

Chapitre 2

Chapitre 3

Liste des figures

Chapitre 2

Chapitre 3

Chapitre 4

Chapitre 5

Liste des photographies

Remerciements

Je tiens à remercier en tout premier lieu mes deux directeurs de thèse. John Ludden tout d'abord, qui m'a acceptée comme étudiante au moment de son déménagement du Canada vers la France. Le soutien de John tout au cours de ce travail, tant financièrement que scientifiquement, a été sans faille. Sans lui, les parties Re-Os et Lu-Hf de cette thèse n'auraient sans doute pas été abordées. Don Francis, initiateur du projet, a été d'une aide incalculable, grâce à sa vigilance scientifique et ses connaissances sur la Cordillère Canadienne et le manteau terrestre. Ses revues détaillées de ce manuscrit ont été une école formidable de rigueur et de précision scientifique. Merci à tous deux pour toute l'aide et les connaissances que vous m'avez apportées.

Un grand merci à Laurie Reisberg également, qui peut être considérée comme un troisième directeur de thèse. Laurie m'a initiée à la chimie, à la spectrométrie de masse par thermoionisation et au système isotopique Re-Os. Sa gentillesse, sa disponibilité et son aide m'ont été infiniment précieuse et de plus travailler avec elle est un vrai plaisir. Je la remercie pour tout ce qu'elle m'a apporté, surtout scientifiquement, mais aussi humainement.

Merci à tous les copains rencontrés au cours de mes périples de thèse. Tout d'abord à l'Université de Montréal, Alain, Isabelle, Martin, Glynn, Jean Kiepura... A McGill, le grand Pierre, roi de l'immiscibilité et passionné de la vie et des météorites, Anne-Claude, "l'Autre Française", Miss basalt et tout le temps en train de rigoler, et Claude Dalpé, amoureux des amphiboles. Grâce à eux trois, mes séjours à McGill ont toujours été joyeux et détendus. Merci pour leur amitié. Merci à Florence, sa joie de vivre et son rire, Yannick et sa gentillesse, et Pavel le grand barbu, au cours de mes séjours à Nancy. Merci à Jérôme et à Franck, dont j'ai partagé le bureau "de fumeurs", et dont l'humour était d'un grand soutien au cours de la rédaction de thèse. Merci à Catherine et Anne-Catherine pour leur aide dans les aléas du Re-Os et la joyeuse ambiance dans le labo. Merci à tous au

CRPG, Pascal Hanon, Benoît, Pascal Audigane, Estelle, Michel Arnold, Daniel et Maryse Ohnenstetter, Nathalie, enfin tous...!

Merci à Long pour l'aide apportée sur le terrain en Colombie Britannique et à Shi Lang pour les discussions sur les xénolites à McGill. Merci beaucoup aussi à Catherine Chauvel qui m'a acceuillie un mois dans son laboratoire à l'Université de Rennes et m'a appris la chimie du Lu-Hf. Merci à Philippe Telouk et Janne Blichert-Toft pour m'avoir acceuillie dans leur laboratoire de l'ENS Lyon pour les analyses Lu-Hf. Merci à Gilles Gauthier pour les discussions sur les techniques analytiques à l'Université de Montréal. Merci à Bertrand Jacquier pour l'aide apportée lors de la chimie du Re-Os, Laurent Z et Bernard Marty pour les analyses d'He, Maryse Ohnenstetter pour le SEM sur des sulfures, Jean Carignan et tout le personnel du SARM pour les analyses ICPMS, Luc Marin pour les analyses de soufre, Caroline Carignan pour la séparation des minéraux et des analyses isotopiques Sr au CRPG. Merci à Harry Becker et Richard Walker à l'Université du Maryland

Je remercie toutes les secrétaires que j'ai tant fait souffrir par ma situation administrative inextricable et internationale: Madame Ouellette, Line Boissonneau, Madame Charbonneau et Louise Terrien à l'Université de Montréal, Madame Lehmann, Suzie Pagel, Valérie Sourlier et Martine Noël au CRPG, Anne Kosowski à McGill. Merci également à Caroline Français pour tous les menus services sans cesse rendus et à Madame Jeannot, la bibliothécaire du CRPG.

Enfin, merci à Reinhard, à mes parents et à Alan, qui tour à tour m'ont encouragée et soutenue au cours de cette thèse.

Pardon à tous ceux que j'ai oublié!

A mes parents

Si j'avais les rimes âpres et rauques
Comme il conviendrait à ce lugubre trou
Sur lequel s'appuient tous les autres rocs,
J'exprimerais le suc de ma pensée
Plus pleinement; mais je ne les ai point,
Et non sans frayeur je m'apprête à parler [...]
Mais que les Muses viennent secourir mes vers
Qui aidèrent Amphion à faire les murs de Thèbes,
Afin que le dire ne soit pas loin du fait.

Dante
(L'enfer, Chant XXXII)

Chapitre 1: Introduction

1.1 CONTEXTE

Le manteau terrestre est essentiellement une enveloppe solide qui sépare le noyau métallique et en partie liquide des roches plus froides de la croûte. S'étendant jusqu'à une profondeur de 2900 km, il constitue environ 83% du volume terrestre et 67% de sa masse. La plupart de ce qui ce passe à la surface de la Terre, de la formation des chaînes de montagnes ou des bassins océaniques, en passant par le volcanisme et même jusqu'à des changements de types de sédimentation, se fait en réponse à des évènements ayant lieu dans le manteau. C'est aussi dans cette partie du globe terrestre que se situent les forces motrices de la tectonique des plaques. Des données séismologiques ont permis de le subdiviser en deux grandes régions grossièrement concentriques, le manteau supérieur et le manteau inférieur que sépare une discontinuité sismique à 670 km de profondeur. C'est du manteau supérieur dont nous nous entretiendrons essentiellement ici. Ce dernier peut encore être subdivisé en deux régions superposées sous les océans (Daly, 1940): (1) la partie mantellique de la lithosphère dont l'épaisseur varie de moins d'un km à 100 km et qui est rigide, et, au dessous (2) l'asthénosphère dont la profondeur est estimée à 200 km et qui se déforme par fluage. La lithosphère océanique s'enfonce dans le manteau au niveau des zones de subduction, mais la profondeur atteinte par la plaque subduite est l'objet de débats: recyclage dans le manteau supérieur (Allègre and Turcotte, 1986), stockage de vieille croûte océanique à la discontinuité sismique de 670 km (Ringwood and Irifune, 1988), percement de cette discontinuté et atteinte du manteau inférieur (van der Hilst, 1995). Les continents quant à eux ont une racine continentale profonde (jusqu`à 400 km de profondeur) définie par thermobarométrie sur minéraux (Boyd et al., 1985), des températures relativement froides (en tomographie sismique, grande vitesse des ondes sismiques (Grand, 1994) et de

hautes viscosités (Jordan, 1988). Cette racine profonde est appelée par certains auteurs tectosphère (Jordan, 1988) . La présence d'une asthénosphère sous la lithosphère continentale est l'objet de débats car on ignore jusqu'à quel point la lithosphère continentale est couplée avec le manteau convectif situé au-dessous (VanDecar et al., 1995; Silver, 1996). Enfin, il n'est toujours pas déterminé si la convection du manteau, moteur de la tectonique des plaques, se fait sur un ou sur deux niveaux, ni quel est le mécanisme principal responsable de cette convection (production de croûte océanique au niveau des rides océaniques, traction par la plaque subduite, montée de panaches mantelliques profonds) (Allègre et al., 1983; Galer and O'Nions, 1985; Christensen, 1995; Hofmann, 1997).

L'étude de la composition du manteau supérieur est possible grâce à l'étude des magmas basaltiques issus de la fusion partielle de celui-ci, mais aussi par l'étude de roches ultramafiques d'origine mantellique. Ces derniers se présentent sous la forme de fragments du manteau remontés par les magmas qui le traversent en arrachant des morceaux aux parois des conduits et des fractures par lesquelles ils remontent vers la surface terrestre. Il s'agit des xénolites du manteau qui constituent l'objet de cette thèse. Les roches ultramafiques sont aussi présentes à la surface de la planète sous forme de vastes éclats de manteau supérieur (parfois atteignant plusieurs km d'envergure) remontés tectoniquement au niveau de la croûte lors d'orogenèses. Il s'agit alors des massifs orogéniques de péridotites et des massifs ophiolitiques, ces derniers étant considérés comme des morceaux de lithosphère océanique. Enfin, une dernière et importante contribution à la connaissance de la composition du manteau supérieur vient de la pétrologie expérimentale qui reproduit en laboratoire les conditions de pression et température élevées du manteau afin de déterminer les phases qui y sont stables. Il est ainsi généralement admis que le manteau supérieur est de composition péridotitique, c'est à dire constitué essentiellement des trois minéraux principaux olivine, orthopyroxene et clinopyroxène. Selon la profondeur, viennent s'ajouter les phases alumineuses spinelle (de 30 à 60 km de profondeur) et grenat

(de 45 à 660 km), les phases hydratées comme l'apatite, l'amphibole ou la phlogopite, et parfois même du diamant. Il est important cependant de noter que la représentativité de ces péridotites vis à vis du manteau supérieur est mal contrainte, et qu'ainsi le manteau en général demeure largement inaccessible.

Photo 1: Affleurement de xénolites du manteau dans leur encaissant de basalte alcalin. Big Timothy Mountain, Colombie Britannique. Noter le xénolite composite à péridotite vert clair recoupée par une veine riche en pyroxènes vert foncé.

La complémentarité des compositions moyennes de la croûte continentale et océanique avec celle du manteau supérieur a conduit à l'élaboration d'un modèle de

formation du manteau supérieur en deux étapes (Hofmann, 1988), à partir d'un manteau primitif issu de la différenciation noyau-manteau initiale (Anderson, 1989). 1.5% de fusion du manteau primitif peut rendre compte de la plupart de la composition de la croûte continentale. Ce processus a sans doute commencé il y a plus de 3.8 Ga (Collerson et al., 1991) et s'est essentiellement déroulé au cours du Précambrien (Taylor and McLennan, 1985). Ensuite, 8 à 10 % de fusion auraient formé la croûte océanique (c'est à dire les MORBs, Mid Ocean Ridge Basalts) mais la période d'initiation de ce processus est l'objet de nombreux débats (Galer and Goldstein, 1991). Cette dernière étape se perpétue continuellement au niveau des rides médio-océaniques et la croûte océanique est constamment recyclée dans le manteau océanique par l'intermédiaire des zones de subduction. Ces processus ont laissé le manteau appauvri en éléments incompatibles par rapport à sa composition initiale, cette dernière devant être celle du manteau inférieur. Cependant la composition du manteau océanique n'est pas uniforme et divers processus sont invoqués pour expliquer cette diversité isotopique et élémentaire (Hofmann, 1997): le recyclage de la croûte océanique déjà mentionné, la délamination de la croûte continentale ou encore l'apport de magmas d'origine profonde comme ceux des OIBs (Océanique Island Basalts), ces derniers pouvant venir du manteau inférieur ou même de la limite noyau-manteau (Wolfe et al., 1997; Brandon et al., 1998). La lithosphère sous-continentale quant à elle est cette partie du manteau située de 100 à 400 km de profondeur sous les continents et considérée comme relativement froide par rapport à l'asthénosphère et suffisamment rigide pour l'empêcher de participer à la convection mantellique. Au contraire elle reste de façon plus ou moins permanente attachée à la croûte continentale. Cela ne l'empêche pas d'avoir une grande diversité de composition comme en témoignent les laves et les xénolites qui en sont issues. Cependant, de grands débats existent quant à sa formation et celle de la croûte qui la surplombe: accrétion d'arc océaniques (Taylor and McLennan, 1985), accrétion de plateaux océaniques (de Witt et al., 1992; Albarède, 1997) ou encore accumulation sous-jascente de matériel de panaches mantelliques (Herzberg,

1993; Choukroune et al., 1997) sont les principaux modèles invoqués. Ainsi, la diversité des roches issues du manteau sous-continental proviendrait de ces divers éléments exotiques qui s'y sont injectés et que l'absence de convection a pu maintenir isolés, ou encore de fluides mantelliques piégés dans ses parties froides (McKenzie and O'Nions, 1989).

Le manteau lithosphérique situé sous la Cordillère Canadienne se situe dans une zone de transition entre manteaux océanique et continental. En effet, la Cordillère Canadienne s'est formée par accrétions successives de terrains tectoniques à la marge occidentale du craton canadien au cours de la fin du Jurassique et du début du Crétacé. Le manteau sous-jascent est donc bordé à l'Est par la lithosphère sous-continentale du craton canadien, et à l'Ouest par la zone de subduction des plaques lithosphériques océaniques du Pacifique. La nature exacte de ce manteau "intermédiaire", son homogénéité, son âge et son origine constituent l'objet de cette thèse.

1.2 OBJECTIFS

Trois grands thèmes de recherche concentrent les efforts des spécialistes de la chimie du manteau. Tout d'abord, le métasomatisme du manteau est l'objet de nombreuses publications. Le métasomatisme se définit par la transformation chimique et/ou modale de la composition originale de la péridotite, issue de la fusion, par le passage de fluides et/ou de liquides de fusion. Lorsque de nouvelles phases minérales apparaissent (apatite, phlogopite, amphibole), on parle de métasomatisme modal. Lorsque le métasomatisme n'est détecté que par un subtil changement de composition en éléments majeurs ou traces des minéraux préexistants, il s'agit de métasomatisme cryptique. De nombreux débats existent sur la nature des agents métasomatiques (fluides ou liquides de fusion, composition carbonatée, siliceuse, CO_2, H_2O, degré d'oxydation) (e.g.(Hawkesworth and Norry, 1983; Menzies and Hawkesworth, 1987), sur leur provenance et leur relation avec

le contexte tectonique (e.g.(Jochum et al., 1989; Hauri et al., 1993; Bedini et al., 1997; Brandon et al., 1998), sur leur circulation à travers les roches du manteau et leur capacité à transporter les éléments (e.g. (McKenzie and O'Nions, 1989; Takazawa et al., 1992), enfin sur la simultanéité ou la postérité de leur action par rapport aux évènements de fusion (e.g. (McDonough and Frey, 1989; Walker et al., 1989; Ionov et al., 1994). L'action de liquides de fusion peut même transformer complètement la composition initiale de la péridotite, masquant les évènements de fusion, comme dans les cas d'interaction liquide de fusion-roche (melt-rock interaction) aboutissant à la cristallisation d'orthopyroxène (Kelemen et al., 1992), de cristallisation d'olivine (Francis, 1987; Niu et al., 1997; Shaw et al., 1998) ou encore de clinopyroxène (Dautria et al., 1992). Dans le cas des xénolites mantelliques de la Cordillère Canadienne, il est donc important de déterminer si leur composition reflète de la fusion et/ou des cas d'interaction liquide de fusion-roche, quel type de métasomatisme les a affecté, en particulier en relation avec leur contexte tectonique entre une zone de subduction et un craton, et quels éléments chimiques ont été affectés par le métasomatisme.

Le deuxième thème majeur qui intéresse les chercheurs est de voir le manteau comme la source du volcanisme terrestre. Toute variation de composition de manteau sera reflètée par les magmas qui en sont issus. De plus, tout magma migrant à travers le manteau dans son chemin vers la surface terrestre est suceptible de réagir chimiquement avec le manteau environnant, voyant ainsi sa composition "tamponnée" par celle du manteau (Francis, 1987). Une part importante des travaux sur le manteau consiste donc à étudier quels types de magmas sont en équilibre avec le manteau, quels types de magmas ont été issus du manteau pour laisser le résidu de fusion que représentent en général les péridotites, enfin s'il y a un lien entre les types de péridotites observés et les types de volcanismes associés géographiquement. Le type de basalte en particulier varie avec le contexte tectonique (Wilson, 1989), et une grande partie de cette variabilité est attribuée au manteau (l'autre l'est à la croûte, généralement aussi traversée par les magmas lors de leur ascension). Le volcanisme de la Cordillère Canadienne est varié, entre la période pré-

accrétion (essentiellement du volcanisme de rift au Protérozoique), le volcanisme propre à chaque terrain tectonique accrété (dominé par du volcanisme de type arc insulaire) et la période post-accrétion (principalement volcanisme calco-alcalin à alcalin à relier au contexte de subduction, mais aussi volcanisme de panache (OIB), l'expression de ces magmas à la surface étant due à des failles de trans-tension dues au jeu entre les plaques Pacifiques et Nord-Américaine) (Souther, 1991). C'est d'ailleurs lors de cette dernière période qu'ont été remontées à la surface par des basaltes alcalins les xénolites du manteau étudiés dans cette thèse. Il sera donc question dans cette thèse de calculer les types de liquides de fusion en équilibre avec la composition des xénolites de la Cordillère Canadienne, de comparer leur composition avec celles de liquides expérimentaux et naturels, enfin de déterminer si la composition de la lithosphère mantellique reflète les variations géographiques et tectoniques des compositions isotopiques des basaltes alcalins récents (Abraham et al., 1998) et des granitoïdes (Armstrong, 1988) de cette région.

Enfin le troisième thème comprend tous les grands modèles de formation de la Terre, du manteau, de la croûte continentale ou océanique évoqués plus haut, ainsi que les relations entre ces divers réservoirs terrestres. En particulier, des études grâce au système isotopique Re-Os de xénolites remontés par des magmas kimberlitiques en contexte cratonique Archéen, suggèrent que le manteau sous-continental de ces régions y est très ancien (3 Ga ou plus). De plus, ces âges de fusion du manteau correspondent à l'âge de formation de la croûte cratonique, suggérant ainsi un lien génétique entre les deux (Walker et al., 1989; Pearson et al., 1995a; Pearson et al., 1995b). Une étude de xénolites mantelliques dans un contexte tectonique de bordure de craton du Protérozoique aboutit aux mêmes conclusions (âge de 2 Ga, (Pearson et al., 1994)). En revanche, l'âge de xénolites Sud-Ouest Australiennes assez similaires à celles de la Cordillère Canadienne est plus ancien que les terrains cambriens de la croûte de cette région, laissant à penser que la lithosphère sous-cratonique de l'Australie se prolonge sous les terrains bordant le craton (Handler et al., 1997). La longévité du manteau lithosphérique non-Archéen est aussi

confirmée par les âges Protérozoiques de péridotites de massifs orogéniques (Reisberg and Lorand, 1995). Dans le cas de la Cordillère Canadienne, il sera en particulier question de la relation du manteau lithosphérique avec les terrains accrétés de la croûte situés au dessus et avec la lithosphère sous-cratonique à l'Est. Ainsi l'âge de formation du manteau lithosphérique sera déterminé et comparé a ceux de ces diverses unités. L'étude des xénolites du manteau de cette région a donc pour but de déterminer dans quelle mesure le manteau situé sous la Cordillère Canadienne est hétérogène, si cette hétérogénéité correspond aux terrains tectoniques de la croûte, ou à l'influence de la subduction ou encore de la lithophère sous-cratonique du Canada, enfin dans quel contexte tectonique s'est formé le manteau lithophérique de cette région. Une comparaison avec d'autres régions du monde permettra d'appréhender le rôle du manteau dans une région orogénique convergente le long d'un craton, comme la Cordillère Canadienne, dans les processus globaux de formation, passée et présente, des continents.

1.3 MÉTHODOLOGIE

Les xénolites du manteau constituant la base de cette étude ont été échantillonnés dans le Sud de la Colombie Britannique au cours de septembre 1995. Des xénolites du Nord de la Cordillère Canadienne, échantillonnés antérieurement (D. Francis, L. Shi) ont aussi été inclus dans cette étude. L'échantillonnage de plusieurs dizaines de xénolites par site se fait de façon aléatoire afin d'assurer une bonne représentativité. Ensuite, les xénolites sont classés en trois groupes en fonction de l'estimation visuelle de leur contenu modal de pyroxène. Enfin, une trentaine de xénolites sont définitivement sélectionnés parmi ces trois groupes en fonction de la proportion de chacun. Chaque xénolite a été examiné en lame mince et l'analyse de la roche totale a été éffectuée par fluorescence X à l'Université McGill (Canada). La composition des minéraux a été déterminée par microsonde sur trois à cinq xénolites par suite, sélectionnés afin de représenter la gamme

entière de composition de roche totale de chaque suite. La composition en éléments traces de ce même sous-groupe a été effectuée par ICP-MS solution au CRPG à Nancy (France). Le début de cette thèse est donc consacré à la pétrologie des xénolites mantelliques de la Cordillère Canadienne, en particulier à leur composition en éléments majeurs et traces (Chapitre 2). Les informations ainsi tirées concernent les évènements de fusion, ainsi que l'interaction liquide de fusion-roche, et le métasomatisme les ayant affecté. Cependant, une grande partie de ce travail a été faite grâce et sur le sytème isotopique Rhénium-Osmium (Chapitres 3 et 4). La chimie et l'analyse sur un spectromètre de masse à thermoionisation négative du Re-Os a été effectuée au CRPG à Nancy (France). Il convient donc de détailler l'intérêt et les particularités de ce système isotopique dans l'étude des roches du manteau. Enfin, un autre système isotopique qui commence tout juste à se développer pour les roches ultramafiques, a été appliqué à quelques xénolites de la Cordillère Canadienne (Chapitre 4). Il s'agit du système Lutétium-Hafnium dont les propriétés vont être également présentées ici. La chimie en a été réalisée à l'Université de Rennes et l'analyse par ICP-MS P54 à l'ENS de Lyon.

Le sytème Re-Os est basé sur la décroissance radioactive β^- du ^{187}Re en ^{186}Os en une période de demi-vie de 45.6 Ga (Lindner et al., 1986). L'Os fait partie des platinoïdes et l'Os et le Re sont des éléments sidérophiles. Le Re est modéremment incompatible (comme le Lu par exemple (Meisel et al., 1996)), alors que l'Os est compatible dans les processus de fusion (Morgan, 1986). C'est cette dernière propriété qui rend unique l'application du Re-Os dans les roches du manteau. En effet, les péridotites, résidus de fusion, sont riches en Os, alors que les liquides résiduels seront appauvris en cet élément. Ainsi, tout fluide ou liquide de fusion circulant dans le manteau sera pauvre en Os et donc ne pourra pas changer la composition en Os des péridotites qu'ils traversent. Une addition de Re est en revanche possible. Ainsi, le système Re-Os est fort différent des autres systèmes isotopiques comme le Rb-Sr, le Sm-Nd ou le Pb par le fait qu'il reste en principe insensible aux processus métasomatiques (Walker et al., 1989). Cette propriété unique a

été utilisée pour dater les évènements de fusion du manteau grâce à des âges modèles, des âges minimum d'appauvrissement en Re (Walker et al., 1989) ou encore à des pseudo-isochrones (Reisberg and Lorand, 1995). Cependant, il a été récemment démontré que l'Os est mobile dans certaines conditions (Brandon et al., 1996), en particulier quand la fucacité d'oxygène est élevée (Wood, 1987). De plus, l'Os ne se trouve vraisemblablement pas dans les phases majeures des péridotites mais est sans doute concentré dans les sulfures (e.g. (Hart and Zindler, 1986). La place du Re dans les péridotites est aussi objet de débats (Hauri and Hart, 1997; Pearson et al., 1998). Etant donné le manque de données expérimentales concernant le comportement des platinoïdes et du Re vis à vis des liquides sulfurés et silicatés, sans compter le comportement des sulfures eux-mêmes lors des processus de fusion, de nombreuses inconnues planent sur les propriétés exactes du système Re-Os dans le manteau. Au cours de cette thèse, le système Re-Os sera utilisé pour dater les évènement de fusion ayant affecté les xénolites de la Cordillère Canadienne. Les comportements du Re et des isotopes de l'Os au cours du métasomatisme seront également traités.

Le système Lu-Hf quant à lui est issu d'une désintégration β du ^{176}Lu en ^{176}Hf en une période de demi-vie de 35.7 Ga. L'Hf et le Lu sont en général considérés comme moins mobiles que les traceurs couramment utilisés que sont le Rb, Sr, Sm, Nd ou Pb. Le Lu est compatible dans le grenat lors des processus de fusion. Le grenat étant une phase importante du manteau à des pressions supérieures à 20 kbar, son influence sur le fractionnement du Lu de l'Hf fait de ce système isotopique un traceur potentiel de la profondeur d'origine des péridotites (Salters and Hart, 1989). Jusqu'à très récemment, les difficultés analytiques ont empêché les mesures isotopiques Lu-Hf dans les roches ultramafiques (Blichert-Toft et al., 1997). Les mesures présentées dans cette thèse sont donc parmi les premières sur des roches du manteau (Salters and Zindler, 1995). L'analyse Lu-Hf de lherzolites permet ici de contraindre le métasomatisme ayant affecté le manteau lithosphérique situé sous le Nord de la Cordillère Canadienne.

L'analyse Lu-Hf de lherzolites permet ici de contraindre le métasomatisme ayant affecté le manteau lithosphérique situé sous le Nord de la Cordillère Canadienne.

1.4 GÉOLOGIE DE LA CORDILLÈRE CANADIENNE

Photo 2: Paysage de la Cordillère Canadienne. Wells Gray Park, Colombie Britannique.

La Cordillère Canadienne s'étend sur plus de 1000 km sur la marge Ouest du Canada et sa longueur est orientée globalement Sud Sud-Est à Nord Nord-Ouest. Elle fait partie de la longue Cordillère qui s'étend à l'Ouest des deux Amériques, de la Terre de Feu à la pointe extrême de l'Alaska. Au Canada, elle a été divisée en cinq grands domaines géomorphologiques qui sont de l'Est à l'Ouest: Avant-Pays, Oménica, Intermontagneux, Côtier et Insulaire (Fig. 1 du Chapitre 2). Des études paléontologiques, magnétiques, tectoniques et pétrologiques ont permis de déterminer qu'elle s'est formée par accrétion de terrains tectoniques de diverses provenances à la marge Ouest du Craton Canadien, ce

Cordillère Canadienne et permettent d'affirmer que le Craton Canadien s'étend au moins jusqu'à la limite entre les Domaines Omenica et Intermontagneux dans cette région (Armstrong et al., 1991). Des données de Sr sur des granitoïdes font affirmer à certains auteurs que cette limite peut être repoussée encore plus à l'Ouest, le long de ce qu'il est devenu commun d'appeler la ligne de Sr 0.704 (Fig. 1 du Chapitre 2, (Armstrong, 1988)). Les terrains accrétés peuvent être classés en deux grandes catégories, les péricratoniques et les allochtones. Les terrains péricratoniques, ainsi nommés parce qu'ils sont toujours restés proches du Craton Canadien au cours de leur histoire, comprennent essentiellement les terrains Yukon-Tanana (YTT) et leur équivalent au Sud, Kootenay (KO). Les principaux terrains allochtones sont Quesnellia (QN), Cassiar (CA), Cache Creek (CC), Stikine (ST), le super-terrain Intermontagneux, et les terrains du Domaine Insulaire qui ne seront pas détaillés ici. Toutes les informations ci-après ont été puisées dans le livre "Géologie de l'orogène de la Cordillère du Canada" édité par Gabrielse et Yorath (Gabrielse and Yorath, 1991a).

Le Domaine de l'Avant-Pays est composé en majorité de roches sédimentaires déposées sur le socle cristallin du Craton Canadien: des sédiments de rift et de marge passive du Protérozoique moyen à la fin du Paléozoique, mais aussi des sédiments d'avant fosse du Mézozoique déposés à l'avant du front de déformation qui a soulevé la Cordillère.

Les terrains accrétés du Domaine d'Omenica se présentent sous la forme de vastes nappes de charriage mises en place sur la marge continentale du Protocontinent Nord-Américain. Cette dernière est constituée par les sédiments et roches volcaniques du Protérozoique au Trias du terrain de Kootenay-Yukon-Tanana. Au dessus ont été charriés au Jurassique les terrains allochtones de Slide Mountain et de Quesnellia, assemblages de milieu océanique du Paléozoique (roches volcaniques mafiques et sédiments clastiques) pour le premier et assemblages essentiellement d'arc volcanique insulaire (Trias, mais aussi des sédiments de l'Ordicicien au Trias) pour le deuxième.

Le Domaine Intermontagneux se compose de divers terrains accrétés au Jurassique précoce et partiellement recouverts de sédiments et roches volcaniques du Tertiaire (volcans boucliers Mount Edziza et Level Mountain et ceinture volcanique d'Anahim). Le terrain Cache Creek, sorte d'éclat de croûte posée sur le terrain Stikinia, a un faciès océanique datant du Mississipien au Trias, essentiellement formé de roches carbonatées. Le terrain Stikinia comprend des strates volcaniques et sédimentaires de bassin marginal et d'arc insulaire du Dévonien Inférieur au Jurassique. Enfin le Domaine Intermontagneux contient une grande partie du terrain de Quesnellia décrit plus haut.

Le domaine Côtier voit sa lithologie dominée par d'énormes plutons granitiques et des roches métamorphiques datant du Crétacé au Tertiaire. Il semble avoir été créé soit dans un environnement de subduction de longue durée, soit par la collision entre les super-terrains Insulaire et Intermontagneux, et représenterait un arc insulaire à maturité.

Le Domaine Insulaire est composé de plusieurs terrains volcaniques et sédimentaires de rift ou de plate-forme de la deuxième moitié du Paléozoique au Trias et accrétés au Crétacé précoce.

Les mouvements tectoniques actuels sont dominés par l'interaction des plaques Pacifiques (Pacifique, Explorer et Juan de Fuca, ainsi que la plaque subduite il y a 43 Ma Farallon) avec la plaque de l'Amérique du Nord. Ces interactions ont eu pour conséquence le passage d'un régime compressif à un régime extensif au cours de l'Eocène par un soulèvement général de la chaîne. La formation de failles en régime extensif a permis l'expression d'un volcanisme alcalin Tertiaire à récent. Les xénolites du manteau étudiés ici ont été trouvés dans ces basaltes. Ainsi le volcanisme de l'ensemble Clearwater-Quesnel (suites de xénolites de West Kettle River, Lightning Peak, Lassie Lake et Kostal Lake) semble être associé aux zones de failles qui limitent le terrain Quesnellia à l'Est et dont la composition va de tholéiitique à alcaline. Les laves d'arrière-arc du Groupe de Chilcotin (suite de xénolites Rayfield River) de composition calco-alcaline sont à lier à la subduction de la plaque Farallon-Juan de Fuca au Tertiaire tardif. La ceinture volcanique d'Anahim

(suite de xénolites de Big Timothy) de composition alcaline à hyperalcaline a été reliée à la trace d'un point chaud mantellique entre 15 Ma et quelques centaines d'années. Le Groupe volcanique d'Endako (suite de xénolites de Summit Lake) datant de l'Eocène-Oligocène doit sans doute son existence à la réactivation d'un ancien complexe de subsidence par les mouvements de subduction à l'Ouest du Domaine Côtier. La chaîne volcanique de Stikine (suites de xénolites Castle Rock, Llangorse, Alligator Lake et Fort Selkirk) de composition de basalte alcalin à olivine jusqu'à felsique hyperalcalin est apparue à la faveur de failles de décrochement dans le contexte d'extension du Néogène mentionné plus haut. La ceinture volcanique de Wrangell enfin (suites de xénolites de Clinton et Prindle), de composition andésitique à calco-alcaline serait un arc continental lié à la convergence de la Plaque Pacifique et Nord-Américaine au Néogène précoce.

Photo 3: Site de Big Timothy Mountain, Colombie Britannique.

Photo 4: Site de Kostal Lake, Wells Gray Park, Colombie Britannique.

1.5 PLAN DE LA THÈSE

Le corps de cette thèse se compose de trois chapitres principaux, correspondant chacun à un article. Ces derniers seront publiés dans des revues internationales. Le chapitre 2 concerne la pétrologie, éléments majeurs et traces, des xénolites du Sud de la Cordillière Canadienne, avec comparaison avec celles du Nord et avec les types variés de péridotites que l'on trouve de par le monde. Le chapitre 3 s'intéresse à l'étude Re-Os des lherzolites de la Cordillère Canadienne, avec discussion de l'âge de la lithosphère mantellique et de l'âge de la croûte située au dessus. Le chapitre 4 est focalisé sur le Re-Os de suites à forte proportion de harzburgites du Nord de la Cordillère Canadienne, et les processus de métasomatisme vis à vis du Re-Os, mais aussi du Lu-Hf, sont discutés. Le chapitre 5 constitue la conclusion générale de la thèse.

Chapitre 2: Petrology and trace element characteristics of the lithospheric mantle beneath the southern Canadian Cordillera

Paper to be submitted to Canadian Journal of Earth Sciences

by Anne H. Peslier, Don Francis and John Ludden

RÉSUMÉ

Dans la Cordillère Canadienne qui borde la marge Pacifique du continent Nord-Américain, de nombreux xénolites à spinelle ont été remontés par des basaltes alcalins de la fin du Tertiaire jusqu'à la période récente. Ces xénolites représentent des échantillons du manteau lithosphérique situé à la transition entre la lithosphère cratonique et la lithosphère océanique en subduction. Les suites de xénolites des sept centres volcaniques sur lesquelles se concentre cette étude sont principalement constituées de péridotites à spinelle et diopside chromifère, mais aussi de wehrlites à spinelle et augite ainsi que de quelques pyroxénites.

La gamme de composition en éléments majeurs des suites à diopside chromifère peut être expliquée par l'extraction de liquides de composition picritique à des degrés variables de fusion partielle d'une source de type pyrolite. De ce point de vue, les suites de lherzolites du Sud de la Cordillère Canadienne sont très semblables à celle de la région nord. L'ampleur de la fusion a sans doute été différente dans chaque suite de xénolites. Quelques-unes des dunites, des harzburgites et des lherzolites appauvries sont cependant trop riches en Fe pour représenter de simples résidus de fusion. Elles sont probablement le

résultat de l'interaction entre un liquide de fusion de composition alcaline et la péridotite, ce qui a conduit à la cristallisation d'olivine au dépens de l'orthopyroxène et du spinelle. Les quelques harzburgites de la région sud sont très différentes des très nombreuses harzburgites que l'on peut trouver dans trois sites de la région nord. Leur présence s'explique par de la fusion induite par un apport récent de fluides. Une comparaison des péridotites à diopside chromifère de la Cordillère Canadienne avec des péridotites provenant d'environnements tectoniques variés, semble indiquer qu'elles ressemblent à celles du manteau océanique, mais sont différentes de celles que l'on trouve dans des contextes tectoniques d'arc. Les teneurs en éléments traces des xénolites suggèrent que la fusion a eu lieu dans le champ de stabilité du spinelle et a été suivie par du métasomatisme. La plupart de ces fluides ou liquides de fusion responsables du métasomatisme étaient enrichis en terres rares légères (LREE) et appauvris en Hf, Zr et Ti. Dans deux sites de xénolites, le métasomatisme a conduit à la cristallisation de minéraux hydratés (amphibole et phlogopite). Il s'exprime sous forme de métasomatisme cryptique partout ailleurs.

Les xénolites de composition wehrlitique à augite représentent vraisemblablement des veines qui recoupent le manteau lherzolitique. La plupart de ces wehrlites sont assez réfractaires par rapport aux suites à augite alumineuse que l'on trouve communément dans les zones continentales post-Protérozoiques.

ABSTRACT

Numerous Spinel peridotite xenolith suites occur in mid-Tertiary to recent alkali-basalts in the Canadian Cordillera, bordering the Pacific margin of the North American continent. The mantle xenoliths from this region are thus samples from the lithospheric mantle at the transition between the cratonic and the oceanic lithosphere. Seven volcanic centers from the Southern Canadian Cordillera contain mantle xenolith suites that comprise

mainly Spinel Cr-diopside peridotites, but also include Spinel augite-wehrlites and minor pyroxenites.

The major element compositional range of the Cr-diopside suites can be explained by the extraction of picritic melts by various degrees of partial melting of a pyrolite type source,with the extent of melting being different in each xenolith suite. The lherzolite suites of the southern region of the Canadian Cordillera are thus similar to those of the Northern region (Francis, 1987). Some of the dunites, harzburgites and depleted lherzolites are, however, too Fe-rich to be the simple residues of melting. They likely result from the interaction of an alkali melt with peridotite, resulting in olivine crystallisation at the expense of orthopyroxene and Spinel. The few harzburgites of the southern region of the Canadian Cordillera are Si and Na-poor, and Fe-rich compared to the more abundant harzburgites at three northern sites, which have been explained by recent fluid-induced melting (Shi et al., 1998). A comparison of the Cr-diopside peridotites from the Canadian Cordillera with peridotites from different tectonic settings indicates that the peridotites from the Canadian Cordillera ressemble those of intraplate oceanic mantle, but are different than those found in arc settings. Trace elements of bulk-xenoliths indicate that melting occurred in the Spinel stability field, and was later followed by metasomatism. The fluids or melts responsible for this metasomatism were enriched in LREE and depleted in Hf, Zr and Ti. At two sites, metasomatism resulted in the crystallization of hydrous minerals (amphibole and phlogopite), but is expressed as cryptic metasomatism everywhere else.

Most of the wehrlites are more refractory than the Al-augite suites found in Phanerozoic continental areas (e.g., Frey and Prinz, 1978). and are likely the result of crystallisation at depth of melts in lithospheric conduits.

2.1 INTRODUCTION

Spinel peridotite xenoliths occur in many alkali basalt centers along the Canadian Cordillera, a Phanerozoic convergent orogen bordering the western edge of the Canadian craton. The petrochemical and isotopic characteristics of xenolith suites in the Northern Canadian Cordillera are now well documented (Francis, 1987; Carignan et al., 1996; Peslier et al., 1998; Shi et al., 1998), while the petrological characteristics of individual xenolith suites in the Southern Cordillera have been adressed by Fiesinger and Nicholls (1977), Fujii and Scarfe (1982), Ross (1983) Brearley and Scarfe (1984); Brearley et al. (1984), Canil et al. (1987), and Canil and Scarfe (1989).

The xenolith suites of the Canadian Cordillera sample the lithospheric mantle at the transition between cratonic continental lithosphere and oceanic mantle. The Canadian Cordillera was formed during the late-Jurassic and Cretaceous through the successive accretion of tectonic terranes of various lithologies (mainly arc-related) to the stable margin of ancestral North America (e.g., Gabrielse et al., 1991). However the nature of the lithospheric mantle beneath these terranes and its tectonic origin is poorly constrained. Moreover this continental magin is bordered in the southern part by a subduction zone (Gabrielse and Yorath, 1991), and as such the Canadian Cordillera lithosphere may have undergone the effects of subduction-related agents. Finally, the major element composition of the mantle lithosphere is of interest as the potential source of terrestrial magmas and also as a compositional buffer for magmas migrating through it on their way to the surface.

This paper presents a synthetic study of the petrochemical characteristics of the Southern Canadian Cordillera xenolith suites, with a systematic comparison to the Northern Canadian Cordillera suites, and other peridotites from around the world. It addresses the origin of both the Cr-diopside xenolith and augite wehrlite xenolith suites in the Canadian Cordillera, using simple melting and crystallisation models to constrain the origin of the compositional variation in these xenoliths and the compositions of melts in

equilibrium with them. A comparison with other types of mantle peridotites helps to constrain the processes of formation of the Canadian Cordillera xenoliths, as well as their probable original tectonic setting.

2.2 OCCURRENCE AND ROCK TYPES OF THE SOUTHERN CORDILLERA MANTLE XENOLITHS

Mantle xenoliths (identified by an X in sample name) were sampled at 7 volcanic centers in the southern Canadian Cordillera: Summit Lake (SL), Kostal Lake (KL), Big Timothy (BT), Rayfiel River (RR), West Kettle River (KR), Lassie Lake (LL) and Lightning Peak (LP; Fig. 1, Table 1). The xenoliths occur as inclusions in lava flows (SL, BT, RR, KR, LL and LP) or as bombs in cinder cones (KL). The host lavas range in composition from alkali olivine basalts (AOB) to olivine nephelinites (Ol-NEPH; Table 1), with eruption ages ranging from mid-Tertiary (SL) to recent (KL; Table 1).

The first description of southern Canadian Cordillera mantle xenoliths was published by Littlejohn and Greenwood (1974). Most studies since then have focused on petrography and geothermobarometry (Fiesinger and Nicholls, 1977; Fujii and Scarfe, 1982; Ross, 1983; Brearley et al., 1984; Canil et al., 1987).

Fig. 1 (next page): Map of the Canadian Cordillera, showing the xenolith sites and the tectonic terranes accreted to the stable margin of North America. White triangles are for dominantly lherzolitic suites, black and white triangles for lherzolitic and harzburgitic suites, grey and white triangles for lherzolitic and wehrlitic suites. Xenolith site name abbreviations: Southern Cordillera sites SL = Summit Lake, KL = Kostal Lake, BT = Big Timothy, RR = Rayfield River, KR = West Kettle River, LL = Lassie Lake, LP = Lightning Peak; location of Northern Cordillera sites (Francis, 1987; Shi et al., 1998) are also shown for reference. Insular, Coast, Intermontane and Foreland are the names of the belts dividing the Canadian Cordillera. Tectonic terrane name abbreviations: YTT = Yukon Tanana (= similar characteristics to the Kootenay terrane (KO) of British Columbia (Mortensen, 1992), CA = Cassiar, QN = Quesnellia, CC = Cache Creek, ST = Stikine. Oceanic plate boundaries are from (Riddihough and Hyndman, 1991).

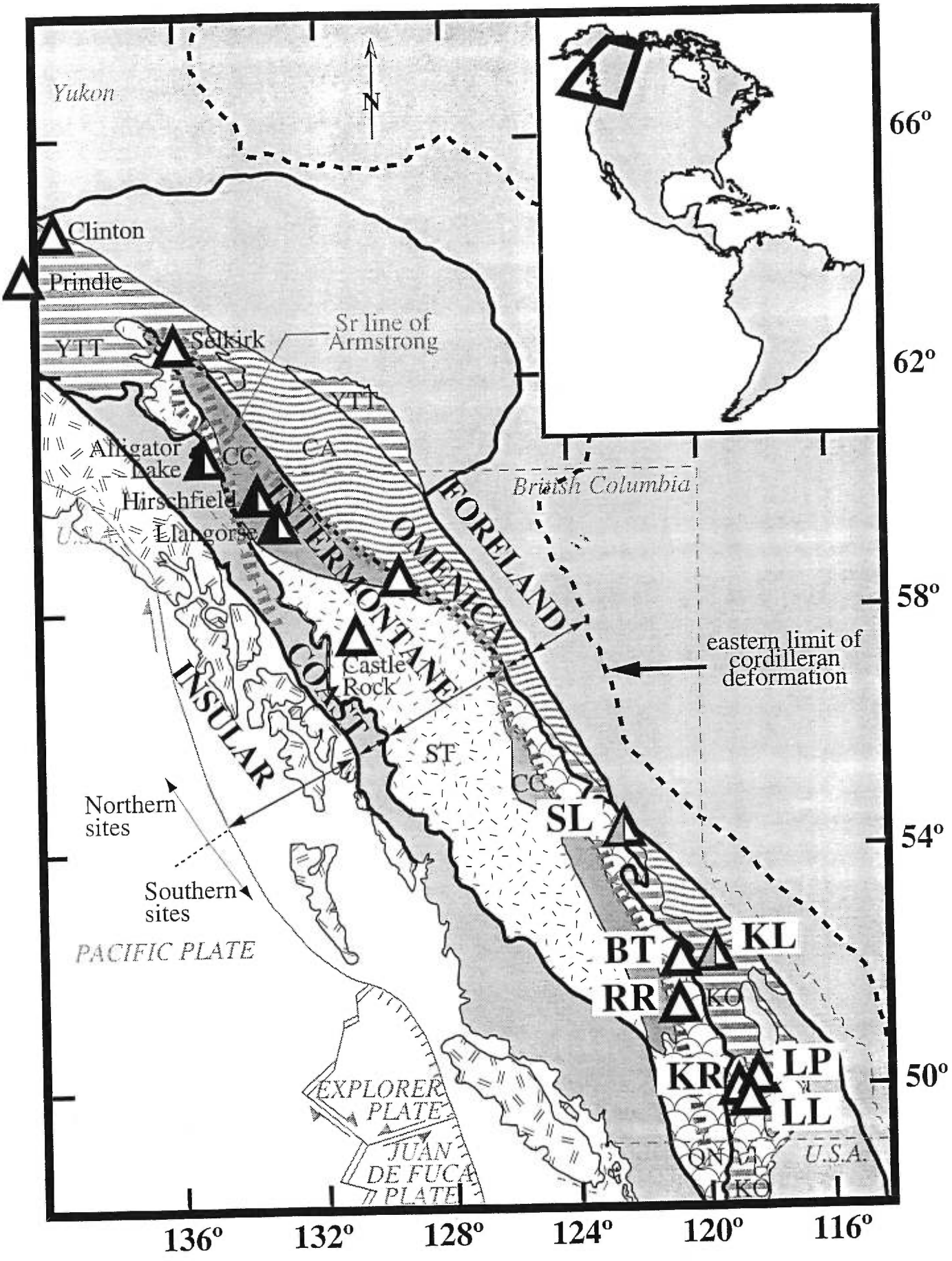
Yukon
N
66°
62°
58°
54°
50°
Clinton
Prindle
YTT
Selkirk
Sr line of Armstrong
YTT
Alligator Lake
CC
CA
Hirschfield
Llangorse
British Columbia
INTERMONTANE
OMENICA
FORELAND
eastern limit of cordilleran deformation
Castle Rock
INSULAR
COAST
ST
CC
SL
Northern sites
Southern sites
PACIFIC PLATE
BT
KL
RR
KO
KR
LP
LL
EXPLORER PLATE
JUAN DE FUCA PLATE
ONT.
U.S.A.
MT
KO
136°
132°
128°
124°
120°
116°

Location	Big Timothy		Kostal Lake	Lassie Lake	Lightning Peak				Rayfield River	Summit Lake	West Kettle River			
	BT		KL	LL	LP				FR	SL	KR			
Latitude	52°5'N	52°5'N	52°10'N	49°36'N	49°53'N	49°53'N	49°53'N	49°53'N	51°20'N	54°31'N	49°47'N	49°47'N	49°47'N	49°47'N
Longitude	119°55'W	119°55'W	119°57'W	118°10'W	118°32'W	118°32'W	118°32'W	118°32'W	121°7'W	122°38'W	119°4'W	119°4'W	119°4'W	119°4'W
N° of xenoliths	34		54	5	24				13	33				10
Basalt sample	BT-1	BT-2	KL-1	LL-1	LP-1	LP-2	LP-3	LP-4	RR-1	SL-1	KR-1	KR-2	KR-3	KR-4
Basalt Type	Ol-NEPH	Ol-NEPH	Basanite	Basanite	Ol-NEPH	Ol-NEPH	Ol-NEPH	Ol-NEPH	AOB	Basanite	Basanite	AOB	AOB	Basanite
Age	0.4±0.04 Ma (1)		7750 B.P. (2)	4.8±0.2 Ma (1)	2.5±0.1 Ma (3)				6-10 Ma (4)	26 Ma (4)	1.2Ma (1)			
SiO_2	41.54	42.32	44.29	45.87	41.80	41.86	41.81	41.86	47.07	46.83	47.63	47.30	47.65	43.07
TiO_2	3.220	3.150	2.683	2.640	3.594	3.593	3.045	2.957	2.399	1.629	2.433	2.443	2.386	3.186
Al_2O_3	13.11	13.19	13.68	14.61	13.76	13.72	11.83	11.66	15.58	16.97	16.42	16.30	16.07	14.19
Fe_2O_3	15.21	14.97	13.81	12.55	15.09	15.22	14.17	13.99	13.30	9.49	12.73	12.73	12.63	13.36
MnO	0.250	0.245	0.178	0.176	0.212	0.214	0.199	0.194	0.181	0.160	0.187	0.196	0.173	0.187
MgO	6.99	7.39	9.84	9.55	7.85	8.14	14.17	14.76	7.73	7.85	5.90	5.71	6.32	8.63
CaO	9.66	9.57	9.55	8.59	9.73	9.71	8.52	8.32	8.39	9.44	9.96	10.00	10.16	9.73
Na_2O	4.90	4.74	3.70	3.15	4.66	4.60	3.89	3.57	3.77	3.08	3.96	3.44	3.27	3.79
K_2O	2.96	2.94	1.58	1.85	2.37	2.25	1.90	1.87	1.31	3.37	1.23	1.17	1.14	1.63
P_2O_5	1.430	1.360	0.596	0.494	0.964	0.954	0.804	0.783	0.645	0.641	0.469	0.471	0.450	0.888
BaO	1309	1299	800	630	970	937	819	785	437	4792	481	476	468	722
Co	35	43	50	45	56	49	71	73	42	34	36	42	49	46
Cr_2O_3	198	225	528	493	135	164	984	958	407	274	144	107	244	318
Ni	133	141	232	394	109	115	517	551	159	127	45	41	54	154
Sc	222	207	19	16	18	18	18	20	13	29	13	15	26	20
LOI	0.00	0.00	0.00	0.71	0.00	0.00	0.00	0.00	0.29	0.27	0.00	0.63	0.32	1.62
Total	99.44	100.05	100.07	100.35	100.16	100.39	100.58	100.20	100.77	100.26	100.99	100.46	100.65	100.41

Table I: Location of xenolith sites, number of xenolith sampled, and age and composition of the host basalts. Ol-NEPH = Olivine nephelinite, AOB = Alkali Olivine Basalt (terminology in (Francis and Ludden, 1990)). Ages from: (1) K-Ar method Sun et al. (1991); (2) Metcalfe (1987); (3) K-Ar method by B.N. Church (Brearley and Scarfe, 1984); (4) Bevier (1983). All data in wt % but BaO, Co and Sc in ppm. LOI = loss on ignition.

Although the sub-lithospheric mantle underlying the southern Canadian Cordillera appears to be largely anhydrous, two occurrences of xenolith suites with hydrous minerals have been described (SL (Brearley and Scarfe, 1984), KL (Canil and Scarfe, 1989)). The most recent studies include the determination of oxidation states (Canil et al., 1990), Rb-Sr (Sun et al., 1991) and Sm-Nd (Xue et al., 1990) isotope systematics, and trace element abundances of whole-rock and minerals (Sun and Kerrich, 1995).

For this study, a total of 175 xenoliths were collected from the seven localities. The number of xenoliths from each suite varies between 4 and 40 (Table 1) and reflects, in part, the amount of sampling these suites have previously experienced. Alteration is minor in most suites, except at BT where about one third of the xenoliths show strong iddingtisation of their olivines. Our sampling at this site was biased towards the fresh samples. Most xenoliths are peridotites, consisting of olivine (Ol), orthopyroxene (Opx), clinopyroxene (Cpx), and Spinel (Sp) in decreasing proportions (Fig. 2). Spinel typically comprises less than 5 % of all samples. Xenoliths from Lightning Peak contain traces (less than 5%) of amphibole, although phlogopite has been reported at KL (Canil and Scarfe, 1989), only one of our samples contained phlogopite. A few pyroxenites (less than 60% olivine) were found at BT, KL, KR and SL, and composite xenoliths are sometimes present at BT, SL and KL.

Fig. 2 (next page): Modal composition of the xenolith suites. The modal compositions were determined by calculating the normative mineralogy of Spinel peridotites from their whole-rock composition and distributing the elements among Ol, Opx, Cpx and Sp. The following equations in molar units were used: $Cpx=X=(Ca+Na+K)$; $Sp=Y^{3+}/2=Cr/2+(Al+2Ti-Na)/2$; $Opx=Y/2=((Mg+Fe+Mn)-Sp-Cpx)/2$; $Si^*=Si-2Cpx-2Opx+Ti$; $Ol=-Si^*$; $Opx=Opx-Ol$. ***Conversion to cation units and normalization to 100% gives the modal proportion. The calculations were carried out assuming a temperature of 1000°C and a pressure of 15 kbars. Grey squares = lherzolites, grey triangles = harzburgites, grey diamonds = dunites, black squares = Opx-poor lherzolites, grey circle = KL wehrlites and dunites, grey circle with cross = SL werhlites, black and white square = pyroxenites.***

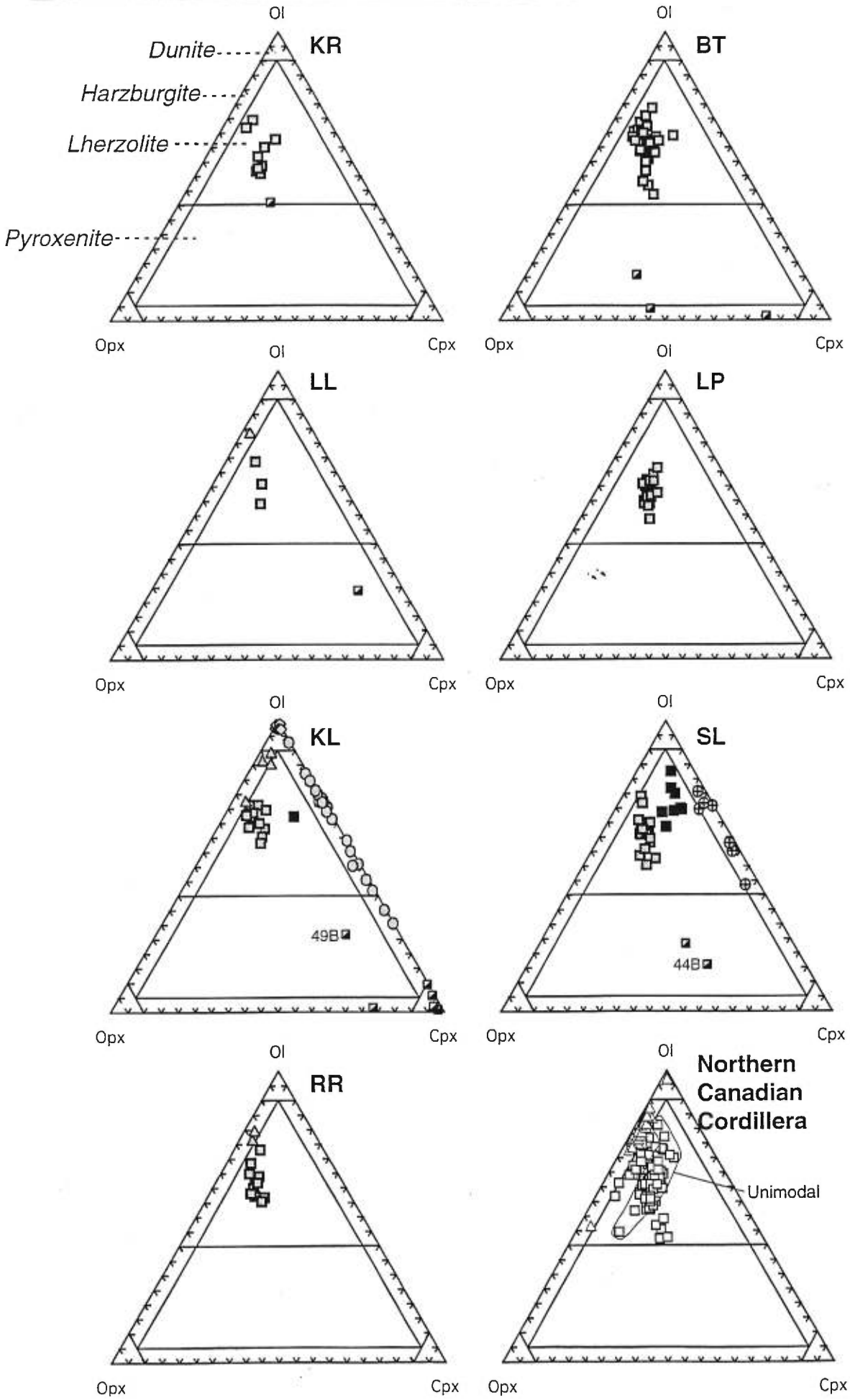
Ol
Dunite
Harzburgite
Lherzolite
Pyroxenite
KR
BT
LL
LP
KL
SL
RR
Northern
Canadian
Cordillera
Unimodal
49B
44B
Opx
Cpx

Most of the peridotites belong to the Type I Cr-diopside defined by Frey and Prinz (1978). Among these, rare harzburgitic xenoliths were found at RR and KL, a few dunites were found at KL, and a few lherzolites from SL and from KL are Opx poor compared to most of the other lherzolites. The dominant xenoliths in all suites are, however, spinel lherzolite, which evedently represent the dominant lithology of the lithospheric mantle beneath the Southern Canadian Cordillera, as well as the Northern Canadian Cordillera (Francis, 1987; Shi et al., 1998).

Wehrlites with less than 5 % Opx are abundant at KL (about 50 % of the xenoliths sampled) and SL (about 25% of the whole suite), the two xenolith sites situated closest to the boundary of ancestral North America (Fig. 1). These wehrlites exhibit cumulate textures similar to these commonly found in the Type II xenoliths of Frey and Prinz ((1978).

The textures of the type I xenoliths are mainly protogranular at LP, RR, KL and SL (according to the scheme of Mercier and Nicolas, 1975), but the xenoliths from SL and RR are finer grained (Ol and Opx < 1mm) than those from LP and KL (1-2 mm). The texture of BT xenoliths range from protogranular to equigranular, but most are protogranular and very coarse grained (2 mm). Porphyroclastic to equigranular textures are found in LL and KR xenoliths, the latter site having moderately coarse grained xenoliths (1 mm). Kink-banding in olivines is common. Spinel grains have shapes and sizes reflecting the texture of the peridotite (Mercier and Nicolas, 1975). For example, spinels in protogranular xenoliths are large, with rounded boundaries, and are associated with Opx, wheareas spinel grains are small and interstitial in the equigranular xenoliths. Clinopyroxene occurs as much smaller grains than Ol and Opx. Type II xenoliths are characterized by large Ol grains or Ol aggregates enclosed in poikilitic augites. The wehrlites are very coarse-grained at KL (2-3 mm), but fined-grained at SL (< 1 mm).

2.3 ANALYTICAL TECHNIQUES

Whole-rock samples were crushed in an alumina mortar and fused with lithium tetraborate. Whole-rock major elements and the trace elements Ba, Sc, Co, Ni and Cr were analysed by X-Ray Fluorescence Spectrometry (XRF) using an α-coefficient technique with a Philips PW 1400 in the Earth and Planetary Sciences Department of McGill University. The analytical precision (in wt%) is estimated to be: Si 0.05, Al 0.03, Cr 0.001, Mg 0.058, Fe 0.01, Mn 0.001, Ni 0.004, Ca 0.01, Na 0.06, K 0.001 and P 0.004, calculated from 20 replicates on one fused disc (Francis, 1987).

The major element compositions of minerals were analysed using a JEOL 8700 Super-probe at McGill University, with an accelerating voltage of 20 kV, a beam current of 20 nA and a beam diameter of 5 μm. All elements were measured with 20 s counting time on peaks and 10 s on background, except for Ni, for which counting times were 50 and 25 s respectively. These results are presented in Table 2, 3, 4, 5, 6 and 7 in which the compositions of each mineral represents the average of 3 spot analyses on different grains. Trace element abundances in whole-rock samples were determined by ICP-MS (Perkin Elmer SCIEX ELAN) analysis of solutions at the CRPG (Nancy, France; Table VIII), after preconcentration on a True Spec resin columns. Reproducibility for most elements is better than 0.1 ppb for most elements as can be seen in two replicates of sample BTX-26 in Table VIII.

2.4 MINERALOGY

Olivines from the Cr-diopside peridotites are homogeneous in composition within individual grains and thin sections. The Cr-diopside lherzolite olivines have Fo contents ranging from 87.4 to 91.3 and are broadly correlated with the modal proportion of olivine (Fig. 3). The olivines of the harzburgites and dunites do not have higher Fo contents than the lherzolites (89.7 to 91.4). Orthopyroxenes are generally homogeneous in composition, but exsolution lamellae of Cpx are present in large Opx crystals at BT and RR. Lherzolite Opx is typically enstatite with Al_2O_3 and CaO varying from 3.4 to 5.3 wt% and 0.5 to 0.8 wt% respectively. Harzburgite Opx have Al_2O_3 and CaO contents of 2 to 3 wt% and 0.8 to 0.9 wt% respectively. The CaO content of Opx at SL is, however, higher (1.1 to 1.2 wt%). Their FeO and Cr_2O_3 contents vary from 2.3 to 3.2 and 0.6 to 1.3 wt% respectively, typical of Cr-diopsides. The FeO content (about 3.5 wt%) of the SL Cpx is higher than that of the Cpx in the other suites (Fig. 4). Spinels have homogeneous compositions within individual xenoliths. The spinels of the harzburgites and dunites are more Cr_2O_3-rich (> 27 wt %) than those of the lherzolites (<24 wt %). The spinels in the harzburgites and dunites are also Fe-rich and Mg-poor compared to the spinels in the lherzolites (Fig. 4). The Cr-diopside peridotites fall in the "OSMA" (olivine-spinel mantle array of Arai ,1994).

Olivine grains from the wehrlite xenoliths are homogeneous in composition within individual samples. Their Fo contents range from 82.4 to 84.2 at KL and from 85.2 and 90.2 at SL. The Fo content of KL olivines correlates positively with the Ol modal proportion (Fig. 3). On the three SL wehrlites, whose Ol have been analysed, two of them have relatively high Fo (> 87) similar to the lowest ones of the Cr-diopside peridodites, and one has a low Fo of 85, similar to those of the KL wehrlites (Fig. 3). The Cpx in the wehrlite suites is black in colour and more Fe rich than the emerald green Cpx of the Cr-diopside peridotites, and is augite in composition.

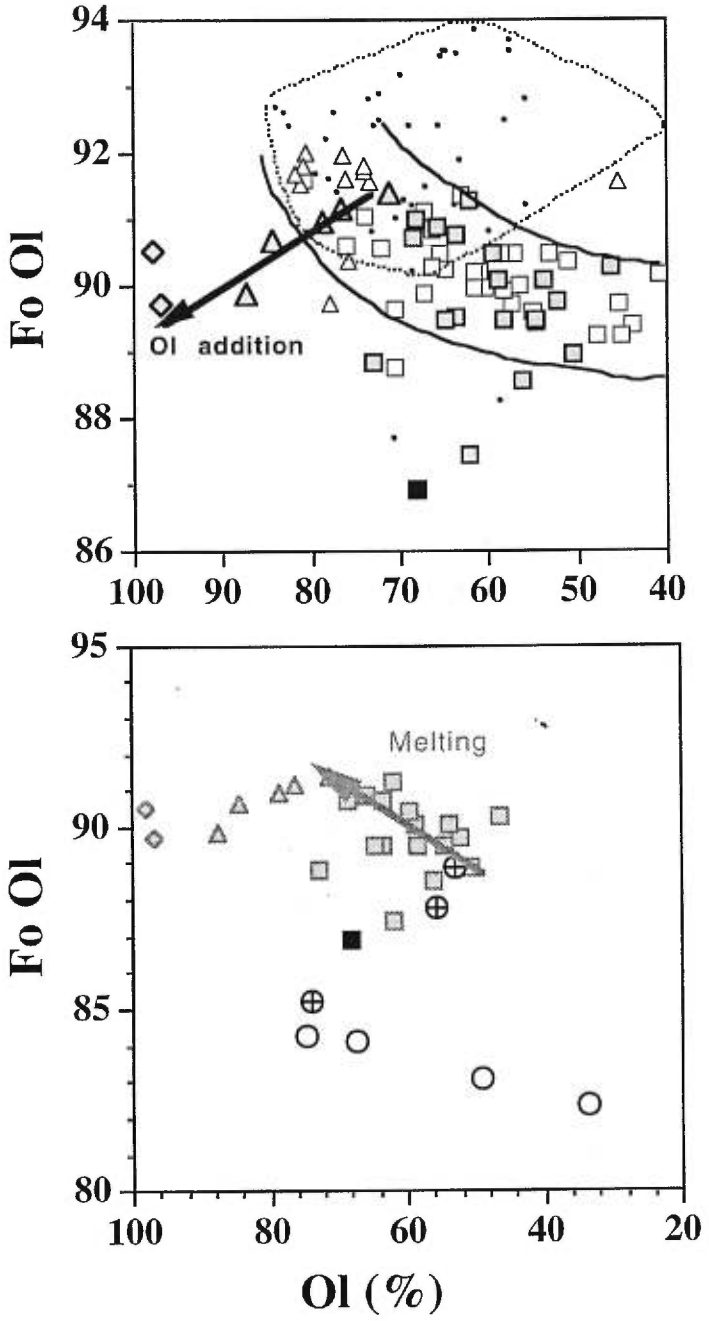

Fig. 3: Forsterite content vs the mode of olivine in xenoliths from the Canadian Cordillera. Black lines define the 'oceanic trend' of Boyd (1989) based on abyssal and ophiolite data, and on which most of the spinel peridotites plot. Dotted line defines the field for Gr-peridotites from cratonic areas (same references as in Fig. 7 and also drawn from Fig. 2 of Boyd, 1989). Northern Canadian Cordillera data are unpublished data from Shi et al. References for Spinel and garnet peridotites as in Fig. 7. Symbols as in Fig. 2 and 7.

The Al_2O_3 content of wehrlite Cpx ranges from 4.8 to 6.2 wt % at KL and from 6.5 to 7.3 wt % at SL. Canil and Scarfe (1989), however, report wehrlite Cpx analyses with Al_2O_3 contents as high as 8.2 wt% at KL. Opx is relatively rare in the wehrlites and is Mg-poor, and Fe, Al and Ca-rich compared to the Opx of the Cr-diopside suites (Fig. 4). Exsolution lamellae of Opx are occasionally observed in the wehrlite Cpx.

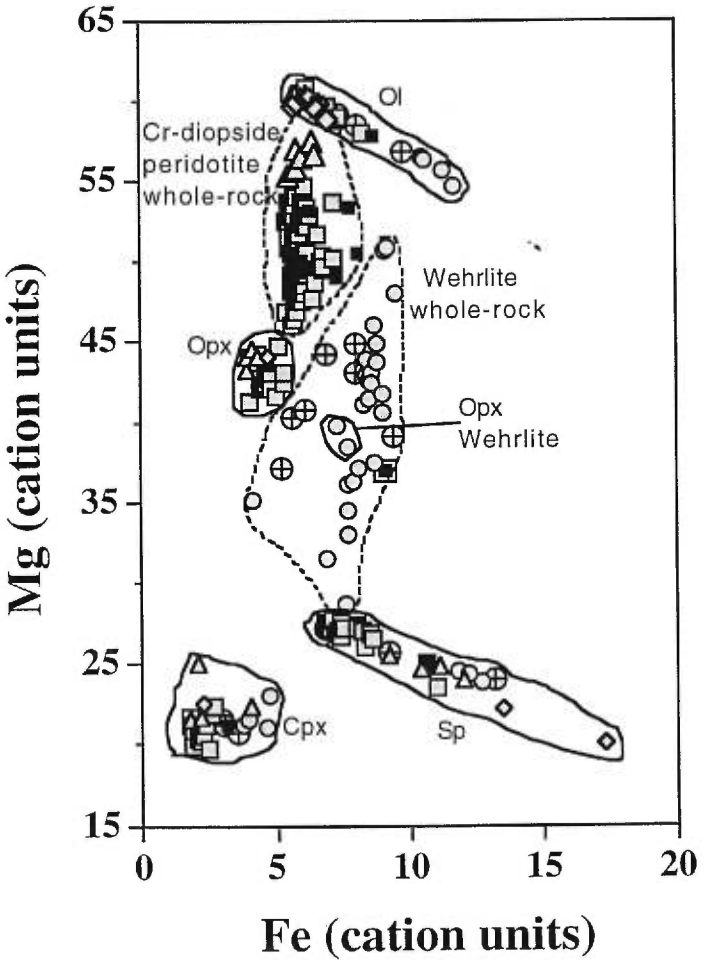

Fig. 4: Mineral and whole-rock compositions in Fe-Mg space in cation units. Symbols as in Fig.2. Black square surrounded by a square is the Opx-poor lherzolite of KL.

2.5 GEOTHERMOMETRY

The most recent and reliable geothermometer for peridotites is that of Brey and Köhler (1990). It is based on the exchange of Ca between Opx and Cpx, but is pressure dependant ($T_{Ca\ in\ Opx}$). As no geobarometer exists for spinel peridotites, the pressure is constrained only by the Spinel stability field (10 to 20 kbar; Green and Hibberson, 1970; O'Neill, 1981). Varying the pressure from 10 to 20 kbar induces a change of about 40 ° C in the calculated temperatures. Other temperature estimates for peridotites can be obtained by the Wells geothermometer (Wells, 1977), which is based on the exchange of Fe^{2+} and Mg^{2+} between Cpx and Opx (T_{Fe-Mg}), and is not pressure dependant. The Wells formulation works for temperatures around 900°C, but underestimates higher temperatures (Brey and Köhler, 1990). Interestingly, using the mineral data given in Tables 4 and 5, the best fit of $T_{Ca\ in\ Opx}$ and T_{Fe-Mg} is obtained using a pressure of 10 kbars in the calculation of $T_{Ca\ in\ Opx}$ (Fig. 5). One sample falls off the 1:1 correlation between the two geothermometers (BTX-23). The majority of the Opx in this sample exhibit Cpx exsolutions, and the microprobe spots may have partly overlapped Cpx lamellae, resulting in higher Ca contents and thus high $T_{Ca\ in\ Opx}$. For most wehrlites, the use of these thermometers was problematic since Opx was scarce or absent.

Most of the calculated temperatures range between 900°C and 1000°C (Fig. 5), which is consistant with previous studies at RR (Canil et al., 1987), KR (Fujii and Scarfe, 1982), LP (Brearley and Scarfe, 1984) and KL (Canil and Scarfe, 1989). SL peridotites (both lherzolites and wehrlites) and KL wehrlites record temperatures slightly greater than 1000°C. Calculated RR peridotites temperatures, on the other hand, are slightly lower than 900°C. However, a temperature range of 860 to 980°C was previously reported for this site (Canil et al., 1987), suggesting that in terms of temperature, RR suite is not different from the other suites of the Canadian Cordillera. The cumulate-textured wehrlite suites appear to yield higher temperatures, but there is no correlation between temperature and

texture in the Cr-diopside suites. The fact that Cr-diopside xenoliths from SL record higher temperatures than most other suites in the Canadian Cordillera suggests that either the geotherm is steeper beneath SL than elsewhere (Brearley et al., 1984), or that the xenoliths originated from a deeper source region (Brearley et al., 1984). Some harzburgites in Northern Canadian Cordillera record similarly high temperatures approximately 100°C hotter than associated lherzolites (Shi et al., 1998). These Northern Canadian Cordillera harzburgites were interpreted to have formed by recent melting of lherzolite, associated with an anomalous zone of low seismic velocity probably related to higher temperatures in the underlying mantle (Shi et al., 1998). The high temperatures of the wehrlite suites (SL and KL) either indicates that these rocks originated at greater depth than the Cr-diopside lherzolites, or that they record higher igneous temperatures while the Cr-diopside suites record lower temperatures of metamorphic origin.

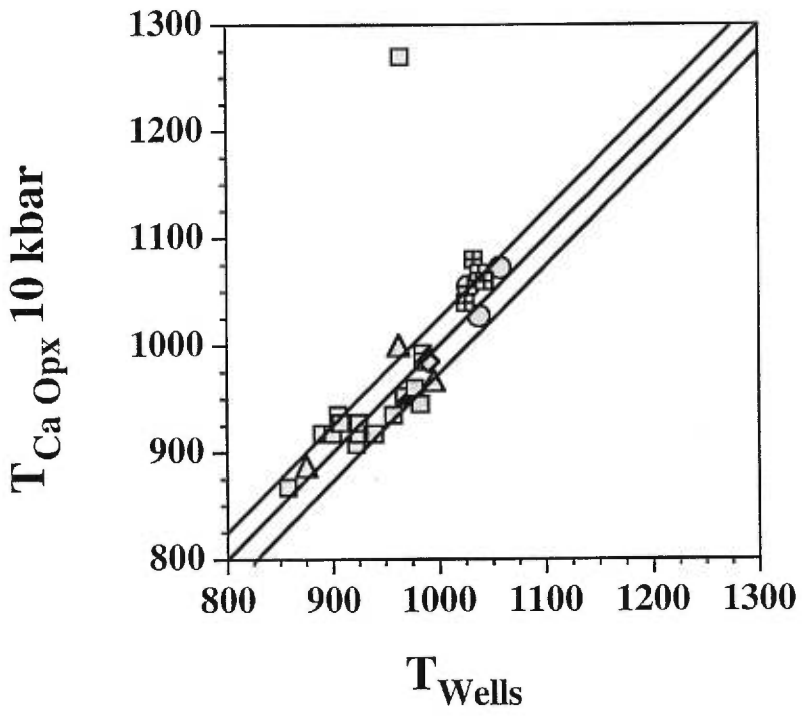

Fig.5: Comparison between two temperature estimates, $T_{Ca\ in\ Opx}$ (Brey and Köhler, 1990) and T_{Wells} (Wells, 1977). Symbols as in Fig. 2. Grey squares with a cross inside = lherzolites from SL.

2.6 WHOLE-ROCK GEOCHEMISTRY

The spectrum of Type I xenoliths varies from Mg-poor lherzolites to Mg-rich lherzolites, harzburgites and dunites. Mg# varies from 88 to 91 and Al_2O_3 from 1.4 to 4.8 wt % for the lherzolites. The distribution of samples within this Al_2O_3 range varies from site to site (Fig. 6), with most KL lherzolites having less than 2.5 wt % Al_2O_3 and most LP and KR lherzolites having relatively high Al_2O_3 contents (2.5-4.5 wt% and 3-5.5.5 wt%). The Al_2O_3 content of RR, KR, BT and SL lherzolites ranges between 2.5 and 3.5 wt %. These ranges in Al_2O_3 can be seen in the modal mineralogy (Fig. 2), with xenoliths ranging from Cpx-rich lherzolites (25 % Cpx) to Ol-rich harzburgites. Dunites (at KL only; Mg# of 89.4 to 91.2) and harzburgites (at KL, RR and LL; Mg# of 89.7 to 91) do not have higher Mg# than the most depleted lherzolites. One harzburgite and three dunites from KL are enriched in FeO compared to most other Cr-diopside peridotites (Fig. 4 and 7).

The wehrlite xenoliths have higher Fe contents and lower Mg contents than the Cr-diopside peridotites (Fig. 4). Their Mg# ranges from 79 to 85 at KL and from 80.6 to 88 at SL. The wehrlite suites from KL have a very wide range of compositions, from Ol-clinopyroxenite, through wehrlite, to dunite (Fig. 2), with MgO contents varying from 27 to 44 wt%. The SL wehrlite suites exhibit a smaller range of compositions, lower Fe, and higher Al contents than the wehrlites at KL (Fig. 2, 4 and 8).

Eight lherzolites from SL and one from KL appear anomalously Opx-poor compared to the other Cr-diopside lherzolites. As such, these Opx-poor lherzolites plot between the "normal" lherzolites and wehrlite xenoliths, with major element compositions that are intermediate between these two (Fig. 8). The Opx-poor lherzolites, whose textures resemble those of Type-I xenoliths, have Mg# between 84 and 89.3, most below 89 (node at 87).

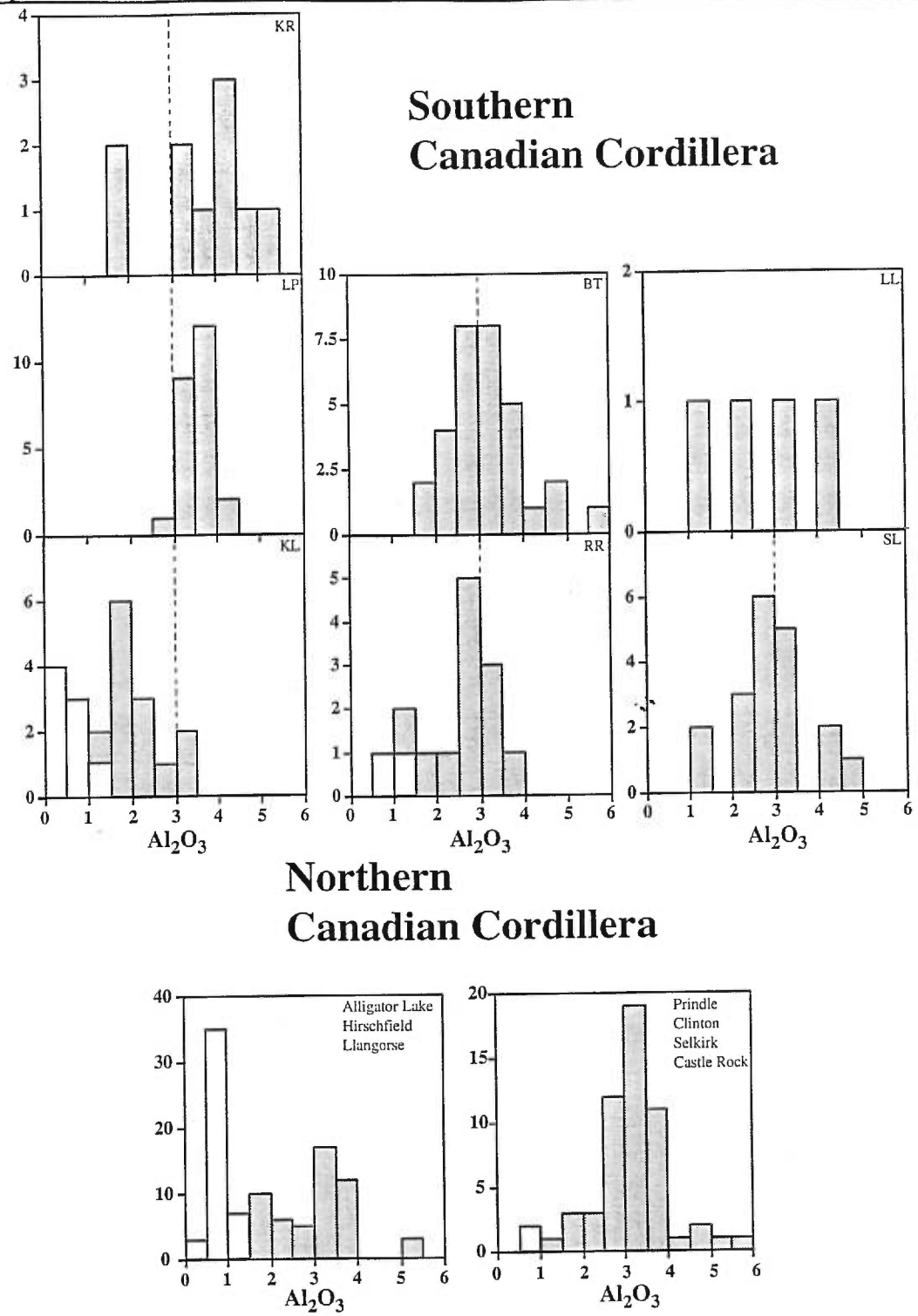

Fig. 6: Histograms of Al_2O_3 for Cr-diopside peridotites from the Canadian Cordillera. In grey, lherzolites, and in white, harzburgites (and dunites in the case of KL). Data for the northern Canadian Cordillera from (Francis, 1987; Shi et al., 1998).

Rare earth element (REE) patterns in the lherzolites vary from light rare earth element (LREE) depleted, through flat, to enriched (Fig.10). Harzburgites from RR have LREE depleted patterns, whereas the harzburgites found at KL and LL have steep REE patterns, enriched in LREE. The middle rare earth elements (MREE) to heavy rare earth elements (HREE) in the lherzolites generally correlate with indexes of fusion such as Al_2O_3, but a broad negative correlation exists between La/Yb ratio and Al_2O_3 content (Fig. 10). Rb and Ba are enriched compared to HREE in all sites. On extended trace element diagrams (Fig. 11), Ta and Nb do not show coherent behavior with Zr, Hf and Ti; SL and BT lherzolites show pronounced negative Zr and Hf anomalies, whereas Nb and Ta define positive, zero or negative anomalies (Fig. 11). Cr-diopside peridotites from BT, LP, SL and KR show negative Zr, Hf and Ti anomalies of varying intensity (Fig. 11). KLX-45, LLX-7 and RRX-10 Cr-diopside peridotites, however, have no or positive Hf and Zr anomalies with no or negative Ti anomalies, and RRX-14 has positive Ti and Zr anomalies, but a negative one for Hf. Finally, LREE enriched harzburgites have positive Zr and Hf anomalies and negative Ti anomalies, while dunites and LREE depleted harzburgite show the opposite characteristics. High field strength elements (HFSE) are difficult to measure because of their low concentrations in mantle rocks (Jochum et al., 1989). In our case, Ta analyses lower than 0.1 times primitive mantle (Sun and McDonough, 1989) are ignored. Moreover, Nb and Ta may reside in secondary oxide phases around spinels (Bodinier et al., 1996), thus complicating the interpretation of whole-rock Ta and Nb data in terms of mantle processes. Only Hf, Zr and Ti are thus here considered reliable for interpretation in terms of mantle processes. Zr and Hf in most Cr-diopside lherzolites broadly correlate with Al_2O_3 (Fig. 12). The three samples that plot off these correlations (LPX-18, KRX-14, LLX-7) are the most LREE enriched ones among the Cr-diopside lherzolites (Fig. 9). The harzburgites that plot off the Zr versus Al_2O_3 and Hf versus Al_2O_3 correlations are also the LREE enriched ones (Fig. 9 and 13).

REE patterns in the SL wehrlites are characterized by LREE enrichment, flat MREE to HREE (Fig. 9), and negative HFSE anomalies (Fig. 11). KL wehrlites, on the other hand, are systematically depleted in HREE compared to MREE, and show a characteristic convex pattern (Fig. 9). KL wehrlites have negative Hf, Zr Nb and Ta anomalies, but no Ti anomalies (Fig. 11).

Fig. 7 (next page): Whole-rock compositions of the Cr-diopside suites of the Southern Canadian Cordillera compared to those of the Northern Canadian Cordillera and other peridotites from around the world. Southern Canadian Cordillera xenoliths: symbols as in Fig. 2. Northern Canadian Cordillera xenoliths: grey squares = lherzolites, grey triangles = harzburgites. Grey plain line = spinel peridotites from around the world. Light black dotted line = garnet peridotites from around the world. Heavy black dotted line = abyssal peridotite field. Straight heavy grey cross = pyrolite composition (Ringwood, 1975), grey X = Primitive Upper Mantle composition (HZPUM; Hart and Zindler, 1986). Spinel peridotites from around the world: Australia (Griffin et al., 1984; O'Reilly and Griffin, 1988; Stolz and Davies, 1988; Chen et al., 1989); Africa (Dupuy et al., 1986); Asia (Song and Frey, 1989; Ionov and Wood, 1992; Ionov et al., 1995); Europe (Dupuy et al., 1987); America (Frey and Prinz, 1978; Boyd, 1981; Roden et al., 1988; Galer and O'Nions, 1989; Brandon and Draper, 1996; Bernstein et al., 1998). Garnet peridotites from South Africa (Boyd, 1981; Nixon et al., 1981; Boyd, 1987; Nixon, 1987; Boyd et al., 1993) and Siberia (Boyd et al., 1997). Abyssal peridotite field drawn from Fig. 6 of Niu et al. (1997).

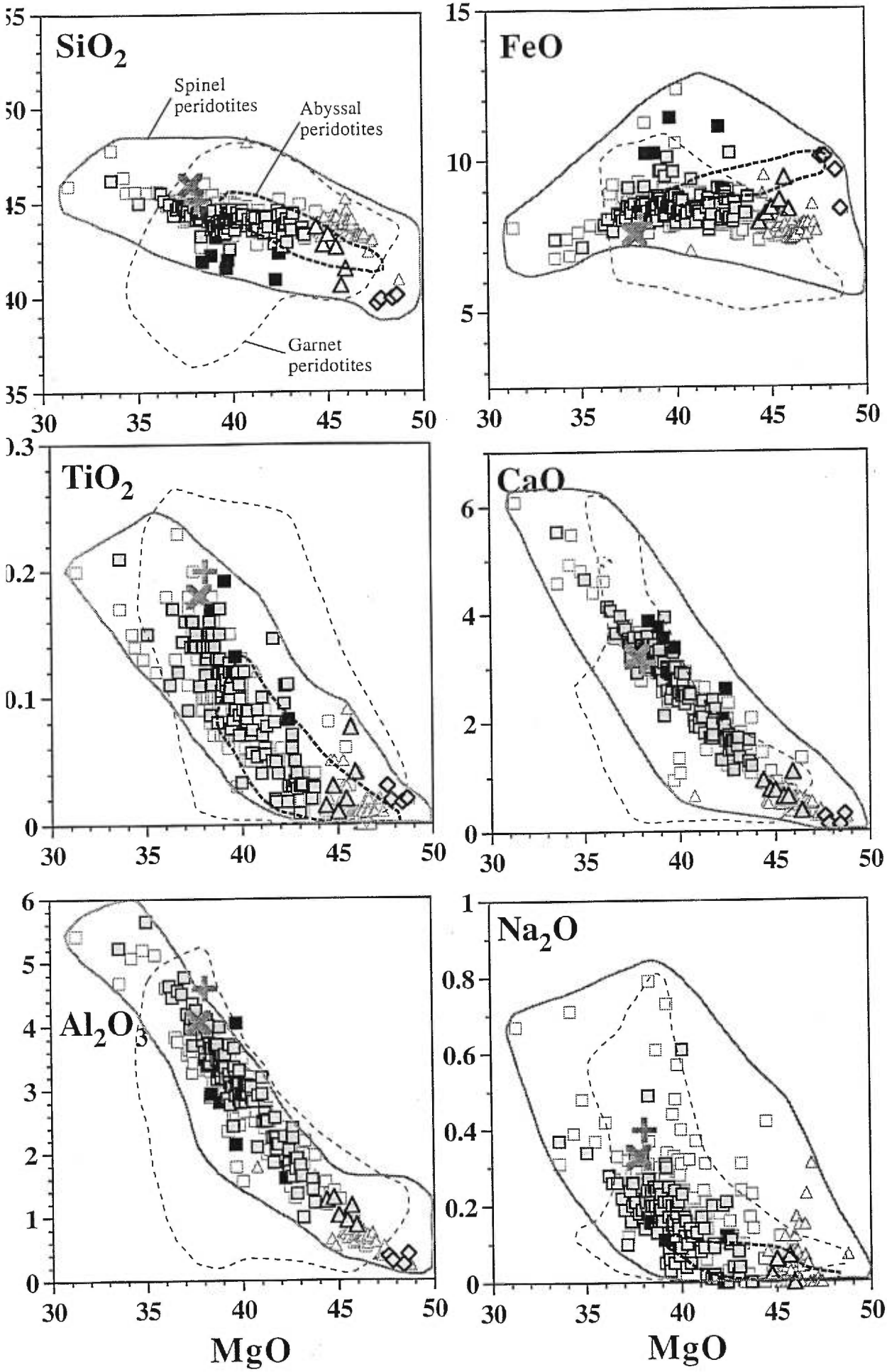
SiO2
Spinel peridotites
Abyssal peridotites
Garnet peridotites
FeO
TiO2
CaO
Al2O3
Na2O
MgO
MgO

	KLX-67 Dunite	KLX-59 Dunite	RRX-21 Harzburgite	KLX-47 Harzburgite	KLX-62 Harzburgite	KLX-57 Harzburgite	LLX-1 Harzburgite	KLX-45 Lherzolite	KLX-49A Lherzolite	KLX-70 Lherzolite	BTX-16 Lherzolite	BTX-23 Lherzolite	BTX-26 Lherzolite	LLX-14 Lherzolite
Cpx	0.69	0.64	3.1	4.49	5.25	3.41	2.695	9.42	15.25	11.6	12.02	10.66	18.36	17.22
Opx	1.34	0.49	16.88	22.86	8.88	7.49	18.767	26.27	25.56	18.22	25.71	21.34	31.5	27.08
Ol	97.04	98	78.72	71.13	84.42	87.43	76.494	62.09	56.29	68.41	59.58	65.78	46.44	52.3
Spi	0.94	0.88	1.3	1.52	1.45	1.67	2.044	2.22	2.89	1.78	2.68	2.22	3.71	3.39
SiO2	39.890	39.920	42.660	43.730	41.510	40.630	42.790	44.290	44.330	43.400	44.320	43.720	44.960	44.360
TiO2	0.019	0.017	0.020	0.015	0.041	0.076	0.030	0.020	0.119	0.146	0.070	0.040	0.120	0.140
Al2O3	0.300	0.240	0.940	1.260	0.860	1.170	1.300	2.260	3.290	1.850	3.050	2.140	4.560	4.060
FeOt	10.100	9.630	8.670	7.950	8.360	9.400	8.230	7.690	8.570	8.670	8.150	8.190	7.660	8.380
MnO	0.139	0.136	0.130	0.130	0.126	0.142	0.130	0.130	0.138	0.139	0.130	0.140	0.130	0.140
MgO	47.790	48.370	45.430	44.370	45.920	45.680	44.740	41.720	38.810	41.650	40.460	41.880	36.670	37.590
CaO	0.120	0.110	0.640	0.940	1.090	0.640	0.770	1.970	3.080	2.280	2.430	2.240	3.640	3.440
Na2O						0.070	0.020	0.020	0.160	0.200	0.140	0.010	0.260	0.210
K2O	0.030		0.010	0.010	0.030	0.080	0.070	0.010	0.010	0.020	0.020	0.010	0.050	0.110
P2O5	0.016	0.017	0.000	0.010	0.033	0.051	0.010	0.010	0.010	0.021			0.010	0.010
NiO	0.410	0.380	0.320	0.330	0.450	0.460	0.340	0.310	0.290	0.310	0.290	0.310	0.260	0.270
Cr2O5	0.382	0.409	0.340	0.399	0.789	0.802	0.670	0.393	0.438	0.421	0.410	0.490	0.500	0.410
Ba					34	63					10			
Co	163	146	132	120	139	143	127	119	114	117	104	119	102	102
Sc				30				31	11		17		86	15
LOI														0.09
Total	100.15	100.09	100.03	99.52	100.06	100.17	99.97	99.24	100.13	100.01	100.34	100.02	99.14	100.1
CATION UNITS														
	KLX-67	KLX-59	RRX-21	KLX-47	KLX-62	KLX-57	LLX-1	KLX-45	KLX-49A	KLX-70	BTX-16	BTX-23	BTX-26	LLX-14
Si	33.000	32.923	35.522	36.521	34.497	33.825	35.718	37.396	37.680	36.592	37.348	36.819	38.529	37.850
Ti	0.012	0.011	0.013	0.009	0.026	0.048	0.019	0.013	0.076	0.093	0.044	0.025	0.077	0.090
Al	0.293	0.233	0.923	1.241	0.843	1.148	1.279	2.250	3.297	1.839	3.030	2.125	4.607	4.084
Fe	6.988	6.642	6.037	5.552	5.810	6.545	5.745	5.430	6.092	6.113	5.743	5.768	5.490	5.980
Mn	0.097	0.095	0.092	0.092	0.089	0.100	0.092	0.093	0.099	0.099	0.093	0.100	0.094	0.101
Mg	58.938	59.469	56.394	55.241	56.891	56.693	55.674	52.513	49.177	52.350	50.828	52.579	46.848	47.814
Ca	0.106	0.097	0.571	0.841	0.971	0.571	0.689	1.782	2.805	2.060	2.194	2.021	3.342	3.145
Na	0.000	0.000	0.000	0.000	0.000	0.113	0.032	0.033	0.264	0.327	0.229	0.016	0.432	0.347
K	0.032	0.000	0.011	0.011	0.032	0.085	0.075	0.011	0.011	0.022	0.022	0.011	0.055	0.120
P	0.011	0.012	0.000	0.007	0.023	0.036	0.007	0.007	0.007	0.015	0.000	0.000	0.007	0.007
Ni	0.273	0.252	0.214	0.222	0.301	0.308	0.228	0.211	0.198	0.210	0.197	0.210	0.179	0.185
Cr	0.250	0.267	0.224	0.263	0.518	0.528	0.442	0.262	0.294	0.281	0.273	0.326	0.339	0.277
Total	100	100	100	100	100	100	100	100	100	100	100	100	100	100
O2-	133.284	133.201	136.103	137.287	135.222	134.666	136.555	138.653	139.425	137.592	138.919	138.056	140.847	139.897
Mg#	0.8940	0.9000	0.9030	0.9090	0.9070	0.8970	0.9070	0.9060	0.8900	0.8950	0.8990	0.9010	0.8950	0.8890

Table II (1): Representative whole-rock analyses of peridotites from the southern Canadian Cordillera. The whole data set is available on request. Mode data in %. Silicate oxydes in wt%. Ba, Co, Sc in ppm.

	KRX-11 Lherzolite	KRX-13 Lherzolite	KRX-14 Lherzolite	LPX-11 Lherzolite	LPX-16 Lherzolite	LPX-18 Lherzolite	RRX-10 Lherzolite	RRX-18 Lherzolite	SLX-4 Lherzolite	SLX-30 Lherzolite	SLX-41 Lherzolite	KLX-53 Dunite	KLX-65 Dunite	KLX-7 Wehrlite
Cpx	7.69	17.05	15.35	16.67	14.08	14.11	8.66	16.56	9.7	5.39	13.36	1.47	2.14	29.55
Opx	22.32	28.69	23.37	25.25	20.87	18.89	25.52	26.53	24.52	20.03	24.75	0.41	0.62	0.77
Ol	68.15	50.64	58.35	54.76	62.12	64.88	63.64	53.69	63.58	72.88	58.95	97.18	96.17	67.38
Spi	1.84	3.62	2.93	3.31	2.93	2.12	2.19	3.22	2.21	1.7	2.94	0.94	1.07	2.3
														1053.93
SiO2	43.820	44.700	43.870	44.240	43.190	43.560	44.610	44.490	43.770	42.910	43.910	39.030	39.280	41.770
TiO2	0.030	0.160	0.170	0.140	0.120	0.120	0.056	0.086	0.053	0.028	0.090	0.037	0.046	0.310
Al2O3	1.810	4.360	3.450	3.920	3.360	3.060	2.870	3.730	2.100	1.360	3.200	0.190	0.330	2.300
FeOt	8.110	8.490	8.780	8.500	9.630	8.750	7.910	8.100	9.360	10.230	8.500	14.410	14.240	12.850
MnO	0.130	0.140	0.140	0.150	0.150	0.140	0.130	0.132	0.155	0.159	0.137	0.179	0.182	0.180
MgO	43.020	37.460	38.860	38.230	39.110	40.110	40.500	38.340	40.780	42.840	39.640	44.360	44.410	35.000
CaO	1.560	3.430	3.050	3.360	2.770	2.490	2.550	3.350	2.030	1.120	2.760	0.280	0.420	5.820
Na2O	0.080	0.200	0.210	0.180	0.210	0.610	0.050	0.170			0.050			0.260
K2O	0.010	0.020	0.200	0.080	0.050	0.200	0.010	0.010	0.050	0.030	0.110	0.010	0.010	0.030
P2O5	0.000	0.010	0.020	0.010	0.010	0.010	0.004	0.003	0.003	0.003	0.005	0.012	0.014	0.020
NiO	0.320	0.260	0.280	0.280	0.280	0.280	0.290	0.270	0.310	0.300	0.300	0.300	0.290	0.190
Cr2O5	0.420	0.420	0.360	0.400	0.380	0.290	0.438	0.523	0.357	0.352	0.406	0.049	0.127	0.350
Ba			32										18	25
Co	118	96	110	114	111	113	117	105	117	125	116	178	175	138
Sc	10	15	18	12	15		23	10			15			15
LOI			0.27				0.180	0.120	0.190	0.020	0.030			
Total	100.15	100.54	100.59	100.39	100.28	100.55	100.43	100.18	100.13	100.41	100.04	100.27	100.79	100.48
CATION UNITS														
	KRX-11	KRX-13	KRX-14	LPX-11	LPX-16	LPX-18	RRX-10	RRX-18	SLX-4	SLX-30	SLX-41	KLX-53	KLX-65	KLX-7
Si	36.691	37.990	37.205	37.557	36.695	36.587	37.626	37.845	37.153	36.105	37.265	33.015	33.070	36.317
Ti	0.019	0.102	0.108	0.089	0.077	0.076	0.036	0.055	0.034	0.018	0.057	0.024	0.029	0.203
Al	1.787	4.369	3.450	3.924	3.366	3.030	2.854	3.741	2.102	1.349	3.202	0.189	0.328	2.358
Fe	5.679	6.034	6.227	6.035	6.842	6.146	5.579	5.762	6.644	7.198	6.033	10.194	10.026	9.343
Mn	0.092	0.101	0.101	0.108	0.108	0.100	0.093	0.095	0.111	0.113	0.098	0.128	0.130	0.133
Mg	53.699	47.462	49.130	48.382	49.536	50.223	50.924	48.619	51.603	53.736	50.152	55.939	55.738	45.365
Ca	1.399	3.123	2.771	3.056	2.522	2.241	2.304	3.053	1.846	1.010	2.510	0.254	0.379	5.422
Na	0.130	0.330	0.345	0.296	0.346	0.993	0.082	0.280	0.000	0.000	0.082	0.000	0.000	0.438
K	0.011	0.022	0.216	0.087	0.054	0.214	0.011	0.011	0.054	0.032	0.119	0.011	0.011	0.033
P	0.000	0.007	0.014	0.007	0.007	0.007	0.003	0.002	0.002	0.002	0.004	0.009	0.010	0.015
Ni	0.216	0.178	0.191	0.191	0.191	0.189	0.197	0.185	0.212	0.203	0.205	0.204	0.196	0.133
Cr	0.278	0.282	0.241	0.268	0.255	0.193	0.292	0.351	0.240	0.234	0.273	0.033	0.085	0.241
Total	100	100	100	100	100	100	100	100	100	100	100	100	100	100
O2-	137.672	140.253	138.899	139.561	138.393	137.681	139.192	139.804	138.333	136.901	138.965	133.157	133.314	137.605
Mg#	0.9040	0.8870	0.8870	0.8890	0.8790	0.8910	0.9010	0.8940	0.8860	0.8820	0.8930	0.8460	0.8480	0.8290

Table II (2): Representative whole-rock analyses of peridotites from the southern Canadian Cordillera. The whole data set is available on request. Mode data in %. Silicate oxydes in wt%. Ba, Co, Sc in ppm.

	KLX-11 Wehrlite	KLX-13 Wehrlite	KLX-17 Wehrlite	SLX-8 Wehrlite	SLX-24 Wehrlite	SLX-39 Wehrlite	SLX-14 Opx-poor Lherz	SLX-51 Opx-poor Lherz	SLX-55 Opx-poor Lherz	SLX-56 Opx-poor Lherz	KLX-51 Opx-poor Lherz
Cpx	45.74	62.14	22.56	38.86	40.44	21.21	18.8	10	17.02	17.4	20.74
Opx	2.1	0.41	0.72	1.55	2.38	2.32	10.51	7.01	12.68	17.62	11.19
Ol	49.12	33.74	74.72	55.76	52.91	74.06	68.06	81.07	66.81	61.85	66.13
Spi	3.04	3.71	2	3.83	4.26	2.41	2.64	1.92	3.48	3.13	1.93
	1100.23				1080.98						
SiO2	43.640	45.170	41.140	42.650	42.610	41.050	42.230	40.950	41.990	43.190	42.640
TiO2	0.480	0.570	0.260	0.313	0.324	0.178	0.150	0.109	0.119	0.192	0.163
Al2O3	3.540	4.610	1.790	4.560	5.340	2.330	2.810	1.610	4.050	3.560	1.580
FeOt	11.640	10.030	13.420	9.040	8.240	12.090	10.230	11.100	8.490	8.740	12.550
MnO	0.170	0.160	0.180	0.166	0.143	0.193	0.170	0.176	0.137	0.138	0.171
MgO	29.890	25.380	37.300	33.600	33.010	38.070	38.840	42.250	39.730	39.130	36.980
CaO	9.060	12.260	4.480	7.770	7.990	4.230	3.760	2.060	3.370	3.550	4.250
Na2O	0.330	0.480	0.170	0.250	0.340	0.140	0.170	0.000	0.200	0.110	0.030
K2O	0.030	0.020	0.020	0.070	0.080	0.040	0.130	0.100	0.280	0.110	0.010
P2O5	0.020	0.020	0.020	0.017	0.021	0.065	0.010	0.021	0.009	0.018	0.015
NiO	0.110	0.110	0.170	0.230	0.230	0.230	0.270	0.280	0.350	0.300	0.240
Cr2O5	0.250	0.480	0.270	0.397	0.356	0.339	0.410	0.266	0.510	0.349	0.224
Ba	53	69	36	42	44	31	24	22	21	35	43
Co	129	98	141	104	105	122	111	127	112	113	147
Sc	23	29	16	27	29	15	13		10	11	14
LOI					0.55	0.06	0.09		0.17	0.12	
Total	100.46	100.4	100.69	100.04	100.12	100.33	100.37	100.11	100.28	100.43	100.22
CATION UNITS											KLX-51
	KLX-11	KLX-13	KLX-17	SLX-8	SLX-24	SLX-39	SLX-14	SLX-51	SLX-55	SLX-56	
Si	38.517	40.341	35.481	36.938	36.995	35.290	35.992	34.664	35.480	36.608	36.949
Ti	0.319	0.383	0.169	0.204	0.212	0.115	0.096	0.069	0.076	0.122	0.106
Al	3.684	4.854	1.820	4.656	5.466	2.362	2.824	1.607	4.035	3.558	1.614
Fe	8.592	7.491	9.679	6.548	5.983	8.692	7.292	7.858	5.999	6.195	9.095
Mn	0.127	0.121	0.131	0.122	0.105	0.141	0.123	0.126	0.098	0.099	0.126
Mg	39.328	33.791	47.957	43.381	42.725	48.790	49.349	53.316	50.046	49.443	47.771
Ca	8.568	11.731	4.140	7.210	7.432	3.896	3.433	1.868	3.051	3.224	3.946
Na	0.565	0.831	0.284	0.420	0.572	0.233	0.281	0.000	0.328	0.181	0.050
K	0.034	0.023	0.022	0.077	0.089	0.044	0.141	0.108	0.302	0.119	0.011
P	0.015	0.015	0.015	0.012	0.015	0.047	0.007	0.015	0.006	0.013	0.011
Ni	0.078	0.079	0.118	0.160	0.161	0.159	0.185	0.191	0.238	0.205	0.167
Cr	0.174	0.339	0.184	0.272	0.245	0.230	0.276	0.178	0.341	0.234	0.153
Total	100	100	100	100	100	100	100	100	100	100	100
O2-	140.488	142.916	136.521	139.376	139.754	136.634	137.438	135.594	137.439	138.495	137.93
Mg#	0.8210	0.8190	0.8320	0.8690	0.8770	0.8490	0.8710	0.8710	0.8930	0.8890	0.8400

Table II (3): Representative whole-rock analyses of peridotites from the southern Canadian Cordillera. The whole data set is available on request. Mode data in %. Silicate oxydes in wt%. Ba, Co, Sc in ppm.

	KLX-67 Ol	KLX-59 gOl	RRX-21 Ol	KLX-47 Ol	KLX-62 Ol	KLX-57 Ol	LLX-1 Ol	KLX-45 Ol	KLX-49 Ol bas	KLX-70 Ol	BTX-16 Ol	BTX-23 Ol	BTX-26 Ol	LLX-14 Ol	KRX-11 Ol	KRX-13 Ol	KRX-14 Ol
SiO2	39.96	40.59	40.82	41.12	40.25	40.31	40.77	40.98	39.90	40.88	40.95	41.02	40.88	40.82	40.63	40.34	40.36
TiO2	0.02	0.00	0.00	0.00	0.01	0.00	0.00	0.00	0.00	0.00	0.00	0.00	0.00	0.00	0.00	0.00	0.00
Al2O3	0.02	0.02	0.01	0.02	0.02	0.02	0.00	0.02	0.02	0.02	0.01	0.01	0.02	0.02	0.00	0.02	0.01
FeOt	9.92	9.32	8.81	8.39	9.12	9.75	8.55	8.53	11.24	9.03	9.27	8.93	9.50	9.92	8.71	10.61	10.09
MnO	0.10	0.21	0.12	0.11	0.13	0.16	0.13	0.12	0.15	0.13	0.13	0.13	0.13	0.16	0.12	0.15	0.15
MgO	48.55	49.70	49.61	49.79	49.67	48.57	49.43	50.02	48.68	49.35	49.35	49.63	49.31	48.71	49.24	47.73	48.06
CaO	0.06	0.07	0.04	0.05	0.08	0.05	0.08	0.09	0.08	0.05	0.04	0.04	0.06	0.12	0.05	0.10	0.09
Na2O	0.01	0.01	0.00	0.02	0.01	0.01	0.00	0.01	0.00	0.01	0.00	0.00	0.01	0.01	0.00	0.01	0.01
NiO	0.33	0.35	0.31	0.33	0.44	0.38	0.30	0.32	0.35	0.30	0.30	0.30	0.29	0.26	0.31	0.29	0.29
Cr2O5	0.01	0.05	0.01	0.07	0.03	0.02	0.02	0.01	0.01	0.01	0.01	0.00	0.00	0.03	0.02	0.01	0.02
Total	98.97	100.31	99.73	99.90	99.75	99.26	99.28	100.10	100.42	99.78	100.05	100.07	100.20	100.05	99.07	99.25	99.07
CATION UNITS																	
	KLX-67 Ol	KLX-59 gOl	RRX-21 Ol	KLX-47 Ol	KLX-62 Ol	KLX-57 Ol	LLX-1 Ol	KLX-45 Ol	KLX-49 Ol bas	KLX-70 Ol	BTX-16 Ol	BTX-23 Ol	BTX-26 Ol	LLX-14 Ol	KRX-11 Ol	KRX-13 Ol	KRX-14 Ol
Si	0.990	0.989	0.999	1.004	0.985	0.996	1.002	0.998	0.978	1.001	1.001	1.001	0.999	1.002	1.001	1.001	1.001
Ti	0.000	0.000	0.000	0.000	0.000	0.000	0.000	0.000	0.000	0.000	0.000	0.000	0.000	0.000	0.000	0.000	0.000
Al	0.000	0.000	0.000	0.000	0.001	0.000	0.000	0.001	0.001	0.001	0.000	0.000	0.000	0.001	0.000	0.000	0.000
Fe	0.206	0.190	0.180	0.171	0.187	0.202	0.176	0.174	0.230	0.185	0.190	0.182	0.194	0.204	0.179	0.220	0.209
Mn	0.002	0.004	0.002	0.002	0.003	0.003	0.003	0.002	0.003	0.003	0.003	0.003	0.003	0.003	0.002	0.003	0.003
Mg	1.793	1.806	1.810	1.812	1.813	1.789	1.811	1.816	1.779	1.802	1.799	1.806	1.796	1.782	1.809	1.766	1.777
Ca	0.002	0.002	0.001	0.001	0.002	0.001	0.002	0.002	0.002	0.001	0.001	0.001	0.002	0.003	0.001	0.003	0.002
Na	0.000	0.000	0.000	0.001	0.000	0.000	0.000	0.000	0.000	0.000	0.000	0.000	0.000	0.001	0.000	0.000	0.001
Ni	0.007	0.007	0.006	0.007	0.009	0.007	0.006	0.006	0.007	0.006	0.006	0.006	0.006	0.005	0.006	0.006	0.006
Cr	0.000	0.001	0.000	0.001	0.001	0.000	0.000	0.000	0.000	0.000	0.000	0.000	0.000	0.000	0.000	0.000	0.000
Total	3.000	3.000	3.000	3.000	3.000	3.000	3.000	3.000	3.000	3.000	3.000	3.000	3.000	3.000	3.000	3.000	3.000
O2-	3.990	3.990	4.000	4.000	3.990	4.000	4.000	4.000	3.980	4.000	4.000	4.000	4.000	4.000	4.000	4.000	4.000
Mg#	0.8972	0.9048	0.9094	0.9137	0.9067	0.8987	0.9116	0.9127	0.8853	0.9069	0.9047	0.9083	0.9025	0.8974	0.9098	0.8892	0.8947

Table III (1): Olivine analyses. Silicate oxydes in wt%

	LPX-11 Ol	LPX-16 Ol	LPX-18 Ol	RRX-10 Ol	RRX-18 Ol	SLX-4 Ol	SLX-30 Ol	SLX-41 Ol	SLX-14 Ol	KLX-7Ol	KLX-11Ol	KLX-13Ol	KLX-17Ol	SLX-8Ol	SLX-24Ol	SLX-39Ol	SLX-44BOl
SiO2	40.74	40.50	40.78	39.67	40.54	40.26	40.28	40.52	39.79	39.25	38.98	39.37	39.04	40.07	40.28	39.50	40.37
TiO2	0.01	0.00	0.00	0.00	0.00	0.00	0.01	0.00	0.01	0.01	0.00	0.01	0.00	0.03	0.01	0.01	0.01
Al2O3	0.00	0.00	0.00	0.01	0.00	0.03	0.03	0.02	0.03	0.03	0.03	0.04	0.02	0.04	0.02	0.01	0.03
FeOt	10.14	12.05	10.11	9.02	9.64	10.23	10.84	9.68	12.55	15.21	16.13	16.49	15.14	11.84	10.78	14.11	9.55
MnO	0.15	0.16	0.15	0.12	0.14	0.15	0.17	0.13	0.14	0.20	0.20	0.20	0.20	0.16	0.17	0.21	0.14
MgO	48.26	47.07	48.30	49.56	48.91	48.83	48.19	49.11	46.70	45.31	44.54	43.23	45.50	47.61	48.40	45.69	49.08
CaO	0.07	0.05	0.06	0.04	0.04	0.10	0.10	0.12	0.16	0.10	0.10	0.09	0.10	0.13	0.13	0.20	0.11
Na2O	0.01	0.00	0.01	0.00	0.01	0.01	0.01	0.01	0.01	0.00	0.00	0.01	0.00	0.01	0.00	0.01	0.01
NiO	0.28	0.28	0.28	0.31	0.30	0.30	0.34	0.30	0.30	0.23	0.16	0.14	0.19	0.28	0.23	0.20	0.29
Cr2O5	0.01	0.00	0.00	0.01	0.01	0.01	0.03	0.02	0.00	0.01	0.00	0.01	0.01	0.01	0.02	0.01	0.03
Total	99.65	100.12	99.69	98.75	99.58	99.92	100.00	99.92	99.69	100.34	100.15	99.57	100.21	100.17	100.04		99.60
CATION UNITS																	
	LPX-11 Ol	LPX-16 Ol	LPX-18 Ol	RRX-10 Ol	RRX-18 Ol	SLX-4 Ol	SLX-30 Ol	SLX-41 Ol	SLX-14 Ol	KLX-7Ol	KLX-11Ol	KLX-13Ol	KLX-17Ol	SLX-8Ol	SLX-24Ol	SLX-39Ol	SLX-44BOl
Si	1.005	1.003	1.006	0.979	0.997	0.989	0.992	0.994	0.991	0.981	0.980	1.000	0.976	0.989	0.991	0.987	0.992
Ti	0.000	0.000	0.000	0.000	0.000	0.000	0.000	0.000	0.000	0.000	0.000	0.000	0.000	0.001	0.000	0.000	0.000
Al	0.000	0.000	0.000	0.000	0.000	0.001	0.001	0.001	0.001	0.001	0.001	0.001	0.001	0.001	0.001	0.000	0.001
Fe	0.209	0.250	0.209	0.186	0.198	0.210	0.223	0.198	0.261	0.318	0.339	0.350	0.317	0.244	0.222	0.295	0.196
Mn	0.003	0.003	0.003	0.003	0.003	0.003	0.004	0.003	0.003	0.004	0.004	0.004	0.004	0.003	0.004	0.004	0.003
Mg	1.775	1.737	1.775	1.824	1.794	1.788	1.770	1.795	1.733	1.688	1.670	1.638	1.696	1.752	1.775	1.703	1.798
Ca	0.002	0.001	0.001	0.001	0.001	0.003	0.003	0.003	0.004	0.003	0.003	0.002	0.003	0.003	0.003	0.005	0.003
Na	0.000	0.000	0.000	0.000	0.000	0.000	0.000	0.000	0.001	0.000	0.000	0.001	0.000	0.000	0.000	0.001	0.000
Ni	0.006	0.006	0.005	0.006	0.006	0.006	0.007	0.006	0.006	0.005	0.003	0.003	0.004	0.006	0.005	0.004	0.006
Cr	0.000	0.000	0.000	0.000	0.000	0.000	0.001	0.000	0.000	0.000	0.000	0.000	0.000	0.000	0.000	0.000	0.001
Total	3.000	3.000	3.000	3.000	3.000	3.000	3.000	3.000	3.000	3.000	3.000	3.000	3.000	3.000	3.000	3.000	3.000
O2-	4.000	4.000	4.010	3.980	4.000	3.990	3.990	3.990	3.990	3.980	3.980	3.980	4.000	3.980	3.990	3.990	3.990
Mg#	0.8945	0.8744	0.8949	0.9074	0.9004	0.8948	0.8879	0.9004	0.8690	0.8415	0.8311	0.8238	0.8427	0.8776	0.8889	0.8523	0.9016

Table III (2): Olivine analyses. Silicate oxydes in wt%

	KLX-67 Opx	RRX-21 Opx	KLX-47 Opx	KLX62 Opx	LLX-1 Opx	KLX-45 Opx	KLX-49A Opx	KLX-70 Opx	BTX-16 Opx	BTX-23 Opx	BTX-26 Opx	LLX-14 Opx	KRX-11 Opx
SiO2	55.71	55.24	56.28	55.43	55.98	54.89	54.77	54.74	55.11	54.68	54.87	54.16	55.38
TiO2	0.02	0.03	0.01	0.10	0.03	0.01	0.08	0.08	0.07	0.06	0.11	0.12	0.04
Al2O3	1.25	2.64	2.94	2.00	2.64	3.76	4.19	3.50	4.48	4.71	5.16	4.99	3.35
FeOt	6.46	5.80	5.53	6.11	5.55	5.65	6.51	5.96	6.26	5.58	6.18	6.45	5.70
MnO	0.09	0.13	0.13	0.22	0.13	0.13	0.14	0.14	0.12	0.13	0.13	0.14	0.14
MgO	33.92	34.79	33.89	34.36	34.58	34.27	33.61	34.05	33.48	32.13	32.99	33.04	34.46
CaO	0.84	0.53	0.85	0.89	0.79	0.64	0.64	0.70	0.65	2.26	0.77	0.83	0.59
Na2O	0.07	0.06	0.13	0.14	0.03	0.09	0.08	0.11	0.08	0.16	0.12	0.11	0.04
K2O	0.00	0.00	0.01	0.00	0.00	0.00	0.00	0.00	0.00	0.01	0.00	0.00	0.00
P2O5	0.02	0.00	0.02	0.00	0.01	0.01	0.00	0.01	0.00	0.01	0.01	0.01	0.01
NiO	0.07	0.08	0.07	0.11	0.09	0.09	0.09	0.10	0.07	0.08	0.09	0.09	0.08
Cr2O5	0.38	0.44	0.60	0.52	0.55	0.37	0.31	0.49	0.36	0.69	0.36	0.31	0.42
Total	98.84	99.74	100.44	99.89	100.39	99.90	100.41	99.87	100.68	100.48	100.78	100.24	100.21

CATION UNITS

	KLX-67 Opx	RRX-21 Opx	KLX-47 Opx	KLX62 Opx	LLX-1 Opx	KLX-45 Opx	KLX-49A Opx	KLX-70 Opx	BTX-16 Opx	BTX-23 Opx	BTX-26 Opx	LLX-14 Opx	KRX-11 Opx
Si	1.943	1.900	1.929	1.910	1.917	1.885	1.879	1.884	1.886	1.881	1.877	1.862	1.898
Ti	0.001	0.001	0.000	0.003	0.001	0.000	0.002	0.002	0.002	0.002	0.003	0.003	0.001
Al	0.052	0.107	0.119	0.081	0.107	0.152	0.170	0.142	0.181	0.191	0.208	0.202	0.135
Fe	0.189	0.167	0.158	0.176	0.159	0.162	0.187	0.171	0.179	0.160	0.177	0.185	0.163
Mn	0.003	0.004	0.004	0.006	0.004	0.004	0.004	0.004	0.003	0.004	0.004	0.004	0.004
Mg	1.764	1.784	1.731	1.765	1.765	1.754	1.719	1.747	1.708	1.647	1.682	1.694	1.760
Ca	0.031	0.020	0.031	0.033	0.029	0.024	0.023	0.026	0.024	0.083	0.028	0.031	0.022
Na	0.005	0.004	0.009	0.009	0.002	0.006	0.005	0.007	0.005	0.011	0.008	0.008	0.003
K	0.000	0.000	0.000	0.000	0.000	0.000	0.000	0.000	0.000	0.000	0.000	0.000	0.000
P	0.001	0.000	0.000	0.000	0.000	0.000	0.000	0.000	0.000	0.000	0.000	0.000	0.000
Ni	0.002	0.002	0.002	0.003	0.003	0.003	0.002	0.003	0.002	0.002	0.002	0.003	0.002
Cr	0.011	0.012	0.016	0.014	0.015	0.010	0.008	0.013	0.010	0.019	0.010	0.008	0.011
Total	4.000	4.000	4.000	4.000	4.000	4.000	4.000	4.000	4.000	4.000	4.000	4.000	4.000
O2-	5.973	5.958	5.993	5.956	5.977	5.964	5.967	5.960	5.981	5.982	5.986	5.967	5.971
Mg#	0.9034	0.9144	0.9162	0.9093	0.9174	0.9153	0.9020	0.9106	0.9051	0.9113	0.9049	0.9013	0.9150
Cr/(Cr+Al)	0.170	0.100	0.121	0.148	0.123	0.062	0.047	0.086	0.051	0.090	0.044	0.040	0.078
Al IV	0.057	0.100	0.071	0.090	0.083	0.115	0.121	0.116	0.114	0.119	0.123	0.138	0.102
AlVI	-0.005	0.007	0.047	-0.009	0.023	0.037	0.049	0.026	0.067	0.071	0.085	0.065	0.033

Table IV (1): Orthopyroxene analyses. Silicate oxydes in wt%

	KRX-13 Opx	KRX-14 Opx	LPX-11 Opx	LPX-16 Opx	LPX-18 Opx	RRX-10 Opx	RRX-18 Opx	SLX-4 Opx	SLX-30 Opx	SLX-41 Opx	KLX-7Opx	KLX-11Opx
SiO2	54.43	54.29	54.65	54.48	54.82	54.33	54.25	53.71	54.73	53.41	52.48	52.07
TiO2	0.11	0.10	0.08	0.10	0.06	0.05	0.08	0.07	0.04	0.11	0.23	0.41
Al2O3	4.39	4.51	4.23	4.01	4.23	3.55	4.12	4.91	3.94	5.23	4.83	6.12
FeOt	6.73	6.52	6.58	7.46	6.53	5.98	6.43	6.74	6.91	6.42	10.00	10.54
MnO	0.16	0.15	0.16	0.16	0.16	0.13	0.15	0.13	0.11	0.14	0.18	0.19
MgO	33.23	33.32	33.46	33.09	33.75	34.29	33.59	32.84	32.12	32.88	30.30	29.36
CaO	0.63	0.68	0.62	0.63	0.64	0.49	0.67	1.16	1.22	1.06	1.00	1.16
Na2O	0.10	0.13	0.07	0.09	0.07	0.05	0.06	0.10	0.09	0.08	0.06	0.12
K2O	0.00	0.00	0.00	0.00	0.00	0.00	0.00	0.00	0.01	0.00	0.00	0.00
P2O5	0.00	0.00	0.00	0.00	0.00	0.01	0.00	0.00	0.01	0.00	0.00	0.01
NiO	0.08	0.09	0.08	0.09	0.08	0.08	0.08	0.09	0.09	0.09	0.05	0.06
Cr2O5	0.25	0.30	0.27	0.25	0.28	0.31	0.33	0.56	0.63	0.43	0.63	0.15
Total	100.10	100.08	100.21	100.36	100.60	99.29	99.77	100.32	99.89	99.87	99.74	100.20

CATION UNITS

	KRX-13 Opx	KRX-14 Opx	LPX-11 Opx	LPX-16 Opx	LPX-18 Opx	RRX-10 Opx	RRX-18 Opx	SLX-4 Opx	SLX-30 Opx	SLX-41 Opx	KLX-7Opx	KLX-11Opx
Si	1.875	1.869	1.879	1.877	1.876	1.878	1.872	1.849	1.900	1.844	1.846	1.827
Ti	0.003	0.002	0.002	0.002	0.001	0.001	0.002	0.002	0.001	0.003	0.006	0.011
Al	0.178	0.183	0.172	0.163	0.171	0.145	0.168	0.199	0.161	0.213	0.200	0.253
Fe	0.194	0.188	0.189	0.215	0.187	0.173	0.185	0.194	0.201	0.185	0.294	0.309
Mn	0.005	0.004	0.005	0.005	0.005	0.004	0.004	0.004	0.003	0.004	0.005	0.006
Mg	1.706	1.710	1.716	1.699	1.722	1.767	1.728	1.685	1.662	1.692	1.588	1.536
Ca	0.023	0.025	0.023	0.023	0.023	0.018	0.025	0.043	0.045	0.039	0.037	0.044
Na	0.007	0.008	0.005	0.006	0.004	0.003	0.004	0.007	0.006	0.005	0.004	0.008
K	0.000	0.000	0.000	0.000	0.000	0.000	0.000	0.000	0.000	0.000	0.000	0.000
P	0.000	0.000	0.000	0.000	0.000	0.000	0.000	0.000	0.000	0.000	0.000	0.000
Ni	0.002	0.003	0.002	0.002	0.002	0.002	0.002	0.003	0.002	0.003	0.001	0.002
Cr	0.007	0.008	0.007	0.007	0.007	0.009	0.009	0.015	0.017	0.012	0.018	0.004
Total	4.000	4.000	4.000	4.000	4.000	4.000	4.000	4.000	4.000	4.000	4.000	4.000
O2-	5.967	5.962	5.969	5.962	5.965	5.954	5.961	5.954	5.987	5.956	5.959	5.963
Mg#	0.8980	0.9011	0.9006	0.8877	0.9021	0.9108	0.9031	0.8968	0.8923	0.9013	0.8438	0.8324
Cr/(Cr+Al)	0.037	0.043	0.041	0.041	0.042	0.056	0.051	0.071	0.097	0.052	0.080	0.016
Al IV	0.125	0.131	0.121	0.123	0.124	0.122	0.128	0.151	0.100	0.156	0.154	0.173
AlVI	0.053	0.051	0.051	0.040	0.047	0.022	0.040	0.048	0.061	0.057	0.046	0.080

Table IV (2): Orthopyroxene analyses. Silicate oxydes in wt%

	KLX-67 Cpx	RRX-21 Cpx	KLX-62 Cpx	KLX-57 Cpx	LLX-1 Cpx	KLX-45 Cpx	KLX-49A Cpx	KLX-70 Cpx	BTX-16 Cpx	BTX-23 Cpx	BTX-26 Cpx	LLX-14 Cpx	KRX-11 Cpx	KRX-13 Cpx	KRX-14 Cpx	LPX-11 Cpx	LPX-16 Cpx
SiO2	52.77	52.15	51.81	51.63	53.52	52.20	51.81	50.09	52.46	52.20	52.10	51.45	52.59	51.59	51.71	51.85	50.11
TiO2	0.15	0.18	0.48	0.92	0.19	0.04	0.36	1.21	0.37	0.18	0.45	0.47	0.18	0.62	0.51	0.46	1.27
Al2O3	3.43	4.45	5.35	3.69	2.53	5.02	6.37	6.60	6.95	6.00	7.21	6.66	4.72	7.21	6.81	6.34	7.12
FeOt	2.93	2.28	2.82	5.34	2.70	2.59	3.20	2.85	2.44	2.50	2.81	3.10	2.30	2.83	3.05	2.82	3.23
MnO	0.05	0.07	0.09	0.18	0.09	0.08	0.10	0.08	0.08	0.08	0.09	0.08	0.08	0.10	0.09	0.09	0.09
MgO	16.66	15.84	16.08	16.46	18.65	16.27	15.79	15.70	14.90	15.56	15.25	15.73	16.14	14.99	15.27	15.39	14.60
CaO	20.39	21.02	20.35	19.43	20.80	21.38	19.93	19.78	20.58	20.84	19.76	20.10	21.49	19.96	19.69	20.81	20.96
Na2O	1.31	1.62	1.49	0.82	0.61	1.25	1.57	1.54	1.82	1.41	1.78	1.49	1.19	1.84	1.86	1.51	1.44
K2O	0.00	0.00	0.00	0.17	0.01	0.00	0.00	0.00	0.00	0.00	0.00	0.00	0.00	0.00	0.00	0.00	0.00
P2O5	0.44	0.01	0.02	0.06	0.02	0.01	0.02	0.04	0.01	0.01	0.01	0.02	0.01	0.01	0.02	0.01	0.03
NiO	0.02	0.04	0.04	0.05	0.05	0.05	0.05	0.04	0.03	0.04	0.04	0.05	0.04	0.04	0.04	0.04	0.06
Cr2O5	1.59	1.41	1.05	1.31	0.95	0.80	0.71	1.26	0.88	1.26	0.76	0.64	1.11	0.67	0.68	0.63	0.79
Total	99.75	99.06	99.59	100.05	100.11	99.68	99.89	99.18	100.52	100.08	100.25	99.78	99.86	99.86	99.73	99.94	99.70

CATION UNITS

	KLX-67 Cpx	RRX-21 Cpx	KLX-62 Cpx	KLX-57 Cpx	LLX-1 Cpx	KLX-45 Cpx	KLX-49A Cpx	KLX-70 Cpx	BTX-16 Cpx	BTX-23 Cpx	BTX-26 Cpx	LLX-14 Cpx	KRX-11 Cpx	KRX-13 Cpx	KRX-14 Cpx	LPX-11 Cpx	LPX-16 Cpx
Si	1.914	1.898	1.876	1.885	1.928	1.887	1.869	1.824	1.881	1.883	1.872	1.858	1.902	1.861	1.867	1.872	1.823
Ti	0.004	0.005	0.013	0.025	0.005	0.001	0.01	0.033	0.01	0.005	0.012	0.013	0.005	0.017	0.014	0.012	0.035
Al	0.146	0.191	0.228	0.159	0.107	0.214	0.271	0.283	0.294	0.255	0.305	0.284	0.201	0.307	0.29	0.27	0.306
Fe	0.089	0.069	0.085	0.163	0.081	0.078	0.096	0.087	0.073	0.076	0.084	0.094	0.07	0.085	0.092	0.085	0.098
Mn	0.002	0.002	0.003	0.005	0.003	0.002	0.003	0.003	0.002	0.002	0.003	0.003	0.002	0.003	0.003	0.003	0.003
Mg	0.901	0.859	0.868	0.896	1.001	0.877	0.849	0.852	0.796	0.837	0.816	0.847	0.87	0.806	0.822	0.828	0.792
Ca	0.792	0.819	0.789	0.76	0.803	0.828	0.77	0.772	0.791	0.806	0.761	0.778	0.833	0.772	0.762	0.805	0.817
Na	0.092	0.114	0.105	0.058	0.043	0.088	0.109	0.108	0.126	0.098	0.124	0.104	0.083	0.129	0.13	0.106	0.101
K	0	0	0	0.008	0.001	0	0	0	0	0	0	0	0	0	0	0	0
P	0.014	0	0.001	0.002	0.001	0	0.001	0.001	0	0	0	0	0	0	0.001	0	0.001
Ni	0.001	0.001	0.001	0.002	0.001	0.001	0.001	0.001	0.001	0.001	0.001	0.001	0.001	0.001	0.001	0.001	0.002
Cr	0.046	0.04	0.03	0.038	0.027	0.023	0.02	0.036	0.025	0.036	0.022	0.018	0.032	0.019	0.019	0.018	0.023
Total	4	4	4	4	4	4	4	4	4	4	4	4	4	4	4	4	4
O2-	5.9878	5.9615	5.9668	5.978	5.9789	5.9632	5.9705	5.9639	5.9875	5.9853	5.9855	5.9703	5.9825	5.9769	5.9712	5.9757	5.9725
Mg#	0.9102	0.9254	0.9104	0.846	0.9249	0.9181	0.8981	0.9075	0.9158	0.9172	0.9064	0.9005	0.9259	0.9043	0.8993	0.9068	0.8896
Cr/(Cr+Al)	0.2378	0.1747	0.1161	0.192	0.2012	0.0963	0.0697	0.1138	0.0784	0.1235	0.0664	0.0601	0.1361	0.0586	0.0627	0.0621	0.0695
Al IV	0.086	0.102	0.124	0.115	0.072	0.113	0.131	0.176	0.119	0.117	0.128	0.142	0.098	0.139	0.133	0.128	0.177
Al VI	0.06	0.089	0.104	0.044	0.035	0.101	0.14	0.107	0.175	0.139	0.177	0.142	0.104	0.168	0.157	0.141	0.129

Table V (1): Clinopyroxene analyses. Silicate oxydes in wt%

	LPX-18 Cpx	RRX-10 Cpx	RRX-18 Cpx	SLX-4 Cpx	SLX-30 Cpx	SLX-41 Cpx	SLX-14 Cpx	KLX-7Cpx	KLX-11Cpx	KLX-13Cpx	KLX-17Cpx	SLX-8Cpx	SLX-24Cpx	SLX-39Cpx	SLX-44BCpx	KLX-49BCpx
SiO2	51.90	51.31	50.84	51.09	51.60	50.45	50.17	49.72	49.06	50.22	49.43	50.29	49.97	50.43	50.18	51.59
TiO2	0.30	0.26	0.42	0.31	0.12	0.41	0.66	0.85	0.89	0.73	1.08	0.68	0.63	0.63	0.41	0.36
Al2O3	5.46	5.57	6.36	5.83	4.95	6.79	6.67	5.98	6.90	5.95	6.67	7.33	7.31	6.57	6.79	6.69
FeOI	2.72	2.37	2.67	3.40	3.53	3.35	4.14	5.20	6.01	6.16	4.85	4.00	3.83	4.71	3.33	3.00
MnO	0.09	0.08	0.08	0.09	0.13	0.10	0.14	0.12	0.13	0.15	0.11	0.10	0.12	0.12	0.09	0.08
MgO	15.79	15.59	15.27	16.50	16.53	16.17	15.71	15.84	15.38	16.83	15.55	15.74	15.91	15.33	16.36	15.45
CaO	21.67	21.45	20.65	19.96	20.43	19.88	20.02	19.88	19.18	16.93	19.63	20.19	19.82	19.85	19.81	20.18
Na2O	1.20	1.46	1.58	1.12	1.00	1.22	1.13	0.83	0.86	0.79	1.00	1.02	1.16	1.09	1.17	1.62
K2O	0.00	0.00	0.00	0.01	0.01	0.00	0.01	0.00	0.00	0.01	0.00	0.00	0.00	0.01	0.00	0.00
P2O5	0.01	0.02	0.02	0.02	0.44	0.02	0.42	0.02	0.03	0.46	0.02	0.45	0.02	0.46	0.01	0.02
NiO	0.03	0.03	0.04	0.04	0.03	0.06	0.02	0.03	0.03	0.02	0.03	0.02	0.04	0.04	0.05	0.04
Cr2O5	0.69	0.90	0.76	1.08	1.17	0.75	0.71	0.97	0.75	1.08	0.97	0.46	0.46	0.77	0.84	0.81
Total	99.87	99.04	98.66	99.44	99.95	99.18	99.80	99.45	99.21	99.31	99.34	100.29	99.25	100.01	99.04	99.84

CATION UNITS

	LPX-18 Cpx	RRX-10 Cpx	RRX-18 Cpx	SLX-4 Cpx	SLX-30 Cpx	SLX-41 Cpx	SLX-14 Cpx	KLX-7Cpx	KLX-11Cpx	KLX-13Cpx	KLX-17Cpx	SLX-8Cpx	SLX-24Cpx	SLX-39Cpx	SLX-44BCpx	KLX-49BCpx
Si	1.877	1.867	1.857	1.855	1.87	1.834	1.822	1.821	1.804	1.842	1.81	1.817	1.818	1.834	1.825	1.863
Ti	0.008	0.007	0.011	0.008	0.003	0.011	0.018	0.0233	0.0245	0.02	0.0299	0.0185	0.0172	0.0172	0.0111	0.010
Al	0.233	0.239	0.274	0.25	0.211	0.291	0.286	0.258	0.299	0.257	0.288	0.312	0.313	0.282	0.291	0.285
Fe	0.082	0.072	0.082	0.103	0.107	0.102	0.126	0.159	0.185	0.189	0.148	0.121	0.117	0.143	0.101	0.091
Mn	0.003	0.003	0.003	0.003	0.004	0.003	0.004	0.004	0.004	0.005	0.003	0.003	0.004	0.004	0.003	0.002
Mg	0.851	0.846	0.831	0.893	0.893	0.876	0.851	0.865	0.843	0.92	0.849	0.848	0.863	0.831	0.887	0.832
Ca	0.84	0.836	0.808	0.776	0.793	0.774	0.779	0.78	0.755	0.665	0.77	0.781	0.772	0.774	0.772	0.781
Na	0.084	0.103	0.112	0.079	0.07	0.086	0.08	0.059	0.061	0.056	0.071	0.071	0.082	0.077	0.082	0.113
K	0	0	0	0	0	0	0	0	0	0.001	0	0	0	0	0	0
P	0	0.001	0	0	0.014	0	0.013	0.001	0.001	0.014	0	0.014	0.001	0.014	0	0.001
Ni	0.001	0.001	0.001	0.001	0.001	0.002	0.001	0.001	0.001	0.001	0.001	0.001	0.001	0.001	0.001	0.000
Cr	0.02	0.026	0.022	0.031	0.033	0.022	0.02	0.028	0.022	0.031	0.028	0.013	0.013	0.022	0.024	0.023
Total	4	4	4	4	4	4	4	4	4	4	4	4	4	4	4	4
O2-	5.9704	5.9561	5.9607	5.9648	5.9803	5.9586	5.9728	5.9591	5.9596	5.9988	5.9636	5.9833	5.9582	5.9860	5.9535	5.9708
Mg#	0.9119	0.9216	0.9106	0.8964	0.893	0.8959	0.8713	0.8444	0.8201	0.8296	0.8511	0.8751	0.8809	0.8531	0.8975	0.9018
Cr/(Cr+Al)	0.0777	0.0981	0.0739	0.1105	0.1365	0.069	0.0664	0.0984	0.0677	0.1083	0.0892	0.0407	0.0402	0.0728	0.0762	0.0751
Al IV	0.123	0.133	0.143	0.145	0.13	0.166	0.178	0.179	0.196	0.158	0.19	0.183	0.182	0.166	0.175	0.137
Al VI	0.11	0.106	0.13	0.104	0.081	0.124	0.108	0.08	0.103	0.099	0.099	0.129	0.131	0.116	0.117	0.148

Table V (2): Clinopyroxene analyses. Silicate oxydes in wt%

	KLX-67Spi	KLX-59 Spi	RRX-21 Spi	KLX-47 Spi	KLX-57 Spi	LLX-1 Spi	KLX-45 Spi	KLX-70 Spi	BTX-16 Spi	BTX-23 Spi	BTX-26 Spi	LLX-14 Spi	KRX-11 Spi	KRX-13 Spi	KRX-14 Spi
SiO2	0.04	0.04	0.00	0.03	0.01	0.00	0.02	0.00	0.00	0.00	0.01	0.03	0.00	0.01	0.01
TiO2	0.16	0.43	0.09	0.01	0.46	0.15	0.01	0.26	0.06	0.07	0.11	0.25	0.06	0.23	0.26
Al2O3	16.41	22.13	41.47	36.78	30.75	33.75	54.24	48.19	56.69	49.19	58.42	58.84	48.61	58.79	57.33
FeOt	19.60	15.84	12.00	13.22	14.85	14.03	10.29	11.62	10.47	11.50	10.07	9.70	10.92	11.35	11.50
MnO	0.11	0.20	0.15	0.19	0.20	0.18	0.12	0.14	0.11	0.12	0.10	0.11	0.13	0.11	0.10
MgO	12.77	14.65	18.59	17.61	16.63	17.56	21.38	20.07	21.20	20.18	21.67	21.71	20.61	21.63	21.23
CaO	0.02	0.02	0.00	0.04	0.00	0.01	0.00	0.01	0.00	0.00	0.00	0.00	0.00	0.00	0.00
Na2O	0.01	0.01	0.00	0.01	0.00	0.00	0.00	0.00	0.00	0.00	0.00	0.00	0.00	0.00	0.00
NiO	0.14	0.10	0.22	0.24	0.24	0.20	0.35	0.30	0.37	0.30	0.39	0.32	0.30	0.39	0.37
Cr2O5	49.87	46.01	27.65	31.96	36.82	34.33	14.18	19.80	10.84	17.78	8.87	9.36	19.66	7.59	9.52
Total		99.43	100.18	100.10	99.97	100.20	100.58	100.38	99.75	99.14	99.63	100.33	100.30	100.09	100.34
	KLX-67Spi	KLX-59 Spi	RRX-21 Spi	KLX-47 Spi	KLX-57 Spi	LLX-1 Spi	KLX-45 Spi	KLX-70 Spi	BTX-16 Spi	BTX-23 Spi	BTX-26 Spi	LLX-14 Spi	KRX-11 Spi	KRX-13 Spi	KRX-14 Spi
Si	0.001	0.001	0.000	0.001	0.000	0.000	0.000	0.000	0.000	0.000	0.000	0.001	0.000	0.000	0.000
Ti	0.004	0.010	0.002	0.000	0.010	0.003	0.000	0.005	0.001	0.001	0.002	0.005	0.001	0.004	0.005
Al	0.614	0.797	1.347	1.223	1.053	1.134	1.653	1.513	1.725	1.551	1.765	1.766	1.520	1.768	1.733
Fe t	0.520	0.405	0.276	0.312	0.361	0.334	0.222	0.259	0.226	0.257	0.216	0.206	0.242	0.242	0.247
Fe3+	0.127	0.071	0.047	0.063	0.081	0.086	0.056	0.060	0.051	0.069	0.051	0.034	0.065	0.070	0.063
Fe2+	0.393	0.334	0.230	0.248	0.280	0.248	0.167	0.199	0.175	0.188	0.164	0.172	0.177	0.172	0.184
Mn	0.003	0.005	0.004	0.005	0.005	0.004	0.003	0.003	0.002	0.003	0.002	0.002	0.003	0.002	0.002
Mg	0.604	0.667	0.764	0.740	0.720	0.746	0.824	0.797	0.816	0.805	0.828	0.824	0.815	0.822	0.812
Ca	0.001	0.000	0.000	0.001	0.000	0.000	0.000	0.000	0.000	0.000	0.000	0.000	0.000	0.000	0.000
Na	0.001	0.001	0.000	0.001	0.000	0.000	0.000	0.000	0.000	0.000	0.000	0.000	0.000	0.000	0.000
Ni	0.004	0.002	0.005	0.005	0.006	0.005	0.007	0.006	0.008	0.006	0.008	0.007	0.006	0.008	0.008
Cr	1.250	1.111	0.602	0.712	0.845	0.774	0.290	0.417	0.221	0.376	0.180	0.188	0.412	0.153	0.193
Total	3.000	3.000	3.000	3.000	3.000	3.000	3.000	3.000	3.000	3.000	3.000	3.000	3.000	3.000	3.000
O2-	3.940	3.960	3.980	3.970	3.960	3.960	3.970	3.970	3.970	3.970	3.970	3.980	3.970	3.970	3.970
Mg#	0.5373	0.6226	0.7342	0.7037	0.6662	0.6905	0.7874	0.7548	0.7831	0.7578	0.7933	0.7997	0.7709	0.7726	0.7670
Cr#	0.6707	0.5823	0.3090	0.3681	0.4453	0.4055	0.1492	0.2160	0.1137	0.1951	0.0924	0.0964	0.2134	0.0797	0.1002

Table VI (1): Spinel analyses. Silicate oxydes in wt%

	LPX-11 Spi	LPX-16 Spi	LPX-18 Spi	RRX-10 Spi	RRX-18 Spi	SLX-30 Spi	SLX-41 Spi	SLX-14 Spi	KLX-7Spi	KLX-11Spi	KLX-17Spi	SLX-8Spi	SLX-24Spi	SLX-39Spi	SLX-44Spi
SiO2	0.00	0.01	0.00	0.00	0.00	0.16	0.02	0.04	0.01	0.02	0.02	0.06	0.02	0.05	0.02
TiO2	0.08	0.09	0.07	0.04	0.07	0.14	0.14	0.25	0.25	0.24	0.57	0.22	0.27	0.35	0.15
Al2O3	59.82	58.69	58.59	55.52	58.16	43.41	58.01	52.71	57.82	60.15	53.09	58.67	61.71	50.77	57.03
FeOt	10.14	11.66	10.34	10.12	10.40	14.25	9.82	14.26	16.88	16.53	17.21	12.75	9.76	17.68	9.89
MnO	0.10	0.10	0.11	0.11	0.11	0.18	0.09	0.16	0.12	0.12	0.14	0.07	0.11	0.10	0.12
MgO	21.19	20.36	21.32	20.95	20.91	17.10	21.55	18.84	18.96	19.15	18.24	19.96	21.61	18.03	21.24
CaO	0.01	0.00	0.01	0.01	0.00	0.01	0.00	0.00	0.00	0.01	0.00	0.01	0.01	0.00	0.00
Na2O	0.00	0.00	0.00	0.00	0.00	0.01	0.00	0.01	0.00	0.00	0.00	0.01	0.00	0.01	0.00
NiO	0.36	0.37	0.35	0.34	0.34	0.25	0.37	0.29	0.27	0.21	0.20	0.35	0.31	0.27	0.31
Cr2O5	8.20	9.11	9.53	13.11	9.84	24.05	10.50	11.99	6.27	3.81	11.00	7.23	6.39	12.08	11.47
Total	99.90	100.38	100.32	100.19	99.84	99.55	100.49	98.54	100.57	100.23	100.47	99.33	100.19		100.24
	LPX-11 Spi	LPX-16 Spi	LPX-18 Spi	RRX-10 Spi	RRX-18 Spi	SLX-30 Spi	SLX-41 Spi	SLX-14 Spi	KLX-7Spi	KLX-11Spi	KLX-17Spi	SLX-8Spi	SLX-24Spi	SLX-39Spi	SLX-44Spi
Si	0.000	0.000	0.000	0.000	0.000	0.004	0.000	0.001	0.000	0.000	0.001	0.002	0.000	0.001	0.000
Ti	0.002	0.002	0.001	0.001	0.001	0.003	0.003	0.005	0.005	0.005	0.011	0.004	0.005	0.007	0.003
Al	1.800	1.775	1.764	1.694	1.764	1.419	1.746	1.661	1.763	1.822	1.653	1.790	1.838	1.607	1.728
Fe t	0.216	0.250	0.221	0.219	0.224	0.330	0.210	0.319	0.365	0.355	0.380	0.276	0.206	0.397	0.213
Fe3+	0.031	0.037	0.041	0.036	0.033	0.041	0.036	0.074	0.099	0.091	0.094	0.050	0.023	0.119	0.032
Fe2+	0.186	0.214	0.180	0.183	0.190	0.289	0.173	0.244	0.266	0.265	0.286	0.225	0.183	0.278	0.180
Mn	0.002	0.002	0.002	0.002	0.002	0.004	0.002	0.004	0.003	0.003	0.003	0.002	0.002	0.002	0.003
Mg	0.806	0.779	0.812	0.808	0.802	0.707	0.820	0.751	0.731	0.733	0.718	0.770	0.814	0.722	0.814
Ca	0.000	0.000	0.000	0.000	0.000	0.000	0.000	0.000	0.000	0.000	0.000	0.000	0.000	0.000	0.000
Na	0.000	0.000	0.000	0.000	0.000	0.001	0.000	0.001	0.000	0.000	0.000	0.001	0.000	0.000	0.000
Ni	0.007	0.008	0.007	0.007	0.007	0.006	0.008	0.006	0.006	0.004	0.004	0.007	0.006	0.006	0.006
Cr	0.166	0.185	0.192	0.268	0.200	0.527	0.212	0.253	0.128	0.077	0.230	0.148	0.128	0.257	0.233
Total	3.000	3.000	3.000	3.000	3.000	3.000	3.000	3.000	3.000	3.000	3.000	3.000	3.000	3.000	3.000
O2-	3.980	3.980	3.980	3.980	3.980	3.980	3.980	3.960	3.950	3.950	3.953	3.970	3.990	3.940	3.980
Mg#	0.7884	0.7568	0.7861	0.7868	0.7818	0.6815	0.7965	0.7020	0.6669	0.6737	0.6539	0.7362	0.7978	0.6451	0.7928
Cr#	0.0842	0.0943	0.0984	0.1367	0.1019	0.2708	0.1082	0.1324	0.0678	0.0407	0.1220	0.0763	0.0649	0.1376	0.1188

Table VI (2): Spinel analyses. Silicate oxydes in wt%

Sample	LPX-11 Amph	LPX-18 Amph	LPX-16 Amph
SiO2	43.24	47.13	42.30
TiO2	2.20	2.03	2.70
Al2O3	15.15	7.71	14.98
FeO	3.89	3.05	4.56
MnO	0.06	0.06	0.09
MgO	17.40	14.20	17.12
CaO	11.50	23.33	11.15
Na2O	3.39	0.58	3.59
K2O	0.10	0.01	0.05
P2O5	0.02	0.03	0.04
NiO	0.08	0.05	0.08
Cr2O3	0.84	1.40	1.00
Total	97.87	99.56	97.66

Table VII: Amphibole analyses. Silicate oxydes in wt%

Ech.#	LLX-1	RRX-19	RRX-21	KLX-47	KLX-57	KLX-59	BTX-26	BTX-26 (2)	BTX-16	BTX-23	BTX-34	RRX-10	RRX-14	KRX-13	KRX-14	KRX-11
Rock Type	Harz	Harz	Harz	Harz	Harz	Dunite	Lherz	Lherz	Lherz	Lherz	Lherz	Lherz	Lherz	Lherz	Lherz	Lherz
La	0.98	0.02	0.01	0.39	1.37	0.09	0.09	0.11	0.04	0.23	0.13	0.05	0.04	0.36	1.46	0.13
Ce	1.25	0.03	0.02	0.89	3.36	0.31	0.31	0.36	0.08	0.47	0.31	0.10	0.12	0.61	2.37	0.11
Pr	0.19	0.01		0.11	0.48	0.04	0.07	0.06	0.02	0.05	0.05	0.02	0.02	0.16	0.43	0.04
Nd	0.70	0.04		0.45	2.28	0.17	0.50	0.45	0.18	0.27	0.45	0.17	0.14	0.90	1.81	0.19
Sm	0.13	0.01	0.01	0.09	0.45	0.03	0.26	0.22	0.09	0.07	0.20	0.10	0.04	0.32	0.42	0.05
Eu	0.03	0.00	0.01	0.02	0.16	0.01	0.11	0.10	0.05	0.03	0.08	0.04	0.02	0.15	0.17	0.02
Gd	0.14	0.02	0.03	0.09	0.40	0.02	0.43	0.42	0.22	0.11	0.29	0.17	0.06	0.51	0.48	0.09
Tb	0.02	0.00	0.00	0.01	0.07	0.00	0.09	0.08	0.05	0.02	0.06	0.04	0.01	0.09	0.09	0.02
Dy	0.11	0.02	0.05	0.06	0.34	0.02	0.64	0.59	0.32	0.18	0.43	0.26	0.12	0.63	0.59	0.12
Ho	0.02	0.01	0.01	0.01	0.06	0.00	0.14	0.13	0.07	0.04	0.11	0.06	0.03	0.13	0.13	0.03
Er	0.07	0.02	0.03	0.04	0.19	0.01	0.41	0.38	0.25	0.12	0.31	0.21	0.09	0.42	0.35	0.08
Tm	0.01	0.00	0.01	0.01	0.03	0.00	0.07	0.06	0.04	0.02	0.05	0.03	0.02	0.06	0.06	0.01
Yb	0.07	0.03	0.05	0.05	0.20	0.02	0.43	0.43	0.26	0.14	0.35	0.21	0.11	0.41	0.34	0.11
Lu	0.01	0.01	0.01	0.01	0.03	0.00	0.07	0.06	0.04	0.02	0.06	0.03	0.02	0.06	0.06	0.02
Sc			7.6025		3.8348		16.6047			11.1580		12.3743		17.2526		9.7645
Ti	197.80	77.94	107.90	89.93	455.60	101.90	749.40		419.70	239.80	599.50	335.70	203.80	971.20	995.20	191.80
Ba	12.0863	1.4507	1.4573	1.9204	40.5865	1.2044	2.2979	2.4433	2.6900	16.6156	2.0709	2.4148	2.6200	5.5685	17.3600	3.3696
Co	104.4540	104.8850	103.1690	97.5966	110.6610	116.8120	81.1148	87.8530	87.4335	97.5704	94.8917	90.5808	88.6204	90.6736	87.6780	93.0713
Cr	4402.24	3262.65	2596.91	2562.66	4864.52	2986.85	3061.75	3301.45	2735.74	2884.97	2707.10	2728.41	2084.17	2734.62	2270.66	2477.45
Cs	0.00	0.01	0.06	0.00	0.06	0.05	0.11	0.04	0.02	0.21	0.03	0.33	0.02	0.07	0.02	0.11
Cu	8.01	7.17	8.89	3.70	2.38	1.11	19.44	20.99	19.24	5.00	23.21	14.50	9.58	19.45	8.65	7.39
Ga	1.31	1.65	1.39	1.03	2.35	0.76	3.87	4.17	2.73	2.02	3.27	2.61	1.69	4.38	4.47	3.94
Hf	0.07		0.01	0.07	0.38	0.01	0.13	0.13	0.06	0.04	0.10	0.13	0.02	0.19	0.25	0.01
Mo	0.34	0.25	0.41	0.25	0.35	0.31	0.28	0.27	0.24	0.29	0.26	0.48	0.23	0.26	0.26	0.35
Nb	0.62			0.18	1.49	0.07	0.04	0.03		0.08	0.06	0.54	0.02	0.19	1.51	0.03
Ni	2331.14	2378.92	2164.07	2162.96	2808.96	2372.64	1546.01	1742.15	1679.51	1944.13	1927.76	1809.88	1709.61	1697.43	1641.41	1855.60
Rb	1.47	0.13	0.32	0.18	2.24	0.07	0.90	0.62	0.45	0.80	0.39	1.32	0.15	0.39	3.59	0.43
Sb	0.02	0.02	0.06	0.03	0.03	0.03	0.01	0.04	0.06	0.04	0.02	0.05	0.05	0.07	0.03	0.07
Sn	0.08	0.07	0.11	0.07	0.15	0.06	0.09	0.15	0.10	0.08	0.11	0.07	0.05	0.13	0.14	0.06
Sr	7.90	1.87	0.53	4.59	16.97	0.93	10.32	11.61	2.84	8.14	4.44	2.03	3.26	22.12	99.27	1.57
Ta	0.04			0.02	0.10	0.01				0.01		0.01		0.01	0.09	
Th	0.06			0.13	0.04	0.12			0.01	0.02	0.01			0.02	0.09	
V	43.48	31.43	26.20	29.58	13.52	12.23	89.12	94.74	65.16	53.32	81.00	60.91	43.02	82.82	71.65	41.26
W		0.03	0.04	0.07	0.01	0.05	0.05	0.24	0.02	0.02		0.09	0.05	0.03	0.03	0.04
Y	0.77	0.17	0.26	0.34	1.97	0.16	3.90	4.01	2.23	1.10	3.05	1.78	0.82	3.94	3.43	0.79
Zn	47.53	46.66	40.76	40.80	74.37	49.83	42.82	47.53	43.47	51.40	44.77	41.97	36.20	45.87	49.92	38.19
Zr	3.59	0.16	0.33	3.46	15.00	0.53	3.91	4.22	1.82	1.20	2.14	4.12	1.35	6.64	9.24	0.37
Ge	0.68	0.75	0.77	0.68	0.76	0.63	0.91	0.81	0.78	0.82	0.75	0.86	0.64	0.86	0.96	0.77
La/Yb	13.10	0.54	0.15	8.18	6.72	4.29	0.21	0.26	0.16	1.64	0.38	0.23	0.31	0.89	4.23	1.20
La/YbN	9.40	0.39	0.11	5.87	4.82	3.08	0.15	0.19	0.12	1.18	0.27	0.17	0.22	0.64	3.04	0.86

Table VIII (1): Trace element content of bulk-rocks (ppm).

Ech.#	KLX-45	LLX-7	LPX-11	LPX-16	LPX-18	SLX-4	SLX-30	SLX-41	SLX-56	SLX-51	SLX-8	SLX-39	KLX-7	KLX-11	KLX-17	KLX-65
Rock Type	Lherz	Lherz	Lherz	Lherz	Lherz	Lherz	Lherz	Lherz	Cpx-rich L	Cpx-rich L	Wehr	Wehr	Wehr	Wehr	Wehr	WehrDun
La	0.14	0.50	0.10	0.10	3.11	0.06	0.21	0.08	0.95	1.14	1.60	4.39	1.25	1.41	0.84	0.22
Ce	0.31	1.19	0.39	0.42	8.94	0.18	0.57	0.25	2.68	3.07	5.54	10.15	3.24	3.92	2.29	0.58
Pr	0.04	0.20	0.09	0.08	1.16	0.03	0.08	0.05	0.40	0.42	0.99	1.30	0.50	0.66	0.37	0.08
Nd	0.16	0.95	0.61	0.51	5.05	0.20	0.31	0.34	2.14	1.80	5.37	5.54	2.47	3.31	1.78	0.36
Sm	0.04	0.28	0.28	0.25	1.00	0.09	0.07	0.18	0.55	0.45	1.27	1.03	0.70	1.03	0.53	0.08
Eu	0.02	0.11	0.13	0.10	0.29	0.04	0.02	0.08	0.19	0.14	0.48	0.32	0.26	0.38	0.19	0.02
Gd	0.05	0.39	0.43	0.36	0.71	0.13	0.07	0.28	0.71	0.40	1.43	1.02	0.82	1.23	0.53	0.08
Tb	0.01	0.08	0.09	0.07	0.12	0.03	0.01	0.06	0.11	0.06	0.25	0.16	0.12	0.19	0.09	0.01
Dy	0.09	0.51	0.57	0.47	0.72	0.20	0.09	0.40	0.75	0.37	1.52	0.88	0.68	1.09	0.51	0.07
Ho	0.03	0.12	0.13	0.10	0.15	0.05	0.02	0.09	0.16	0.09	0.31	0.18	0.13	0.20	0.09	0.01
Er	0.10	0.34	0.41	0.31	0.46	0.15	0.08	0.31	0.43	0.24	0.91	0.49	0.32	0.47	0.22	0.04
Tm	0.02	0.05	0.06	0.05	0.07	0.03	0.01	0.05	0.08	0.03	0.14	0.08	0.04	0.06	0.03	0.01
Yb	0.13	0.33	0.42	0.30	0.47	0.18	0.10	0.31	0.43	0.24	0.86	0.46	0.24	0.40	0.20	0.04
Lu	0.02	0.06	0.07	0.05	0.08	0.03	0.02	0.05	0.06	0.04	0.13	0.08	0.03	0.05	0.03	0.01
Sc	10.8212	13.8901		13.2645				13.1083			24.0192		16.3583			
Ti	119.90	707.40	839.30	689.40	719.40	317.70	167.90	539.60	1151.00	653.50	1876.00	1067.00	1829.00	2854.00	1547.00	275.80
Ba	2.0000	6.7617	10.6923	2.7992	24.9247	3.3810	1.8877	4.3000	21.0343	28.2770	18.5409	23.3548	9.3678	8.7179	8.3528	1.6988
Co	90.3000	91.3164	96.6899	89.9324	90.9803	105.3370	102.0250	88.0000	102.0150	111.1340	83.5978	101.3750	117.4510	97.2059	125.5240	136.5270
Cr	2541.00	2894.57	2844.53	2507.87	2551.45	2546.96	2408.67	2497.00	2266.45	1634.81	2616.42	2226.67	2394.97	1666.38	1835.98	904.55
Cs	0.05	0.09	0.04	0.07	0.03	0.03	0.04	0.17	0.04	0.03	0.07	0.04	0.09			
Cu	2.50	22.60	29.39	7.40	19.53	17.39	2.87	19.30	26.19	9.51	22.40	25.61	48.17	26.09	24.23	8.66
Ga	1.56	3.22	4.05	3.09	3.95	1.98	1.95	2.93	5.11	2.68	5.63	3.09	4.34	5.86	3.31	0.85
Hf	0.04	0.17	0.17	0.16	0.24	0.05	0.02	0.10	0.28	0.15	0.49	0.33	0.39	0.65	0.32	0.04
Mo	0.24	0.31	0.26	0.25	0.25	0.22	0.28	0.21	0.49	0.26	0.21	0.17	0.20	0.13	0.19	0.20
Nb	0.09	0.30		0.06	2.09	0.03	0.11	0.72	1.10	1.01	0.75	1.29	0.83	0.91	0.54	0.07
Ni	1894.00	1764.77	1927.13	1718.61	1962.70	2103.12	2101.83	1742.00	1915.98	1749.28	1476.48	1597.26	1281.43	775.34	1292.40	2228.67
Rb	0.10	1.62	0.72	0.59	3.05	0.58	0.32	1.80	1.67	1.60	1.09	0.75	0.80	0.54	0.38	0.06
Sb	0.04	0.04	0.01	0.03	0.02	0.01	0.01	0.06	0.18	0.02	0.02	0.04	0.07	0.03	0.03	0.03
Sn	0.09	0.10	0.10	0.06	0.16	0.02	0.00	0.07	0.14	0.09	0.21	0.16	0.33	0.31	0.27	0.06
Sr	1.74	13.13	7.49	7.96	70.05	3.89	4.90	5.57	15.24	12.56	48.98	32.29	32.60	43.88	20.69	3.52
Ta	0.01	0.02			0.07		0.01	0.01	0.09	0.08	0.09	0.13	0.07	0.08	0.05	0.01
Th	0.21	0.02		0.01	0.03				0.05	0.04	0.05	0.28	0.10	0.09	0.05	0.02
V	33.50	71.87	86.14	65.95	73.32	52.85	34.37	62.90	80.90	50.58	156.62	73.64	98.72	165.66	83.14	14.53
W	0.03	0.01		0.05	0.01			0.02	0.02	0.00	0.03		0.02			
Y	0.83	3.38	3.87	2.85	4.15	1.44	0.72	2.70	4.54	2.39	8.80	5.12	3.36	5.60	2.67	0.37
Zn	39.00	42.23	52.51	56.64	41.13	44.96	50.15	39.20	51.04	62.18	49.04	55.28	74.13	62.21	76.76	78.89
Zr	1.74	7.00	4.92	5.16	9.37	1.53	0.72	3.08	9.02	5.75	14.15	12.59	12.69	18.00	9.06	1.63
Ge	0.82	0.87	0.82	0.87	0.78	0.68	0.70	0.87	0.74	0.63	1.02	0.70	1.08	1.01	0.84	0.73
La/Yb	1.03	1.50	0.25	0.32	6.67	0.33	2.00	0.27	2.19	4.80	1.88	9.55	5.11	3.51	4.11	5.69
La/YbN	0.74	1.08	0.18	0.23	4.79	0.24	1.43	0.19	1.57	3.44	1.35	6.85	3.67	2.52	2.94	4.08

Table VIII (2): Trace element content of bulk-rocks (ppm).

2.7 DISCUSSION

The discussion is divided into two parts. The first part involves the origin of the Cr-diopside peridotites, while the second part addresses the origin of the wehrlite xenoliths and the Opx-poor lherzolites.

2.7.1 The origin of the Cr-diopside suites

Lherzolites and harzburgites have typically been interpreted as the residues of various degrees of melting of a pyrolite type source (e.g., Frey and Prinz, 1978). This melting event, or several events, may have been followed by secondary metasomatic processes involving fluids or melts that reset trace element contents and eventually resulted in the crystallization of secondary hydrous phases (e.g., McDonough and Frey, 1989). However, recent studies suggest that the composition of some peridotites cannot be explained simply by partial melting, but require refertilisation or melt-rock interaction. This appears particularly to be the case for some abyssal peridotites (Elthon, 1992; Niu et al., 1997) and for most of the very depleted garnet xenoliths from cratonic settings (Kelemen et al., 1992).

2.7.1.1 Comparison to other continental spinel bearing xenoliths

When compared to continental spinel peridotite xenoliths brough to the surface by alkali basalts from around the world, those of the Canadian Cordillera are very similar in terms of whole-rock major element composition (Fig. 7). MgO correlates negatively with SiO_2, TiO_2, Al_2O_3, CaO and NaO (Fig. 7), and positively with NiO (not shown). These correlations can be interpreted as reflecting various degrees of extraction of a basaltic melt from the most fertile (lowest MgO) leaving the more depleted (highest MgO)

compositions as solid residues. The Canadian Cordillera xenoliths also display a negative correlation between La/Yb_N and Al_2O_3 which is characteristic of spinel xenoliths (Fig. 10; McDonough and Frey, 1989). Little concensus exists on the explanation of this paradox, i.e. the most depleted peridotites in terms of major elements being the most enriched in incompatible trace elements. This paradox could be caused by the physical properties of the peridotites, Ol-poor rocks being less permeable to melts than Ol rich ones (Toramaru and Fujii, 1986), and REE migrating more rapidly in Cpx-poor rocks than in Cpx-rich ones (McKenzie, 1984; Takazawa et al., 1992).

Fig. 8 (next page): Whole-rock compositions of the wehrlite suites and of the pyroxenites from the southern Canadian Cordillera compared with those of the Cr-diopside suites from the same region and the Al-augite suites taken from the literature. Circles = KL wehrlites and two dunites. Circle with cross = SL wehrlites. Black squares = Opx-poor lherzolites from SL. Black square with a surrounding square = Opx-poor lherzolite from KL. Grey symbols = Cr-diopsie suites from the Canadian Cordillera (symbols as in Fig. 3). Black and white squares = pyroxenites from the Canadian Cordillera (KL, SL, LL, BT). Pyroxenites from KL and SL are represented as black and white squares surrounded with the respective symbols of the KL (circle) and SL (circle with cross) wehrlites. Inclined triangles labelled KL-1, SL-1 and L2 are respectively the host-rock of KL xenoliths, the host-rock of SL xenoliths, and the melt L2 produced by the melting of Cr-diopside lherzolites. Asterisks = Al-augite suites from the literature (Frey and Prinz, 1978; Irving, 1980; Griffin et al., 1984; Aoki, 1987; Gamble and Kyle, 1987; Hunter and Upton, 1987; Griffin et al., 1988; Kepezhinskas et al., 1995).

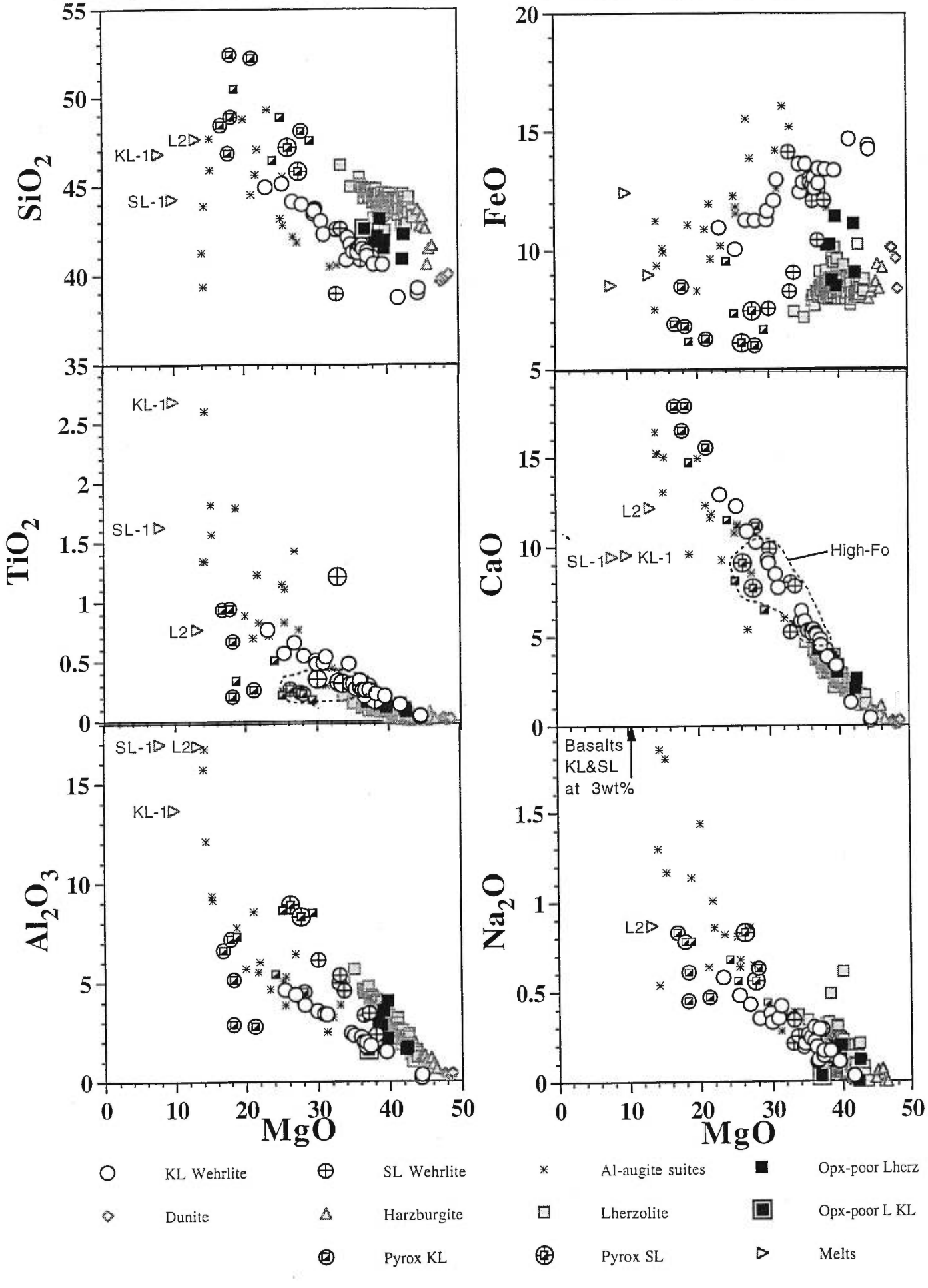
SiO2
TiO2
Al2O3
FeO
CaO
Na2O
MgO
MgO
KL-1
L2
SL-1
High-Fo
Basalts
KL&SL
at 3wt%
KL Wehrlite
SL Wehrlite
Al-augite suites
Opx-poor Lherz
Dunite
Harzburgite
Lherzolite
Opx-poor L KL
Pyrox KL
Pyrox SL
Melts

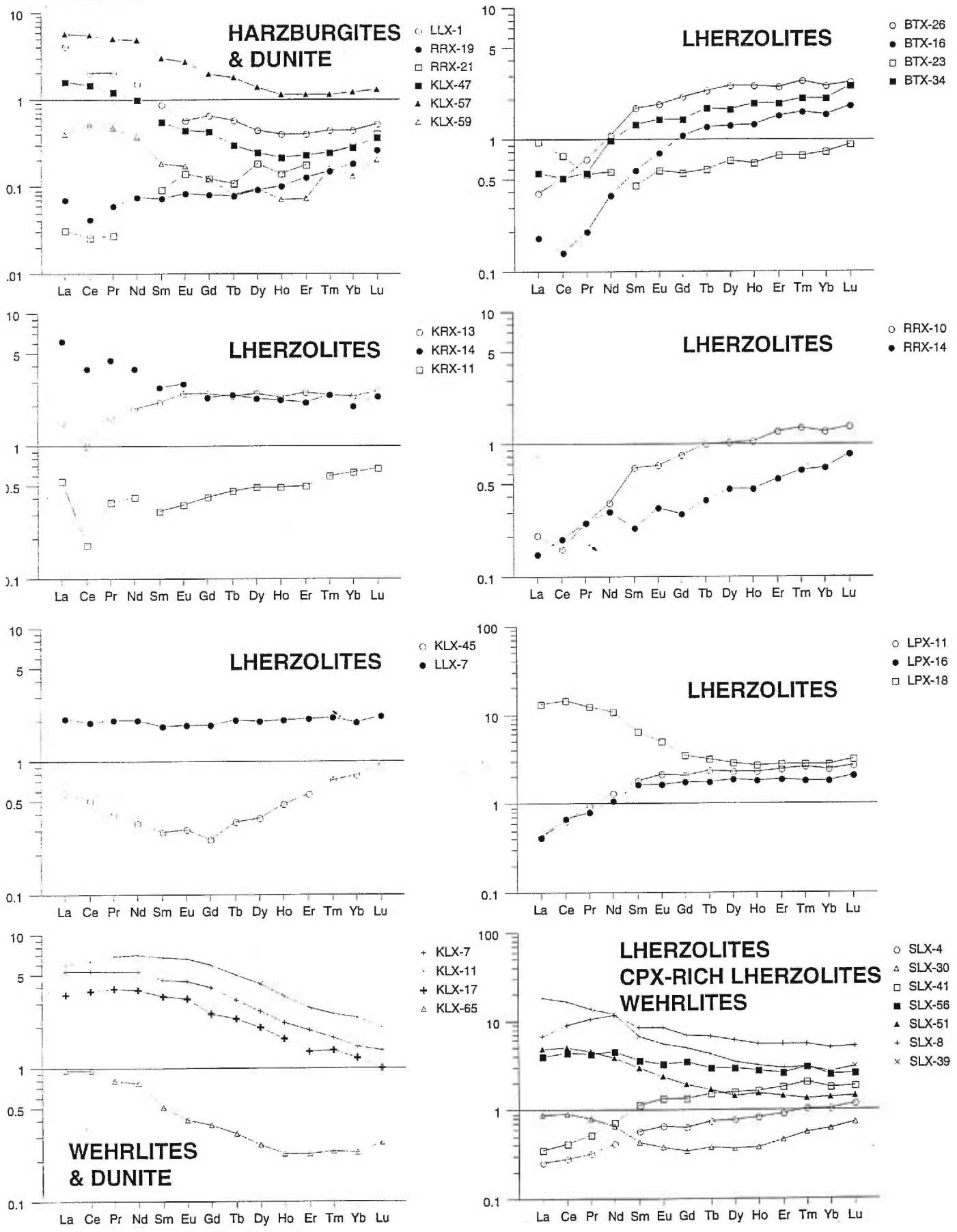

Fig. 9: Chondrite normalized (Sun and McDonough, 1989) whole-rock REE patterns of the Southern Canadian Cordillera xenoliths.

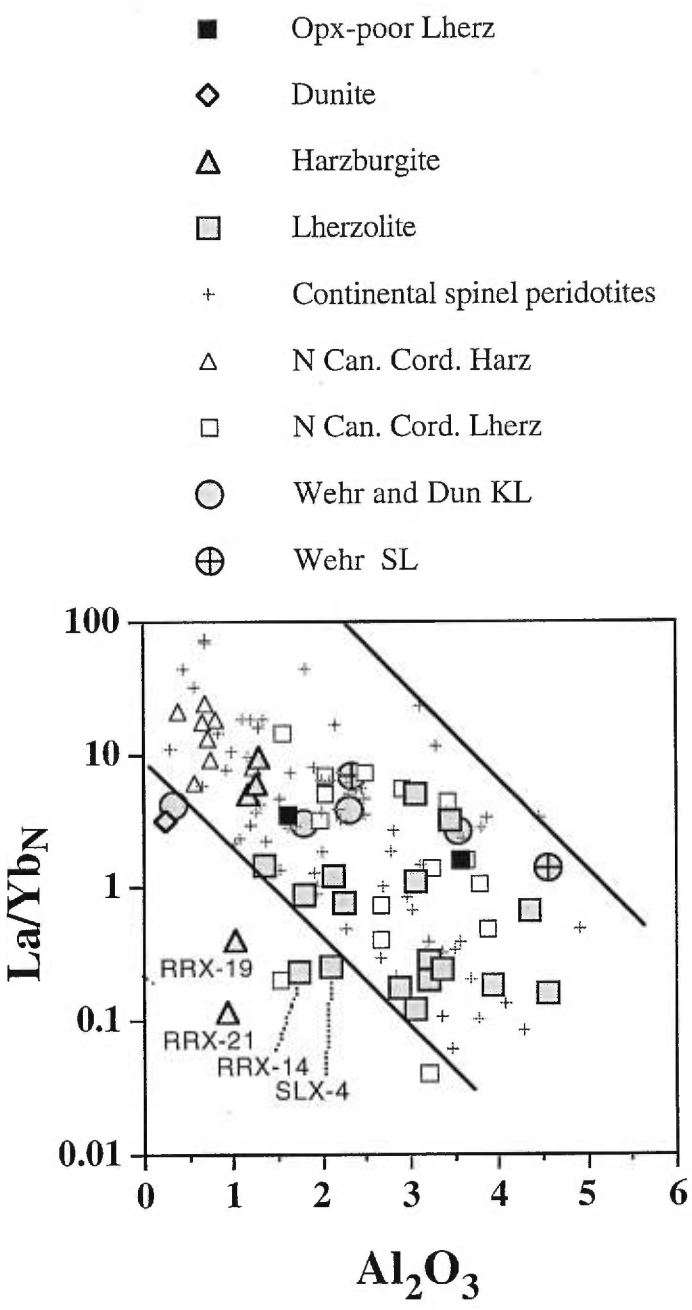

Fig. 10: Chondrite normalized (Sun and McDonough, 1989, and references therein) La/Yb ratio vs Al_2O_3 of the Cr-diopside suites of the Southern Canadian Cordillera, compared to other spinel peridotites from around the world. References are the same as in Fig. 5. Symbols as in Fig.2. Black lines underline the worldwide negative correlation.

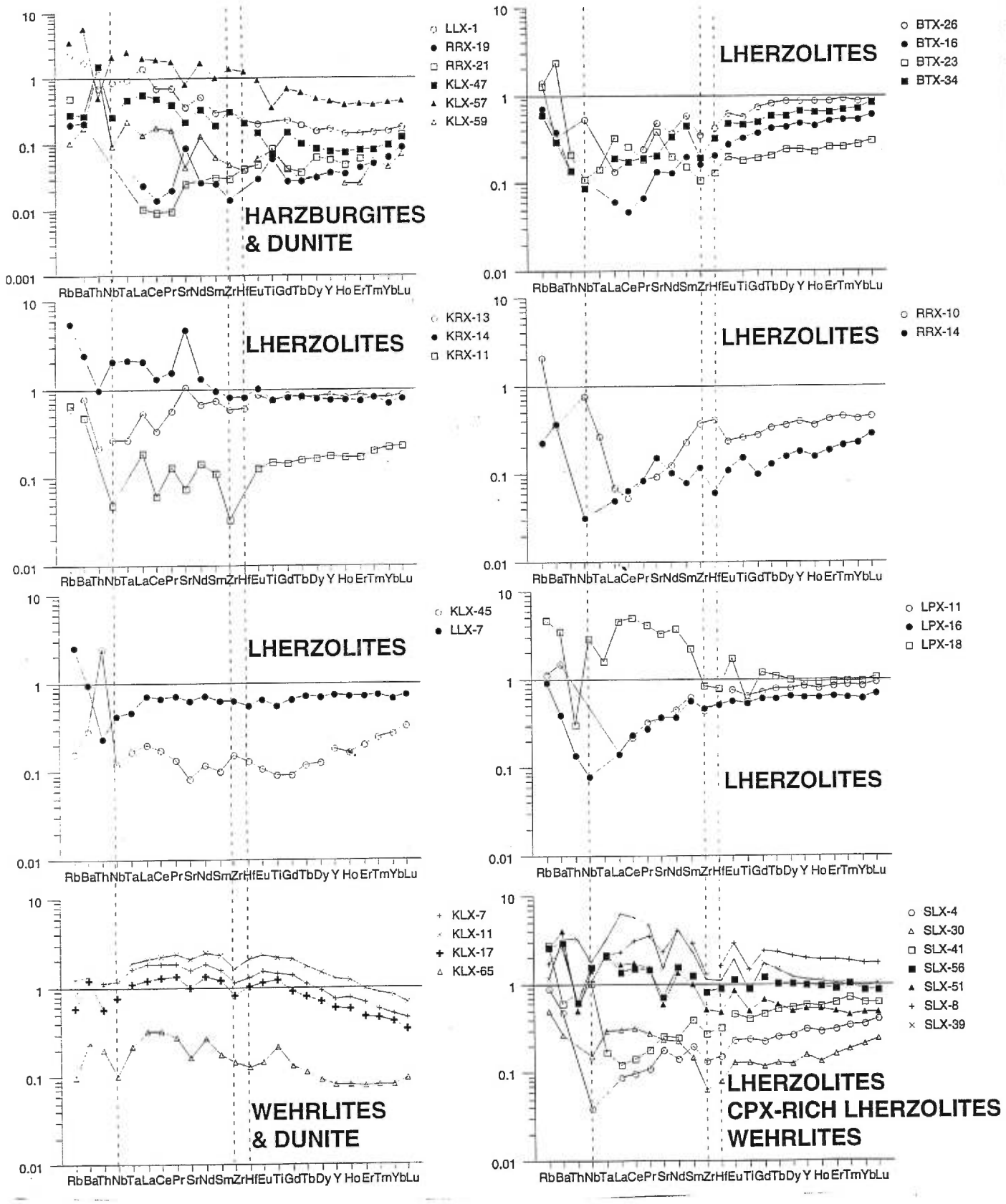

Fig.11: Primitive-mantle normalized (Sun and McDonough, 1989) whole-rock extended trace-element diagrams of the Southern Canadian Cordillera xenoliths.

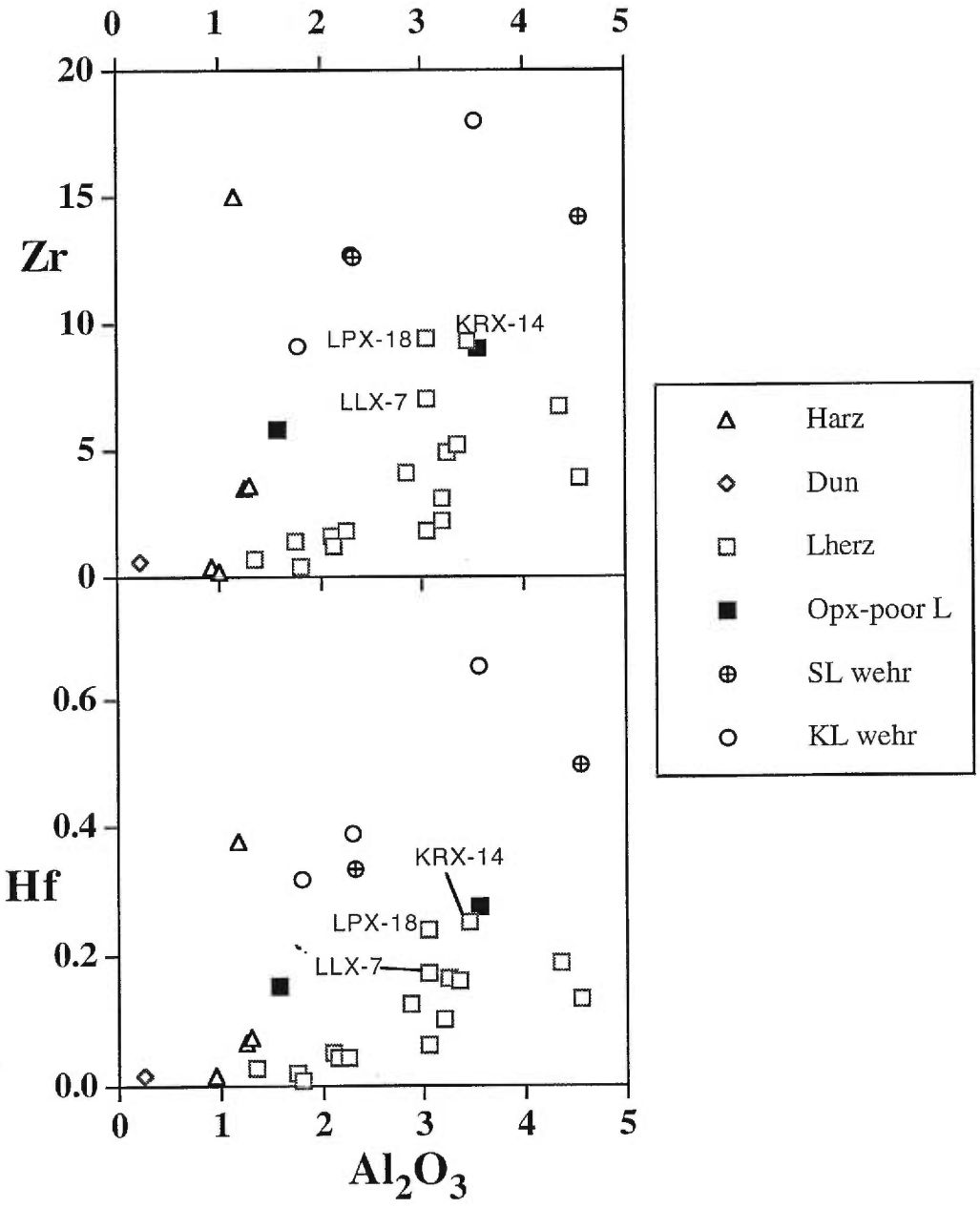

Fig. 12: Zr and Hf contents (ppm) of the southern Canadian Cordillera xenoliths versus the Al_2O_3 content (wt%). Symbols as in Fig. 2.

2.7.1.2 Processes responsible for the Cr-diopside suite compositional range

Variable degrees of partial melting may be responsible for the compositional range observed in the Southern Canadian Cordillera xenolith suite. In a diagram of a compatible element (e.g. Ni) versus a relatively incompatible element (e.g. Al or Yb), melting a fertile composition should produce a series of residues with relatively little variation for compatible elements compared to that for incompatible elements. Crystallization produces a series of cumulates with comparatively steep trends with large variations in compatible elements compared to those of incompatible element (Francis, 1987). In the melting model presented here, the source compositions are taken as the most fertile of our samples, KRX-8 and LPX-18. The equilibrium and fractional melting equations of Shaw were used to calculate the compositions of the residues produced by the melting of these source compositions (Shaw, 1979). Both equilibrium and fractional melting trends can reasonably reproduce the range of xenolith data (Fig. 13). Very similar values are obtained with either Al or Yb as an incompatible element. Using low partition coefficients (D_{Yb}= 0.104, D_{Al}=0.1, D_{Ni}=3.7), 15% fractional melting is sufficient to reproduce the entire Al-Ni and Yb-Ni lherzolite trends, while equilibrium melting models require 35-40%. Using higher partition coefficients for Ni and Yb (D_{Yb}= 0.14, D_{Ni}=13.05) reduces the amount of melting to about10%. Similarly, the harzburgites could be the residue of 25% (fractional) to 50% (equilibrium) melting and the dunites of 35% (fractional) to 60% (equilibrium) melting, using the lower set of partition coefficients for Ni and Yb. At first glance, the compositional range of the Cr-diopside peridotites can thus be interpreted as the residues of melting of a source with a composition equivalent to fertile lherzolite KRX-8. The LP xenoliths, however, have a very narrow range of relatively fertile compositions, whereas the KL xenoliths range from fertile lherzolites to depleted dunites (Fig. 2 and 6). The extent of melting thus differed in each suite, although overall the average degree of melting is about 7%.

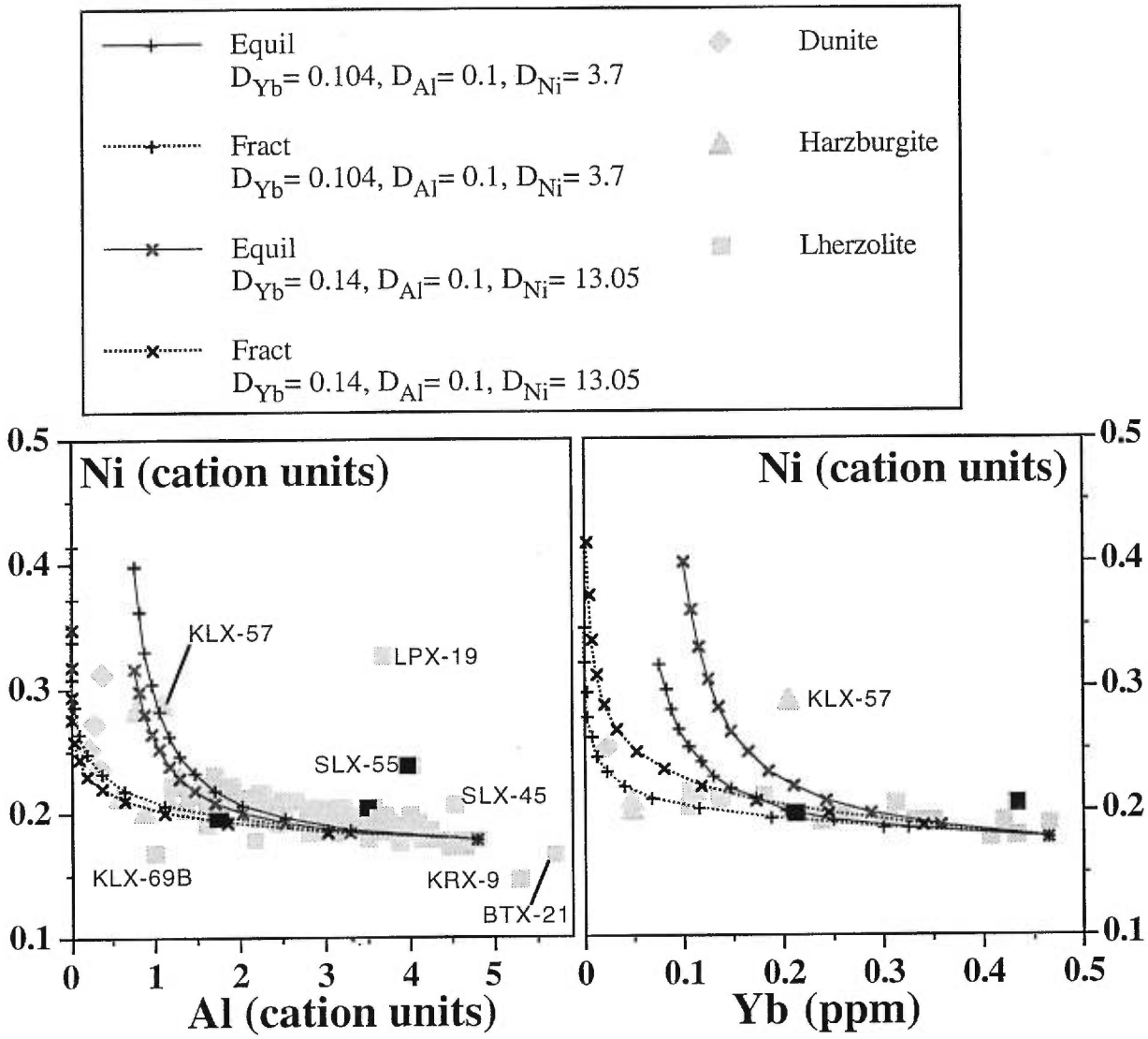

Fig. 13: Modelling of melting process and comparison with Cr-diopside suite data from the Southern Canadian Cordillera. Trace element equilibrium and fractional melting equations are from Shaw (1979). Source composition is taken as sample KRX-8 for the Al and Ni content, and as sample LPX-18 for the Yb content. Distribution coefficients between whole-rock and liquid (D) were calculated assuming a peridotite composed of 60% olivine, 25% orthopyroxene and 15% clinopyroxene and with the following mineral partition coefficients (Green, 1994): D_{Ni} Ol = 5 to 20; D_{Ni} Opx= 1.5 to 3; D_{Ni} Cpx= 2; D_{Yb} Ol = 0.02 to 0.04; D_{Yb} Opx= 0.2to 0.3; D_{Yb} Cpx= 0.2 to 0.8. Al partition coefficient was assumed to be around 0.1. Black plain line = equilibrium melting. Black dashed line = fractional melting. Lines with vertical crosses: partition coefficients between liquid and bulk-rock solid = 3.7 for Ni, 0.1 for Al, 0.104 for Yb. Lines with inclined crosses: partition coefficients between liquid and bulk-rock solid = 13.05 for Ni, 0.1 for Al, 0.14 for Yb. Increments are of 5%. Symbols as in Fig. 2.

A few samples, however, plot off the melting trends (Fig. 13). One harzburgite (KLX-57) has an elevated Yb content compared to its Al and Ni contents. Moreover, the total REE content of this sample is higher than that of other harzburgites, and even of that of lherzolites (Fig. 9). This sample contains Cpx-rich veinlets and might reflect the influx of fluids or melts rich in incompatible trace elements (Dautria et al., 1992). A few samples (LPX-19, SLX-55 and SLX-45) have high Ni contents, though their major element characteristics are similar to those of other samples. One lherzolite that plots below the melting trend in the Ni vs Al or Yb diagrams (KLX-69B) is a lherzolite vein from a harzburgite xenolith that was analysed separately from its host (KLX-69A).

Another process that may have affected the southern Cordilleran xenoliths is Ol addition at low pressure. Most dunites from the Canadian Cordillera plot at the MgO-rich end of the field of abyssal peridotites and one harzburgite and several depleted lherzolites plot within the field of abyssal peridotites (Fig. 7). Moreover, depleted lherzolites and harzburgites from the Southern Cordillera are within the abyssal field in a SiO_2 vs Mg diagram. In contrast, harzburgites from the Northern Canadian Cordillera (open triangles, Fig. 6) are richer in SiO_2 and Na_2O but poorer in FeO than that of the southern Cordilleran harzburgites (Francis, 1987; Fig. 6). However, the harzburgites and dunites of the Southern Canadian Cordillera are similar to another rare type of Fe-rich harzburgite in the Northern Canadian Cordillera (Fig. 7), which Francis (1987) interpreted to have suffered interaction with an alkaline melt at depth. By analogy with reactions observed between host lava and xenoliths, such a reaction is likely to preferentially enrich a Spinel peridotite in Fe, and deplete it in Al and Si, resulting in a more Ol-rich peridotite by the consumption of pyroxene and spinel (Francis, 1987). This process has recently been investigated by experiments at 1 atmosphere, which showed that very siliceous melts could be produced at the Opx-melt boundary by the reaction of peridotite with Si-undersaturated alkaline melts (Shaw, 1979). Orthopyroxene dissolution by alkali melt reacting with

peridotite may be responsible for the Fe rich composition of some of the depleted lherzolites, harzburgites and dunites in the southern Canadian Cordillera.

The extraction of melt should produce a correlation between the Ol content of peridotites and the Fo content of the Ol, the most depleted peridotites having Ol with the highest Fo contents (the "oceanic trend" of Boyd, 1989; Fig. 3). Olivine added from a migrating melt, on the other hand, should have a lower Fo content than that of the most depleted peridotites, leading to an opposite trend in which Fo content decreases with increasing Ol content, as has been proposed in abyssal peridotites (Niu and Hékinian, 1997). Two dunites, and a few harzburgites and lherzolites from the Southern Canadian Cordillera appear to reflect this process, having lower Ol Fo contents at high Ol contents.

Another possible origin for the range of peridotite compositions is melt/rock interaction transforming lherzolites into harzburgites by Opx addition (Kelemen et al., 1992), although due to the small porportion of harzburgites compared to lherzolites, we consider that this process is likely a minor one in the southern Canadian Cordillera.

2.7.1.3 Calculation of melt compositions in equilibrium with the Cr-diopside peridotites

The compositions of melts extracted from the Cr diopside peridotites were estimated using a simple mass balance calculation (source = residue + melt). Knowledge of the average Fo content of a residual xenolith and the Ol-liquid Fe/Mg equilibrium constant (K_D of 0.332 at 15 kbar and 1150°C (Ulmer, 1989), the degree of fusion can be estimated from the MgO and FeO contents of any chosen source and residue composition (Francis, 1987). Three different residual compositions were tested using KRX-8 as a source composition; a depleted lherzolite, and the average compositions of the harzburgites and of the dunites. Anomalously Fe-rich and Si-poor compositions were not included. Once the degree of fusion is determined (F), the compositions of melts (Table 9 and in Fig.

14) in equilibrium with the Ol in the residue were calculated by solving mass balance equations for each element (Francis, 1987).

Liquids L and H, calculated with the lherzolite, harzburgite and dunite as residues correspond to 20, 24.7 and 30% partial melting respectively. The compositions of liquids L and H (Fig. 14) do not resemble Mg-rich alkali basalts from the Canadian Cordillera (which are too Ca poor) or komatiites (which are too Al-poor and Fe-rich) or Mg-rich andesites (which are too Si-rich), but are similar to picritic liquids (Fig. 14). The only natural lavas known to have the high MgO contents and SiO_2 contents of melt D, are high Mg andesites from Japan (Tatsumi and Ishizaka, 1982) or ankaramites from the Canadian Cordillera (Johnston et al., 1996). These lavas however appear to be too Fe- and Ca-poor compared to melt D (Fig. 14)

The composition of experimental melts varies with pressure, temperature and H_2O content (Table 9). In particular, higher pressure favors lower SiO_2 and higher Na_2O and FeO, while higher H_2O content favors high SiO_2, Al_2O_3, Na_2O and lower FeO (Table 9). Comparing the compositional range of the Cr-diopside peridotites with simple mixing models between a depleted end member and experimental melts at different pressures can thus give an indication of the pressure at which melting occurred. KLX-61 was chosen as the depleted end-member (residue of melt L) and melts at 2 kbar (Falloon et al., 1988), 10, 15 and 30 kbar (Hirose and Kushiro, 1993), and one at 10 kbar and 0.5 wt% H_2O (Hirose and Kawamoto, 1995), were used as the other end-members (Fig. 15, Table 9). The mixing line that best fits the data involves an experimental melt produced at 15 kbar. The Cr-diopside peridotites are thus likely the result of melting around 15 kbar. However, many of the xenoliths have FeO contents which are high compared to the mixing lines with experimental melts.

Fig. 14 (next page): Melt compositions generated with the Southern Canadian Cordillera xenolith compositions compared to experimental data and primitive lava fields. In grey, melts caculated with the initial composition of lherzolite KRX-8. Open symbols, melts calculated with the initial composition KLB-1 (Hirose and Kushiro, 1993). Squares = melting to generate lherzolite KLX-61 (melt L). Triangles = melting to generate the average composition of harzburgites (melt H), excluding two Fe rich ones. Diamonds = melting to generate dunite KLX-66 (melt D). White crosses = experimental melts under anhydrous conditions at 10, 15, 25 and 30 kb (Hirose and Kushiro, 1993). Black stars = experimental melts under hydrous conditions (Hirose and Kawamoto, 1995). See Table 9 for details on the experimental conditions. Grey square boxes indicate the fields of primitive type lavas: P = picrites (references in Francis, 1995), K = komatiites (references in (Bernstein et al., 1998), A = high Mg andesite lavas (Tatsumi and Ishizaka, 1982), CC = primitive lavas from the Canadian Cordillera (Eiché et al., 1987), ANK = ankaramites from the Canadian Cordillera (Johnston et al., 1996).

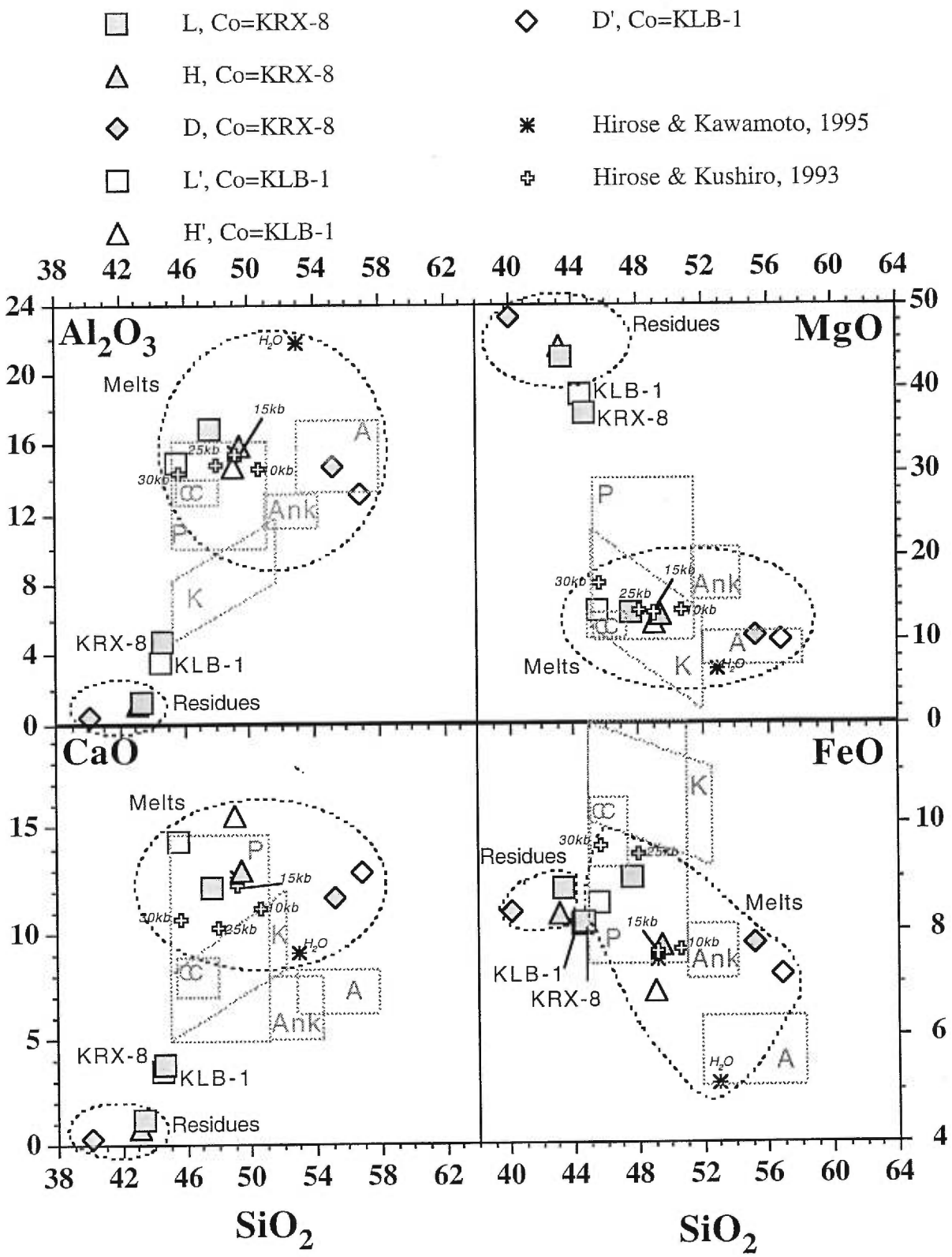
L, Co=KRX-8
H, Co=KRX-8
D, Co=KRX-8
L', Co=KLB-1
H', Co=KLB-1
D', Co=KLB-1
Hirose & Kawamoto, 1995
Hirose & Kushiro, 1993
Al2O3
Melts
Residues
KRX-8
KLB-1
MgO
CaO
FeO
SiO2
SiO2
15kb
25kb
30kb
10kb
H2O
A
Ank
cc
P
K

The compositions of the calculated liquids can be compared to experimental melts obtained by fusion of KLB-1, a fertile lherzolite from Kilbourne Hole (Hirose and Kushiro, 1993; Hirose and Kawamoto, 1995). Liquid compositions (L', H', D', Fig. 14) were recalculated using KLB-1 as a source. Melts L corresponds well to experimental melts generated at 15-25 kbar under dry conditions (Fig. 14), and corresponding to 13-19% melting (Hirose and Kushiro, 1993), while melt H corresponds well to an experimental melt produced at 10 kbar for which only Ol remains in the residue (Fig. 9). Moreover, the Ol Fo contents (89.9 and 91.2) of the lherzolite and harzburgite residues for liquids L' and H' correspond well with that in equilibrium with the closest experimental liquid (90.5 and 91). The degrees of fusion are similar for melt L' and the experimental melt at 15 kbar (20% and 18.9% respectively), but the degree of fusion for melt H' is slightly higher than that of the experimental liquid having Ol as the sole residue (24.7 and 20% respectively).

Fig. 15 (next page): Mixing models of depleted lherzolite KLX-61 with experimental melts at various pressure and H_2O content, and comparison with Cr-diopside suite data from the Southern Canadian Cordillera. Basaltic melts compositions from the experiments of Falloon et al. (1988), Hirose and Kushiro (1993), Hirose and Kawamoto (1995) The experimental melts are given in Table 9. Symbols as in Fig. 2.

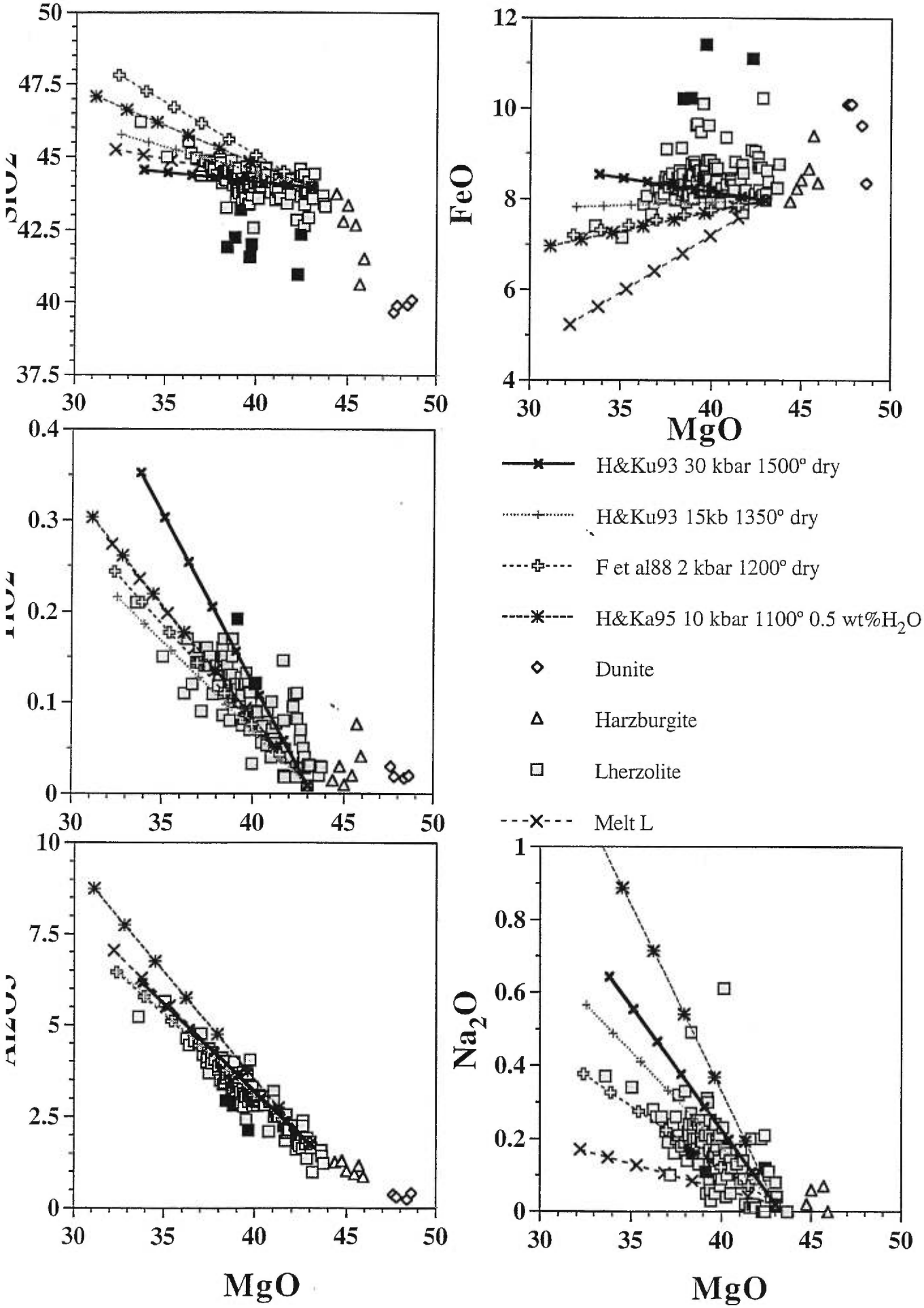
SiO2
FeO
TiO2
Na2O
Al2O3
MgO
MgO
H&Ku93 30 kbar 1500° dry
H&Ku93 15kb 1350° dry
F et al88 2 kbar 1200° dry
H&Ka95 10 kbar 1100° 0.5 wt%H2O
Dunite
Harzburgite
Lherzolite
Melt L

	Co KRX-8	Residue KLX-61	Liq L KRX-8 KLX-61	Residue Harz av	Liq H KRX-8 Harz av	Residue KLX-66	Liq D KRX-8 Dun av
Fo			89.89		91.16		90.1
F % melt			20		24.66		30.4
SiO2	**44.69**	43.95	47.66	43.13	49.46	40.09	55.20
TiO2	**0.16**	0.009	0.77	0.02	0.59	0.02	0.48
Al2O3	**4.77**	1.75	16.88	1.13	15.89	0.41	14.73
FeO	**8.17**	7.97	8.97	8.32	7.73	8.35	7.76
MnO	**0.13**	0.128	0.14	0.13	0.13	0.13	0.13
MgO	**37.04**	43	13.18	44.89	13.07	48.62	10.58
CaO	**3.77**	1.67	12.19	0.78	12.92	0.31	11.68
Na2O	**0.19**	0.02	0.87	0.04	0.65	0.00	0.62
K2O	**0.09**	0	0.45	0.03	0.29	0.01	0.27
P2O5	**0.01**	0.002	0.04	0.01	0.01	0.01	0.01
NiO	**0.26**	0.32	0.02	0.33	0.04	0.50	-0.29
Cr2O5	**0.38**	0.394	0.32	0.46	0.13	0.90	-0.81
Total	**99.66**	99.213	101.50	99.79	100.90	99.68	100.37

	Co KLB-1	Residue KLX-61	Liq L' KRX-8 KLX-61	Residue Harz av	Liq H' KRX-8 Harz av	Residue Dun KLX-(	Liq D' KRX-8 Dunite av
Fo			89.89		91.16		90.1
F % melt			13.1		17.43		24.4
SiO2	**44.48**	43.95	45.55	43.13	49.08	40.09	56.89
TiO2	**0.16**	0.009	1.10	0.02	0.80	0.02	0.58
Al2O3	**3.59**	1.75	14.95	1.13	14.71	0.41	13.17
FeO	**8.1**	7.97	8.50	8.32	6.83	8.35	7.17
MnO	**0.12**	0.128	0.06	0.13	0.07	0.13	0.09
MgO	**39.22**	43	13.53	44.89	11.95	48.62	9.88
CaO	**3.44**	1.67	14.36	0.78	15.50	0.31	12.87
Na2O	**0.3**	0.02	2.04	0.04	1.48	0.00	1.20
K2O	**0.02**	0	0.14	0.03	0.00	0.01	0.05
P2O5				0.01	0.12	0.01	0.09
NiO				0.33	-0.14	0.50	-0.51
Cr2O5	**0.31**	0.394	-0.23	0.46	-0.40	0.90	-1.49
Total	**99.74**	98.89	100.00	99.79	100.00	99.68	100

	Hirose et Kawamoto 1995			Hirose et Kushiro 1993					Falloon88
	KLB-1	Run 36	Run 40	**KLB-1**	Run 16	Run 19	Run 23	Run 25	Run 26
	Co	10kb	10kb	**Co**	10kb	15kb	25 kb	30kb	2 kb
		1100ºC	1300º		1350º	1350º	1425º	1500º	1200º
Residual phases		OlOpx CpxSp	OlOpx CpxSp		Ol Opx	OlOpx Cpx	OlOpx Cpx	OlOpx Cpx	OlOpx CpxSpPl
Fo	**89.1**	89.6	91.7	**89.1**	91	90.6	90.5	90.1	92.8
F % melt		7	17.8		20	18.9	12.6	16.6	81
H2O wt %		0.5	0.1						
SiO2	**44.48**	52.89	49.2	**44.48**	50.67	49.13	47.97	45.67	54.99
TiO2	**0.16**	0.85	0.57	**0.16**	0.42	0.6	0.83	0.99	0.68
Al2O3	**3.59**	21.73	15.55	**3.59**	14.61	15.18	14.88	14.33	15.18
FeO	**8.1**	5.11	7.46	**8.1**	7.64	7.54	9.43	9.59	
MnO	**0.12**	0.19	0.18	**0.12**	0.13	0.14	0	0.17	5.78
MgO	**39.22**	6.58	12.56	**39.22**	13.39	13.11	13.36	16.73	0
CaO	**3.44**	9.06	12.69	**3.44**	11.17	12.28	10.23	10.64	8.94
Na2O	**0.3**	3.49	1.62	**0.3**	1.5	1.58	2.37	1.8	12.67
K2O	**0.02**	0.07	0.06	**0.02**	0.19	0.08	0.82	0.07	1.04
Cr2O5	**0.31**	0.03	0.11	**0.31**	0.28	0.36	0.11	0.21	
Total	**99.74**	100	100	**99.74**	100	100	100	100	99.28

Table IX: Composition of computed melts in equilibrium with 2 depleted lherzolites (KRX-8 and SLX-27), average harzburgites and average dunites. Experimental melts, their starting compositions and the experimental conditions.

Melt D' was calculated for a dunite residue with an Ol of composition Fo 90. Experimental melts for which only Ol remains in the residue, however, are in equilibrium with more forsteritic Ol (92 to 93; Falloon et al., 1988). Although the dunite chosen for residue in the melt calculation was the lowest in Fe, it still may be linked to other processes than melting.

2.7.1.4 Trace element variations

Incompatible elements such as Rb, Ba and sometimes Sr are relatively mobile in sub-surface environments (Pearce, 1983) and may also reside in interstitial accessory phases. Rb and Ba, for example, have been shown to reside in a layer of oxides surrounding spinel grains (Bodinier et al., 1996). Highly incompatible elements have very low concentrations in mantle xenoliths, and the composition of bulk xenoliths is thus very sensitive to alteration or host magma infiltration. Most Cr-diopside xenoliths from the southern Canadian Cordillera have relatively high Rb and Ba primitive-mantle normalized contents compared to HREE, and two of them (KRX-14 and RRX-19) exhibit a positive anomaly in Sr (Fig.11). These are likely due to post-eruption alteration processes by a sub-surface fluid enriched in Rb, Ba and Sr compared to the peridotite, however, no particular alteration features were noted in the thin sections.

The HREE and MREE correlate with indices of fusion such as MgO or Al_2O_3 in the Southern Canadian Cordillera xenoliths. The Tb/Yb ratio has been used to distinguish between melting in the spinel and garnet facies (Bodinier et al., 1988), because HREE such as Yb, are strongly partitionned into garnet during melting. The Tb/Yb ratio will decrease rapidly during the first 10 % of fusion in the garnet stability field, whereas this ratio will be less affected in the spinel stability field (Fig. 16; Bodinier et al., 1988; McDonough and Frey, 1989). Most of the lherzolites from the Canadian Cordillera follow the melting trend calculated for the Spinel stability field, from the fertile lherzolite to the harzburgites. The

Southern Cordillera xenoliths thus appear to be residues of melting in the Spinel stability field. Two harzburgites (RRX-19 and RRX-21) have very depleted REE patterns, consistent with partial melting. This is unusual for continental Spinel Cr-diopside suites where the most major element depleted peridotites are generally enriched in incompatible trace elements (McDonough and Frey, 1989; and Fig. 10). Xenoliths that plot above the Tb/Yb vs Al_2O_3 trend may have suffered sufficient metasomatism that the MREE were affected.

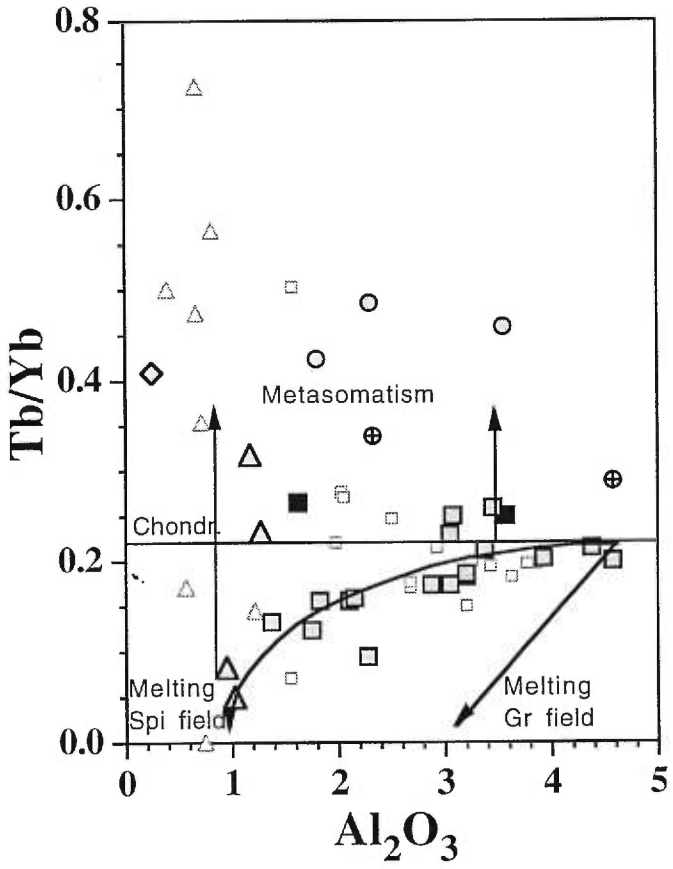

Fig. 16: Tb/Yb vs Al_2O_3 in Canadian Cordillera xenoliths and trends for melting in the Spinel and garnet stability field and for metasomatism. Northern Canadian Cordillera data are unpublished data from Shi et al. Symbols as in Fig. 2 and 4.

The majority of the Cr-diopside lherzolites have depleted REE patterns (Fig.9), most likely the result of melting with loss of the most incompatible elements into the melt

(e.g. BT, RR, 2 SL lherzolites). These lherzolites generally have a MREE/HREE< 1 (gently sloping REE pattern from HREE to MREE) consistent with the increasing degree of compatibility from MREE to HREE. Samples from LP and LL, and two samples from KRX, however, have MREE/HREE about 1 (flat REE pattern from HREE to MREE). This might be explained by the low degree of melting that depleted the samples in the most incompatible REE, but did not affect the more compatible elements like MREE and HREE.

BT samples are selectively enriched in LREE and are consistent with chromatographic metasomatic process, controlled by equilibration at the grain surface and volume diffusion in the minerals (Takazawa et al., 1992). A LREE enriched melt percolating through a LREE depleted peridotite first affects La (similar to BTX-16), then Ce (similar to BTX-34) and then Nd (similar to BTX-23), i.e. in the order of increasing partition coefficient values. The same process can explain the REE patterns of KR, RRX-10, KLX-45, LLX-7 and SLX-30. The KR lherzolites are the only ones, however, to show a systematic negative Ce anomaly compared to La and Pr. As seawater typically has negative Ce anomalies, which in turn creates Ce anomalies in altered Mid Ocean Ridge Basalts (MORB), and some marine sediments, it has been suggested that Ce anomalies in mantle rocks could be due to metasomatism by melts or fluids derived from subducting slab (Ionov et al., 1995, and references therein). However, this feature is not seen in the two other xenoliths sites close to KR (LP and LL). Although three LP lherzolites analysed for trace elements (LPX-11, 16 and 18) contain amphibole, only one shows the strong LREE enrichment (more than 10 times chondrites) typical of hydrous lherzolites (McDonough and Frey, 1989). Finally, the steep REE patterns of most harzburgites and of the two dunites are typical of major-element depleted spinel-peridotites (Bedini et al., 1997; Shi et al., 1998; see also Fig. 10). These patterns could be explained by chromatographic effects involving the porous flow of small melt fractions (Bodinier et al., 1990; Bedini et al., 1997), by the different physical properties of harzburgites compared to

lherzolites (McKenzie, 1984; Takazawa et al., 1992), or by the simultaneous melting of lherzolites to give harzburgites enriched in incompatible elements, triggered by the influx of fluids or melts (Ionov et al., 1994; Shi et al., 1998).

The behavior of High Field Strength Elements (HFSE) in the mantle is a controversial subject. The debate on HFSE has mainly focused on the relationship between peridotites and subduction zone lavas, many of which exhibit negative Nb and Ta anomalies. Salters and Shimizu (1988) argued for a world-wide lithospheric mantle depleted in HFSE, based on trace element analyses of Cpx. In the Canadian Cordillera whole-rock trace element patterns (Fig. 11), HFSE depletion is common but not systematic, as for example lherzolites RRX-10, KLX-45, harzburgites LLX-1 and KLX-47, and dunite KLX-57 do not have negative Hf and Zr anomalies. Indeed, studies of mineral separates showed that the HFSE depletion seen by Salters and Shimizu (1988) in Cpx is compensated by positive anomalies in other minerals (e.g., Rampone et al., 1991), and that HFSE characteristics of mantle xenoliths are inconsistent with these rocks being the residues of island arc magmatism (Jochum et al., 1989). In a study of Southern Canadian Cordillera xenoliths (KR, BT, LL and Jacque Lake sites), Sun and Kerrich (1995) related the size of the HFSE anomalies to the modal proportions of minerals, because Zr, Hf and Ti mainly reside in Cpx, while Nb and Th are as abundant in Opx as in Cpx. The Zr and Hf contents of the Cr-diopside lherzolites showing a broad correlation with Al_2O_3, an index of fusion, appear to be mainly controlled by melting processes (Fig. 12). The three samples (LLX-7, LPX-18 and KRX-14) plotting off these correlations likely suffered metasomatism, as shown by their enriched LREE patterns compared to those of the other Cr-diopside lherzolites (Fig. 9)

Enrichment in LREE coupled with negative anomalies in Ti, Zr and Hf has been attributed to carbonate metasomatism (Hauri et al., 1993; Rudnick et al., 1993). These features appear to be characteristic of xenoliths containing apatite that is rich in REE, but very poor in HFSE (Ionov et al., 1993). Carbonate metasomatism may be responsible for

the trace element characteristics of BT, because of the marked negative HFSE anomalies in the xenoliths at this site. KR shows similar characteristics as BT, besides its Ce negative anomaly. LP has similar HFSE characteristics to BT, but the presence of modal amphibole in this suite also argues for a hydrous rather than a carbonatitic fluid. It is thus hard to distinguish the type of metasomatic agents active in the Southern Canadian Cordillera suites. They may be subduction related fluids. Most analysed xenoliths have negative Zr, Hf and Ti anomalies, and varing enrichment in LREE. These may be the dominant characteristics of fluids or melts percolating in the lithospheric mantle beneath the Southern Canadian Cordillera.

2.7.1.5 Comparison with other peridotites from around the world

2.7.1.5.1 Comparison to northern Canadian Cordillera xenoliths

All suites from northern Canadian Cordillera are relatively fertile in compositions, i.e. most samples of each suite have lherzolites with Al_2O_3 contents higher than 3 wt% (Fig. 6). The most fertile suite is that of Fort Selkirk with Al_2O_3 contents up to 6 wt % (Francis, 1987). In the South, only two xenolith suites have a majority of samples with Al_2O_3 content higher than 3, LP and RR, the southern most sites in the Canadian Cordillera. The other sites are more depleted, and KL shows the most extreme depletion with most of its samples having Al_2O_3 below 2.5 wt %. No relation between the degree of fertility and tectonic terrane or belt is apparent.

Some of the northern xenolith suites (Llangorse, Alligator Lake and Hirshfield) are, however, bimodal, i.e. characterized by high proportions of both harzburgites and lherzolites (Fig. 6; Francis, 1987; Shi et al., 1998) These three sites are geographically close and the harzburgites are interpreted to result from recent metasomatism-induced melting, linked to an underlying region of anomalously hot mantle that has been detected

teleseismically (Frederiksen et al., 1998; Shi et al., 1998). The lherzolites of the bimodal suites range from Cpx-rich (25%) to Cpx-poor (5%) lherzolite, similar to the lherzolites of the Southern Canadian Cordillera (Fig. 2). The lherzolites from the unimodal suites, comprised only of lherzolites in the northern Canadian Cordillera, have a narrower range of Cpx contents, from about 10 to 15%, and a wider range of Opx contents (10 to 40% Opx) (Shi et al., 1998), compared to the lherzolites in southern Canadian Cordillera and in the bimodal suites (20-35% Opx) (Fig. 2). When compared to the melting-model trends calculated for the southern Canadian Cordillera, the range of most lherzolites in the unimodal suites of the northern Canadian Cordillera require only a small range in degree of fusion (Fig. 17). For example, they can be produced by 2.5 to 7.5 % of fusion of a pyrolite type source with a fractional melting model and 2.5 to 10% for equilibrium melting. These differences between the unimodal suites of Northern Canadian Cordillera and the lherzolites from the Southern Canadian Cordillera may reflect overall lower degrees of fusion in the North compared to the South.

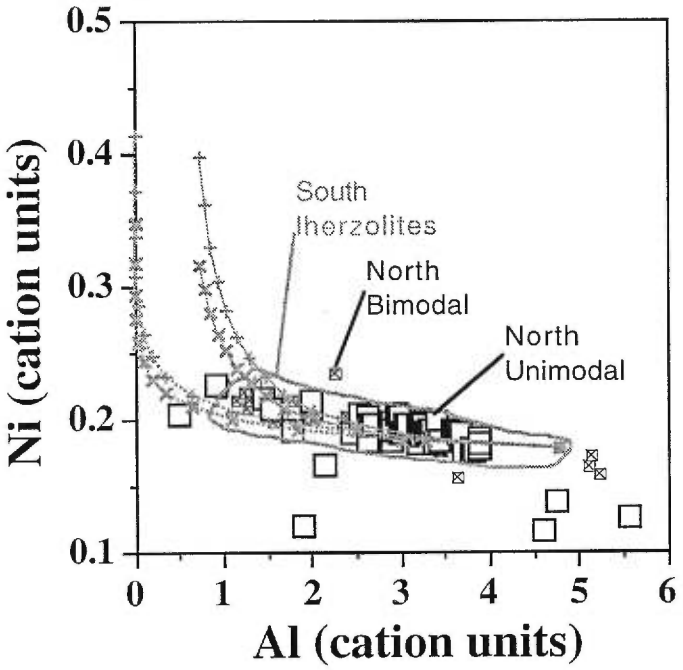

Fig. 17: Modelling of melting process and comparison with Cr-diopside suites from northern Canadian Cordillera. Modelling as in Fig. 8. Big white squares = unimodal suites (i.e. mainly comprised of lherzolites) from northern Canadian Cordillera; small squares with a cross = lherzolites from bimodal suites (i.e. comprising the same amount of both harzburgites and lherzolites) from northern Canadian Cordillera; grey field = Cr-diopside lherzolites from the southern Canadian Cordillera.

Finally, Sr and Nd isotopes of the Southern Canadian Cordillera, and one Sr and Pb analysis for the unimodal suites (Selkirk) in the northern Canadian Cordillera, plot within the MORB field (Xue et al., 1990; Sun et al., 1991; and unpublished data of Carignan). The bimodal suites, on the other hand, range from MORB-like to higher than MORB Sr and Pb ratios, reflecting a greater degree of metasomatism (Carignan et al., 1996).

2.7.1.5.2 Comparison to peridotites from various tectonic settings

Canadian Cordilleran peridotites are very different from continental garnet peridotite xenoliths, in which the major element correlations are less well developed (Fig. 7). In particular, the SiO_2 range of garnet peridotite is wider than that of Spinel peridotites (Fig. 7), and garnet peridotites found in some cratonic settings tend to be more Opx-rich (Boyd, 1989). Boyd (1989) used a plot of modal olivine vs forsterite content to distinguish between cratonic and "oceanic" lithosphere (Fig. 3). In this diagram abyssal and ophiolitic peridotites form a concave upward trend that Boyd called "oceanic trend". Low-temperature garnet peridotites from kimberlites in cratonic settings plot above this trend and the high-temperature ones plot at the high Fo end of the "oceanic trend". Spinel peridotites in alkaline basalts plot along the "oceanic trend", as do the Canadian Cordillera Cr-diopside peridotites (Fig. 3). The "oceanic trend" is likely due to partial melting, while peridotites plotting off this trend, such as cratonic xenoliths, have suffered additional processes; such as depleted harzburgites being formed by melt/rock interaction (with Opx forming at the expense of Ca-Cpx in the upper mantle), and have a deeper origin in the continental lithosphere (Boyd, 1989; Kelemen et al., 1992). The similarity between the spinel peridotite and the oceanic trend led Boyd (1989) to suggest that these xenoliths may be derived from oceanic lithosphere accreted at the margin of archean cratons.

Fig. 18 (next page): Comparison of the Canadian Cordillera xenolith compositions with that of oceanic peridotites. Sp Cr# = Cr/(Cr+Al) of Spinel; Sp Mg# = Mg/(Mg+Fe^{2+}) in Spinel with Fe^{2+} calculated using the structural formula AB_2O_4 for spinel (Table 6); Fo Ol = forsterite content of olivine caculated as Mg/(Mg+Fe), Fe being all Fe as Fe^{2+}. The grey lines delimitate the "OSMA" (Olivine-Spinel Mantle Array) trend of Arai (1994). Thick dashed curve delimitates the field for abyssal peridotites (Arai, 1994; Niu et al., 1997). Thick dashed curve delimitates the field for back-arc to arc peridotites from Japan, and in diagram 19b from Japan and Kamtchatka (Aoki and Shiba, 1973; Arai, 1980; Takahashi, 1980; Aoki, 1987; Ozawa, 1988; Arai, 1991; Kepezhinskas et al., 1993; Ozawa, 1994; Kepezhinskas et al., 1995; Umino and Yoshizawa, 1996) and from Fig. 4D of Arai (1994). Black curve = arc peridotites (Bloomer and Fisher, 1987; Neal, 1988; Maury et al., 1992; Parkinson and Pearce, 1998). Thick black cross = intraplate oceanic lithosphere, mantle xenoliths from Hawaii (Jackson and Wright, 1970; Goto and Yokoyama, 1988; Sen, 1988). Thick cross with a circle = intraplate oceanic lithosphere, mantle xenoliths from Tahiti (Tracy, 1980). Gray points (squares, triangles and diamonds, symbols as in Fig. 2 and 4) = Canadian Cordillera Cr diopside xenoliths (this study and Francis, 1987; Shi et al., 1998).

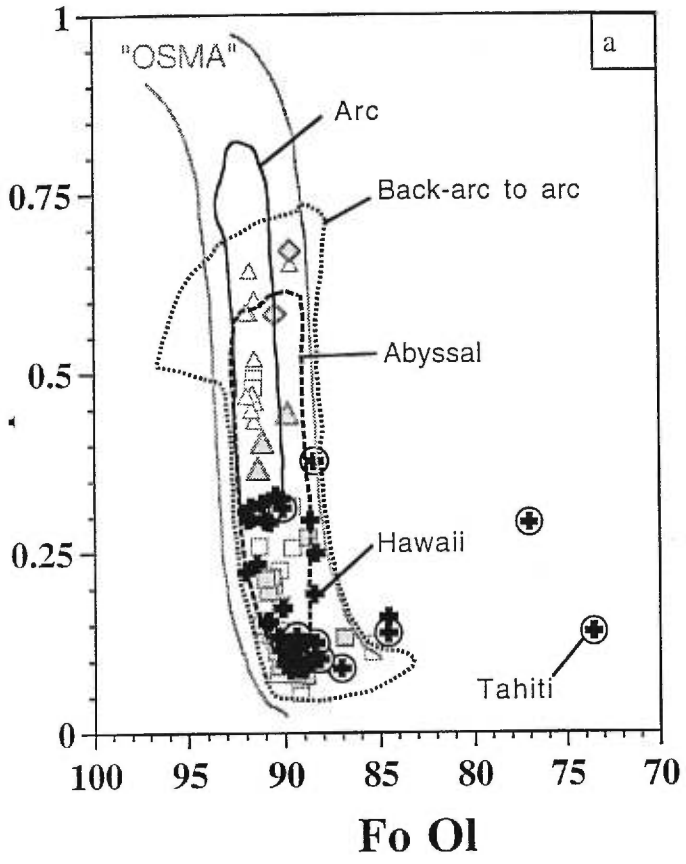
a
"OSMA"
Arc
Back-arc to arc
Abyssal
Hawaii
Tahiti
1
0.75
0.5
0.25
0
100
95
90
85
80
75
70
Fo Ol

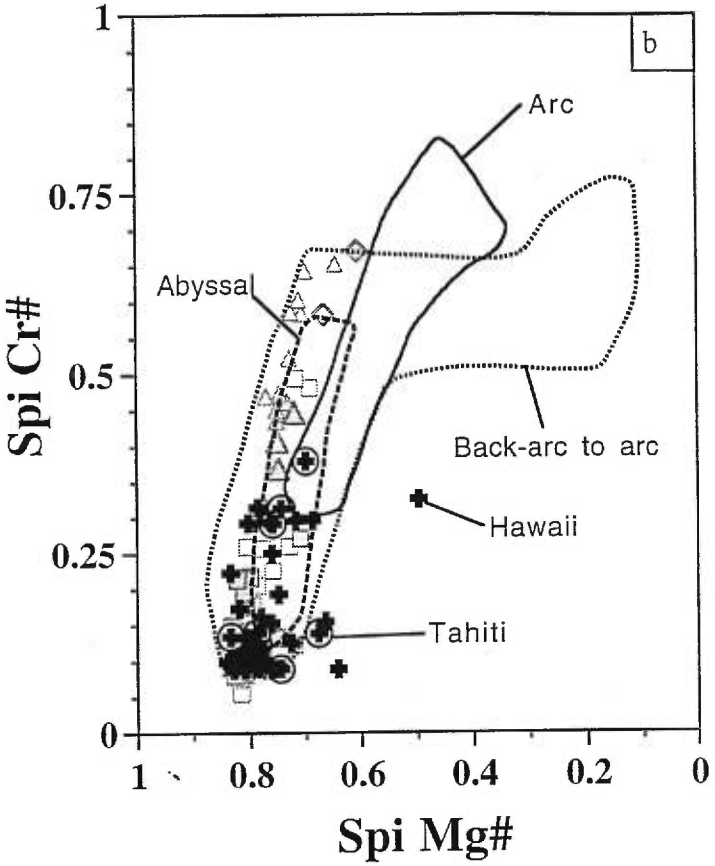
b
Arc
Abyssal
Back-arc to arc
Hawaii
Tahiti
Spi Cr#
1
0.75
0.5
0.25
0
1
0.8
0.6
0.4
0.2
0
Spi Mg#

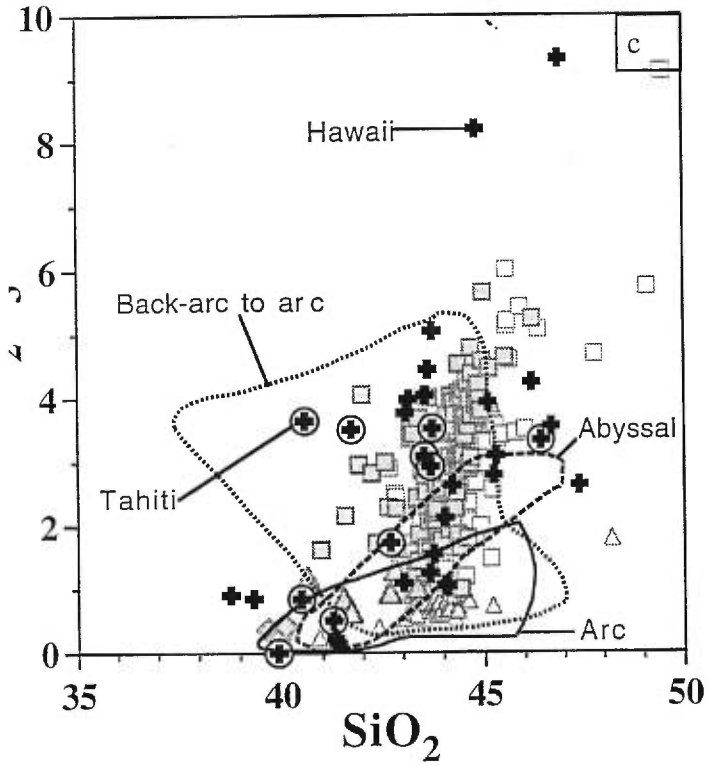
c
Hawaii
Back-arc to arc
Tahiti
Abyssal
Arc
10
8
6
4
2
0
35
40
45
50
SiO2

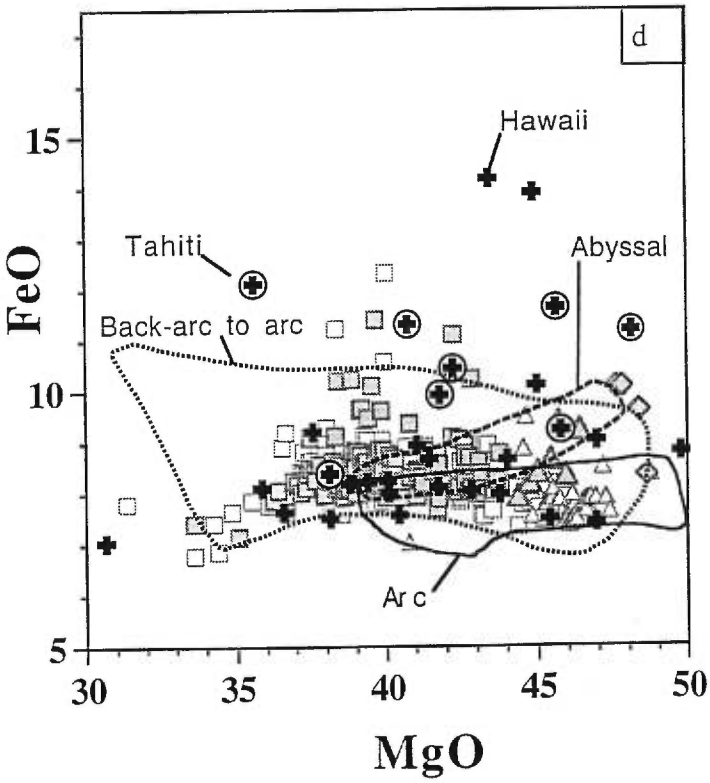
d
Hawaii
Tahiti
Abyssal
Back-arc to arc
Arc
FeO
15
10
5
30
35
40
45
50
MgO

A comparison of continental spinel peridotites with abyssal peridotites (Fig. 7) shows that the latter have a narrower range of whole rock compositions and define more depleted compositions. Unlike the continental peridotites, FeO may correlate positively with MgO in abyssal peridotites (Niu et al., 1997), and NaO is higher at a given MgO in abyssal peridotites than in other types of peridotites (Elthon, 1992; Fig. 7). These particularities of the abyssal peridotites have been interpreted as the result of low pressure refertilisation by melts (Elthon, 1992) or Ol crystallization from percolating melts (Niu et al., 1997). All abyssal peridotites have clinopyroxene REE patterns systematically depleted in LREE (Johnson et al., 1990), wheareas the REE patterns of continental spinel peridotites range from depleted to enriched types (e.g., McDonough and Frey, 1989), Fig. 9). The composition of chromian Spinel has been used to discriminate between different types of peridotites, their petrogenesis and tectonic setting (Dick and Bullen, 1984; Arai, 1994; Fig. 18). Cr-diopside suites from the Canadian Cordillera plot within the Olivine Spinel Mantle Array ("OSMA") defined by Arai as the locus of most Spinel xenoliths (oceanic and continental) and orogenic massifs and ophiolites. Abyssal peridotites broadly overlap the field for the Canadian Cordillera xenoliths in the Spinel Cr# vs forsterite content of olivine and Spinel Cr# vs Spinel Mg# diagrams.

Mantle xenoliths brought up by OIB lavas are also samples of the oceanic mantle, but sampled at greater depth. Hawaiian xenoliths typically have low Sp Cr# compared to abyssal peridotites and overlap the Canadian Cordillera lherzolite range in all diagrams. Tahitian xenoliths are, however, poorer in SiO_2 and richer in FeO, and their Ol have lower Fo contents than those from Hawaii and the Canadian Cordillera. The low Ol Fo contents of most Tahitian xenoliths compared to the "OSMA" trend may argue against these xenoliths being representative of typical oceanic mantle. Spinel lherzolites from continental settings such as the Canadian Cordillera xenoliths resemble intraplate oceanic lithosphere represented by Hawaiian xenoliths.

Arc related peridotites can be divided in two groups; forearc peridotites such as on the Solomon islands, the Izu-Bonin-Marianas and Tonga Trenches, and "transitional" arc peridotites from fore-arc to back-arc settings, such as the Japanese and Kamtchatka peridotites (Arai, 1994). Fore-arc peridotites are very depleted (high MgO, low FeO, low Al_2O_3) and have systematically high Sp Cr# and Sp Mg#. Their high Sp Mg#, distinguishes them from the depleted harzburgites from the Canadian Cordillera, which have relatively low Sp Mg#. These high Mg# for Sp have been attributed to low temperature equilibration (Dich and Bullen, 1984) or to high oxygen fugacity, thought to be typical of arc settings (Wood and Virgo, 1989; Wood et al., 1990; Brandon and Draper, 1996; Parkinson and Pearce, 1998) which results in the transformation of spinel + olivine to pyroxene + magnetite (Bernstein et al., 1998). Transitional arc peridotites have compositions varying from those of oceanic intraplate settings like back-arc peridotites to that of true arc peridotites. Canadian Cordillera lherzolites have lower Sp Cr#, Sp Mg# and MgO content, and higher FeO and Al_2O_3 than peridotites in arc setting, but are similar to those of back-arc setting peridotites. The southern Canadian Cordilleran xenoliths have equilibrated at low oxygen fugacities (Canil et al., 1990) compared to arc peridotites (Parkinson and Pearce, 1998). As such, the Canadian Cordillera xenoliths are not likely to be the residues of melting in an arc tectonic setting. The southern Canadian Cordillera lherzolites are very similar to those of Sikhote-Alin, the southeastern edge of Siberia, in terms of composition and oxygen fugacity (Ionov and Wood, 1992; Ionov et al., 1995). The tectonic setting of the Sikhote-Alin is similar to that of the Canadian Cordillera as it formed by the accretion of terranes to the edge of a craton, and was bordered by a subduction zone during the Mesozoic (Ionov and Wood, 1992; Ionov et al., 1995). The characteristics of the Canadian Cordillera lherzolites is thus not unique, and appears to be typical of the lithospheric mantle beneath young orogenic belts bordering cratons.

2.7.2 The wehrlite suites

The major element compositions of the wehrlite xenoliths extend to more FeO-rich compositions with lower MgO, and much higher TiO_2 and Na_2O than those of the most fertile lherzolites (Fig. 8). As a first remark, host lavas KL-1 and SL-1 are too low in Si, Ca and too high in Ti, Al, Fe and Na to have any genetical link with the wehrlite suite xenoliths (Fig. 2). Secondly, the wehrlites can be divided in two groups; one with low Fo contents of Ol (<86), which includes all the KL and part of the SL wehrlites. Three of the clinopyroxenites from KL align perfectly with the KL wehrlite major element trends, and are thus likely to be included in this group (Fig. 8); the second group has high Fo content of Ol (>87) (similar Fo contents as the Ol of the Cr-diopside peridotites), which includes the rest of the SL wehrlites (Fig. 3). The latter have FeO contents that have the same range as those of the Cr-diopside peridotites (Fig. 8). Two pyroxenites from SL also align with the high-Fo SL wehrlites, and are thus included in the group (Fig. 8).

In order to test whether the wehrlite compositional ranges reflect melting, model calculations were compared to the wehrlite data in a diagram of a compatible (Ni) vs an incompatible element (Al or Yb; Fig. 19). The most Al-rich wehrlite in each suite was chosen as a possible source (KLX-27 for the low-Fo group and SLX-54) for the high-Fo group. For the Yb content, that of KLX-11 was used because KLX-27 has not been analysed for trace elements. Equilibrium and fractional melting equations of Shaw (1979) were used, with the same partition coefficients as those used when modelling the Cr-diopside peridotites (see caption of Fig. 8). As can be seen in Fig. 19, the low-Fo wehrlites from KL have a too wide range in Ni content to be the residues of partial melting. KL wehrlites present a steep positive correlation of FeO content vs MgO content (Fig. 8), which may not be compatible with a series of residues during a melting process (Niu et al., 1997). The wehrlite suites at KL are thus, not likely the residues of partial melting processes. The high-Fo SL wehrlites, on the other hand, fit the melting trend, although

their scatter around the melting lines is relatively large (Fig. 19). However, the positive correlation between FeO and MgO for this group suggests an interaction between a melt and peridotite, such as was described for the Fe-rich depleted Cr-diopside peridotites. This is in agreement with the alignment of the two SL pyroxenites with these four wehrlites in all major element diagrams (Fig. 8) and which may represent the composition of the melt. Also, SLX-8, belonging to the high-Fo group, is enriched in trace elements, HREE included, compared to melting residues such as the Cr-diopside peridotites (Fig. 9 and 12).

Another possibility is that the wehrlite peridotites represent the crystallisation of a liquid passing through the Canadian Cordillera lithospheric mantle. Crystallisation is consistent with the wide range of Ni contents displayed by the KL wehrlites (Fig. 14), and with the low Fo content of olivine compared to that of the Cr-diopside suites (Fig. 15). A cumulate origin has been invoked for the origin of Al-augite suites (some of which have the poikiloblastic texture seen in the wehrlites; e.g., Frey and Prinz, 1978) and of the pyroxenite layers found in peridotite orogenic massifs (e.g., Bodinier et al., 1987; Becker, 1996). The composition of the Canadian Cordillera wehrlites is, however, different from that of the Al-augite suites and from the pyroxenites, in that most Canadian Cordillera wehrlites are more refractory than the majority of Al-augite suite xenoliths (Fig. 8). With the three KL pyroxenites included in the KL wehrlite suite, the latter resembles other Al-augite xenoliths from the literature. The KL and SL suite extend, nevertheless, to more refractory compositions than the majority of Al-augite suites. Simple modelling of the compositions as crystal cumulates of a magma undergoing crystallisation was calculated using the equations of Allègre and Minster (1978). The composition of the initial melt was taken as that of a melt in equilibrium with Al-poor wehrlites KLX-65. Simple crystallisation cannot, however, reproduce the data, as the Ni content of the cumulate of simple crystallisation drops too quickly compared to the wehrlite trend (Fig. 19).

The KL wehrlites may thus represent physical mixtures of Ol and Cpx during crystallisation, the dunites defining the highest Mg and Fe, and the lowest Si, Ti, Al, Ca

and Na values, the clinopyroxenites having the opposite characteristics, the wehrlites being intermediate. The oikocrystic Cpx in these rocks may be in part trapped liquid. Such a process can be modelled in the Ni versus Al diagram by a crystallization process involving the trapping of part of the melt phase. The starting liquid composition is taken as that of a liquid in equilibrium with dunite KLX-65. The fractional crystallization calculation is the same as that done previously (Allègre and Minster, 1978), except that an increasing amount of trapped liquid (x_i) is included during the process, with the equation: $C_{wehr} = C_s + x_i.C_l$. , with C_s being the composition of the cumulate, and C_l the composition of the liquid, calculated with fractional crystallisation equations. With 5% increments of trapped liquid proportion during the fractional crystallisation process ($x_{i+1} = x_i+5\%$), the entire KL trend can be reproduced after 65% of crystallization. The KL werhlites thus represent the cumulates of a crystallizating liquid, which includes liquids trapped between the cumulus phases. The low-Fo SL-wehrlite may be the result of a similar process, but there are not enough samples from this group to allow effective modelling as for the KL wehrlites.

Fig. 19 (next page): Modelling of melting and crystallization processes for the wehrlite suite. Same symbols as in Fig. 2 and 14. Trace element melting and crystallization equations are from Allègre and Minster (1978) and Shaw (1979). For the KL suite melting modelling (black lines), source composition is taken as sample KRX-27 for the Al and Ni content (6.01 and 0.058 cations units respectively), and as sample KLX-11 for the Yb content (0.403 ppm). For the KL suite crystallisation modelling (vertical grey lines), the composition of the crystallized composition is obtained from a magma initially in equilibrium with dunite KLX-65 (Al = 0.328 cation units, Ni = 0.196 cation units, Yb = 0.04 ppm). Distribution coefficients between whole-rock and liquid (D) were calculating using a whole-rock composition of 65% Ol and 35% Cpx and the same distribution coefficients as in Fig. 13. Black plain line = equilibrium melting. Black dashed line = fractional melting. Lines with vertical crosses: partition coefficients between liquid and bulk-rock solid = 3.95 for Ni, 0.1 for Al, 0.083 for Yb. Lines with inclined crosses: partition coefficients between liquid and bulk-rock solid = 13.7 for Ni, 0.1 for Al, 0.306 for Yb. Same symbols but in grey for the equilibrium and fractional crystallisation modelling. Lower diagram; fractional crystallization with 1 or 5% increments of trapped liquid amounts (see text for explanation)

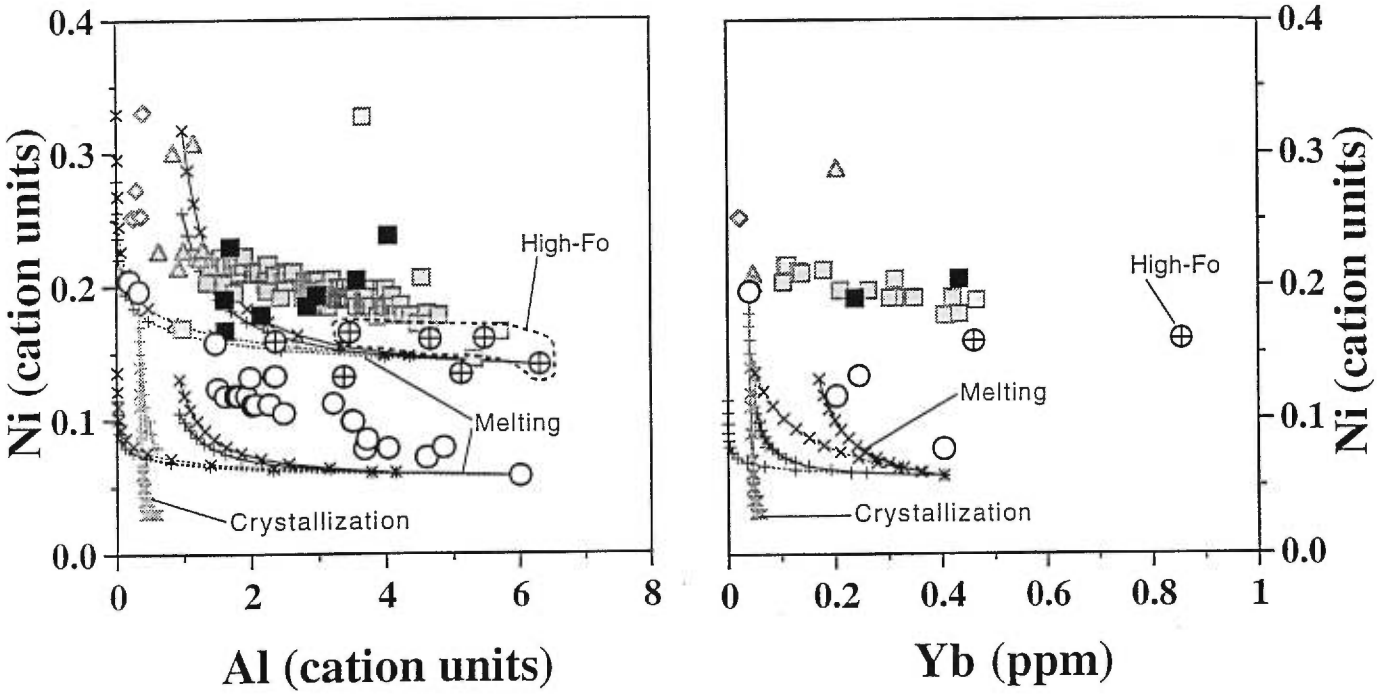

KL Wehr ⊕ SL Wehr ■ Opx-poor L

◇ Dunite △ Harz □ Lherz

Fract. crystallization with increasing proportion of trapped liquid (by5% steps)

Fract. crystallization with increasing proportion of trapped liquid (by 1% steps)

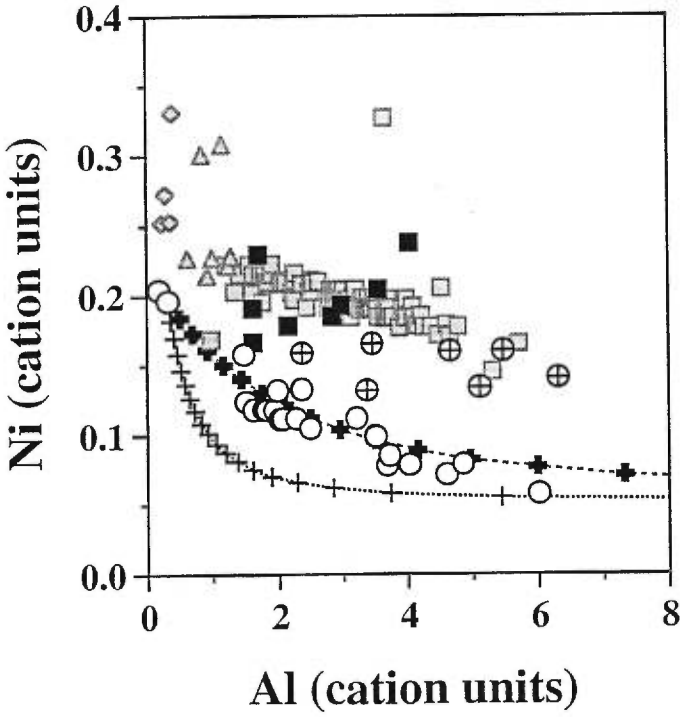

The Opx-poor lherzolites which have textures similar to the "normal" lherzolites (i.e. non poikilitic), have intermediate compositions between the Cr-diopside suites and the wehrlite suites in terms of major (Fig. 16) and trace (Fig. 9 and 10) elements. Mineral compositions were analysed in only one sample (SLX-14). The Fo content of Ol (Fo = 87, Fig. 18) in SLX-14 is as low as in most SL wehrlites. The Cpx of SLX-14 is similar to that in the SL wehrlites for most elements but has higher Cr_2O_3 (Table 5). The Opx-poor lherzolites may represent the products of reaction of Cr-diopside peridotite with the melt that produced the low-Fo wehrlite xenoliths.

As the KL wehrlites appear to represent melts, their actual trace element compositions represent that of the liquid. The fact that melt L2, produced by the melting of the Cr-diopside lherzolites, plots near the KL clinopyroxenites in all major element diagrams but for Al2O3 may imply that the wehrlite melt is generated by the melting of the Cr-diopside peridotites. The trace element composition of melts produced by fractional melting of the Cr-diopside lherzolite KLX-45 were calculated, using the equation of Allègre and Minster (1978) and whole-rock partition coefficients calculated from the mode of KLX-45 and the average of mineral partition coefficients compiled by Green (1994). The same calculation was applied to LREE depleted LPX-11. None of the calculated REE patterns resemble those of the KL wehrlites, which are in particular depleted in HREE (Fig. 20). The melts that produced the werhlite are thus not the product of melting of the Cr-diopside peridotites. The relative depletion in HREE compared to LREE may suggest that these melts result from melting in the garnet stability field.

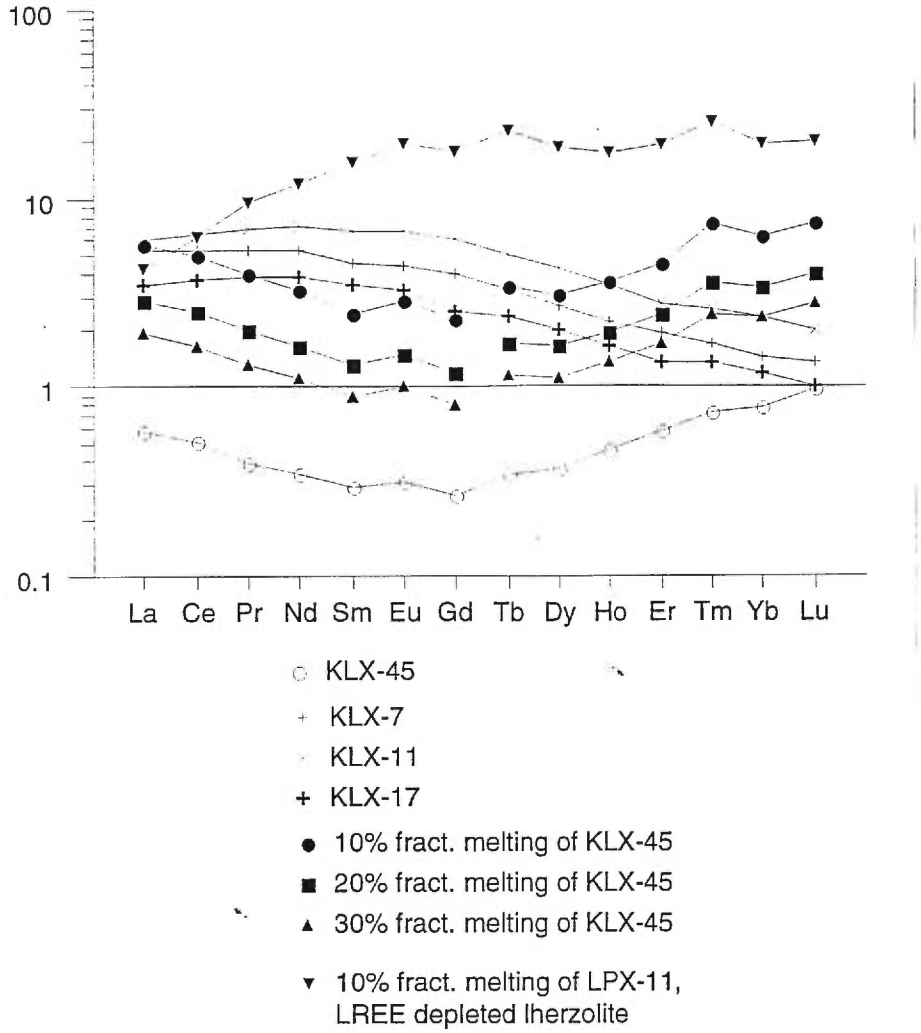

Fig. 20: Chondrite normalized trace element patterns (Sun and McDonough, 1989) of lherzolite KLX-45, wehrlites KLX-7, 11 and 17, and melts produced by fractional melting of KLX-45 and LPX-11. Calculation was made using the trace element composition of the lherzolites (Table 8), their modal mineralogy (Table 2), and the mineral-melt partition coefficients compiled by Green (1994).

2.8 CONCLUSION

The xenoliths brought to the surface by alkaline basaltic lavas from the Canadian Cordillera comprise mainly spinel lherzolites, with minor harzburgites, wehrlites and pyroxenites. The spinel lherzolite compositional range can be explained by up to 15% partial melting from a pyrolite like source resulting in picritic melts. Major element characteristics of bulk-rocks and minerals of the lherzolites resemble those of intraplate oceanic mantle, but are different from peridotites found in arc settings. Subtle differences between the northern and southern Cordillera indicate generally higher degrees of partial melting for the southern Canadian Cordillera. The rare harzburgites, dunites and some of the depleted lherzolites from southern Canadian Cordillera are too Fe-rich, however, to be simple residues of melting. They may result from the interaction of an alkaline melt with peridotite at depth, that crystallized Ol at the expense of Opx and Sp. Wehrlites are abundant in xenolith sites close to the craton, and likely represent mixtures of cumulates and trapped melt. In general, most wehrlites from the Canadian Cordillera are more refractory than Al-augite suites found elsewhere. Most of the Canadian Cordillera lithosphere is anhydrous except that two sites which contain minor amphibole or phlogopite are evidence of later metasomatism (Brearley and Scarfe, 1984; Canil and Scarfe, 1989). Enriched trace element patterns are also evidence of cryptic metasomatism, and indicate that the metasomatic fluids or melts were LREE-enriched and HFSE-depleted. The melts from which the wehrlites were derived are depleted in HREE and were not derived from the Cr-diopside lherzolites.

Chapitre 3: Re-Os systematics in mantle xenoliths; age constraints on the Canadian Cordillera lithosphere

Paper submitted to Chemical Geology

by Anne H. Peslier, Laurie Reisberg, John Ludden and Don Francis

RÉSUMÉ

Les rapports $^{187}Os/^{188}Os$ des lherzolites des différentes suites de xénolites de la Cordillère Canadienne sont corrélés avec l'Al_2O_3 et les terres rares lourdes (HREE), indépendamment des terrains tectoniques où ces xénolites ont été échantillonnés. L'intersection de la corrélation des rapports isotopiques de l'Os en fonction du Lu, avec l'axe des ordonnées suggère un âge modèle de 1,12 ± 0,26 Ga pour le manteau lithophérique tout au long de la Cordillère Canadienne. Les âges de formation crustale (âges modèles Nd) des terrains tectoniques formés loin du craton Nord Américain et plus tard accrétés à sa marge Ouest, sont cependant beaucoup plus jeunes que l'âge du manteau déterminé grâce à l'Os. La base de la croûte continentale affleure uniquement dans le Sud-Est de la Colombie Britannique et présente le même âge (1,9 à 2,3 Ga) que la croûte du craton Nord-Américain adjascent. Elle est cependant plus vieille que le manteau lithosphérique situé sous la Cordillère Canadienne. L'âge modèle de 1,1 Ga de ce manteau est en revanche le même que celui de zircons détritiques dont la provenance est inconnue mais que l'on trouve dans l'ensemble de la Cordillère. Cette différence d'âge entre la formation de la croûte et celle du manteau sous-jascent suggère un découplage croûte-

manteau au cours de l'évolution de la Cordillère Canadienne. Ceci contraste fortement avec les zones cratoniques Archéennes et les ceintures Protérozoiques où croûte et manteau semblent avoir le même âge de formation.

ABSTRACT

The $^{187}Os/^{188}Os$ ratios of lherzolites from various xenolith suites from the Canadian Cordillera show a correlation with Al_2O_3 and heavy rare earth elements (HREE) which appears to be independent of tectonic terrane. The intercept of the correlation suggests a lithospheric mantle model age of 1.12±0.26 Ga throughout the Canadian Cordillera. Crustal formation ages of tectonic terranes formed far away from the North American craton are, however, significantly younger than the mantle Os age. Early Proterozoic basement is exposed only in southeastern British Columbia and has the same age (1.9 to 2.3 Ga) as the ancestral North American crust, older than the age inferred for the mantle lithosphere underlying the Canadian Cordillera. The Cordilleran mantle is thus probably not a simple extension of the North American cratonic lithosphere beneath the adjacent mobile orogenic belt of the Canadian Cordillera. The mantle model age is however consistent with those of detrital zircons of unknown crustal provenance found throughout the Cordillera (Ross, 1991a). The difference in age between the formation of the crust and the formation of the underlying mantle suggests mantle-crust decoupling during Canadian Cordillera evolution. This contrasts strongly with Archean cratonic zones and Proterozoic belts where crust and mantle appear to have the same formation age.

3.1 INTRODUCTION

Due to the compatible behavior of Os during mantle processes, the Re-Os isotopic system is considered to be relatively immune to the effects of metasomatism that often disturb the Sr, Nd and Pb systematics of mantle rocks. Although Re, being moderately incompatible, may be mobile during the percolation of fluids or melts in the mantle, the Re-Os system is nonetheless presently the most useful isotopic system for age estimation of mantle rocks. Two types of ages may be calculated for peridotites with the Re-Os system: a minimum age of Re-depletion (Walker et al., 1989) and model ages based on Os isotopic ratio vs aluminium content correlation (Reisberg and Lorand, 1995).

The possibility of dating mantle rocks allows better constraints to be placed on the relationships between mantle and its overlying crust. Times of crustal extraction can be estimated using Nd model ages of sediments, granitoids, or lavas and Pb dating of zircons from sediments. Indeed, while crustal rocks provide information on the tectonic development of modern orogenic belts or Archean cratons, mantle xenoliths are critical for understanding the inaccessible part of the lithosphere and its role in crustal formation. In Archean cratonic environments and Proterozoic belts, mantle and overlying crust seem to have similar formation ages (Walker et al., 1989; Carlson and Irving, 1994; Pearson et al., 1994; Pearson et al., 1995a; Pearson et al., 1995b), implying contemporaneous formation, if not necessarily a genetic link between crust and lithospheric mantle in these regions. Proterozoic model ages have been found under Cambrian terranes close to craton margins (Handler et al., 1997), suggesting a lateral extension of the cratonic lithosphere beneath the adjacent crustal units. There are few geochemical constraints, however, on the genetic link between crust and the underlying lithospheric mantle. The Canadian Cordillera is one of the most extensively studied Phanerozoic accretionary tectonic zones, and is thus an ideal region to study the role of the lithospheric mantle in continental lithospheric formation.

3.2 REGIONAL GEOLOGY

The Canadian Cordillera spans more than 1000 km north-south along the edge of the North American craton, and includes more than a dozen Late-Tertiary to Recent volcanic centers containing innumerable fresh mantle xenoliths (Fig.1). It is composed of numerous tectonostratigraphic terranes that were accreted to the stable margin of North America from the Jurassic to the early Tertiary, many of which have oceanic-island arc affinities (Monger et al., 1982; Umhoefer, 1987; Gabrielse and Yorath, 1991b and references therein). These terranes can be distinguished from each other by their specific stratigraphic, paleontological and paleomagnetic signatures that indicate that they formed at various distances from the American protocontinent (Gabrielse et al., 1991). The main terranes are Quesnellia (QN), Cache Creek (CC), Stikinia (ST) and the terranes composing the Coast Belt (Fig.1). Between the American continent and these accreted terranes, are located the pericratonic terranes (Yukon-Tanana YTT, Kootenay KO and Cassiar CA belonging to the Omenica belt) which formed close to and never moved far away from the American continent, and as such presents stratigraphic affinities with this continent (Gabrielse et al., 1991). The Canadian Cordillera, one of the best studied Phanerozoic orogenic belts, has been considered to be a modern analogue of Proterozoic crustal growth (Samson et al., 1989; Samson and Patchett, 1991). A regional geographic sampling of mantle xenoliths was analysed for Re-Os in order to constrain the age of the lithospheric mantle beneath the accreted terrains of the Canadian Cordillera. The age obtained is compared with that of the overlying crust and implications for the formation of the continental lithosphere is discussed.

Fig. 1 (next page): Map of the Canadian Cordillera, showing the xenolith sites and the tectonic terranes accreted to the stable margin of North America. White triangles are for unimodal suites, and black and white triangles for bimodal suites. Xenolith site name abbreviations: CL = Clinton, FS = Fort Selkirk, AL = Alligator Lake, LG = Llangorse, BT = Big Timothy, RR = Rayfield River, KR = West Kettle River, LP = Lightning Peak. Tectonic terrane name abbreviations: YTT = Yukon Tanana (= similar characteristics to the Kootenay terrane (KO) of British Columbia (Mortensen, 1992)), CA = Cassiar, QN = Quesnellia, CC = Cache Creek, ST = Stikine. Proterozoic basement exposures: MO = Monashee, VA = Vaseaux formation. Oceanic plate boundaries are from Riddihough and Hyndman (1991). A-B corresponds to the cross-section of Fig. 6.

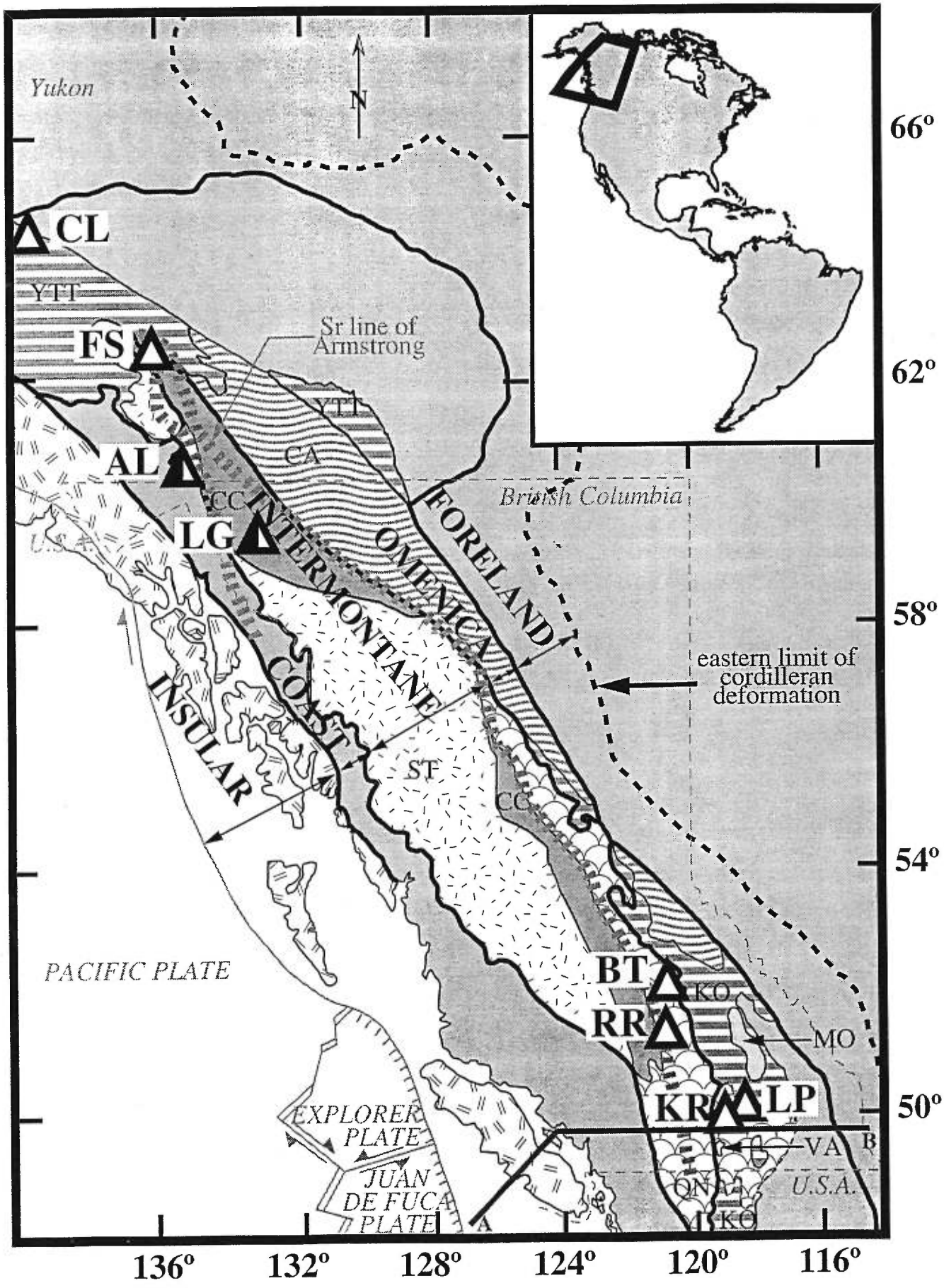
Yukon
N
CL
YTT
FS
Sr line of Armstrong
YTT
AL
CA
CC
INTERMONTANE
OMENICA
FORELAND
British Columbia
LG
eastern limit of cordilleran deformation
INSULAR
COAST
ST
CC
PACIFIC PLATE
BT
KO
RR
MO
KR
LP
EXPLORER PLATE
JUAN DE FUCA PLATE
VA
B
ON
U.S.A.
MI
KO
A
66°
62°
58°
54°
50°
136°
132°
128°
124°
120°
116°

3.3 SAMPLE DESCRIPTION

The 13 fresh spinel-lherzolite samples of this study were derived from suites composed almost solely of lherzolites, with only minor harzburgites (≈ 5%). This type of suite is referred to as "unimodal" in contrast to some "bimodal" suites in the Northern Canadian Cordillera, which contain a large proportion of harzburgite as well as lherzolite xenoliths (Francis, 1987; Shi et al., 1998). All xenoliths analysed here have major and trace element compositions reflecting various degrees of fusion (Peslier et al., 1999) and belong to the Type I Cr-diopside peridotite group defined by Frey and Prinz (1978). Only one suite, that from Lightning Peak, contains significant hydrous minerals, around 5% modal amphibole.

3.4 ANALYTICAL PROCEDURES

Re-Os chemical procedures are based on those described by Shirey and Walker (1995) and Roy-Barman (1993), and only a brief summary is given here. The Carius tube digestion technique was used on 1.5 g of whole-rock powder splits. Os was separated from matrix by a double distillation technique. Os was then further purified by microdistillation. Re was purified from matrix via AG1X8 anion columns. Os was analysed on a Finnigan MAT 262 mass spectrometer as negative ions (Creaser et al., 1991; Volkening et al., 1991; CRPG-CNRS, Nancy, France), with Os total blanks typically about 5 pg. Re was analysed on an Elan 6000 ICP-MS (CRPG-CNRS, Nancy, France). Owing to high Re blanks obtained using this chemical procedure, several samples were redone for Re. Powder splits were dissolved in a 3HF:1HNO_3 mixture at 140°C for three days, and Re was then purified through one AG1X8 anion column (Reisberg et al., 1991). Re blanks by this procedure are 7-25 pg.

$^{187}Os/^{188}Os$ ratio precision is better than ±0.3% (2σ-m) (Table 1). Reproducibility of $^{187}Os/^{188}Os$ ratios measured on duplicate powder splits for 2 samples is within 1%. Os contents were less reproducible, perhaps reflecting a nugget effect. In addition, separate pieces of samples KRX-11 and BTX-26 (quoted P in Table 1) crushed in an agate crusher have $^{187}Os/^{188}Os$ ratios and Al_2O_3 compositions (ICP emission) that differ from the values found in the powders prepared in an alumina crusher. These variations, however, probably reflect cm-scale heterogeneity in the sample, rather than pollution related to the crushing method, as the shifts in composition are not systematic in the two samples (KRX-11 P has a lower $^{187}Os/^{188}Os$ ratio and Al_2O_3 content than KRX-11, while BTX-26 P has higher values of these parameters than BTX-26). The high Al_2O_3 content of BTX-26 P (5.37 wt %) in particular may indicate that the piece of the xenolith used to make the second powder may have contained a small unobserved mafic vein, thus explaining its high $^{187}Os/^{188}Os$ ratio compared to the piece of the same xenolith crushed in alumina.

3.5 RESULTS

Most samples have whole-rock Os concentrations between 0.25 ppb and 2.5 ppb, except sample CL-3 which contains 3.12 ppb Os (Table 1). The $^{187}Os/^{188}Os$ ratios of the xenoliths (Table 1) are sub-chondritic to chondritic and similar to present-day values of orogenic peridotite massifs and non-cratonic mantle xenoliths (e.g. Reisberg and Lorand, 1995; Handler et al., 1997). $^{187}Os/^{188}Os$ ratios do not, however, correlate with the $^{187}Re/^{188}Os$ ratios. This lack of correlation has been noted in other peridotite suites and may reflect Re and/or Os mobility during metasomatism or alteration. For this reason, model age calculations (Walker et al., 1989), based on the $^{187}Re/^{188}Os$ ratio, often lead to aberrant values (both future ages and ages older than the Earth, Table 1). In contrast, $^{187}Os/^{188}Os$ ratios of the lherzolites correlate well with indices of melt extraction, such as

whole-rock Al_2O_3 and HREE concentrations (Fig. 2). This is surprising, since the samples come from widely-spaced locations situated in several different tectonic terranes (Fig.1). The sole amphibole-rich lherzolite (LPX-18) plots on the correlation of $^{187}Os/^{188}Os$ with Al_2O_3 but falls below the correlation with Lu, reflecting an unusually high Lu content for this sample relative to its Al_2O_3 content. It is one of the most REE (especially LREE) enriched xenoliths analysed in the Canadian Cordillera. In this suite however amphibole bearing samples also sometimes have bulk-rock LREE depleted patterns. Because of its unusual characteristics, sample LPX-18 is excluded from the following discussion. Finally, the Os isotopic ratio of "fertile" lherzolite, deduced from the lherzolite $^{187}Os/^{188}Os$-Lu trend (at a Lu value of 0.068 ppm) is 0.130, which agrees with the primitive upper mantle (PUM) value of 0.129 proposed by Meisel et al. (1996).

Location name	Tectonic terrane	Sample	Rock type	[Re] (ppb)	[Os] (ppb)	$^{187}Os/^{188}Os$	$^{187}Re/^{188}Os$	T_{MA} (Ga)	T_{RD} (Ga)	S (ppm)	Al_2O_3 (wt %)	Mg#	Yb (ppm)	Lu (ppm)
West Kettle River	Quesnel	KRX-11	lherz	0.011	1.1728	0.12363±21	0.0451	0.8363	0.7488	27	1.81	90.44	0.1077	0.0166
KR	thrust onto				0.7684	0.12494±43								
	Kootenay		P		1.4517	0.12220±22					1.73			
	KO	KRX-14	lherz		1.8037	0.12860±33			0.0561	29	3.45	88.75	0.3441	0.0586
Lightning Peak		LPX-18	lherz	0.198	0.9236	0.12797±25	1.0298	*<0*	0.1443		3.06	89.10	0.4652	0.0780
Big Timothy	Quesnel	BTX-26	lherz	0.054	1.0532	0.13090±58	0.2463	*<0*	*<0*	29	4.56	89.51	0.4326	0.0684
BT	QN			0.071	1.2346	0.13111±22								
			P		1.2044	0.13790±45					5.37			
		BTX-23	lherz	0.018	0.3021	0.12670±28	0.2862	0.9660	0.3217	32	2.14	90.12	0.1376	0.0227
		BTX-16	lherz	0.081	2.1703	0.12640±31	0.1793	0.6242	0.3635	57	3.05	89.85	0.2629	0.0448
Rayfield River		RRX-10	lherz		0.7731	0.12745±56			0.2170	42	2.81	90.13	0.2098	0.0344
RR		RRX-14	lherz		1.8258	0.12416±61			0.6750	35	1.75	89.76	0.1120	0.0209
Fort Selkirk	Stikine	VM-10	lherz	0.161	1.5186	0.13010±44	0.5092	0.8074	*<0*	66	3.86	88.97	0.3694	0.0625
FS	ST	FS-41	lherz		1.7983	0.12651±13			0.3482	83	2.81	90.15	0.2764	0.0397
Clinton	Kootenay	CL-3	lherz		3.1171	0.12512±25			0.5417	71	1.99	90.13	0.1687	0.0262
CL	KO	CL-17	lherz		0.2502	0.12774±11			0.1764	34	2.62	89.33	0.2427	0.0418

Table I: Os isotope data from mantle xenoliths of the Canadian Cordillera. Precision on $^{187}Os/^{188}Os$ ratio listed corresponds to 2σ run statistics.

P = samples crushed in agate instead of carbon carbide crusher (see text for explanations). Model age calculations (T_{MA}) and minimum Re depletion age (T_{RD}) were made using a $\lambda = 1.666\ 10^{-11}\ y^{-1}$ (Smoliar et al., 1996) and a present primitive mantle $^{187}Os/^{188}Os$ ratio of 0.1290 and $^{187}Re/^{188}Os$ ratio of 0.428 (Meisel et al., 1996). Al_2O_3 compositions were determined by a Philips PW1400 X-ray fluorescence spectrometer at McGill University, Canada. Lu and Yb concentrations (dosability = 10 x detection limit = 0.001 ppm) were analysed by ICP-MS at the CRPG-CNRS, Nancy, France. S contents were analysed by combustion followed by impulsion coulometry at the CRPG, and reproducibility ranges from 10 to 40%. Uncertainties on the Lu and Al_2O_3 contents are respectively ± 0.1 ppb (analytical precision calculated from 3 replicate analyses of two solutions at 6.5 ppb and 1.2 ppb, method developped at CRPG) and 0.03 wt % (analytical precision calculated from 20 replicate analysis).

3.6 DISCUSSION

3.6.1 The correlation between $^{187}Os/^{188}Os$ and indices of melt extraction

Correlations between Os isotopic ratios and indices of peridotite fusion have already been reported in orogenic peridotite massifs (Reisberg et al., 1991; Reisberg and Lorand, 1995) and individual mantle xenolith suites (Walker et al., 1989; Meisel et al., 1996). These correlations have been interpreted to be the result of radiogenic ingrowth following partial melting, possibly associated with lithospheric stabilization. Reisberg and Lorand (1995) consider the y-intercept of the $^{187}Os/^{188}Os$-Al_2O_3 correlation to represent the Os isotopic ratio of the convective mantle when it was incorporated into the sub-continental lithospheric mantle (SCLM). This y-intercept value, projected onto the mantle evolution curve, can be used to determine a model age of the lithosphere.

Fig. 2 (next page): a) $^{187}Os/^{188}Os$ vs Al_2O_3 (wt%). Ronda, Pyrenees, SW Australia and Dreiser Weiher data are from (Reisberg and Lorand, 1995; Meisel et al., 1996; Handler et al., 1997). b) $^{187}Os/^{188}Os$ vs Lu (ppb). The triangle corresponds to the depleted harzburgite AL-49 from Alligator Lake. This harzburgite was not tincluded in the calculation of the regression line. White squares = lherzolites from southern Canadian Cordillera; squares with a x inside = lherzolites from the bimodal suite of Alligator Lake; squares with a cross inside = lherzolites from the bimodal suite of Llangorse.

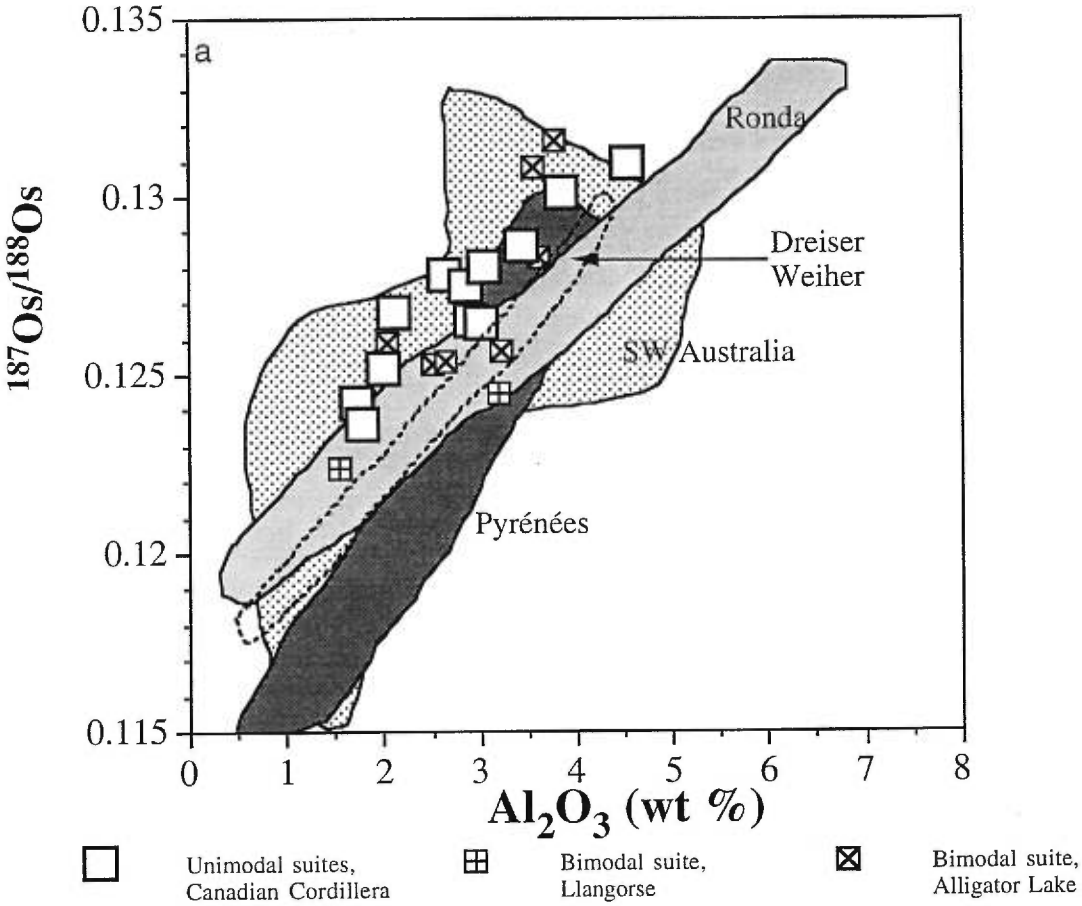
a
Ronda
Dreiser
Weiher
SW Australia
Pyrénées
$^{187}Os/^{188}Os$
Al_2O_3 (wt %)
0.135
0.13
0.125
0.12
0.115
0
1
2
3
4
5
6
7
8
Unimodal suites, Canadian Cordillera
Bimodal suite, Llangorse
Bimodal suite, Alligator Lake

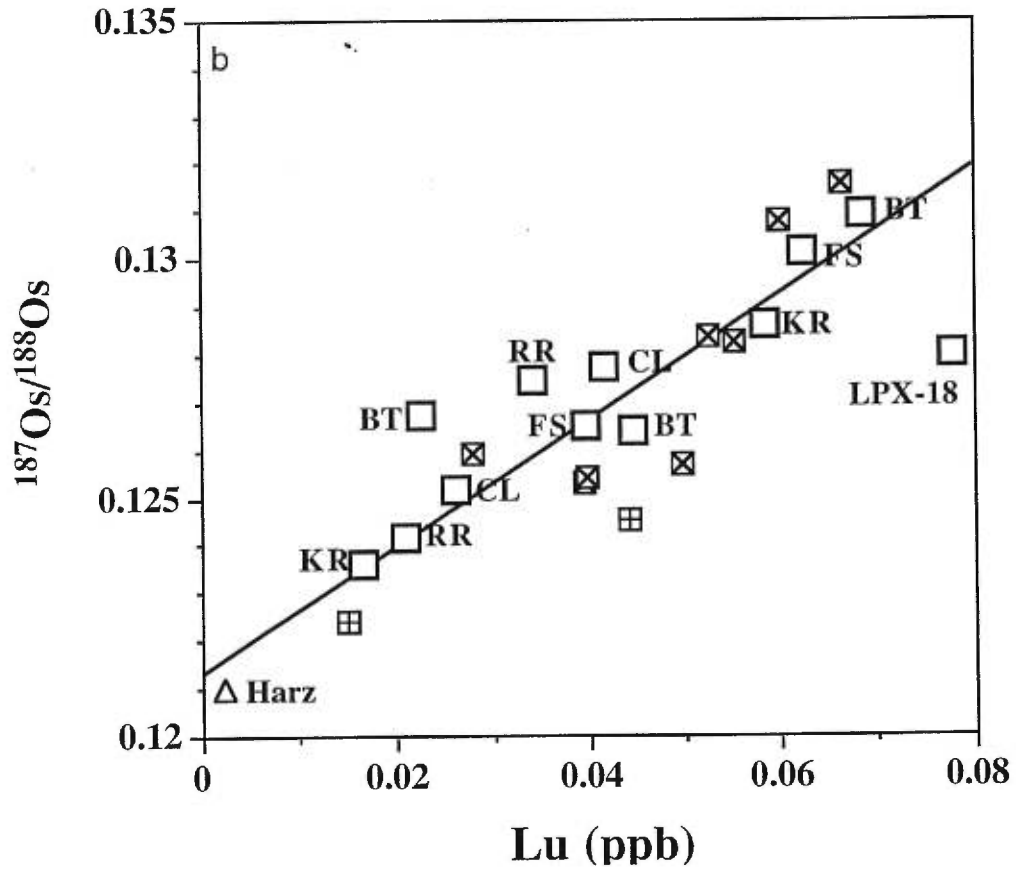
b
BT
FS
KR
RR
CL
LPX-18
BT
FS
BT
CL
RR
KR
Δ Harz
$^{187}Os/^{188}Os$
Lu (ppb)
0.135
0.13
0.125
0.12
0
0.02
0.04
0.06
0.08

The "age" obtained is subject to uncertainties. These arise from (1) errors in the determination of the mantle evolution curve (Reisberg and Lorand, 1995), (2) the quality of the least-square fit of the line to the data, (3) the adequacy of the element chosen as the Re/Os-ratio proxy and (4) the appropriateness of the use of the y-intercept as the "initial" $^{187}Os/^{188}Os$ ratio.

(1) Tighter constraints on the age calculation may be placed by assuming that the Canadian Cordillera lherzolites were derived from a source similar to the fertile mantle, as our most fertile samples have Os ratios equal to that proposed for primitive mantle (Meisel et al., 1996). The lowest value for chondritic (enstatite and ordinary) mantle evolution curve (Meisel et al., 1996) produces ages systematically 0.1 Ga younger than those obtained using the primitive mantle evolution curve. This age shift is small compared to the uncertainties calculated on the ages (Table 2).

(2) The error in the fit of the correlation line to the data can be calculated using expanded uncertainties on the y-intercept and which mainly reflect the amount of scatter of the data about this line (McIntyre et al., 1966; York, 1969; Titterington and Halliday, 1979; Table 2).

(3) The y-intercept of the $^{187}Os/^{188}Os$-Lu correlation differs somewhat from that of the correlation with Al_2O_3 (0.11943 for Al_2O_3 and 0.12093 for Lu), giving an age difference of 0.21 Ga for the entire Canadian Cordillera. The fit to the data is generally better for Lu than for Al_2O_3 (see uncertainties in Table 2).

Lu is probably a better choice for a proxy for the Re/Os ratio since Re and Lu seem to be similarly incompatible during peridotite melting (Hauri and Hart, 1997). The reasons for the similar behavior of Re and Lu are not well understood. HREE are mainly hosted by clinopyroxene (Stosch, 1982; Bodinier et al., 1996) . Experimental studies of Re partitioning between silicate and sulfur melts under mantle conditions are quite scarce, recent data (Schiano et al., 1997b; Righter and Hauri, 1998) suggest that Re may be stored largely in silicate phases as well. Nevertheless, the possibility of some Re control by

sulfide trace phases (Pearson et al., 1998), as seems to be the case for Os (e.g., Hamlyn and Keays, 1986; Crocket et al., 1997), cannot yet be ruled out. S contents of the Canadian Cordillera lherzolites (Table 1) show no relationship with Re-Os systematics, or with indices of melt extraction. This could reflect post-eruption alteration of the xenoliths (S loss during secondary oxihydration of mantle sulfides (Lorand, 1990), or the difficulty of measuring low S contents in mantle xenoliths. Lorand (1989) has observed a correlation between S and clinopyroxene contents in orogenic peridotites not affected by melt contamination, suggesting that sulfide and clinopyroxene are removed at similar rates during fusion processes. Consequently, the HREE content and the Re/Os ratio of mantle rocks may be proportional during melting processes.

(4) The interpretation of an initial $^{187}Os/^{188}Os$ ratio at 0 ppm Lu (or Al_2O_3) assumes that both Re and Lu are completely removed from the residue at similar degrees of melting. The Re contents of the Canadian Cordillera unimodal suite lherzolites are comparable to those of other xenolith suites worldwide (e.g., Handler et al., 1997), and show a broad correlation of Re with HREE (Fig. 4). The correlation line intersects the HREE axis at a positive value, thus indicating that HREE were still present in the residue after Re was totally exhausted. The initial $^{187}Os/^{188}Os$ ratio (at 0 ppm Lu) used for model age determinations in the Canadian Cordillera might thus be slightly underestimated, leading to model ages somewhat older than the true ages. On the other hand, lherzolites from the bimodal Canadian Cordillera suites have higher Re concentrations for similar Yb contents (Peslier et al., 1998b), comparable to those measured in orogenic massifs such as those of the E. Pyrenees (Burnham et al., 1998; Fig. 3). Pyrenean samples thought to be free of exotic sulfur (selected on the basis of their Cu/S ratios; see Burnham et al., 1998) define a correlation that intersects the Re axis at a positive value of Yb. This suggests an opposite conclusion compared to our unimodal suite data, i.e., HREE are exhausted after Re. Further investigation is needed to determine the exact similarities and differences of behavior between Re and HREE. For the purpose of age estimation using the Os isotopic

ratio vs. HREE correlation, uncertainties in the HREE concentration equivalent to 0 ppm Re will induce ambiguity in the proper choice of an "initial" $^{187}Os/^{188}Os$ ratio, which will translate into uncertainties in the estimated model age. However these errors are smaller than those related to scatter in the data and uncertainty in the appropriate mantle evolution curve.

A final remark concerning the choice of Lu instead of Al_2O_3 for the Re/Os ratio proxy is that the precision of Lu measurements by the ICP-MS is good (± 0.1 ppb). This leads to a relative precision similar to that of Al_2O_3 analyses (±0.03 wt%, absolute precision). Analytical precision thus is not a determining factor in this choice.

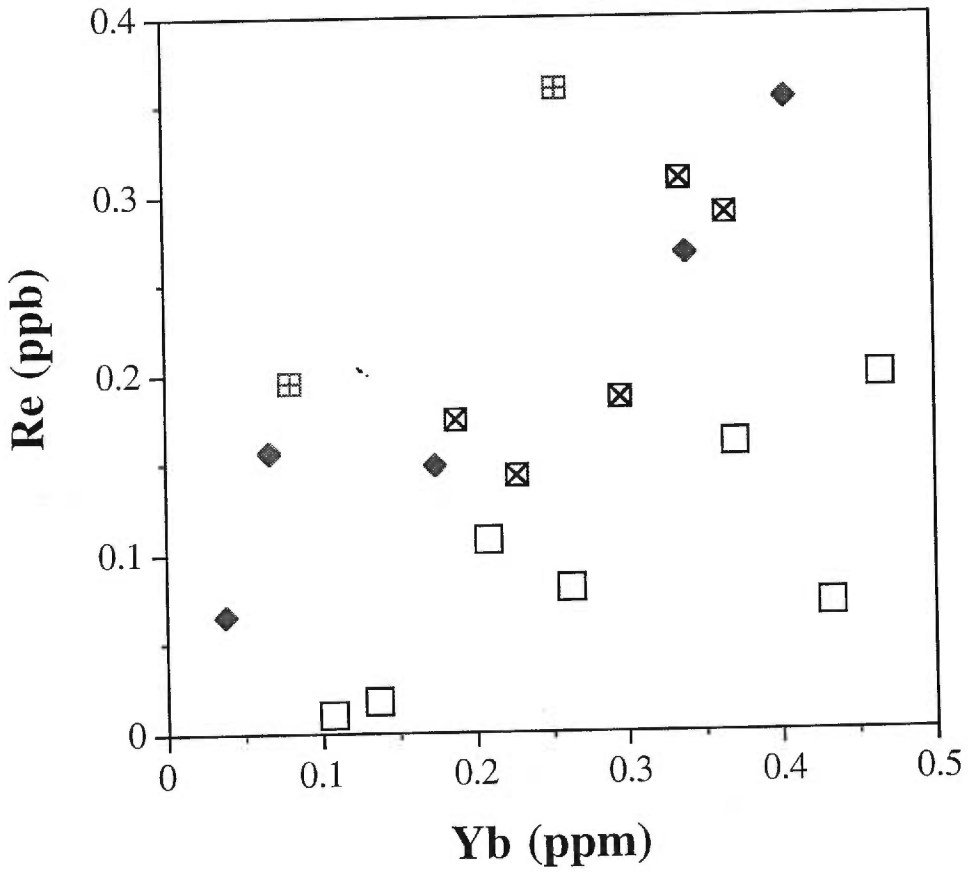

Fig. 3: Re vs Yb in the Canadian Cordillera. Diamonds are the E. Pyrenean data of Burnham et al. (1998), including only those points thought by Burnham et al. to be free of interaction with an exotic sufur component. Other symbols as in Fig. 2.

3.6.2 Model ages and mantle domains

Model age calculations are made by projecting the initial value of the $^{187}Os/^{188}Os$-Lu correlation onto a mantle evolution curve, defined by the present day primitive upper mantle (PUM) values of 0.1290 for $^{187}Os/^{188}Os$ and 0.428 for $^{187}Re/^{188}Os$ (Meisel et al., 1996). This method yields older ages than the "Re depletion" ages commonly used to estimate the melting age of the mantle in studies of xenoliths from cratonic regions (Walker et al., 1989; Pearson et al., 1995a; Pearson et al., 1995b). The concept of Re depletion age is based on the assumption that the peridotite lost all Re during melting (Walker et al., 1989). Thus Re depletion ages are minimum values. These values approach the true values of melting for very depleted peridotites such as those of Archean cratons, as Re is assumed to have left the residue almost completely during melting (Walker et al., 1989). The oldest Re depletion age of an entire xenolith suite is generally assumed to be the best estimate of the melting age because later Re addition may have occurred in many xenoliths (Walker et al., 1989). Peridotites from alkali basalts, such as the Canadian Cordillera xenoliths studied here, are much less depleted than cratonic peridotites from kimberlite pipes (Boyd, 1989). The Re-depletion ages of the Canadian Cordillera lherzolites range from 0.06 to 0.74 Ga (Table 1). These ages probably greatly underestimate the true melting age due to the fact that Re was still present after melting in the residue. The only Canadian Cordillera harzburgite whose Os composition was apparently undisturbed by later metasomatism lies very close to the pseudo-isochron in Fig. 2b. This highly depleted sample, which is from one of the bimodal suite of the northern Cordillera (Peslier et al., 1998b), yields a Re depletion age of 1.1 Ga.

The model ages of the mantle lithosphere inside individual mantle domains, defined on the basis of the overlying tectonic terrane or belt boundaries (Fig. 1, Table 2), were calculated by the pseudo-isochron method. In these calculations, the 11 samples of this

study (LPX-18 excluded), as well as the 10 lherzolite samples of Peslier et al. (1998b) were taken into account. The significance of these model ages is quite limited due to the small number of Os results available for each domain. Nevertheless, this calculation allows us to determine whether any tectonically logical sub-group of the total data set suggests a markedly different model age from that given by all the data from the Canadian Cordillera, including samples from the bimodal suites discussed elsewhere (Peslier et al. 1998b; Fig. 5).

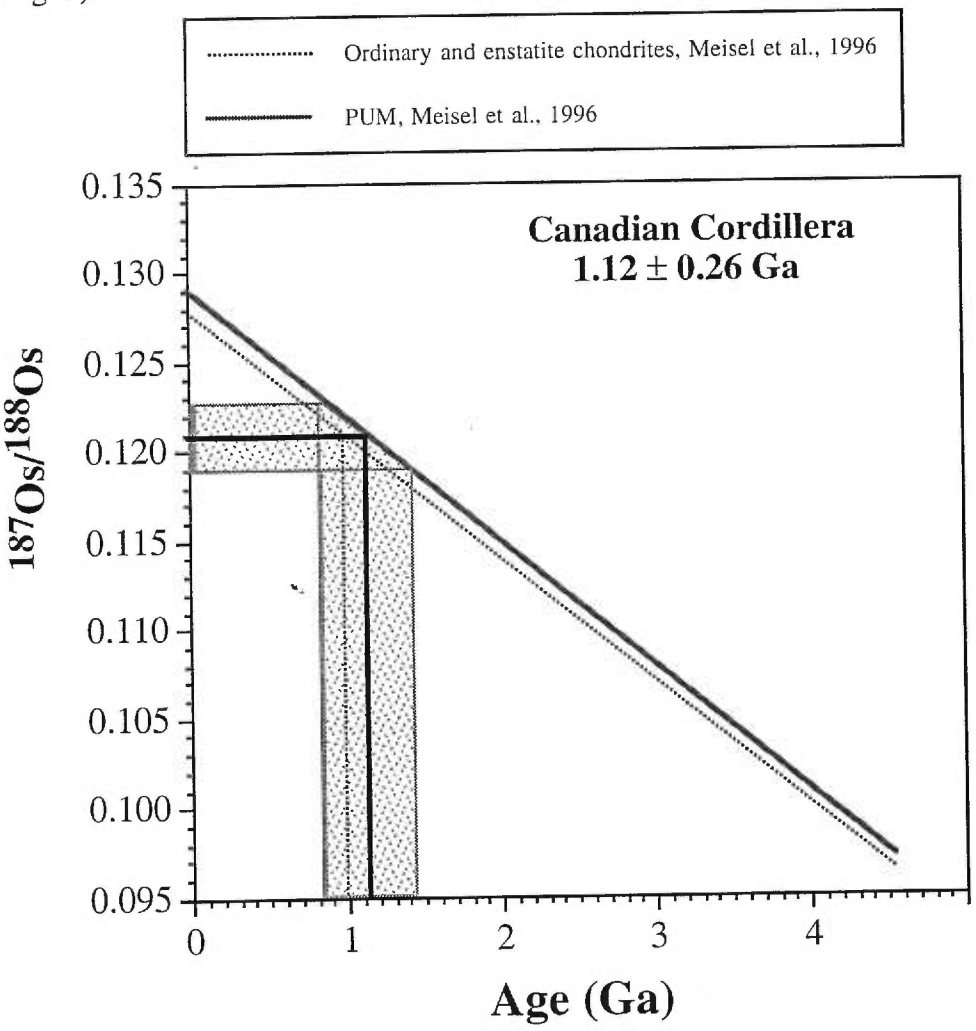

Fig. 4: Os mantle evolution curve and model age determination. Parameters used are $\lambda = 1.666\ 10^{-11}\ y^{-1}$ *(Smoliar et al., 1996) and a present primitive mantle* $^{187}Os/^{188}Os$ *ratio of 0.1290 and* $^{187}Re/^{188}Os$ *ratio of 0.428 (Meisel et al., 1996). Lower curve from Meisel et al. (1996), representing the lowest value for enstatite and ordinary chondrites. The model age obtained for the Canadian Cordillera is 1.12±0.26 Ga.*

(1) The southern sites (KR, LP, RR, BT) versus the northern sites (LG, AL, FS, CL; Fig.1). The southern sites are situated closer to the craton border than the northern sites and are separated by a xenolith-free region about 300 km in length. Model-age estimates of the mantle yield 0.91±0.27 Ga for the southern region, and 1.33±0.43 Ga for the northern region (Fig. 5). The fit of the correlation line to the data is better in the South than in the North (table 2, Fig. 5).

(2) Orogenic belts. The belts of the Canadian Cordillera are defined by various lithological, structural, tectonic and physiographic criteria (Gabrielse et al., 1991). More interestingly for our study, isotopic data on granitoids (Armstrong, 1988) and basalts (Abraham et al., 1998) in the northern part of the Canadian Cordillera define a region of lower $^{87}Sr/^{86}Sr$ ratios, lower Pb isotopic ratios and higher $^{143}Nd/^{144}Nd$ broadly corresponding to the Intermontane Belt (Fig. 1), compared to other parts of the Canadian Cordillera. These igneous rocks may reflect heterogeneity of mantle source regions corresponding to the Canadian Cordillera Belts (Abraham et al., 1998). The four Os data available for the Omenica Belt (sites CL, KR) yield an age of 1.04±0.25 Ga, despite the fact that the two samples from the south and the two from the north are separated by about 800 km. The model age found for the Intermontane Belt (sites FS, LG, BT, RR) is 0.97±0.45 Ga. The only xenolith site from the Coast Belt (AL) yields a model age estimation of 1.55±0.72 Ga, but gives 1.21±0.48 Ga when the harzburgite lying on the correlation is included (Peslier et al., 1998b).

(3) Tectonic terranes. According to the number of samples analysed per terrane, three different tectonic terranes can be considered. Five samples from the Quesnellia terrane (sites BT, RR) yield a mantle model age of 0.67±0.46 Ga, which is younger than all the ages found previously. The two other terrane groupings were already discussed in (2): the Yukon Tanana-Kootenay terrane (i.e., the Omenica Belt) and the Coast Belt. Note that the West Kettle River samples were included in the Kootenay terrane as this site lies on an

overthrusting of the Kootenay terrane by the Quesnellia terrane (Gabrielse and Yorath, 1991b; Fig. 1).

Finally, applying the pseudo-isochron method to all the samples from the Canadian Cordillera, regardless of their geographic provenance, gives an overall model age of 1.12±0.26 Ga for the Canadian Cordillera (Fig. 4). This calculation takes into account the Os isotopic ratios of lherzolites from bimodal suites (Peslier et al., 1998b). Given that the lherzolites were collected over a very large geographic area spanning several accreted terranes, it is somewhat surprising to find a single, fairly well-defined trend in Fig. 2. Thus possible origins for this correlation other than melt depletion linked to lithosphere formation must be considered. One possibility is that it results from mixing between depleted harzburgites and basaltic melts, but this is untenable, as such mixtures would produce strongly curved and poorly defined arrays (Reisberg and Lorand, 1995). Futhermore the apparent uniformity of the trend would imply single basaltic and harzburgititic endmembers for the entire Cordillera, which is highly unlikely. A more plausible alternative is that the correlation reflects a global trend resulting from continuous processes in the convecting upper mantle. However, the fact that similar correlations noted elsewhere in the world (Fig. 2a) display different slopes and y-intercepts argues against this interpretation. Thus the simplest explanation for the trend is that it records an ancient melting event or series of events closely spaced in time. If the convecting mantle is less well-mixed than is commonly believed, as suggested by the recent data of Parkinson et al.(1998), it may be possible for the traces of such a melting episode to be preserved for very long time periods outside of the lithosphere. If not, melt extraction associated with lithospheric stabilization remains the most likely explanation of the data. In either case, the well-defined correlation observed here suggests that the mantle lithosphere currently underlying the Canadian Cordillera, or all the domains of which it is composed, underwent melting about 1.1 Ga ago.

Tectonic Unit	Xenolith sites	Number of data used	Age (Ga) Lu	Uncertainty	Age (Ga) Al2O3	Uncertainty
Canadian Cordillera	All	21	1.1212	0.2621	1.3273	0.4254
South	KR, RR, BT	7	0.9144	0.2686	1.2821	0.3718
North	LG, AL, FS, CL	14	1.3369	0.4253	1.3356	1.1046
Intermontane Belt	FS, LG, BT, RR	9	0.9710	0.4543	1.1666	0.6222
Omenica Belt, KO-YTT	CL, KR	4	1.0372	0.2500	1.5710	0.5586
Coast Belt	AL	8	1.5519	0.7163	1.6352	0.5209
Coast Belt incl. 1 Harz	AL	9	1.2093	0.4775	1.3424	0.5608
Quesnellia (QN)	BT, RR	5	0.6694	0.4566	0.9172	0.5216

Table II: Mantle ages in the possible domains of the Canadian Cordillera. Ages are calculated using the method of Reisberg and Lorand (1995) but with Lu as a Re/Os ratio proxy. The error on the fit of the correlation line of the data can be calculated using expanded uncertainties on the y-intercept (McIntyre et al., 1966; York, 1969; Titterington and Halliday, 1979) The data used in this table are from this study and from Peslier et al. (1998b)

In summary, owing to the uncertainties on these calculated ages, no fundamental age difference can be seen in the different possible mantle domains of the Canadian Cordillera (Table 2, Fig. 5). The ages are all about 1 Ga and are in agreement with the Re-depletion age calculated for the depleted harzburgite. The younger age found for the Quesnellia terrane grouping is likely due to the reduced number of samples used for the correlation (5). The overall model age of 1.12±0.26 Ga is thus a reasonable estimate for the lithospheric mantle underlying the Canadian Cordillera, taking into account the uncertainties discussed above on the method used to calculate this age. This could mean that the mantle beneath each of the accreted terranes experienced melting at roughly the same time, about 1.1 Ga ago, or alternatively that a mantle of mid to late Proterozoic age is attached to the Canadian craton. The question whether this mantle was all formed by one event, or several events occuring within a short period of time is difficult to answer. In order to better constrain this problem, the link between the accreted terrains and the mantle must also be addressed in terms of formation age, as is done in the next paragraph. Finally, the Re-Os Proterozoic ages found in the Canadian Cordillera confirm the long-term stability of the continental lithospheric mantle, as previously noted both in cratonic

and off-cratonic environments (e.g., Walker et al., 1989; Pearson et al., 1995b; Reisberg and Lorand, 1995).

3.6.3 Relations between crust and mantle

Some authors (Armstrong and Ghosh, 1990; Ghosh, 1995), based on Sr and Nd isotopic values of granitoids, locate the western boundary of the North American basement in the Southern Canadian Cordillera almost at the limit between the Intermontane and the Coast Belts and following the 0.704 Sr line of Armstrong (1988; Fig. 1). However, recent seismic results (Clowes et al., 1995; Clowes et al., 1998) indicate that North-American crustal basement extends in the lower crust as far as the limit between the Intermontane and the Coast belt. Furthermore, Proterozoic metamorphic rocks, such as the Monashee complex (MO on Fig. 1) or similar outcrops in southeastern British Columbia (VA in Fig. 1; Armstrong et al., 1991; Parrish, 1991), provide evidence that the North American crustal basement crops out west of the terrane accretion boundary (western margin of the Foreland Belt) along the North American continent in this southern region, and at the limit between the Intermontane and Omenica Belts at the latitude of the Canada-US border (Armstrong et al., 1991). The crustal residence ages of these Precambrian exposures range from 1.9 to 2.3 Ga (Armstrong et al., 1991). This age corresponds to the age of the cratonic North American crust east of the Canadian Cordillera (Parrish, 1991) but is older than the 1.12±0.26 Ga age proposed here for the mantle lithosphere. This age discrepancy suggests that there is no direct genetic link (i.e. a melt-residue relation) between the mantle and the crustal basement in the southeastern region of the Canadian Cordillera. This differs from what has been observed in Archean and early Proterozoic regions (Walker et al., 1989; Pearson et al., 1994; Pearson et al., 1995a; Pearson et al., 1995b), where mantle and the oldest crustal rocks share the same formation age. It also suggests that the Proterozoic

mantle under the Cordillera may not represent the extension of the ancestral continental lithosphere as was proposed for SE Australia (Handler et al., 1997).

With the exception of those in southeastern British Columbia, no other Precambrian basement exposure has been reported in the Canadian Cordillera (Parrish, 1991). Thus interpretation of crust-mantle relationships must be based on Nd model ages or zircon U-Pb ages for crustal extraction, and on tectonic relationships between the crustal units. Sediments from the easternmost terranes (Kootenay KO and Cassiar CA), the closest to the stable margin of North America, have negative ε_{Nd} and Nd model ages older than 1.7 Ga. These values likely reflect derivation of the sediments in these accreted terranes from the North American craton (Patchett and Gehrels, 1998). The Yukon-Tanana terrane (YTT on Fig.1) has been close to the North American margin throughout its history, and the nature of its basement is unknown (Mortensen, 1992). Most of the Nd depleted mantle model ages and the U-Pb zircon ages in the YTT range from 1.24 to 2.3 Ga (Stevens et al., 1995; Creaser et al., 1997; and references in Samson et al., 1991b); these ages might simply reflect a North-American cratonic source. Negative ε_{Nd} in Omenica Belt plutons in southeastern British Columbia suggest that they result from crustal antexis of early Proterozoic basement rocks exposed in this region (Samson et al., 1991b; Brandon and Lambert, 1993; Brandon and Lambert, 1994; Brandon and Smith, 1994).

Most of the Nd model ages on sediments and volcanics from the Quesnel, Cache Creek and Stikinia oceanic terranes, which developed far from the craton, are around 0.55 Ga, 0.35 Ga and 0.55 Ga respectively (Fig. 5; Samson et al., 1989; Patchett and Gehrels, 1998). The few Proterozoic Nd model ages (Fig.4) are thought to reflect addition of sediments from the American continent in Triassic time, i.e. after terrane assembly (Patchett and Gehrels, 1998). The young crustal formation age of the Cache Creek terrane (CC on Fig.1) compared to the age of the mantle lithosphere (Fig. 5) is no surprise as this terrane is believed to be a slice of crust lying on top of the Stikinia terrane (Monger et al.,

1982; Mihalynuk et al., 1994), and probably completely decoupled from its original mantle root. The Stikinia terrane (ST on Fig. 1) may also be a crustal unit lying on top of the Yukon-Tanana terrane (Samson et al., 1991b). As such, these terranes were likely decoupled from their mantle roots during accretion and now rest unconformably on other crustal units.

The majority of plutonic and metamorphic rocks of the Coast Belt have positive εNd and Nd model ages around 0.35 Ga (Fig. 5; Cui and Russel, 1995; Friedman et al., 1995). The northern Coast Belt plutonic and metamorphic rocks define a peak in Nd model age distribution around 0.75 Ga (Fig. 5; Armstrong, 1988; Samson et al., 1991b; Patchett et al., 1997). Some of the Coast Belt rocks, however, have Proterozoic and Precambrian Nd model ages and were tectonically interleaved in the Coast Mountains (Patchett et al., 1997; Fig.4). The origin of these older metasediments is unclear and they may be derived from an ancient assemblage formerly at the latitude of the Southern Canadian Cordillera and situated to the West of the Coast Belt terranes (Patchett et al., 1997). These Proterozoic Nd model ages thus likely result from crustal contamination by an older crust of unclear origin (Patchett et al., 1997). The Northern Coast Belt plutons were likely derived from a mixed source of old metasediments and younger rocks of the region (Patchett et al., 1997), thus explaining why the peak of the crustal age distribution is different in the North and in the South of the Coast Belt. The Nd model ages around the 0.35 Ga distribution peak (Fig. 5) are probably the best representatives of the Coast Belt formation in terms of its time of extraction from its mantle source. These crust formation ages are considerably younger than the 1.12±0.26 Ga of the mantle.

An age difference between mantle and crust is thus strongly indicated in the Cache creek (LG xenolith site) and Stikinia (FS xenolith site) terranes and the Coast Belt. A similar age difference is likely between the Quesnellia (BT and RR xenolith sites) terrane and its underlying lithospheric mantle, because the 0.67±0.46 Ga found for the mantle there (about the range of the crustal Nd model ages (Fig. 5) is based only on a few data.

Finally the formation age of the crust is difficult to evaluate for the pericratonic Yukon-Tanana (Clinton xenolith site)-Kootenay (West Kettle River xenolith site) terrane because of derivation of crustal sediments from the adjacent craton.

To summarize, in the southeastern region of the Canadian Cordillera basement exposures indicate that cratonic rocks with crustal residence ages of about 2 Ga overlay a mantle lithosphere with an age of about 1.1 Ga (Fig. 6). In contrast, in the more western terranes lithospheric mantle of this age is overlain by crust with mostly Phanerozoic crustal formation ages (Fig. 6). If the mantle is indeed of different age than the overlying crust, several inferences can be drawn: 1) the mantle underlying the terranes may not represent the mantle from which the terranes were derived; 2) alternatively, if the mantle is related to the overlying terranes, it may have preserved mantle with older melt-extraction ages 3) the Proterozoic mantle to the west of the limits of the cratonic crustal rocks may not represent the prolongation of the ancestral North American cratonic mantle.

If the terranes are separated from their mantle roots, it raises the question of what has become of the crust associated with this 1.1 Ga mantle. One intriguing clue to this puzzle comes from the presence of xenocrystic zircons of 1.0-1.1 Ga in diatremes from southeastern British Columbia and detrital zircons of this age throughout the Cordillera (Ross, 1991b, and references therein). According to Ross, these zircons testify to the existence of a 1.0-1.1 Ga old crust whose location and present state are unknown, but which may have been widespread before exotic terrane accretion and tectonic shortening started. Another question raised by the age difference between crust and mantle is the mechanism by which the mantle and the overlying crust were separated. Before trying to answer this question, we discuss below several possible interpretations of the apparent 1.1 Ga mantle age.

Fig. 5 (next page): Os model ages of the mantle obtained by the Reisberg and Lorand method (Reisberg and Lorand, 1995) and depleted-mantle Nd model ages of crustal tectonic units (Quesnel and Cache Creek data from Patchett and Gehrels (1998) and Coast Belt data from Samson et al.(1991b), Samson et al.(1991a), and Patchett et al.(1997)

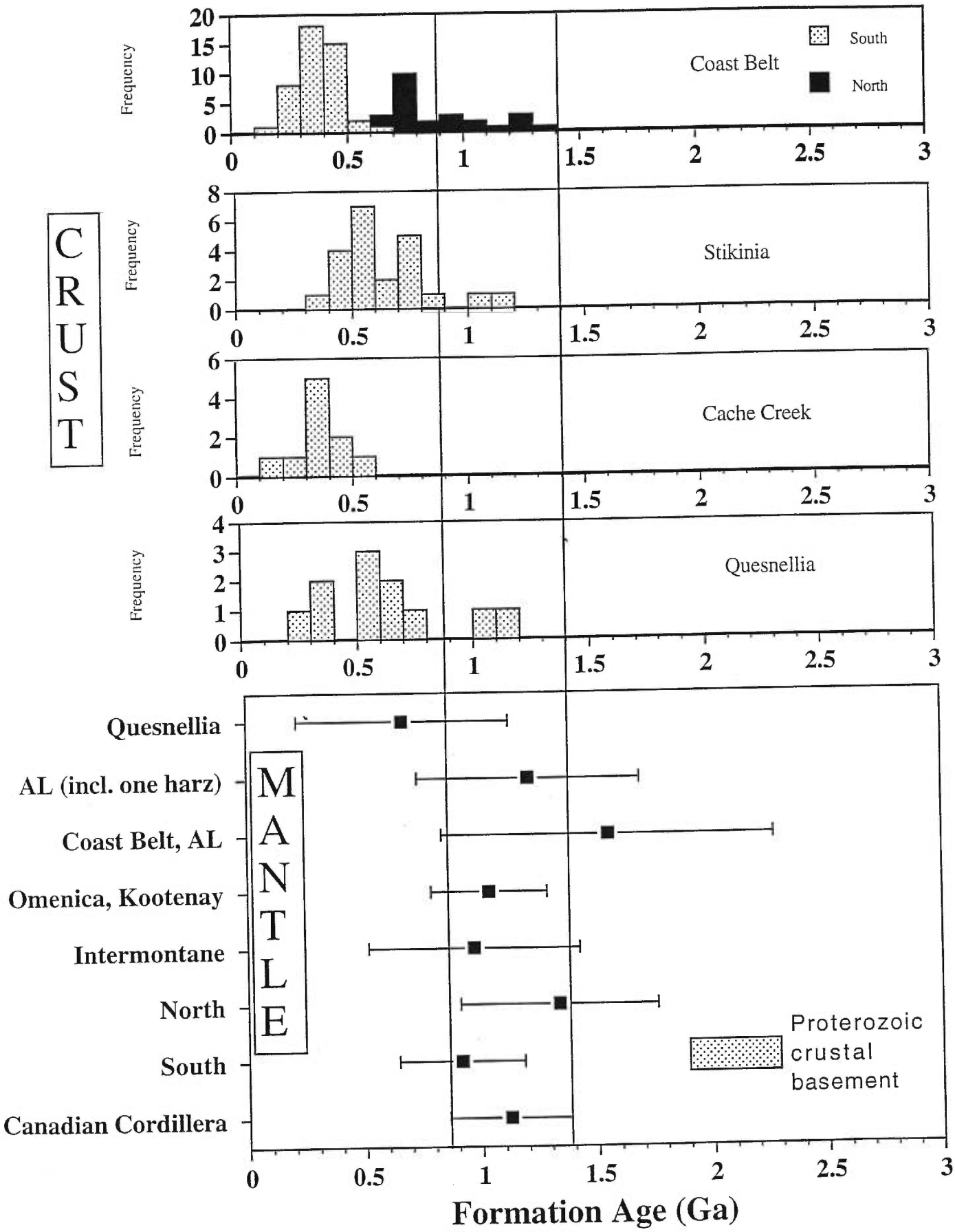
CRUST
Frequency
Coast Belt
South
North
Stikinia
Cache Creek
Quesnellia
MANTLE
Quesnellia
AL (incl. one harz)
Coast Belt, AL
Omenica, Kootenay
Intermontane
North
South
Canadian Cordillera
Proterozoic crustal basement
Formation Age (Ga)

3.6.4. Possibility of long-term isolation in the convective mantle

Re-Os systematics suggest that Phanerozoic continental spinel xenoliths (this study; Handler et al., 1997), as well as peridotite orogenic massifs (Reisberg and Lorand, 1995), appear to record Proterozoic melting ages. However, spinel lherzolites such as the ones analysed here have major element compositions very similar to those of oceanic mantle lithosphere, and in particular to those of mantle xenoliths found in Hawaiian lavas (Peslier et al., 1999, and references therein). Thus we must consider the possibility that the mantle currently underlying the Canadian Cordillera was not incorporated into the subcontinental lithosphere at the time of melting about 1.1 Ga ago, but rather was preserved within the convective oceanic mantle for the ensuing time period. Such a process may be typical of convergent settings at craton margins as spinel continental xenoliths from these regions share similar compositional and isotopic characteristics (e.g., Ionov et al., 1995; Brandon et al., 1996; Brandon and Draper, 1996; Handler et al., 1997). Results from unaltered abyssal peridotites (Snow and Reisberg, 1995, and references therein) suggest that the upper mantle ($^{187}Os/^{188}Os$ ratio ~0.1246 ± 0.0014 - 1σ) has been relatively well homogenized by convection. However two recent studies throw doubt on this inference. One involves xenoliths from the Kerguelen islands. Re depletion ages of xenoliths from the Kerguelen are as old as 1.36 Ga (Hassler and Shimizu, 1998). Geophysical and geochemical arguments, however, suggest that the lithosphere beneath Kerguelen may actually be derived from delaminated subcontinental Gondwana lithosphere incorporated in the oceanic mantle during the initiation of the Indian Ocean (Hassler and Shimizu, 1998, and references therein). More convincing evidence for the long-term preservation of the traces of ancient residual mantle in the convective oceanic mantle comes from a study of peridotites from the Izu-Bonin-Mariana forearc basin (Parkinson et al., 1998). The Re-depletion ages of these depleted peridotites range from 0.82 to 1.23 Ga. These authors suggest that peridotites with such ancient ages may be preferentially preserved in the

forearc mantle because they are depleted and thus buoyant (Parkinson et al., 1998). These new studies and the one presented here, indicate that estimates of the age of sub-continental lithospheric mantle, although representing melt extraction, may not necessarily represent the age of stabilisation of the sub-continental lithosphere.

If the mantle beneath the Canadian Cordillera really is of oceanic character, two possible scenarios may explain the age difference between mantle and upper crust. One would imply that older mantle within the Os-heterogeneous oceanic mantle was accreted and incorporated to the sub-continental lithosphere at the time of tectonic accretion of the terranes. However the widespread age of 1.1 Ga for mantle below the Canadian Cordillera, and the geophysical evidence for the extension of the North American basement beneath most southern Cordillera, argues for a homogeneous mantle in this region, and not a heterogeneous mixture of old and young mantle material as appears to be the case for the two modern examples (Kerguelen and Izu-Bonin) sited above. A second scenario would imply an oceanic mantle generated 1 Ga ago at the North American continental margin. Two episodes of rifting in the Proterozoic affected crustal rocks of the western edge of North America; one around 1.2-1.3 Ga and another starting at 0.8 Ga (Gabrielse and Yorath, 1991b). The melting age of the lithospheric mantle beneath the Canadian Cordillera (1.1 ±0.26 Ga) is roughly equivalent to these events. Young, warm and thin oceanic lithophere created in a young ocean or in back-arc basins is not easily subductable (Meissner and Wever, 1988), and may stay stable at a continental edge if the oceanic basin never gets very large. Such a mechanism would have been followed much later by crustal accretion on top of this oceanic mantle and thinned continental crust.

3.6.5 Continental lithosphere formation

Despite the note of caution introduced above, we believe that the most plausible interpretation of the data is that the Canadian Cordillera peridotites have been isolated within the sub-continental lithosphere for about 1.1 Ga. This is consistent with the widespread 1.1 Ga age for the lithospheric mantle, with the presence of 1.1 Ga detrital zircons throughout the Canadian Cordillera, and with the seismic evidence for Ancestral North America lower crust as far as the Coast Belt. The nature and age of this lower crust is, however, unknown, but may represent the crust associated with the 1.1 Ga old mantle. Decoupling thus appears to have occured between the upper crust, represented by the accreted terranes, and the lower crust. In Archean cratonic areas, the harzburgitic character of the lithospheric mantle is invoked to explain its stability over several Ga, because of its density contrast with the more fertile, and thus more Fe-rich, convective mantle (Walker et al., 1989 and references therein). The lithospheric mantle underlying non-cratonic regions such as the Canadian Cordillera is less depleted than cratonic lithosphere and as such the density contrast relative to the convective mantle is smaller. Nonetheless, a significant compositional difference exists between non-cratonic lithosphere as represented by continental spinel peridotite xenoliths and the average convective mantle composition (determined by mass balance after continental crust extraction). For example, the average Al_2O_3 content of worldwide spinel xenolith samples is about 2.3 wt% (McDonough, 1990); 3 wt % for average lherzolites from the Canadian Cordillera (Peslier et al., 1999) ,much lower than the convective mantle Al_2O_3 content of about 3.9 wt% obtained by mass balance for the convective mantle (assuming primitive mantle with 4.06% Al_2O_3 and continental crust with 15 wt% Al_2O_3; Hofmann, 1988). It is not clear whether such differences in major element composition are sufficient to explain the stability of the sub-continental non-cratonic lithosphere, or if another mechanism is required. Given the result for the Kerguelen Plateau, whose ancient mantle may well have been preserved in the

oceanic lithosphere created at the ocean-continent boundary, it is possible that old continental lithosphere which was partially melted during rifting of the western North America, may underlie much of the Canadian Cordillera.

This study suggests that mantle underlying mobile orogenic belts surrounding ancestral continents may not have the same age as the upper-crust terranes of these belts. Proterozoic Os model ages in mantle xenoliths have also been found as far as 500 km south-eastward off the Australian craton, underlying Cambrian greenstone belts (Handler et al., 1997). In contrast, Re-Os studies of mantle xenoliths from Archean (e.g. Walker et al., 1989; Pearson et al., 1995b) and early Proterozoic areas (Pearson et al., 1994) suggest that the age of the mantle corresponds to the oldest ages found in the overlying crustal rocks, and thus implies long term mantle-crust coupling in these Precambrian regions. These differences may simply be related to different mechanisms of preservation in the ancient geological record relative to the present.

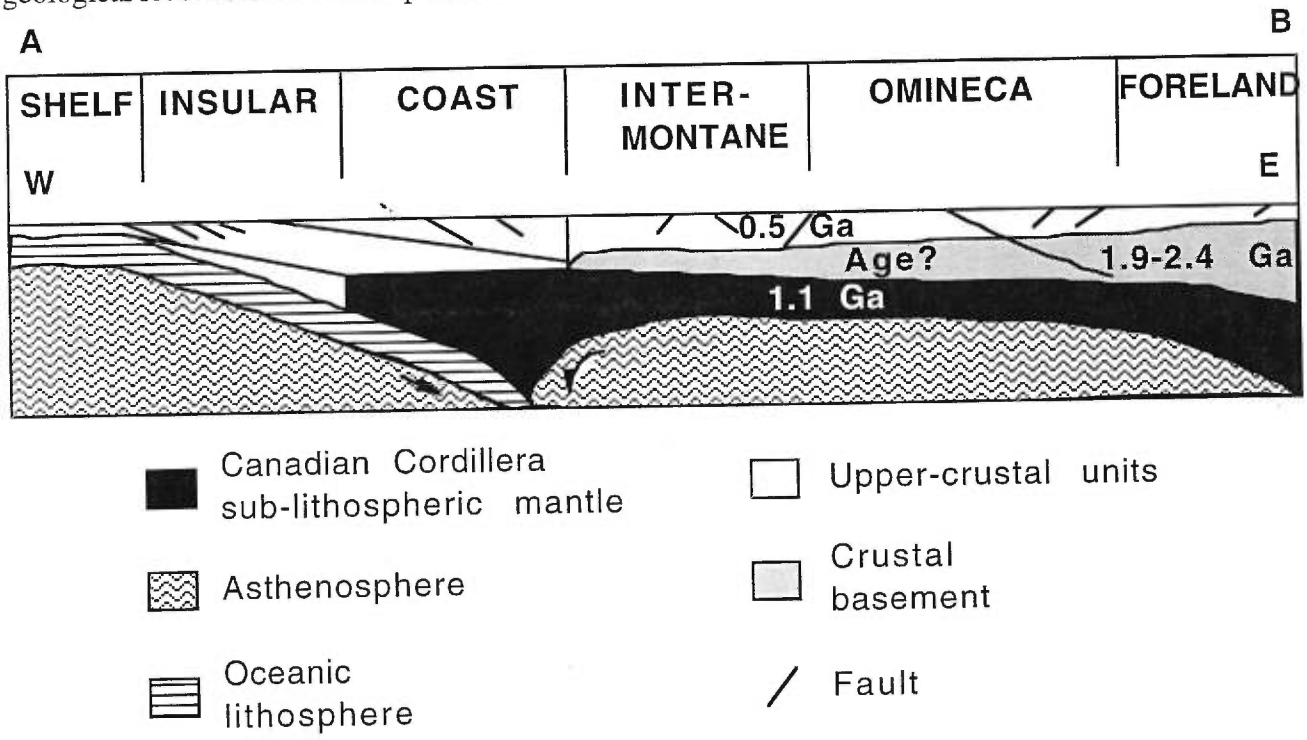

Fig. 6: schematic cross-section of the Canadian Cordillera, drawn after Clowes et al. (1998). See text for discussion on the ages. Total depth is about 150 km. A-B corresponds to the A-B line on the map of Fig. 1.

3.7 CONCLUSION

Lherzolite xenoliths from the Canadian Cordillera were sampled by alkali basalts from a mantle with long term melt depletion since about 1 Ga. This contrasts with the model ages of the upper-crust and supports a tectonic model of decoupling of lower crust from upper-crust during accretion of the Canadian Cordillera. Increasingly old Os model ages have been found in young tectonic settings in both arc, oceanic and continental regimes. In addition to the tectonic decoupling postulated for the Canadian Cordillera, these ages may indicate local preservation of ancient lithosphere in the convecting mantle, either by delamination associated with extension in continental margins or by preferential accumulation of depleted buoyant mantle in zones of tectonic convergence.

ACKNOWLEDGEMENTS

We thank J. Patchett for sending us his unpublished data and H. Becker for giving hints on uncertainty calculations. We are grateful to A.D. Brandon for an earlier revision of the manuscript. Thank you to C. Spatz and A.-C. Pierson-Wickmann for help with the Re-Os analyses.

Chapitre 4: Melting and metasomatism of the lithospheric mantle beneath the Northern Canadian Cordillera: a Re-Os and Lu-Hf study

Paper submitted to Earth and Planetary Science Letters

by Anne H. Peslier, Laurie Reisberg, John Ludden, Don Francis and Catherine Chauvel

RÉSUMÉ

L'étude isotopique de l'Os permet de mettre en évidence une différence significative entre la genèse des lherzolites et celle des harzburgites trouvées sous forme de xénolites dans le Nord de la Cordillère Canadienne. Le rapport $^{187}Os/^{188}Os$ des lherzolites est correlé avec l'Al_2O_3 et les terres rares lourdes (HREE). Cette corrélation reflète probablement le fractionnement du rapport Re/Os au cours de la fusion partielle du manteau, suivie par une longue période de croissance radiogénique. Les données Re-Os et Lu-Hf indiquent que cette fusion a eu lieu au cours du Protérozoique. Les isotopes de l'Os des harzburgites quant à eux se placent au dessus de la corrélation régionale des lherzolites. Les harzburgites semblent donc avoir subi un autre processus que celui qui a affecté les lherzolites, et celui-ci semble avoir opéré tout au long de la Cordillère Canadienne. Il semble que ce processus résulte d'une fusion récente de la lithosphère lherzolitique provoquée par l'arrivée de fluides ou liquides de fusion asthénosphériques, qui ont en même temps laissé aux harzburgites ainsi créées leur signature enrichie en éléments incompatibles (Shi et al., 1998). Ces agents métasomatiques avaient un contenu d'Os

faible mais des rapports isotopiques $^{187}Os/^{188}Os$ élevés. Une région du manteau dans la partie Nord de la Cordillère Canadienne ayant une température anormalement élevée et détectée récemment par des méthodes télésismiques (Frederiksen et al., 1998), pourrait être à l'origine de la forte proportion de harzburgites dans les suites de xénolites trouvées à l'aplomb (Shi et al., 1998). L'interaction lithosphère-asthénosphère au-dessus de cette zone semble aussi avoir perturbé les caractéristiques isotopiques Pb, Sr (Carignan et al., 1996), Lu-Hf et Sm-Nd des lherzolites de la région. Ces fluides ou liquides de fusion ont interagi avec le manteau lithosphérique de la Cordillère Canadienne il y a moins de 170 Ma et semblent avoir eu des caractéristiques isotopiques de type EMII.

ABSTRACT

Os isotopes provide evidence for a definitive difference between the genesis of lherzolite and harzburgite xenoliths of the Northern Canadian Cordillera. The $^{187}Os/^{188}Os$ ratios of the lherzolites show a correlation with Al_2O_3 and heavy rare earth elements (HREE), which probably reflects Re/Os fractionation during various degrees of mantle melting, followed by a long period of radiogenic ingrowth. Re-Os and Lu-Hf data indicate that this melting occurred during the Proterozoic. Harzburgite Os isotopic ratios, however, plot above the regional correlation of the lherzolites. The harzburgites thus appear to have been disturbed by another process, which may have operated throughout the Canadian Cordillera lithospheric mantle. This process may have been melting triggered by the ingress of asthenospheric fluids or melts, which simultaneously imprinted an incompatible trace element enriched signature (Shi et al., 1998). These metasomatic agents had low Os contents, but high $^{187}Os/^{188}Os$ ratios. An anomalously hot region of the mantle recently detected teleseismically in the northern part of the Cordillera (Frederiksen et al., 1998) may be responsible for the high proportion of harzburgites in the overlying xenolith suites (Shi et al., 1998). Asthenosphere-lithosphere interaction above this zone also appears to have

reset the Pb, Sr (Carignan et al., 1996), Lu-Hf and Sm-Nd isotopic characteristics of the lherzolites from this region. The fluid/melts interacted with the Canadian Cordillera lithospheric mantle less than about 170 Ma ago and may have had EMII type isotopic characteristics.

4.1 INTRODUCTION

The great advantage of the Re-Os isotopic system over other isotopic systems used to study mantle rocks is that Os behaves compatibly, while Re is moderately incompatible during melting processes. Consequently, the Os budget of a mantle rock is assumed to be insensitive to percolating melts and fluids, in contrast to the behavior of the elements of other isotopic systems such as Rb-Sr, Pb-Pb, and Sm-Nd (Reisberg et al., 1991; Wilson et al., 1996; Handler et al., 1997). In peridotites, this unique property of the Re-Os system has been used to calculate minimum and model ages of melt depletion in the sub-continental lithosphere (e.g. (Walker et al., 1989; Reisberg and Lorand, 1995; Burnham et al., 1998)). Nonetheless, correlations between Nd, Pb and Os isotopes in mantle xenoliths from beneath oceanic arcs suggest that Os may be mobilized by oxidizing fluids related to subduction (Brandon et al., 1996; Brandon and Draper, 1996). Moreover, the chalcophile behavior of Re and Os may induce movement of these elements together with sulfur during post-volcanic alteration processes of mantle xenoliths, or during grain-boundary percolation of PGE (platinum group element)-bearing sulphidic fluids in the sub-continental mantle (Lorand, 1990; Lorand, 1997).

A second isotopic system of great interest for mantle rocks is Lu-Hf. Hf and Lu are less mobile elements in mantle processes than the commonly used tracers Rb, Sr, Sm, Nd or Pb. Lu preferentially partitions into garnet which is a stable phase in mantle peridotite at pressures greater than approximately 20 kbars. The influence of garnet in Lu-Hf fractionation potentially offers the possibility of distinguishing between shallow and

deep-seated origins in the continental lithosphere. Until recently, analytical difficulties have limited the application of the Lu-Hf system to mantle peridotites and data on these rocks are scarce (Salters and Zindler, 1995). Our data are thus an important contribution to the Lu-Hf data record of mantle rocks.

In this paper we demonstrate that the Os systematics of the lherzolitic mantle lithosphere below the northern Canadian Cordillera preserves evidence for melt extraction during the Proterozoic. The harzburgite xenoliths from this region and from other parts of the Canadian Cordillera, on the other hand, record a more recent melting or metasomatic event. This event reset the Os-isotope systematics of the lowermost lithosphere and resulted in the loss of Os and the enrichment of other trace elements due to the percolation of fluids or melts, probably derived from the asthenosphere.

Fig. 1 (next page): Map of the Canadian Cordillera and mantle xenolith site locations. White triangles are for unimodal suites, and black and white triangles for bimodal suites. Xenolith site name abbreviations: CL = Clinton, FS = Fort Selkirk, AL = Alligator Lake, LG = Llangorse, BT = Big Timothy, RR = Rayfield River, KR = West Kettle River, LP = Lightning Peak. Tectonic terrane name abbreviations: YTT = Yukon Tanana (= similar characteristics to the Kootenay terrane (KO) of British Columbia (Mortensen, 1992), CA = Cassiar, QN = Quesnellia, CC = Cache Creek, ST = Stikine. Oceanic plate boundaries are from Riddihough and Hyndman (1991).

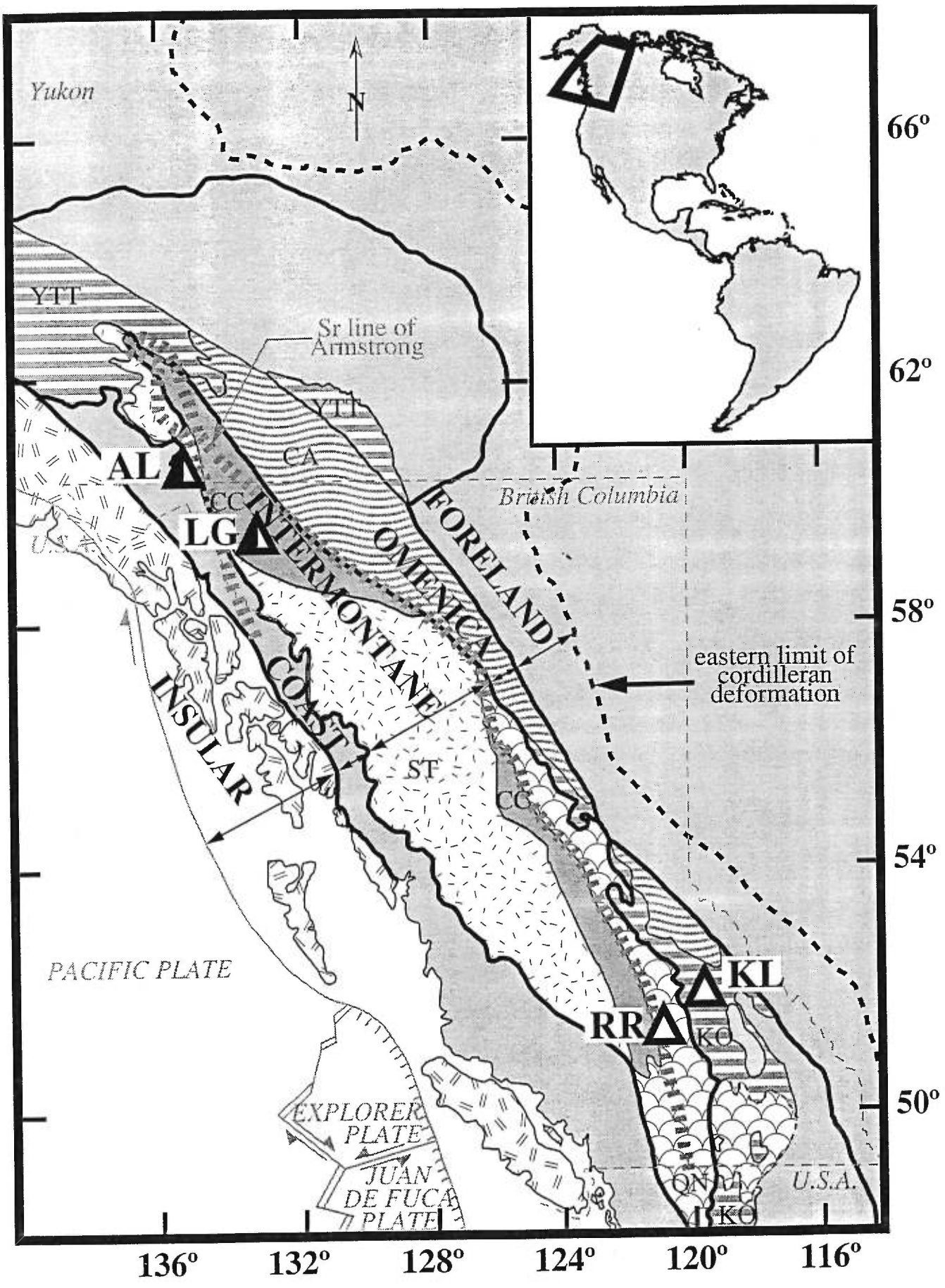
Yukon
N
YTT
Sr line of Armstrong
YTT
CA
AL
CC
LG
INTERMONTANE
OMINECA
FORELAND
British Columbia
COAST
INSULAR
ST
CC
eastern limit of cordilleran deformation
PACIFIC PLATE
KL
RR
KO
EXPLORER PLATE
JUAN DE FUCA PLATE
ON
U.S.A.
KO
66°
62°
58°
54°
50°
136°
132°
128°
124°
120°
116°

4.2 GEOLOGICAL SETTING AND PREVIOUS STUDIES

The Canadian Cordillera formed between 150 and 50 Ma by the accretion of diverse tectonic terranes to the North American protocontinent (Gabrielse and Yorath, 1991b; Fig. 1). For the past 60 Ma, the tectonics of the Canadian Cordillera have been dominated by interactions with Pacific oceanic plates (Kula (subducted), Pacific, Juan de Fuca and Explorer plates), being subducted beneath the margin of the Northern American continental plate (Gabrielse and Yorath, 1991b; Fig. 1). Late Tertiary to recent basaltic volcanism occurred throughout the Canadian Cordillera and appears to be related to zones of trans-tension reflecting lateral movement between these plates (Souther, 1991). A zone of anomalously hot mantle has been discovered through teleseismic studies that appears to reflect a Tertiary to recent thermal event in the Northern Cordillera (Frederiksen et al., 1998). Volcanic centers above this zone contain a high proportion of cryptically metasomatized harzburgite xenoliths. In contrast xenoliths suites outside this zone are dominated by lherzolites (Shi et al., 1998). These two types of mantle xenolith suites are referred to respectively as bimodal (comprising approximately equal proportions of lherzolites and harzburgites) and unimodal (composed almost solely of lherzolites, with only minor harzburgites ($\approx 5\%$)).

4.3 SAMPLE DESCRIPTION

All the xenoliths of this study were derived from mid-Tertiary to recent alkali basaltic lavas. They include fresh spinel-peridotites of two bimodal xenolith suites: 17 xenoliths from Alligator Lake and 4 xenoliths from Llangorse and 3 additional harzburgite samples from unimodal suites of the Southern Canadian Cordillera (Fig. 1). These three harzburgites were included here because their chemical characteristics are similar to those of the bimodal suite harzburgites. Lherzolites from the Southern Canadian Cordillera are

studied elsewhere (Peslier et al., 1998a). Major and trace element compositions for Alligator Lake and Llangorse xenoliths are reported in Francis (1987) and Shi et al. (1998) respectively. All the analysed xenoliths are Type I Cr-diopside peridotites as defined by Frey and Prinz (1978). Furthermore, major element trends, such as negative correlations of CaO, Al_2O_3, TiO_2, SiO_2 and FeO with MgO, and a positive correlation of NiO with MgO, indicate that the xenoliths are the residues of melt extraction (Francis, 1987; Shi et al., 1998). However, as often observed in spinel Cr-diopside suites (McDonough and Frey, 1989), clinopyroxenes in the harzburgites are enriched in incompatible trace elements compared to those of the lherzolites (Shi et al., 1998), opposite to what is expected for melt extraction.

The combination of the teleseismic studies conducted in the Northern Canadian Cordillera (Frederiksen et al., 1998) and trace element laser ICP-MS of clinopyroxenes from the bimodal suites led Shi et al. (1998) to elaborate the following model for the genesis of the harzburgites. The influx of fluids/melts from the hot anomalous zone induced melting of the overlying mantle lithosphere, represented by the lherzolites which is the dominant peridotite type in the region. The harzburgites thus represent the residue after this melting. The fluids/melts were likely enriched in incompatible trace elements, and thus were also responsible for the concomitant incompatible trace element enrichment of the harzburgites. On the other hand, a Sr-Pb study of the bimodal suites (Carignan et al., 1996) concluded that some of the lherzolite and harzburgite isotopic characteristics were disturbed by a recent metasomatic event, probably linked to subduction related fluids.

4.4 ANALYTICAL PROCEDURES

Samples for Re-Os analysis were digested by the Carius tube technique, and Os was extracted by double distillation (Shirey and Walker, 1995). Typically 1.5 g of sample powder were digested. Os was further purified through a microdistillation procedure

(Roy-Barman, 1993). Os was analysed as negative ions [(Creaser et al., 1991; Volkening et al., 1991) on a Finnigan MAT 262 mass spectrometer, in peak jumping mode on an electron multiplier. Measurements of 70 standards (>40 pg) yielded $^{187}Os/^{188}Os$ ratios = 0.17398±0.00040 (σ). Os total blanks were between 5 and 7 pg. Precision on the isotopic ratios is less than ± 0.3% (2σ–m) (Table 1).

At first, Re was extracted from the distillation using two successive AG1X8 anion columns. However, this procedure yielded very high and variable blanks and the reproducibility of replicate samples was poor. For this reason, all samples for which sufficient powder remained were reanalysed for Re using the following chemical procedure. Powder splits were dissolved in $3HF+1HNO_3$ and left for 3 days in an oven at 140°C. Re was then extracted on one AG1X8 anion column following the procedure described in Reisberg et al. (Reisberg et al., 1991), and then analysed by ICP-MS. Blanks by this latter method were about 30 pg. Because of the lower and less variable Re blanks, this technique likely yielded more reliable results. Since these Re concentrations were measured on different powder splits than the corresponding Os analyses, powder heterogeneity may introduce some uncertainty in the Re/Os ratios and partly explain the lack of correlation between $^{187}Os/^{188}Os$ and Re/Os.

Lu-Hf chemical and analytical procedures follow those described by Blichert-Toft et al. (Blichert-Toft et al., 1997). Chemistry was performed at the Université de Rennes (France). The procedure of Blichert-Toft et al. was applied to 150 mg of carefully hand-picked Cpx separates previously washed with purified H_2O, after initial separation by a Frantz magnetic separator. Samples were spiked for both Lu-Hf and Sm-Nd. Lu and Hf were analysed at the ENS-Lyon on a VG Elemental multi collector ICP-MS ("Plasma 54"). Measurements of standard JMC 475 typically gave $^{176}Hf/^{177}Hf$ = 0.282160±25. However, reproducibility could only be tested on one peridotite sample (AL-40) via the analysis of two clinopyroxene separate splits (Table 2). The result is that the replicate "AL-40 Cpx" is within the 2σ-m in run precision of the other replicate "AL-40 Cpxbis". Two

samples (AL-40 and AL-47) have large errors (2σ-m) on their $^{176}Hf/^{177}Hf$ ratios (Table 2). These were due to the low signal intensities on the mass spectrometer, which resulted from poor yields during chemistry. Comparison of the Lu contents obtained by isotope dilution (Table 2) with those determined by ICP-MS (Table 1 for the whole-rock data, see Shi et al., 1998, for the clinopyroxene data) shows that the inter-method reproducibility is between 1 and 14% for whole-rocks and between 1 and 10% for the clinopyroxenes. Hf contents of clinopyroxenes determined by isotope dilution (Table 2) and by ICP-MS (Shi et al., 1998) also agree within 10 to 18%.

Aliquots for Sm-Nd in the clinopyroxenes were taken before the REE solution was loaded onto a cation-exchange column for Lu separation. The same Sm-Nd chemistry and analytical procedure were applied to 1.5 to 2 g of whole-rock powder. Nd was then separated using 0.1 ml True Spec resin and 2 ml HDEHP resin columns at the Université de Rennes (France). Finally Nd was analysed on a Finnigan MAT 262 mass spectrometer at the CRPG-CNRS (Nancy, France), after loading with phosphoric acid onto Re evaporation filaments in a double Ta and Re filament assembly. Nd concentrations were thus obtained by isotope dilution. Fractionation was corrected to $^{146}Nd/^{144}Nd = 0.721900$ and repeated measurements of the Johnson and Matthey standard gave $^{143}Nd/^{144}Nd = 0.511127\pm13$. Comparison of Nd contents obtained by Isotope Dilution (Table 2) and by ICP-MS (Table 1) indicate a difference of 30-42 % in the whole-rock analysis (based on one sample, AL70WR), and of 11.5-16% for the Cpx (Table 2 and (Shi et al., 1998). Sm contents on the other hand were analysed by ICP-MS solution and its dosability (10 times the detection limit) is approximately 0.005 ppm. Lastly, S contents were analysed by combustion followed by impulsion coulometry at the CRPG, with reproducibility ranging between 10 and 40%.

Location name	Tectonic terrane	Sample	Rock type	[Re] (ppb)	[Os] (ppb)	$^{187}Os/^{188}Os$	$^{187}Re/^{188}Os$	T_{MA} (Ga)	T_{RD} (Ga)	S (ppm)	Al_2O_3 (wt %)	Mg#	Nd (ppm)	Sm (ppm)	Yb (ppm)	Lu (ppm)	Hf (ppm)
Alligator Lake (B)	Coast Belt	AL-40	lherz		2.2331	0.12840±25			0.0841	30	3.43	89.49	0.5462	0.2077	0.3050	0.0526	0.0587
		AL-42	lherz	**0.187**	1.4981	0.12568±13	0.5995	*<0*	0.4638		3.24	89.66	0.8986	0.2958	0.2951	0.0496	0.0723
		AL-46	lherz		0.1460	0.13081±58			*<0*		3.53	89.25				0.0600	
		AL-47	lherz		2.1930	0.12541±37			0.5014		2.66	89.62	0.2699	0.1196	0.2274	0.0398	0.0353
		AL-70	lherz								1.56	85.30	1.8240	0.4779	0.1028	0.0126	0.1281
		AL-75	lherz	**0.174**	1.0574	0.12591±28	0.7904	*<0*	0.4318		2.05	89.78	2.9348	0.6184	0.1877	0.0280	0.0798
				0.090													
		AL-76*	lherz	**0.310**	1.8090	0.12830	0.8220	*<0*	0.0981	35	3.63	88.28	0.5552	0.1677	0.3352	0.0552	
		AL-86	lherz	**0.144**	0.7252	0.12531±37	0.9537	*<0*	0.5153		2.50	89.07	1.7911	0.2985	0.2285	0.0394	0.0721
		AL-88*	lherz	**0.289**	1.5297	0.13160	0.9075	0.3246	*<0*	58	3.77	89.50	0.5341	0.2062	0.3652	0.0662	
		AL-41	harz	**0.179**	1.1437	0.12554±34	0.7518	*<0*	0.4833	38	0.62	91.33	0.5111	0.0761	0.0186	0.0036	
		AL-49	harz		0.6816	0.12098±34			1.1143	27	0.44	90.86	0.2742	0.0424	0.0117	0.0023	
		AL-52*	harz	**0.093**	0.7779	0.12740	0.5742	*<0*	0.2240	27	0.58	91.18	0.3389	0.0633	0.0289	0.0041	
		AL-53	harz		1.7068	0.12531±24			0.5153		0.72	91.20	0.4988	0.0849	0.0305	0.0047	
		AL-54	harz	0.057	1.7564	0.12648±49	0.2987	1.1585	0.3524		0.66	91.44	1.3028	0.2729	0.0478	0.0061	
		AL-56	harz	**0.082**	1.0233	0.12724±25	0.3849	2.4024	0.2463		1.22	89.94	0.3589	0.0552	0.0619	0.0110	
Llangorse (B)	Cache Creek	XLG-30N	lherz	0.360	4.4654	0.12450±29	0.3872	*>4.5*	0.6278	80	3.13	90.71	0.0485	0.0474	0.2562	0.0441	0.0250
		XLG-29A	lherz	**0.195**	0.5086	0.12236±43	1.8416	*<0*	0.9241	65	1.49	89.73			0.0817	0.0149	0.0001
		XLG-12A	harz	**0.003**	0.4128	0.12957±36	0.0349	*<0*	*<0*	36	0.71	91.31	0.0679		0.0089	0.0083	0.0107
		XLG-25A	harz	0.014	0.0502	0.13728±76	1.3403	0.5423	*<0*	33	0.84	91.59	0.8672	0.1597	0.0372	0.0083	0.1008
Rayfield River (U)	Quesnellia	RRX-19	harz	0.082	3.1418	0.12443±30	0.0290	0.6837	0.6375			90.50	0.0351	0.0111	0.0311	0.0065	0.0086
				0.045													
		RRX-21	harz	**0.019**	1.7967	0.12532±21	0.0680	0.6072	0.5111	41	0.94	90.33		0.0138	0.0478	0.0098	0.0125
Kostal Lake (U)	Kootenay	KLX-47	harz	**0.028**	1.2642	0.12661±39	0.1064	*<0*	0.3342		1.17	89.65	0.4546	0.0850	0.0473	0.0091	0.0657

*Table 1: Os isotope data from mantle xenoliths of the Canadian Cordillera. Precision on $^{187}Os/^{188}Os$ ratio listed corresponds to 2σ run statistics. Uncertainties on the Lu and Al_2O_3 contents are respectively ± 0.001 ppm (analytical precision calculated from 10 replicate analyses of a REE standard) and 0.03 wt % (analytical precision calculated from 20 replicate analysis). Re contents determined on samples dissolved in HF-HNO_3 are denoted in boldface and corrected for 30 pg blank, while those digested by the Carius Tube technique are listed in plain type and corrected for a 50 pg blank. Os isotopic ratios were normalized to $^{192}Os/^{188}Os$ = 3.08271. U = Unimodal suites, B = Bimodal suites, * = samples analysed by J. Carignan (Carignan et al., 1996). Model age calculations (T_{MA}) and minimum Re depletion age (T_{RD}) were made using a λ= 1.666 10^{-11} y^{-1} (Smoliar et al., 1996), a present primitive mantle $^{187}Os/^{188}Os$ ratio of 0.1290 and $^{187}Re/^{188}Os$ ratio of 0.428 (Meisel et al., 1996).*

Sample	Hf (ppm)	Lu (ppm)	$^{176}Hf/^{177}Hf$	2σ-m	$^{176}Lu/^{177}Hf$	TM (Ga)	Nd (ppm)	Sm (ppm)	$^{143}Nd/^{144}Nd$	$^{147}Sm/^{144}Nd$
AL70Cpx	1.79	0.08	0.283241	6.60E-05	0.00635	<0				
AL70WR		0.02					1.28	0.42	0.512735±5	0.1984
AL75Cpx	2.21	0.16	0.282916	4.40E-05	0.01029	0.47	28.6		0.512788±5	
AL75WR		0.03								
AL47Cpx	0.64	0.25	0.283496	2.90E-04	0.05514	1.02				
AL47WR		0.04								
AL40Cpx	0.78	0.27	0.283595	1.93E-04	0.04825	2.32	3.57	1.41	0.51303±5	0.2397
AL40Cpxbis	0.77	0.25	0.283928	3.67E-04	0.04576					
AL40Opx	0.03	0.06	0.283919	1.95E-04	0.26971	0.17				
AL88Cpx		0.23								
AL88WR		0.06								
AL52Cpx		0.06								
AL53Cpx							32.2	3.66	0.512774±1	0.0691

Table II: Lu-Hf and Sm-Nd data from mantle xenoliths of the Canadian Cordillera. For Lu and Hf concentrations, in-run precisions are about ± 0.000005 and 0.0004 Model age calculations (T_{MA}) were made using a $\lambda = 1.94\ 10^{-11}\ y^{-1}$ (Sguigna et al., 1982), a depleted mantle $^{176}Hf/^{177}Hf$ ratio of 0.283176 (middle of the range 0.283040-0.283311 (Nowell et al., 1998) and a $^{176}Lu/^{177}Hf$ ratio of 0.03912 (calculated with a mantle evolution line from chondritic (Blichert-Toft, et al. 1997) to depleted MORB).

4.5 RESULTS

Os and Re concentrations and $^{187}Os/^{188}Os$ ratios are given in Table 1, as well as 3 data points from the study of Carignan et al. (1996). The Os contents of all the analysed xenoliths range from 0.05 ppb to 4.5 ppb, most being less than 2.5 ppb (Table 1). These values are comparable to results reported for other spinel peridotite xenolith suites (McBride et al., 1996; Handler et al., 1997), but less than the values usually found in peridotite massifs (e.g., Reisberg et al., 1991; Fig. 2). Sulfur contents (Table 1) are also lower than typical peridotite massif values, as is often the case in mantle xenoliths (Lorand, 1990). Re contents range from 0.014 to 0.310 ppb, which are typical upper mantle values, and are generally lower in the harzburgites than in the lherzolites (Fig. 3). A broad correlation exists between Re contents and Al_2O_3 and HREE (Heavy Rare Earth Elements; Fig. 3)

Although no correlation is observed between $^{187}Re/^{188}Os$ and $^{187}Os/^{188}Os$, the $^{187}Os/^{188}Os$ ratios of the lherzolites define a good correlation with fusion indexes such as Al_2O_3 and HREE (Fig. 4). This trend is not seen in the harzburgites from either the bimodal suites or the unimodal suites, whose $^{187}Os/^{188}Os$ ratios are, however, correlated with their 1/Os contents (Fig. 5). One of the harzburgites (XLG-25A) has a $^{187}Os/^{188}Os$ ratio of 0.1373, which is markedly higher than the primitive mantle value of 0.1290 (Meisel et al., 1996). Furthermore this sample also has the lowest Os concentration of all the xenoliths and falls below the 1/Os harzburgite correlation (Fig. 5). Another harzburgite xenolith from the Llangorse site (XLG-12A) also possesses a high Os isotopic ratio with a relatively low Os concentration, but nonetheless plots on the $^{187}Os/^{188}Os$-1/Os trend of the other harzburgites. Harzburgite AL-49 also falls off the harzburgite correlation and is the only harzburgite that appears to lie on the $^{187}Os/^{188}Os$-Al_2O_3 correlation line defined by the lherzolites, despite exhibiting the LREE enriched patterns typical of most other

harzburgites (Fig. 3). Finally, no correlation was observed between Os isotopes and Pb isotopes (Carignan et al., 1996) in lherzolites or harzburgites.

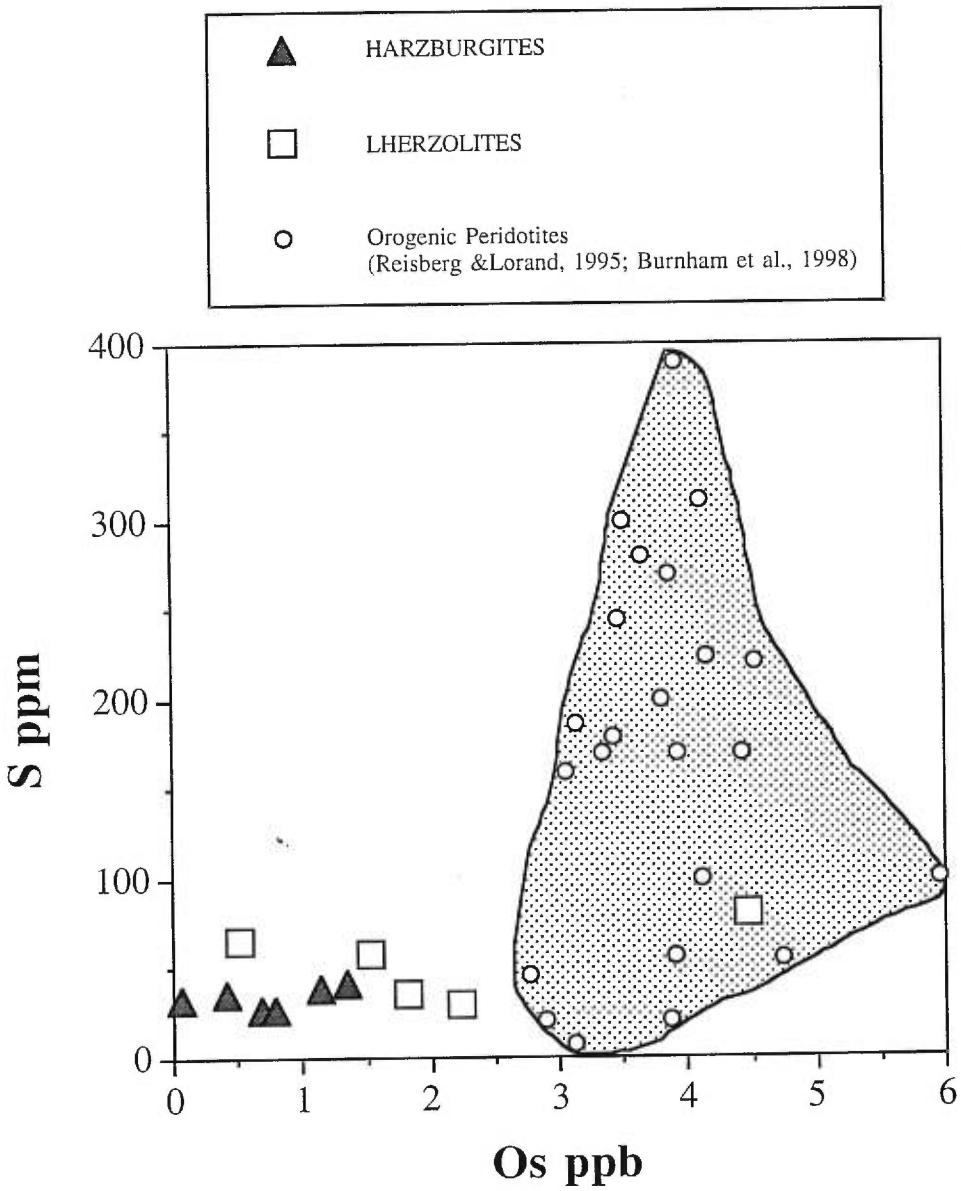

Fig. 2: S content versus Os content of Canadian Cordillera xenoliths and comparison with orogenic peridotite (Reisberg and Lorand, 1995; Burnham et al., 1998). Grey area represents orogenic peridotite field.

The Lu-Hf data for 4 lherzolite samples are presented in Table 2. The $^{176}Hf/^{177}Hf$ ratios of clinopyroxenes vary over a wide range, from as low as typical OIB (Oceanic Island Basalts) values to slightly more radiogenic than the MORB field (Fig. 6). Interestingly, the low $^{176}Hf/^{177}Hf$ ratio (0.282916) of AL-75 Cpx is the lowest ever measured in a peridotite sample. The $^{176}Hf/^{177}Hf$ ratio of orthopyroxene in sample AL-40 is within error of one of the clinopyroxene replicates, but outside the errors of the other. The average $^{176}Hf/^{177}Hf$ ratio between the two Cpx replicates from AL-40 is 0.283762, which is slightly lower than the Opx $^{176}Hf/^{177}Hf$ ratio. A $Kd^{Cpx/Opx}$ for Hf of 23.2 can be calculated for sample AL-40, which is in agreement with previously published data on natural samples (Salters and Zindler, 1995), but lower than results from mineral/melt experiments ($Kd^{Cpx/Opx}$ for Hf ~ 62, using data from Green (Green, 1994). When plotted against Hf concentration, the Hf isotopic ratios of the Cpx and Opx define a negative correlation (Fig 7). Finally, there is no correlation between Hf and Os isotopes or between Hf isotopes and any trace element, but the small number of Hf data prevents us from drawing strong conclusions.

The $^{143}Nd/^{144}Nd$ ratios of three clinopyroxenes, from two lherzolites and one harzburgite, are within the range reported for similar spinel peridotites (e.g., Menzies, 1983; Brandon et al., 1996; Zangana et al., 1997) though in the relatively unradiogenic part of this field ($\leq$ 0.51303) with the harzburgite Cpx being the least radiogenic of the three. One whole-rock analysis of lherzolite AL-70 gives a relatively unradiogenic $^{143}Nd/^{144}Nd$ ratio of 0.512735. These Nd isotopic ratios are lower than MORB values and within the OIB range (Fig. 6). Finally the possibility of correlations between Pb (Carignan et al., 1996) isotopes and Hf or Nd isotopes could not be tested due to the limited number of samples which could be analysed for Nd and Hf.

Most of the harzburgite whole rocks have steep light rare earth element enriched patterns, except at one unimodal suite (Rayfield River) where the two harzburgites analysed are depleted in LREE (Fig.8a). Lherzolites have whole-rock depleted to enriched LREE

patterns (Fig. 8a). Harzburgite Cpx (Shi et al., 1998) have steeper REE patterns than harzburgite whole-rocks (Fig 8b), which is consistent with the fact that the partition coefficient for LREE is higher for Cpx than for the other peridotite minerals (Green, 1994), and that no other mineral phase that preferencially hosts LREE is present in the harzburgites (Ionov et al., 1995). On the other hand, in the bimodal suites, LREE/HREE ratios (Shi et al., 1998) of the clinopyroxenes are generally lower than in whole-rocks (Fig 8b), such as observed by Eggins et al. in similar xenoliths (Eggins et al., 1998). They explain this discrepancy by cpx and amphibole breakdown products defining the REE pattern of the bulk-rock (Eggins et al., 1998). However no such amphibole breakdown is observed in the lherzolites of the bimodal suites (Francis, 1987). Either other phases contain LREE concentrations comparable to those of the cpx (such as fluid or melt inclusions in the major minerals) or the cpx is not in equilibrium with the other minerals of the lherzolites.

4.6 DISCUSSION

4.6.1 Re-Os systematics

4.6.1.1 The lherzolites

Lherzolites with similar major element and Os isotopic characteristics to those of the bimodal suites studied here are the most abundant type of mantle xenoliths found throughout the entire Canadian Cordillera, suggesting that this rock type is volumetrically dominant in the mantle lithosphere underlying this orogenic belt. No correlation is observed between $^{187}Os/^{188}Os$ and $^{187}Re/^{188}Os$ among these samples despite the existence of a good correlation between $^{187}Os/^{188}Os$ and Al_2O_3 or HREE contents. A similar lack of correlation between $^{187}Re/^{188}Os$ and $^{187}Os/^{188}Os$ in other peridotite suites

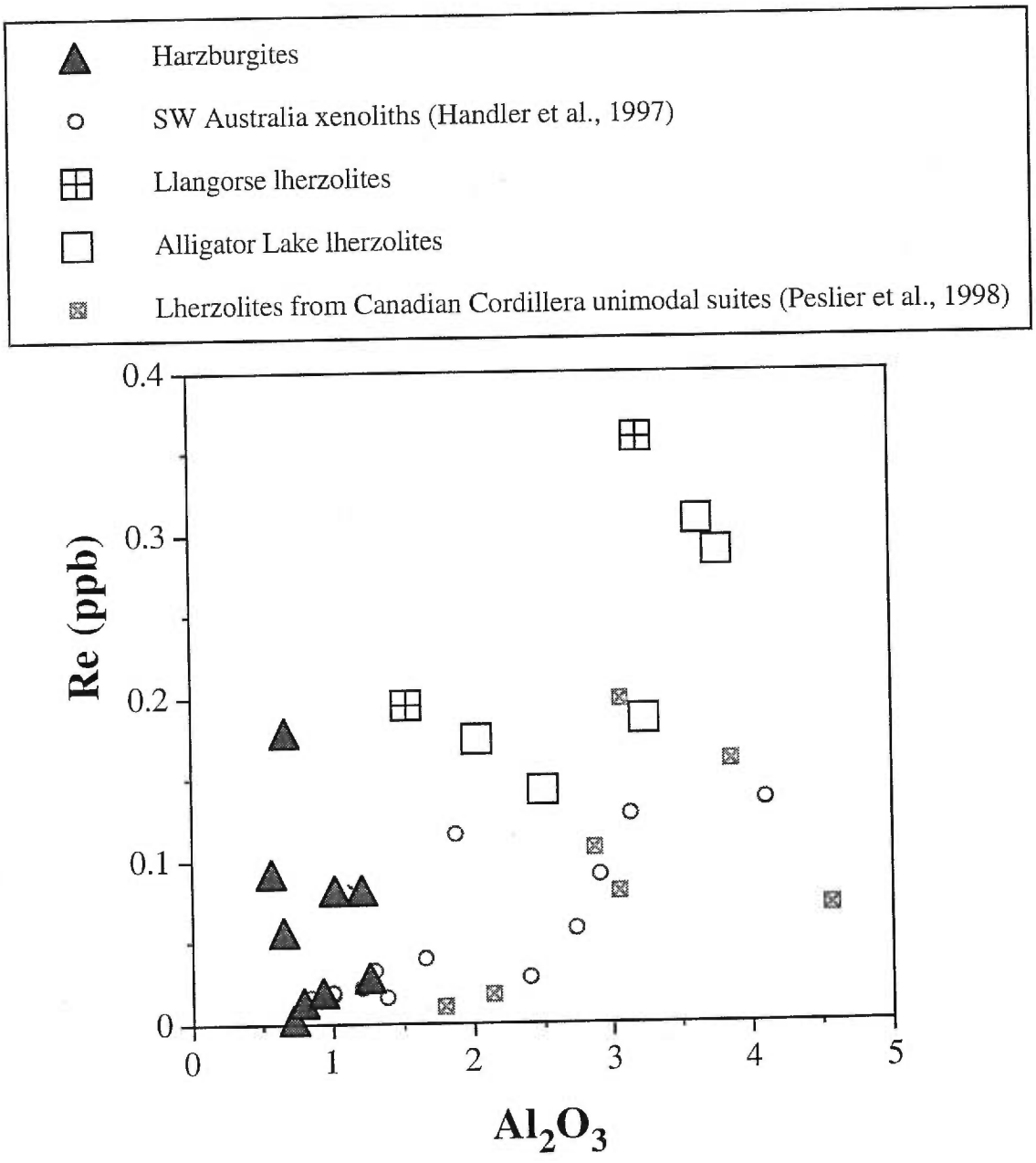

Fig. 3: Re contents (ppb) versus Al_2O_3 contents (wt %).

has often been attributed to disturbance of the moderately incompatible element Re by metasomatic processes (e.g., Reisberg and Lorand, 1995). The Re content of the lherzolites and harzburgites of the suites studied here correlates roughly with that of Al_2O_3

and HREE content (Fig. 3), but the Os content does not. Re concentrations of harzburgites moreover are lower than those of lherzolites, and the Re contents of the most fertile lherzolites approach those observed in fertile orogenic lherzolites (~ 0.3 ppb). This Re concentration is higher than that observed in similar xenolith suites (Handler et al., 1997) and in lherzolites from unimodal Canadian Cordillera suites (Peslier et al., 1998a; Fig. 3). The rough correlation of Re and Al_2O_3 of the lherzolites suggests that these samples may have experienced substantial recent Os loss. Alternatively, their higher Re contents compared to those of the other xenoliths shown in Fig. 3 may indicate that Re was added to them. The $^{187}Re/^{188}Os$ ratios of nearly all the lherzolites are considerably higher (Table 1) than that of the fertile upper mantle (~ 0.4; Reisberg and Lorand, 1995), despite their normal Os isotopic ratios (Table 1). Thus regardless of which process (Os loss or Re addition) was more important, the increase of the Re/Os ratios must have been recent.

The decoupling of $^{187}Re/^{188}Os$ and $^{187}Os/^{188}Os$ observed in the Canadian Cordillera xenolith data also affects the calculation of Os model ages, and leads to "future" ages or ages older than the Earth (Table 1). Calculated minimum ages, assuming a Re/Os of zero (Walker et al., 1989), range from 0.08 to 1.11 Ga, with no significant difference between lherzolites and harzburgites, but four xenoliths still yield "future" ages (Table 1). Since the lherzolites almost certainly had Re/Os ratios significantly higher than zero after melt extraction these "Re depletion ages" seriously underestimate the true ages of the melting events. The good correlation between $^{187}Os/^{188}Os$ vs Al_2O_3 in the lherzolite xenoliths permits the use of the method of Reisberg and Lorand (Reisberg and Lorand, 1995) to estimate the age of the last depletion event. In this method, Al_2O_3 is taken as a proxy for the Re/Os ratio, and gives an age of 1.64 ± 0.52 Ga for the Alligator Lake lherzolites. Following Meisel et al. (1996) and Hauri et al. (1997), who consider Lu and Re as similarly incompatible, we however prefer to use the Lu content of the whole rock as a Re/Os ratio proxy. The $^{187}Os/^{188}Os$ vs Lu correlation for the Alligator Lake lherzolites (Fig. 3) yields a model age of 1.55 ±0.72 Ga. If the harzburgite AL-49 is included in the

correlation (see discussion in 5.1.2), the model age is 1.21 ± 0.48 Ga (1.34 ± 0.56 using Al_2O_3). These ages were calculated using a mantle evolution curve similar to that of primitive mantle (Meisel et al., 1996). If the lowest value for the "chondritic" mantle evolution curve (ordinary and enstatite chondrites; Meisel et al. 1996) is used instead, the estimated ages decrease by 0.1 Ga. The uncertainties on the ages are based on the expanded uncertainties on the y-intercept, and mainly reflect how well the data fit an "isochron" line (McIntyre et al., 1966; York, 1969; Titterington and Halliday, 1979). A conservative interpretation of these uncertainties suggests that the Alligator Lake lherzolites are the residues of melting events which took place between 0.73 and 2.27 Ga ago, i.e. during the Proterozoic. It is quite possible, however, that most melt extraction associated with lithosphere formation was limited to a much shorter time interval within this period.

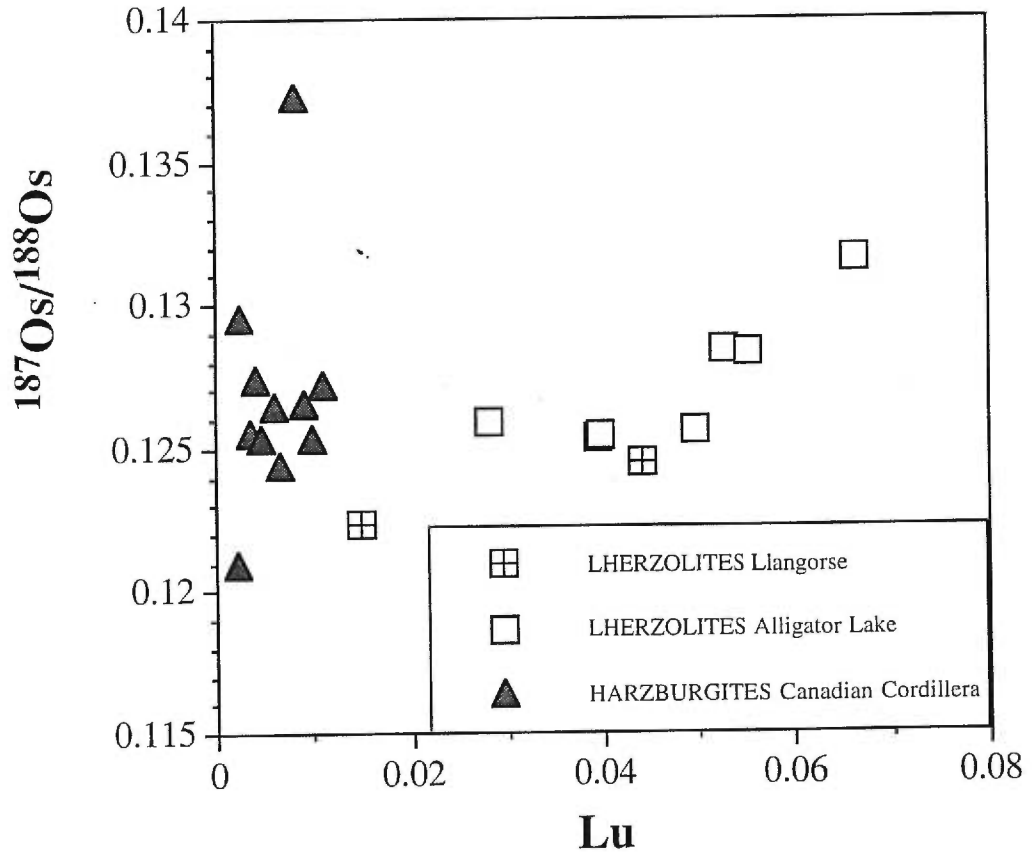

Fig. 4: $^{187}Os/^{188}Os$ vs Lu. Lu concentrations in ppm.

4.6.1.2 The harzburgites

The $^{187}Os/^{188}Os$-1/Os correlation

In contrast to the lherzolites, the Os isotopic ratios of the harzburgites show no relation with HREE or Al_2O_3. The positive correlation between $^{187}Os/^{188}Os$ and 1/Os, observed in harzburgites from both bimodal and unimodal suites (Fig. 5), however, suggests a mixing process between peridotite and a component with radiogenic Os. Sample Al-49 lies off this correlation, although it is enriched in incompatible elements like most other harzburgites (Shi et al., 1998). It may represent a depleted end-member of the lherzolite trend. The exceptionally low Os content of XLG-25A (0.05 ppb), on the other end, suggests that it may have been affected by post-eruptive Os loss (Lorand, 1990), or a different metasomatic agent. The two harzburgites having the highest Os isotopic ratios (XLG-25A and XLG-12A) are the only harzburgites analysed from the Llangorse site. In contrast to the Alligator Lake site, where the xenoliths were removed from scoria, mantle xenoliths at Llangorse were extracted from a lava lake and may have exchanged Os with their host lava. However, lherzolite xenoliths from the Llangorse suite do not show similar Os isotopic enrichments or particularly low Os contents (Table 1), suggesting the Os values for the Llangorse harzburgites are primary.

Finally, the harzburgite $^{187}Os/^{188}Os$-1/Os correlation (Fig. 5) indicates that the Os concentration variation in the harzburgites is not the result of sulfur loss through post-eruptive alteration processes such as described by Lorand (Lorand, 1990), and that such processes are not responsible for the low Os contents of spinel xenoliths compared to those of orogenic peridotitic massifs. Such processes would lower the Os contents of the harzburgites, but not change their Os isotopic ratios. The phenomenon responsible for the Os concentration difference between xenoliths and orogenic peridotitic massifs (Fig. 2) thus remains unclear, but it was probably pre-eruptive.

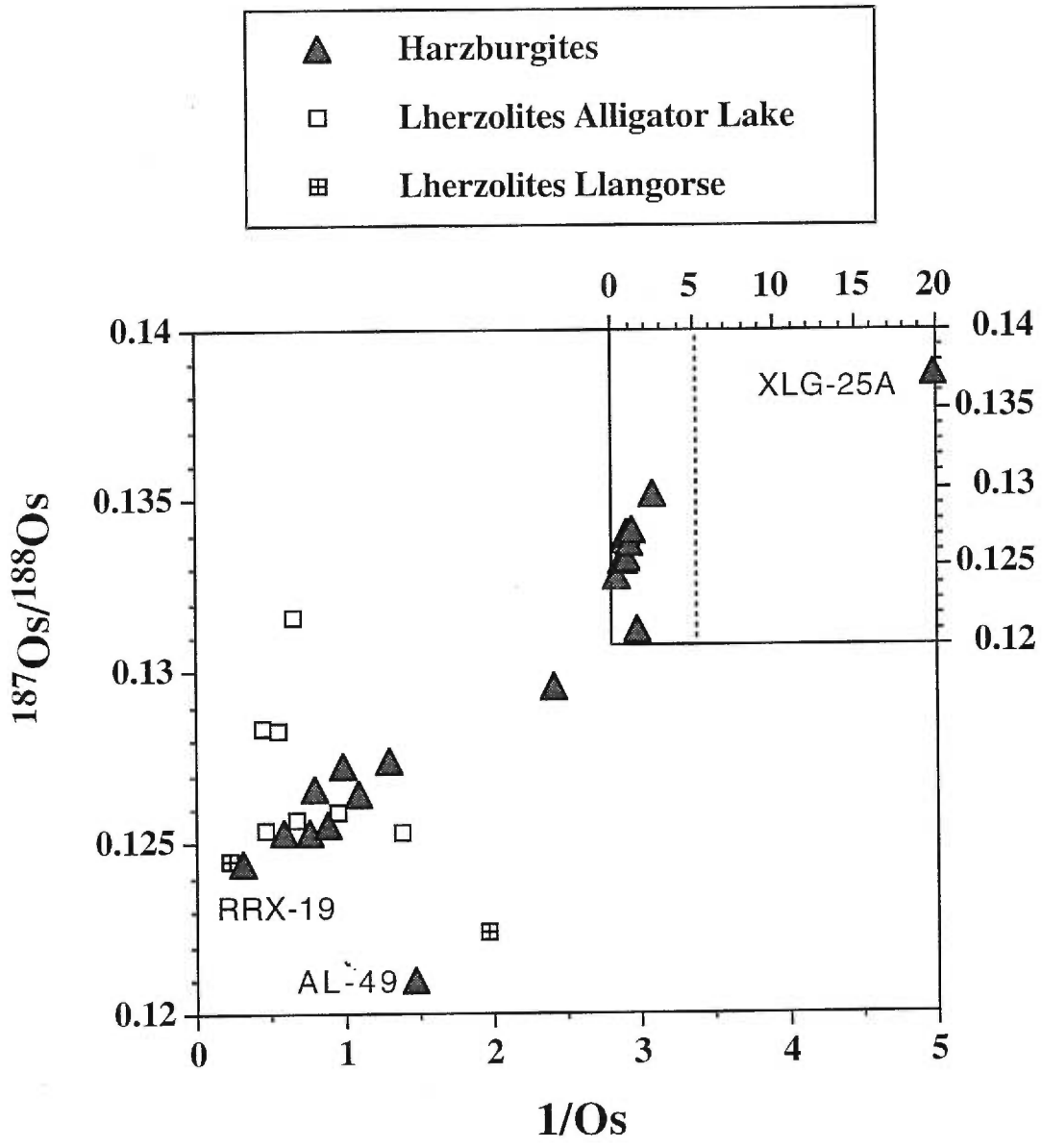

Fig. 5: $^{187}Os/^{188}Os$ vs 1/Os for the harzburgitic xenoliths, derived from both bimodal and unimodal suites. The larger graph is an expanded view of the dashed portion of the small graph.

Harzburgite formation

The Os isotopic systematics (Fig. 4), as well as the trace element geochemistry (Shi et al., 1998), demonstrate that harzburgites do not merely represent higher degrees of melting of the lherzolitic source mantle. It is unlikely that the harzburgites represent the

asthenospheric mantle, such as the high-temperature mantle detected teleseismically under the bimodal suites (Frederiksen et al., 1998), for three reasons. (1) No garnet is present and no petrological indication of former garnet can be detected (Shi et al., 1998). (2) The harzburgites would produce faster seismic velocities than the lherzolites, and not lower ones as required for the teleseismic mantle anomaly (Shi et al., 1998). (3) Four of nine harzburgites fall above the typical $^{187}Os/^{188}Os$ ratio range for abyssal peridotite (0.1221 to 0.1270), which can be taken as representative of the asthenosphere (Snow and Reisberg, 1995).

20-25% partial melting is required to reproduce the bulk-rock major-element and clinopyroxene HREE contents of the most depleted harzburgite from the most fertile lherzolite (Francis, 1987; Shi et al., 1998). Recent simple melting however cannot explain the harzburgite Os data. This process could have produced the harzburgites from the lherzolites without changing the $^{187}Os/^{188}Os$ ratios, thus causing them to plot above the lherzolite trend in Fig. 4. However it could not have produced harzburgite XLG-25A with a $^{187}Os/^{188}Os$ ratio (0.137) exceeding that of fertile mantle (0.1290; Meisel et al., 1996). Also simple recent remelting should also have produced cpx-poor lherzolites that would also plot above the lherzolite trend, and these are not observed. Hamlyn and Keays (1986), based on the enhanced PGE content of boninitic magmas compared to that of MORB (Mid-Ocean Ridge Basalts), have developed a model in which second stage melting of depleted mantle could decrease the PGE content of the residue by complete dissolution of the sulfide phases. No significant Os content difference can be seen between harzburgites and lherzolites of the Canadian Cordillera (Table 1), thus providing a further line of evidence that the Os content range of the harzburgites do not reflect recent remelting of the lithosphere (represented by the lherzolites of Proterozoic age). Finally again, melting alone would not generate the $^{187}Os/^{188}Os$-1/Os correlation.

From the previous remarks, metasomatic enrichment is the process most likely to explain the Os isotopic characteristics of the harzburgites. The $^{187}Os/^{188}Os$-1/Os

correlation (Fig. 5) could be a mixing line representing the interaction of low-Os content, high-Os isotopic ratio metasomatic fluids or melts with the depleted mantle lithosphere. If the harzburgite-correlation is modeled as simple mixing between a low-Os isotopic ratio, high Os content harzburgite (e.g., sample RRX-19) and a high Os isotopic ratio, low Os content mixing component, at least 80 % of the radiogenic component would be required to reproduce the Os content range of the harzburgites. This is clearly unrealistic from a major element bulk addition perspective. Instead, this simple calculation indicates that high fluid-rock ratios would be required to produce the Os isotopic signature of the harzburgites.

Two hypothetical scenarios may explain the fact that only the harzburgite type xenoliths display $^{187}Os/^{188}Os$ ratios that fall above the regional lherzolite trend. One possibility is that metasomatic melts/fluids with high Os isotopic ratios preferentially migrated through preexisting harzburgites and reset their Os isotopic characteristics. This is in agreement with the fact that these distinct Os features are displayed by not only the harzburgites of the bimodal suites, but also by the harzburgites of the unimodal suites located far from the thermal mantle anomaly. Moreover, two of the latter samples have LREE depleted whole-rock patterns, unlike the distinctly LREE enriched patterns from the other harzburgites, suggesting that Os and LREE metasomatism may have been decoupled. Metasomatism of preexisting harzburgites nicely explains the $^{187}Os/^{188}Os$-1/Os trend, but offers no explanation for the preferential association of harzburgites with the underlying mantle thermal anomaly.

A second hypothesis is that harzburgite formation was triggered by the ingress of melts or fluids (e.g., Kelemen et al., 1992; Shi et al., 1998) with radiogenic Os compositions. Harzburgite formation could then result from either lherzolite melting (increasing magma volume; Shi et al., 1998) or by lherzolite-magma interaction (constant or decreasing magma volume) in reaction zones surrounding melt conduits (e.g., Kelemen et al., 1992). In either case, interaction with such fluids could have simultaneously enhanced the incompatible trace element contents of the residual peridotite (Shi et al., 1998)

and increased their $^{187}Os/^{188}Os$ ratios. The existence of such melts at depth is consistent with the presence of the low-velocity seismic anomaly in the region (Frederiksen et al., 1998; Shi et al., 1998). This melting-metasomatism process was particularly intense above the thermal mantle anomaly above which harzburgite xenoliths are more abundant than in other parts of the Canadian Cordillera. We imagine a process in which a passing Os poor, $^{187}Os/^{188}Os$ radiogenic fluid triggers melting and scavenges Os, while enriching the trace elements and increasing the Os radiogenic isotopic ratios of the residual peridotite. However, as noted above, trace element and Os exchange may be largely decoupled, as there is no relationship between Os ratio and LREE content in the harzburgites. It is difficult to model the process of Os exchange as the behavior of Os under mantle conditions is so poorly constrained. It is however well known that PGE (Platinum Group Element) such as Os are known to be mobile under certain conditions of temperature, oxygen fugacities and chlorine fugacities (Wood, 1987).

4.6.2 Lu-Hf and Sm-Nd in the Alligator Lake lherzolites

4.6.2.1 Origin of the lherzolite isotopic characteristics

The compatibility of HREE in garnet allows the Lu-Hf system to serve as a potential tracer of deep melting of mantle peridotites. Among the Canadian Cordillera lherzolites analysed here, none have the very high $^{176}Hf/^{177}Hf$ or $^{143}Nd/^{144}Nd$ ratios that would be expected to result from melt extraction in the garnet stability field followed by a prolonged period of radiogenic ingrowth (Salters and Hart, 1989; Pearson et al., 1995b; Witt-Eickschen and Kramm, 1997). In addition, there is no petrographic evidence of the former presence of garnet in the Alligator Lake xenoliths (Shi et al., 1998), and the trace element characteristics of Alligator Lake lherzolite clinopyroxenes seem to preclude a major role for residual garnet (Shi et al., 1998). However, any petrographic evidence of

former garnet may have been erased by more than one Ga of slow reequilibration of the lherzolites in the spinel stability field. Moreover, as shown below, the lherzolites at Alligator Lake also record younger events than the primary melting about 1.5 Ga ago. These secondary events might have reset their trace element characteristics.

Interaction with the host lava is likely to lower the Lu/Hf ratio of the xenolith minerals and with time lead to lower $^{176}Hf/^{177}Hf$ ratios. However, this effect is insignificant, considering the long half-life of ^{177}Lu and the young age of the Alligator lake lava (3.5 to 6.8 Ma; Hart C., personnal communication). Direct modification of the xenolith $^{176}Hf/^{177}Hf$ ratios by the magma is a potentially a larger concern. However, one sample (AL-70) that exibits pronounced mineral zoning and partial melting textures probably produced by interaction with its host magma (Francis, 1987) yields a Cpx Hf isotopic ratio which lies within the MORB field or the upper part of the OIB field. On the other hand lherzolite AL-75 that displays no obvious host lava interaction features has the lowest Cpx $^{176}Hf/^{177}Hf$ ratio (0.282916) of the four lherzolites. Finally, host lava-xenolith interaction will tend to homogenize the isotopic compositions of the xenoliths and thus cannot explain the wide isotopic range observed.

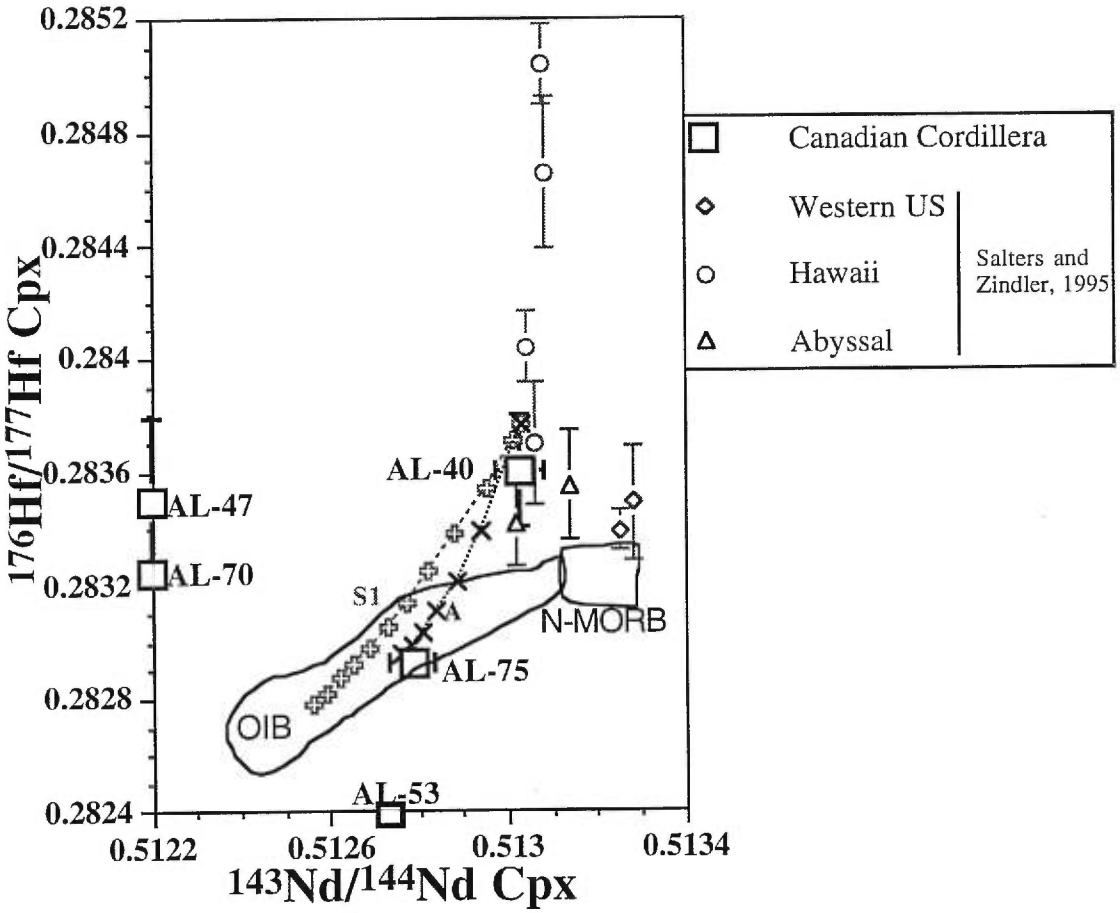

Fig. 6: $^{176}Hf/^{177}Hf$ vs $^{143}Nd/^{144}Nd$ of clinopyroxenes. Data for which the Hf or Nd isotopic value only is known are plotted on the graph axes. Also included are peridotite data from Salters and Zindler (1995). MORB and OIB fields from Nowell et al. (1998). The dashed-lines (Trends A and S1 of Fig. 3) correspond to simple mixing between an OIB type component (Trend A; parameters used are $^{143}Nd/^{144}Nd$ = 0.51265 and Nd content = 20 ppm, which could correspond to an EMII type OIB) or a slab type component (Trend S1; parameters used are 80% MORB $^{143}Nd/^{144}Nd$ = 0.5132 at 175 Ma = 0.51317 and Nd content = 7.3 ppm (Sun and McDonough, 1989) + 20% sediments at $^{143}Nd/^{144}Nd$ =0.51231 and Nd content = 18.5 ppm, which is the turbidite with the lowest $^{176}Hf/^{177}Hf$ ratio from the Northern Pacific measured so far (Vervoort et al., 1998) and an initial composition taken as the $^{176}Hf/^{177}Hf$ of AL-40 Cpx (average of the two replicates) and the Hf content of AL-47. Ticks on the line mark 5 % mixing increments.

Simple bulk mixing calculations can be used in order to constrain the origin of the broad range of Hf isotopic data. One end-member is assumed to be the most depleted mantle-like sample in terms of Hf isotopes (average of AL-40 Cpx replicates). This end-member is mixed with various possible metasomatic components. Simple mixing between AL-40 Cpx and less than 25% of an OIB type component ([Hf] = 7.8 ppm; Sun and McDonough, 1989), $^{176}Hf/^{177}Hf$ = 0.2828, typical EMII Hf isotopic ratio (Salters and Hart, 1991) can reproduce the $^{176}Hf/^{177}Hf$ ratio vs Hf content trend of our Cpx data (Fig. 7, trend A) and goes from AL-40 Cpx to AL-75 Cpx in the $^{176}Hf/^{177}Hf$- $^{143}Nd/^{144}Nd$ diagram (Fig. 6). Increasing the Hf concentration in the OIB component up to 8.8 ppm Hf, which is a higher end value for OIB (Weaver et al., 1987), reproduces our data as well (Fig. 3, trend B). Lowering the Hf concentration down to 4.4 ppm, a lower value for OIB (Weaver et al., 1987), would increase the amount of this component necessary to more than 30% (Fig. 7, trend D). Lowering the $^{176}Hf/^{177}Hf$ ratio of the OIB component to the lower end of the OIB field (0.2826) produces a mixing trend that falls below the $^{176}Hf/^{177}Hf$-Hf trend (Fig. 7, trend C). Such simple bulk mixing is unrealistic as it would completely change the major element composition of the peridotite. It is possible that the metasomatic component was a low fraction melt derived from an OIB source. Such a melt would probably have a high Hf content. The metasomatic agent may also have been a fluid that was more enriched in Hf than the end-members used above. Consequently a lower amount of this component would be needed to produce the Hf characteristics of the mantle xenoliths. These possibilities are of course very poorly constrained and difficult to test. Nevertheless, the Pb-Sr characteristics of the Alligator Lake xenoliths (both lherzolites and harzburgites) show a trend from depleted mantle values towards EMII type of mantle (Carignan et al., 1996), reinforcing the need for some sort of enrichment process.

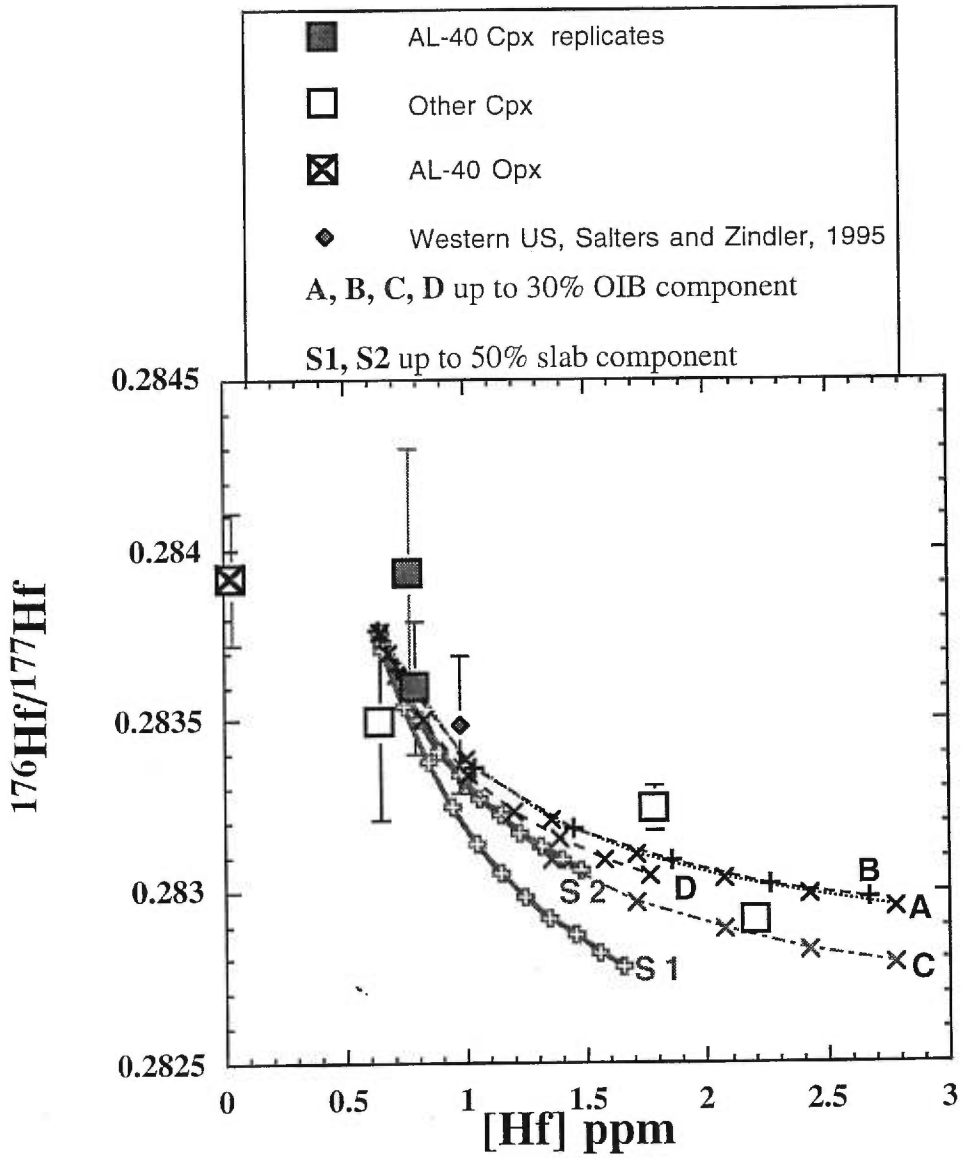

Fig. 7: Graph $^{176}Hf/^{177}Hf$ vs Hf content of clinopyroxenes and orthopyroxene. Dashed lines correspond to the mixtures A, B, C, D, S1 and S2 described in text. Trend A: OIB, [Hf] = 7.8 ppm, $^{176}Hf/^{177}Hf$ = 0.2828; Trend B: OIB, [Hf] = 21 ppm, $^{176}Hf/^{177}Hf$ = 0.2828; Trend C: OIB, [Hf] = 7.8 ppm, $^{176}Hf/^{177}Hf$ = 0.2826; Trends S1 and S2: slab, 80% MORB (0.283176; Nowell et al., 1998), 2.05 ppm Hf; Sun and McDonough, 1989), which is allowed to evolve 175 Ma, age of the Pacific plate, giving 0.2833081), 20% sediments (0.282467, 5.1 ppm Hf for S1 and 0.2828, 3.37 ppm Hf for S2; Vervoort et al., 1998)). S1 corresponds to the lowest $^{176}Hf/^{177}Hf$ ratio measured in a northern Pacific sediment (a turbidite), S2 corresponds to the average of the four $^{176}Hf/^{177}Hf$ ratios of sediments (turbidites) measured so far in the Northern Pacific (Vervoort et al., 1998). Increments are 5 %.

Comparison of the Pb isotopic characteristics of Aleutian Arc lavas with those of Northern Pacific sediments led Carignan et al. (1996) to conclude that the subcontinental lithosphere underlying the Northern Canadian Cordillera had been recently enriched by subduction related fluids/melts. By taking the lowest Hf isotopic ratio measured for a Northern Pacific ocean sediment (0.282467; Vervoort et al., 1998), the lowest value of our Hf isotopic ratios (0.282916 for AL-75 Cpx) can be reached by simple mixing with 35% of a slab component composed of 80% MORB-20% sediment (0.283131), but the Hf content range is not reproduced and the Nd isotopic ratio range is too wide compared to the data (Fig. 6 and 7, trend S1). By taking an average of the $^{176}Hf/^{177}Hf$ ratios of the Northern Pacific sediments (0.282670), much more than 50% of slab component is needed in order to obtain a value as low as that of AL-75, which is totally unrealistic (Fig. 7, trend S2). It is more plausible to propose that the metasomatic agent was a melt or fluid with a high Hf content derived from a downgoing slab, but this model is too poorly constrained to be tested In conclusion, although metasomatism by subduction related fluid/melts cannot be totally excluded based on the few contraints we have from Hf isotopes, a more likely explanation of our data is that it reflects the interaction of a subcontinental mantle slightly more radiogenic than MORB with a fluid/melt of EMII type isotopic characteristics. This fluid/melt partly reset the Lu-Hf characteristics of the lherzolites, leaving two of our analysed samples (AL-40 and AL-47) with depleted mantle Lu-Hf values and the other two (AL-70 and AL-75) with values approaching those of OIBs. This is in agreement with the more LREE enriched patterns of AL-70 and AL-75 compared to those of AL-40 and AL-47 (Fig. 8a). Moreover, AL-40 and AL-47 have higher than chondritic Lu/Hf ratios (0.23; Sun and McDonough, 1989)), consistent with the result of melt extraction, while AL-70 and AL-75 have lower than chondritic Lu/Hf ratios, requiring an enrichment process. This interpretation is in agreement with the model developed for the Re-Os characteristics of the harzburgites. Low Os content, Os radiogenic fluids/melts of

asthenospheric origin percolated through the lherzolites, transforming them to harzburgites while increasing their Os isotopic ratios. This process also disturbed the Sm-Nd and the Lu-Hf characteristics of the pre-existing lherzolites of this region.

4.6.2.2 Timing of melting and metasomatism

The two samples (AL-70 and AL-75) which have apparently interacted with enriched melts or fluids yield one "future" Hf model age and 0.465 Ga. The latter age is significantly younger than the Proterozoic age found with the Re-Os method. This is to be expected, as the Lu-Hf and Hf isotopic ratios have been recently modified. Cpx separates from the two other samples (AL-47 and AL-40), which have suffered little or no recent Lu/Hf perturbation, yield ages of 1.02 and 2.32 Ga respectively. The latter age is older than the Re-Os model age, but was calculated on AL-40 for which the error on the Hf isotopic ratio is the largest of the samples analysed. Because minerals such as opx (around 10 times less Hf than Cpx from our data), or spinel microinclusions (Bodinier et al., 1996) may contain a significant fraction of Hf in peridotite, a bulk-rock model age would be more meaningful, especially if cpx and opx were recently in Hf isotopic equilibrium. Using the mineral proportions of sample AL-40 (cpx 16% and opx 24%), the bulk-rock age is calculated to be 1 Ga. The 1.02 Ga model age for AL-47 (cpx) is on the other hand in the range of Re-Os model ages calculated above for the Alligator Lake lherzolites.

Fig. 8 (2 next pages): a) REE patterns of whole-rock lherzolites and harzburgites. b) Comparison of REE patterns between clinopyroxenes (Shi et al., 1998) and whole-rock samples. Data normalized to Sun and McDonough (1989) C1 chondrite. The whole-rock REE patterns were obtained by ICP-MS at the CRPG-CNRS, Nancy, France and are unpublished data by Shi and ourselves.

Fig. 8a

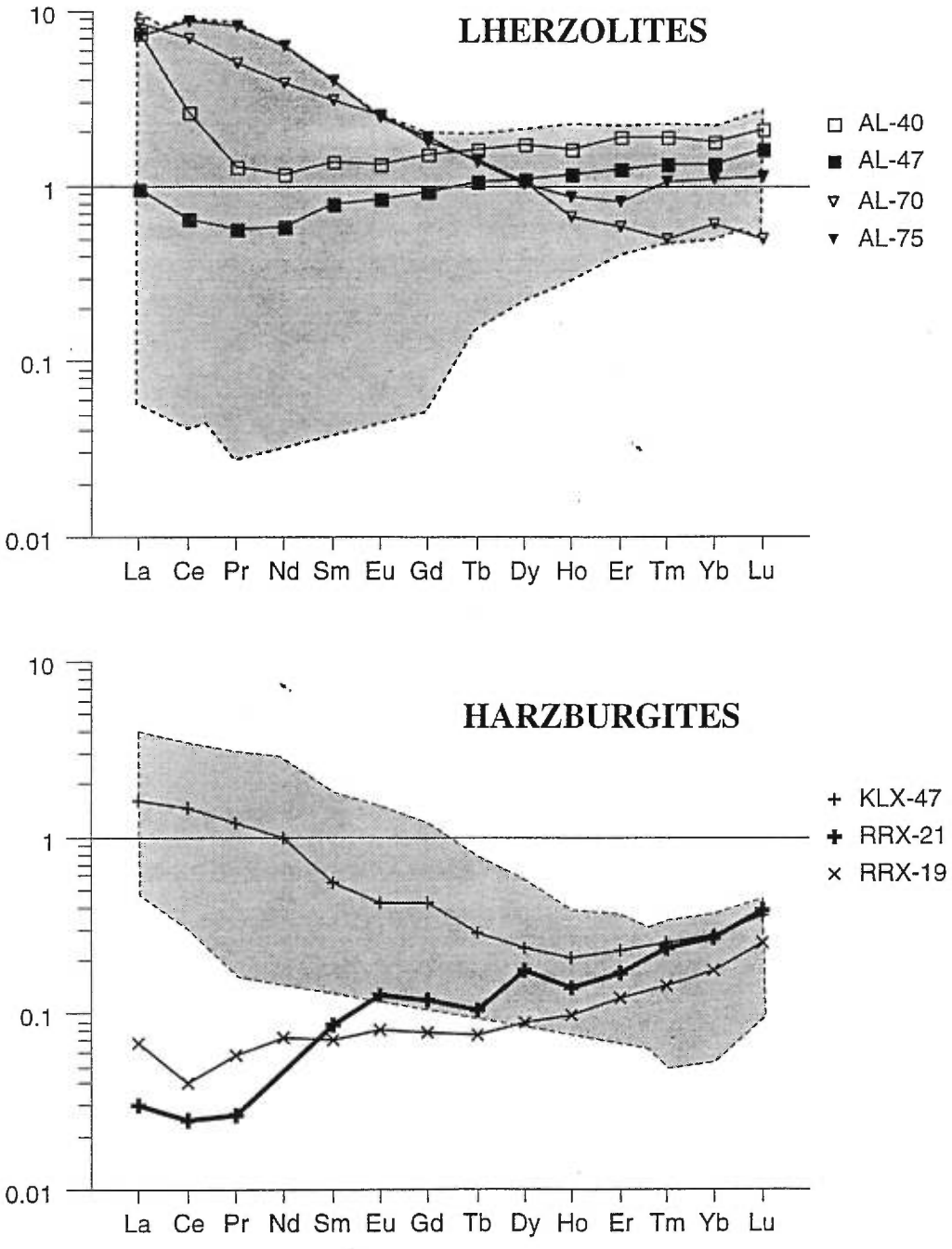
LHERZOLITES
10
1
0.1
0.01
La Ce Pr Nd Sm Eu Gd Tb Dy Ho Er Tm Yb Lu
AL-40
AL-47
AL-70
AL-75
HARZBURGITES
10
1
0.1
0.01
La Ce Pr Nd Sm Eu Gd Tb Dy Ho Er Tm Yb Lu
KLX-47
RRX-21
RRX-19

Fig. 8b

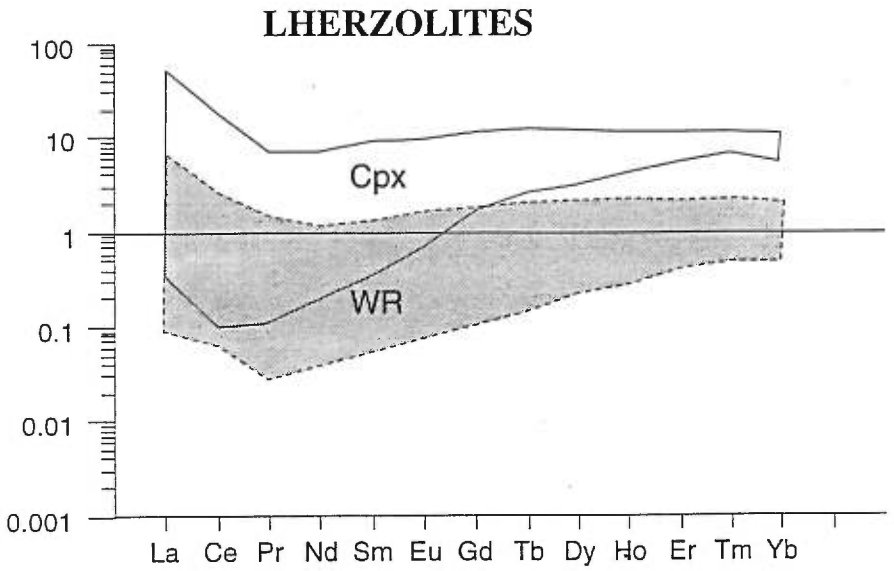
LHERZOLITES
100
10
1
0.1
0.01
0.001
Cpx
WR
La Ce Pr Nd Sm Eu Gd Tb Dy Ho Er Tm Yb

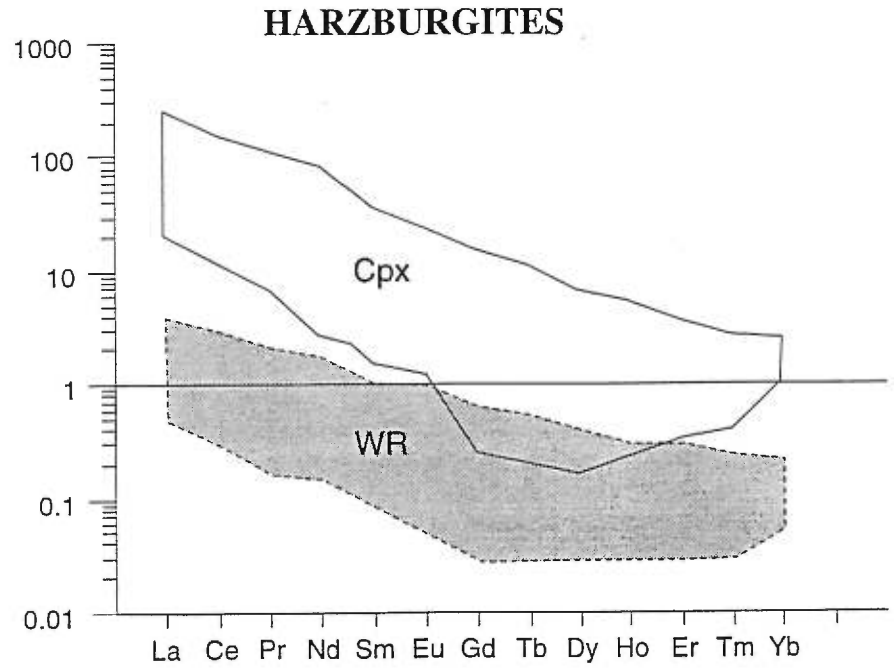
HARZBURGITES
1000
100
10
1
0.1
0.01
Cpx
WR
La Ce Pr Nd Sm Eu Gd Tb Dy Ho Er Tm Yb

The calculated Nd model ages for the lherzolites are either "future" values or unreasonably old (>4 Ga). The only Nd model age for a harzburgite is 0.398 Ga. Because metasomatism likely reset the Nd isotopic characteristics of the xenoliths, such model ages are not meaningfull. A Sm-Nd study of similar spinel lherzolites from unimodal suites in alkali basalts situated in southern British Columbia in the Canadian Cordillera records Proterozoic model ages and $^{143}Nd/^{144}Nd$ ratios which plot within the MORB field (Xue et al., 1990). These samples were located far from the thermal anomaly (more than 1000 km away) underlying southeastern Yukon where Alligator Lake is located. Our preferred scenario is thus reinforced i.e. the isotopic characteristics of the bimodal suites can be explained by OIB-type fluids associated with the thermal anomaly, forming the harzburgites and resetting the Sm-Nd and Lu-Hf characteristics of the lherzolites. On the other hand, in regions far away from this type of deep hot mantle upwelling, asthenosphere-derived melts locally induced the formation of harzburgites with reset Os isotopic characteristics, but these melts did not penetrate extensively enough to leave a signature in the Sm-Nd characteristics of the overall lherzolitic mantle.

At first glance it is tempting to draw an isochron through the four Cpx data in a $^{176}Hf/^{177}Hf$-$^{176}Lu/^{177}Hf$ diagram. An age of 0.55±0.20 Ga is obtained. However several observations suggest that this age is likely to be meaningless. First, all Hf is assumed to be in the clinopyroxene whereas our data suggest that at least 10% of the Hf is also in Opx (Table 2). Second, as discussed previously, in two of our samples (AL-70 and AL-75) $^{176}Hf/^{177}Hf$ ratios likely reflect a metasomatic process post-dating the original melting. Finally, the uncertainty of 0.20 Ga, reflecting mainly the uncertainties on the Hf isotopic ratios (McIntyre et al., 1966; York, 1969; Titterington and Halliday, 1979), is quite high for a "classical" isochron method.

The Hf systematics can also be used to determine the time at which the system cooled beneath the closure temperature for Hf. A two point isochron can be drawn between the Cpx and Opx Lu-Hf data of lherzolite AL-40. We find an age 75 Ma, which

would correspond to the most recent isotopic equilibration undergone by this rock at the mineral scale. The errors on the Hf isotopic ratios of both Cpx and Opx induce a range of ages between 0 (Cpx-Opx equilibrium) and 167 Ma (with the lowest Hf isotopic ratio of AL-40 Cpx and the highest Hf isotopic ratio of Al-40 Opx). Interestingly, 75 Ma corresponds to the age of the Carmacks volcanism (late Cretaceous), which is located just north of the Alligator Lake site, and has been interpreted to be plume-related (Johnston et al., 1996). We also note however that one of the interpretations for the mantle thermal-anomaly is that it represents asthenospheric upwelling related to a slab-window which was in place under the Northern Cordillera about 45 Ma ago (Frederiksen et al., 1998). Finally Pb data for the Alligator lake xenoliths suggest that the metasomatic event affecting the Sr-Pb characteristics of the Northern Canadian Cordillera mantle occurred less than 30 Ma ago (Carignan et al., 1996). We are consequently more tempted to link the Lu-Hf isochron age to a metasomatic event, related to a plume or slab-window, than simply to the end of inter-mineral diffusive equilibria after a period of slow cooling since the last melt depletion event.

4.6.2.3 Origin of the metasomatic agent

In summary, the Re-Os characteristics and REE patterns of the harzburgites and the Hf isotopic characteristics of the lherzolites require the presence of a metasomatic agent. Two possible origins for this agent can be examined.

(1) Subduction related fluids or melts. A Sr-Pb study of lherzolites and harzburgites from the Alligator Lake site (Carignan et al., 1996) concluded that there may have been a slab-related metasomatic enrichment of the Canadian Cordillera lithosphere. The material of a downgoing slab is likely to be enriched in radiogenic Os (Righter and Hauri, 1998), thus providing a potential source of high-$^{187}Os/^{188}Os$ fluids or melts. Simple mass balance calculations on the Simcoe harzburgite suite from a similar tectonic

setting in the US Cordillera and having a similar $^{187}Os/^{188}Os$ range (excluding our two exceptional samples AL-49 and XLG-25A) to that of the Canadian Cordillera led Brandon et al. (Brandon et al., 1996) to suggest that Os might have fluid/melt affinities when the Os-undersaturated fluid/melt from a slab reacts with a relatively Os rich peridotite in the presumably more oxidizing conditions of a mantle wedge (Brandon et al., 1996). While metasomatism by slab-derived fluids could explain our Os harzburgite data and possibly our Hf lherzolite data, it is not our preferred explanation, since a slab derived fluid mechanism does not explain the association of harzburgites with the thermal anomaly.

(2) Asthenosphere derived metasomatic agent. A model for inducing melting in the lithosphere via the influx of fluids from the anomalously hot mantle detected teleseismically beneath the northern Canadian Cordillera (Frederiksen et al., 1998) was developed for the bimodal suites by Shi et al. (Shi et al., 1998), based on trace element data for clinopyroxenes. This model could explain the Os data if the fluids were derived from either an OIB-type (e.g. (Widom and Shirey, 1996)) or MORB source, if MORBs indeed have radiogenic Os ratios as suggested by the data of Schiano et al. (Schiano et al., 1997a). However, our Sm-Nd and Lu-Hf data, as well as the Sr-Pb data (Carignan et al., 1996), favor an OIB-type metasomatic agent. The correspondence between geophysical and petrological observations in the northern part of the Canadian Cordillera favors a model in which the genesis of the bimodal suites is linked to the presence of the thermal anomaly. However, as the rare harzburgites from unimodal suites located far from the mantle anomaly record similar Re-Os systematics to those associated with the anomaly, fluid-lithosphere interaction may occur throughout the length of the Canadian Cordillera. The increased number of harzburgite xenoliths at the sites overlying the anomaly may indicate that the phenomenon was more intense there than in the other parts of the Canadian Cordillera.

4.7 CONCLUSION

Re-Os, Lu-Hf and Sm-Nd measurements in mantle xenoliths from the Canadian Cordillera indicate the occurence of two mantle processes:

(1) The lherzolite xenoliths record various degrees of melt depletion which suggest a middle Proterozoic model age. The REE patterns, and the Lu-Hf systematics, were later modified by interaction with an enriched melt or fluid. The Os isotopic ratios of the lherzolites were unaffected by this latter process.

(2) The harzburgite xenoliths were formed by a more recent magmatic process (< 167 Ma) triggered by the influx of OIB-type fluids or melts bearing radiogenic Os. This process was particularly intense over a hot mantle anomaly detected teleseismically beneath the southeastern Yukon (Frederiksen et al., 1998; Shi et al., 1998), suggesting that the fluids originated in the sub-lithospheric mantle.

ACKNOWLEDGEMENTS

We wish to thank Tarik Ahmedali for the XRF analyses and Luc Marin for the S analyses. Thanks also to Catherine Spatz and Anne-Catherine Pierson-Wickman for help with the Re-Os chemistry and analyses. We are grateful to Shi Lang for providing samples he collected. Thanks a lot to A. D. Brandon for an earlier revision of the manuscript. We thank J. Vervoort for sending us his paper in press.

Chapitre 5: Conclusion

En se condensant, le feu s'humidifie; et,
en se resserrant plus encore, il engendre l'eau;
et quand l'eau cristallise, elle se change en terre.

Héraclite

La compréhension de l'évolution de la Terre au cours du temps implique l'étude des divers réservoirs géochimiques qui la composent. Cette thèse a pour thème la lithophère mantellique, et tout particulièrement celui situé sous les zones de croûte continentale post-Précambriennes. Les études des réservoirs terrestres se focalisent en général sur les roches d'une région bien particulière puis les comparent à celles d'autres endroits du monde et/ou d'un âge différent. Ici, notre attention s'est concentrée sur la Cordillère Canadienne, formée par l'accrétion de terrains tectoniques à la marge occidentale du continent Nord-Américain au cours du Crétacé-Jurassique, et dont la lithosphère mantellique est accessible grâce à de nombreux xénolites péridotitiques remontés par des basaltes alcalins de la fin du Tertiaire à la période actuelle. Enfin, les outils géochimiques utilisés pour l'analyse des roches sont en constante évolution due à l'amélioration des techniques analytiques, et à ce titre nécessitent d'être bien contraints afin de pouvoir correctement interpréter les données. Ainsi, une partie importante de cette thèse a été consacré au système isotopique Re-Os dont beaucoup de paramètres géochimiques demeurent mal connus, mais aussi au système Lu-Hf dont l'application aux roches ultramafiques en est à ses premiers balbutiements.

BILAN DE LA PÉTROGENÈSE DE LA LITHOSPHÈRE MANTELLIQUE DE LA CORDILLÈRE CANADIENNE

Un des objectifs de cette thèse était de déterminer si le manteau lithosphérique situé sous la Cordillère Canadienne est homogène, si il correspond aux découpages tectoniques et géochimiques des roches de la croûte située au dessus et par quels processus il s'est formé. Ainsi, les suites de xénolites ont été échantillonnées sur une aire géographique large, allant du Sud de la Colombie Britannique jusqu'en Alaska, et se répartissent dans les divers terrains tectoniques et ceintures orogéniques de la Cordillère Canadienne. Le type de péridotite le mieux représenté est celui des lherzolites à spinelle, et ainsi le manteau lithosphérique de la Cordillère Canadienne semble en être essentiellement constitué. L'étude des éléments majeurs de la roche totale et des minéraux de ces lherzolites a permis de montrer qu'elles représentent le résidu de degrés variables de fusion partielle résultant en l'extraction de liquides de type picritique, vers 45 km de profondeur. L'ampleur de cette fusion a été différente pour chaque suite de xénolite et en particulier il semblerait que les suites lherzolitiques de la région Nord (Francis, 1987; Shi et al., 1998) ont subi une fusion plus faible que celles du Sud. Du point de vue du métasomatisme, chaque suite présente un degré variable d'enrichissement en LREE, allant d'un profil appauvri en LREE jusqu'à 7 fois le manteau primitif (PUM), et même plus de 10 fois PUM lorsque de l'amphibole est présente. A ce propos, la majeure partie du manteau lithosphérique de la Cordillère Canadienne semble anhydre, avec seulement du métasomatisme cryptique, mais deux sites, LP et KL, ont des minéraux hydratés dans leurs xénolites. La plupart des xénolites des suites dominées par des lherzolites (sauf RR et KL) sont caractérisées par une anomalie négative de Hf, Zr et Ti par rapport aux REE, et ceci est valable du Nord au Sud de la Cordillère Canadienne. Les rapports isotopiques du Sr et du Nd des suites dominées par des lherzolites tombent dans le champ des MORBs (Xue et al., 1990; Sun et al., 1991) et données non publiées de Carignan). Cependant, il existe dans le Nord des suites qui ont

une forte proportion de hazburgites en plus des lherzolites (suites appelées bimodales; AL, LG, HF). Les lherzolites des suites bimodales ont des rapports isotopiques du Sr et du Pb élevés (Carignan et al., 1996) et de l'Hf bas, reflètant du métasomatisme. Ce dernier pourrait être du à des fluides ou liquides de fusion de type EMII, ou provenant de la zone de subduction (Carignan et al., 1996). Les rapports isotopiques de l'Os varient sur la même gamme (0.122 à 0.132) sur l'ensemble des lherzolites d'une même suite, qu'elle soit unimodale ou bimodale. Leur corrélation avec des indices de fusion comme l'Al_2O_3 ou les HREE est attribuée à la croissance radiogénique en ^{187}Os après un événement de fusion ancien.

Un autre type de péridotite après celui des lherzolites est assez abondant dans le Nord de la Cordillère Canadienne. Il s'agit des harzburgites des suites bimodales (Francis, 1987; Shi et al., 1998). Ces harzburgites semblent avoir été le résultat d'une fusion récente induite par du métasomatisme (Francis, 1987; Shi et al., 1998). En effet, ces harzburgites sont très riches en éléments traces incompatibles (Shi et al., 1998). Les agents métasomatiques semblent avoir été issus d'une zone anormalement chaude dans le manteau détecté par télésismique à plus de 100 km de profondeur (Frederiksen et al., 1998; Shi et al., 1998). Les isotopes de l'Os ont enregistré ce métasomatisme puisque les rapports $^{187}Os/^{188}Os$ des harzburgites sont corrélés avec 1/Os et se placent au dessus de la corrélation en fonction de l'Al_2O_3 ou des HREE des lherzolites. Des harzburgites et même des dunites sont présentes aussi dans les sites de xénolites du Sud de la Cordillère Canadienne mais sont assez rares. La composition en éléments majeurs de certaines d'entre elles, assez riches en Fe pour des péridotites appauvries, suggère qu'elles sont le résultat de l'interaction entre un liquide de fusion alcalin et la péridotite. Parmi les harzburgites du Sud analysées pour les éléments traces, trois sont enrichies en éléments traces incompatibles, mais deux (à RR) en sont appauvries. Par contre, toutes les harzburgites du Sud présentent des rapports isotopiques d'Os situés aussi au dessus de la corrélation régionale des lherzolites.

Enfin, le dernier type de péridotite regroupe des wehrlites, des pyroxénites et des dunites. Ces types de roches sont abondants dans les deux suites situées près du craton (SL et KL). Il semblerait qu'elles se soient formées par le passage de liquides de fusion mantelliques dans les péridotites lherzolitiques.

Ainsi, aucune relation entre la composition des suites de xénolites et les terrains tectoniques ou les ceintures orogéniques de la croûte n'a pu être dégagée. Cependant, une étude de basaltes alcalins récents du Nord de la Cordillère Canadienne semble indiquer des différences de source de ces laves entre les différentes ceintures orogéniques (Abraham et al., 1998), et ceci correspond à des données antérieures sur des granitoïdes (Armstrong, 1988). En particulier, les ceintures orogéniques de Intermontane et de l'Avant-Pays ont des basaltes et des granitoïdes dont les rapports $^{87}Sr/^{86}Sr$ sont moins élevés et les rapports $^{143}Nd/^{144}Nd$ plus élevés que ceux des ceintures Côtière et Omenica. Le fait que ces variations ne soient pas mises en évidences dans les xénolites peut être interprété soit par l'hypothèse que les variations isotopiques des basaltes et des granitoïdes proviennent de processus de contamination crustale, soit par l'hypothèse que la source des basaltes alcalins est différente du manteau lithosphérique qu'ils échantillonnent en remontant vers la surface et qui est représenté par les xénolites.

Datation des événements ayant affecté la lithosphère mantellique

Cette thèse avait aussi pour but d'utiliser les systèmes isotopiques comme le Re-Os et le Lu-Hf pour avoir des informations temporelles sur les événements ayant affecté la lithosphère mantellique étudiée. Une application du système Re-Os dans les roches du manteau est la détermination de l'âge de la dernière fusion les ayant affecté. Les âges modèles classiques (comme ceux utilisés avec le Nd) Re-Os sont peu utilisés car le rapport $^{187}Re/^{188}Os$ a souvent été perturbé par du métasomatisme postérieur (Walker et al., 1989). Afin de s'affranchir du Re, des âges minimums d'appauvrissement en Re (T_{RD}) sont

calculés, assumant que tout le Re est parti lors du dernier événement de fusion (Walker et al., 1989). Les T_{RD} sont vraisemblables uniquement pour les péridotites très appauvries comme les harzburgites. Dans la Cordillère Canadienne, une harzburgite dont le rapport isotopique de l'Os n'a pas été perturbé par du métasomatisme a un âge T_{RD} de 1 Ga. Cependant, les rapports isotopiques de toutes les autres harzburgites analysées ayant été perturbés par du métasomatisme, seules les lherzolites ont pu fournir une information temporelle. Ainsi, une troisième méthode de datation Re-Os a été mise en application. L'intersection de la corrélation $^{187}Os/^{188}Os$ en fonction du Lu avec l'axe des abscisses donne la valeur du rapport isotopique initial des suites de lherzolites. La projection de cette valeur sur une courbe d'évolution des rapports $^{187}Os/^{188}Os$ du manteau primitif au cours du temps permet de calculer un âge modèle pour les suites de xénolites (Reisberg and Lorand, 1995). Ce calcul a été appliqué à divers groupements de lherzolites de la Cordillère Canadienne (par ceinture orogénique, par terrain tectonique, Nord-Sud) et donne systématiquement 1 Ga environ. Ainsi le calcul appliqué à l'ensemble des lherzolites analysées résulte en un âge de 1.12 ± 0.26 Ga pour la lithosphère mantellique de la Cordillère Canadienne. Enfin, deux lherzolites dont les rapports $^{176}Hf/^{177}Hf$ des clinopyroxènes n'ont pas été perturbés par du métasomatisme ont des âges modèles Lu-Hf du même ordre de grandeur.

Des âges Protérozoiques ont été trouvés dans des massifs péridotitiques orogéniques (Reisberg and Lorand, 1995), dans le manteau situé sous des terrains Cambriens (Handler et al., 1997) et même dans la lithosphère océanique (Hassler and Shimizu, 1998; Parkinson et al., 1998). Bien que le manteau convectif ne soit peut-être pas si homogène que l'on pense généralement, la lithosphère mantellique de la Cordillère Canadienne représente sans doute de la lithosphère continentale stabilisée en tant que telle il y a 1 Ga. La composition des xénolites à spinelle comme celles étudiées ici est moins appauvrie que celle des xénolites à grenat des cratons. Dans ces derniers, la stabilité des racines continentales depuis plus de 3 milliards d'années a été expliquée par le contraste de

densité entre leur composition appauvrie et celle du manteau convectif plus enrichi (e.g. (Walker et al., 1989). Le contraste de composition entre la lithosphère mantellique de la Cordillère Canadienne et le manteau convectif est moindre mais semble avoir été suffisant pour qu'elle reste stable pendant 1 Ga.

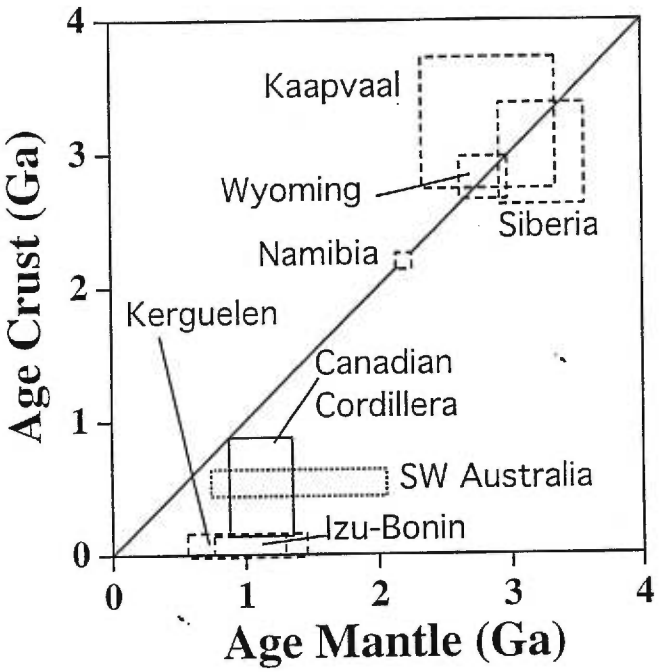

Fig. 1: Age de la croûte en fonction de l'âge du manteau sous-jascent dans différentes régions du monde. Pointillés fins= âge du manteau déterminé par âge modèle Os; pointillés épais = âge du manteau déterminé par âge minimum d'appauvrissement en Re. Sources: Kaapvaal: Walker et al. (1989), Pearson et al. (1995a); Sibérie: Pearson et al. (1995b); Namibie: Pearson et al. (1994); Sud Ouest de l'Australie: Handler et al. (1997); Izu-Bonin: Parkinson et al. (1998); Kerguelen: Hassler et al. (1998).

L'âge de 1 Ga du manteau contraste avec les âges modèles Nd des roches de la croûte supérieure qui sont plus jeunes (0.5 Ga en moyenne). Cette différence d'âge semble impliquer que lors de leur accrétion les terrains tectoniques ont vu leur racine mantellique délaminée. Ceci est en accord avec les profils sismiques réalisés dans le Sud de la Cordillère Canadienne qui montrent l'extension de la croûte inférieure du craton jusqu'à la limite entre les ceintures Côtière et Intermontane (Clowes et al., 1998) et sur laquelle les terrains de la croûte supérieure semblent posés.

Les processus de formation des harzburgites ne pouvant être datés par le système Re-Os, il faut se référer à d'autres systèmes isotopiques. Les isotopes du Pb avaient déjà permis de situer le métasomatisme ayant affecté la suite bimodale d'AL à moins de 30 Ma (Carignan et al., 1996). Un isochrone Lu-Hf sur seulement deux minéraux d'une lherzolite suggère moins de 175 Ma pour l'équilibrage isotopique le plus récent. Ainsi le métasomatisme, sinon la fusion des harzburgites si elle lui est associée (Shi et al., 1998), de la lithosphère mantellique sous AL est récent.

Comportement des éléments Re, Os, Lu et Hf lors de la fusion et du métasomatisme du manteau

Cette étude a permis de rappeler que l'Os peut être mobile dans le manteau, en particulier en conditions oxydantes (Wood, 1987; Brandon et al., 1996). En effet les rapports $^{187}Os/^{188}Os$ des harzburgites sont beaucoup plus élevés que ce que l'on attend si ces harzburgites étaient le simple produit de fusion des lherzolites. De plus, cette corrélation ne peut être expliquée uniquement par de la fusion partielle, mais semble exiger un processus de mélange comme le métasomatisme. Il semblerait donc que les fluides ou les liquides de fusion responsables du métasomatisme des harzburgites aient eu des rapports $^{187}Os/^{188}Os$ élevés. Ces agents métasomatiques ont donc "extrait" de l'Os de la péridotite, tout en l'enrichissant en éléments traces incompatibles (Shi et al., 1998) et en

augmentant ses rapports $^{187}Os/^{188}Os$. La relation entre l'enrichissement en éléments traces incompatibles et l'augmentation des rapports $^{187}Os/^{188}Os$ n'est cependant peut-être pas si simple. En effet, deux des harzburgites analysées et venant du site RR, sont appauvries en LREE, mais ont un rapport $^{187}Os/^{188}Os$ aussi élevé que toutes les autres harzburgites. Ceci suggère que le métasomatisme affectant l'Os n'est pas forcément couplé avec celui affectant les REE. Il faut rappeler que l'Os est sans doute concentré dans les sulfures, alors que la plupart des éléments traces incompatibles sont dans les phases majeures de la péridotites, en particulier les clinopyroxènes. Les comportements différenciels de ces différentes phases lors du métasomatisme et de la fusion doivent être à l'origine de ce découplage.

D'autre part, le fait que les rapports $^{187}Os/^{188}Os$ corrèlent avec 1/Os met en doute l'hypothèse d'altération post-éruptive invoquée pour expliquer les concentration basses en Os des xénolites par rapport aux massifs péridotitiques. L'explication de cette différence en concentration est sans doute à chercher dans des processus mantelliques.

Le Re, étant modéremment incompatible lors de la fusion et du métasomatisme, est mobile au cours de ces processus. Ceci est particulièrement évident lorsque l'on compare le contenu en Re des suites unimodales et celui des suites bimodales. Dans ces dernières, le contenu en Re est globalement plus élevé, et cela est sans doute du au métasomatisme plus important qui les a affecté en comparaison à celui subi par suites unimodales.

Le Lu n'a pas été perturbé par le métasomatisme puisqu'il est corrélé avec les indices de fusion comme l'Al_2O_3. L'Hf en revanche, ainsi que les isotopes de l'Hf sont sensibles au métasomatisme. En particulier, le contenu en Hf des Cpx augmente et les rapports $^{176}Hf/^{177}Hf$ diminuent, plus le métasomatisme, mis en évidence par l'enrichissment en LREE, est important dans les lherzolites. Ainsi le comportement de l'Hf et celui des rapports isotopiques de l'Hf semblent couplés avec les LREE lors du métasomatisme des lherzolites.

Questions en suspend

Comme le bilan ci-dessus l'a mis en évidence, une étude comme celle-ci engendre plus de questions qu'elle n'apporte de réponses. Ainsi, pourquoi les xénolites semblent-elles indiquer que le manteau est homogène sous la Cordillère alors que les données sur les basaltes suggèrent le contraire? Comment le manteau lithosphérique s'est-il formé il y a 1 Ga, comment est-il resté stable pendant tout ce temps et comment s'est passé le processus d'accrétion de terrains de la croûte supérieure plus jeune au dessus? Quelle est la nature et l'âge de la croûte inférieure que l'on voit en sismique et cette croûte est-elle couplée avec le manteau Protérozoique sous-jascent? Comment expliquer les âges anciens de certaines péridotites océaniques? Pourquoi l'Os est-il mobile dans certaines conditions? Pourquoi et quand le comportement de l'Os est-il couplé avec celui d'autres éléments comme les LREE lors du métasomatisme et pourquoi parfois ne l'est-il pas? Quelles phases gouvernent les comportements de l'Os et du Re?

Les champs d'investigation futurs pouvant apporter des réponses à ces questions sont en particulier les suivants. Des analyses Re-Os seraient nécessaires sur d'avantages de xénolites de la Cordillère Canadienne, mais aussi sur des xénolites du craton afin en particulier de déterminer l'âge de la lithophère sous le craton canadien. Il serait intéressant de déterminer la fugacité d'oxygène sur les harzburgites pour voir si le métasomatisme influant l'Os est forcément couplé à un fort degré d'oxydation. D'autres analyses Lu-Hf sur des péridotites du manteau sont nécessaires pour essayer de contraindre le comportement de ces éléments, mais aussi pour obtenir des informations sur le métasomatisme ou la profondeur d'origine de ces roches. En particulier, il serait nécessaire de faire des analyses Lu-Hf sur les harzburgites de la Cordillère Canadienne. Les analyses de Re-Os s'effectuant jusqu'à présent sur la roche totale, il serait intéressant d'analyser des grains individuels de sulfures où semble se concentrer l'Os dans les péridotites et ainsi mieux contraindre ce que signifie un rapport isotopique de l'Os tels que ceux présentés dans cette thèse. Le manque

de données expérimentales se fait d'autre part cruellement sentir en ce qui concerne le comportement des platinoïdes, des liquides sulfurés ou silicatés et les coeffients de partition de l'Os et du Re. La meilleure maîtrise de tous ces paramètres permettrait de mieux contraindre la datation des péridotites par le système Re-Os.

Bibliographie

Abraham, A.-C., Francis, D., Polvé, M. and Ludden, J., 1998. Source differences and terrane dependance in recent alkaline basaltic magmas accross the accreted terranes of the Northern Canadian Cordillera. Goldschmidt, Toulouse, Mineralogical Magazine, 62A, 7-8.

Albarède, F., 1997. The growth of continents. EUG 9, Strasbourg,Terra Nova, , 81.

Allègre, C.J., Hart, S.R. and Minster, J.-F., 1983. Chemical structure and evolution of the mantle and continents determined by inversion of Nd and Sr isotopic data, II. Numerical experiments and discussion. Earth Planet. Sci. Lett., 66 , 191-213.

Allègre, C.J. and Minster, J.F., 1978. Quantitative models of trace element behavior in magmatic processes. Earth Planet. Sci. Lett., 38 , 1-25.

Allègre, C.J. and Turcotte, D.L., 1986. Implications of a two component marble-cake mantle. Nature, 323 , 123-127.

Anderson, D.L., 1989. Theory of the Earth. Blackwell Scientific Publications, 366 pp.

Aoki, K., 1987. Japanese island arc: xenoliths in alkali basalts, high-alumina basalts, and calc-alkaline andesites and dacites. In: P.H. Nixon (Editor), Mantle xenoliths. J. Wiley & sons Ldt, 319-333.

Aoki, K.-I. and Shiba, I., 1973. Pyroxenes from lherzolite inclusions of Itinome-gata, Japan. Lithos, 6 , 41-51.

Arai, S., 1980. Dunite-harzburgite-chromitite complexes as refractory residue in the Sangun-Yamguchi zone, Western Japan. J. Petrol., 21 (1), 141-165.

Arai, S., 1991. The Circum-Izu peridotite, Central Japan, as back-arc fragments of the Izu-Bonin arc system. In: T. Peters, A. Nicolas and R.G. Coleman (Editor), Ophiolite genesis and evolution of the oceanic lithosphere. Kluwer Academic Publishers, Dordrecht, 801-816.

Arai, S., 1994. Characterization of spinel peridotites by olivine-spinel compositional relationships: review and interpretation. Chem. Geol., 113 , 191-204.

Armstrong, R.L., 1988. Mesozoic and early Cenozoic magmatic evolution of the Canadian Cordillera. Geological Society of America Special Paper(218), 55-91.

Armstrong, R.L. and Ghosh, D.K., 1990. Westward movement of the 87Sr/86Sr=0.704 line in southern B.C. from Triassic to Eocene time: monitoring the tectonic overlap of accreted terranes of North America. , Geological Association of Canada, P.w. abstracts, 15, 4.

Armstrong, R.L., Parrish, R.R., van der Heyden, P., Scott, K. and Runkle, D., 1991. Early Proterozoic basement exposure in the southern Canadian Cordillera: core gneiss of Frenchman Cap, Unit I of the Grand Forks Gneiss, and the Vaseaux Formation. Can. J. Earth Sci., 28 , 1169-1201.

Becker, H., 1996. Crustal trace element and isotopic signatures in garnet pyroxenites from garnet peridotite massifs from Lower Austria. J. Petrol., 37 (4), 785-810.

Bédard, J.H., 1994. A procedure for calculating the equilibrium distribution of trace elements among the minerals of cumulate rocks, and the concentration of trace elements in the coexisting liquids. Chem. Geol., 118 , 143-153.

Bedini, R.M., Bodinier, J.-L., Dautria, J.-M. and Morten, L., 1997. Evolution of LILE-enriched small melt fractions in the lithospheric mantle: a case study from the East African Rift. Earth Planet. Sci. Lett., 153 , 67-83.

Bernstein, S., Kelemen, P.B. and Brooks, C.K., 1998. Depleted spinel harzburgite xenoliths in Tertiary dykes from East Greenland: restites from high degree melting. Earth Planet. Sci. Lett., 154 , 221-235.

Bevier, M.L., 1983. Regional stratigraphy and age of Chilcotin Group basalts, south-central British Columbia. Can. J. Earth Sci., 20 , 515-524.

Blichert-Toft, J., Chauvel, C. and Albarède, F., 1997. Separation of Hf and Lu for high-precision isotope analysis of rock samples by magnetic sector-multiple collector ICP-MS. Contrib. Miner. Petrol., 127 , 248-260.

Bloomer, S.H. and Fisher, R.L., 1987. Petrology and geochemistry of igneous rocks from the Tonga trench - a non-accretionary plate boundary. J. Geol., 95 , 469-495.

Bodinier, J.-L. et al., 1996. Distribution of niobium, tantalium, and other highly incompatible trace elements in the lithospheric mantle: the spinel paradox. Geochim. Cosmochim. Acta, 60 (3), 545-550.

Bodinier, J.L., Dupuy, C. and Dostal, J., 1988. Geochemistry and petrogenesis of eastern pyrenean peridotites. Geochim. Cosmochim. Acta, 52 , 2893-2907.

Bodinier, J.L., Guiraud, M., Fabriès, J., Dostal, J. and Dupuy, C., 1987. Petrogenesis of layered pyroxenites from the Lherz, Freychinède and Prades ultramafic bodies (Ariège, French Pyrénées). Geochim. Cosmochim. Acta, 51 , 279-290.

Bodinier, J.L., Vasseur, G., Vernieres, J., Dupuy, C. and Fabries, J., 1990. Mechanism of mantle metasomatism: geochemical evidence from the Lherz orogenic peridotite. J. Petrol., 31 (3), 597-628.

Boyd, F.R., 1981. Ultramafic xenoliths in terrestrial volcanics and mantle magmatic processes, Basaltic Volcanism on the Terrestrial Planets. Pergamon, New-York, 282-291.

Boyd, F.R., 1987. High- and low-temperature garnet peridotite xenoliths and their possible relation to the lithosphere-asthenosphere boundary beneath southern Africa. In: P.H. Nixon (Editor), Mantle xenoliths. John Wiley & Sons Ldt, 403-412.

Boyd, F.R., 1989. Compositional distinction between oceanic and cratonic lithosphere. Earth Planet. Sci. Lett., 96 , 15-26.

Boyd, F.R., Gurney, J.J. and Richardson, S.H., 1985. Evidence for a 150-200 km thick Archean lithosphere from diamond inclusion thermobarometry. Nature, 315 , 387-389.

Boyd, F.R., Pearson, D.G., Nixon, P.H. and Mertzman, S.A., 1993. Low-calcium garnet hazburgites from southern Africa: their relations to craton structure and diamond crystallisation. Contrib. Miner. Petrol., 113 , 352-366.

Boyd, F.R. et al., 1997. Composition of the Siberian cratonic mantle: evidence from Udachnaya peridotite xenoliths. Contrib. Miner. Petrol., 128 , 228-246.

Brandon, A.D., Becker, H., Carlson, R.W. and Shirey, S.B., 1998. Isotopic constraints on time scales and mechanism of slab material transport in the mantle wedge: evidence from the Simcoe mantle xenoliths, Washington, USA. Chem. Geol., Special volume (Submitted).

Brandon, A.D., Creaser, R.A., Shirey, S.B. and Carlson, R.W., 1996. Osmium Recycling in Subduction Zones. Science, 272 , 861-864.

Brandon, A.D. and Draper, D.S., 1996. Constraints on the origin of the oxidation state of mantle overlying subduction zones: an example from Simcoe, Washington, USA. Geochim. Cosmochim. Acta, 60 (10), 1739-1749.

Brandon, A.D. and Lambert, R.S., 1993. Geochemical characterization of mid-Cretaeous granitoids of the Kootenay Arc in the southern Canadian Cordillera. Can. J. Earth Sci., 30 , 1076-1090.

Brandon, A.D. and Lambert, R.S., 1994. Crustal melting in the Cordilleran interior: the Mid-Cretaceous White Creek batholith in the Southern Canadian Cordillera. J. Petrol., 35 (1), 239-269.

Brandon, A.D. and Smith, A.D., 1994. Mesozoic granitoid magmatism in southeast British Columbia: Implications for the origin of granitoid belts in the North American Cordillera. J. Geophys. Res., 99 (B6), 11879-11896.

Brandon, A.D., Walker, R.J., Morgan, J.W., Norman, M.D. and Prichard, H.M., 1998. Coupled 186Os and 187Os evidence for core-mantle interaction. Science, 280 , 1570-1573.

Brearley, M. and Scarfe, C.M., 1984. Amphibole in a spinel lherzolite xenolith: evidence for volatiles and partial melting in the upper mantle beneath southern British Columbia. Can. J. Earth Sci., 21 , 1067-1072.

Brearley, M., Scarfe, C.M. and Fujii, T., 1984. The petrology of ultramafic xenoliths from Summit Lake, near Prince George, British Columbia. Contrib. Miner. Petrol., 88 , 53-63.

Brey, G.P. and Köhler, T., 1990. Geothermobarometry in four-phase lherzolites II. New thermpbarometers, and practical assessment of existing thermobarometers. J. Petrol., 31 (6), 1353-1378.

Burnham, O.M., Rogers, N.W., Pearson, D.G., Van Calsteren, P.W. and Hawkworth, C.J., 1998. The petrogenesis of the eastern pyrenean peridotites: an integrated study of their whole-rock geochemistry and Re-Os isotope composition. Geochim. Cosmochim. Acta, in press .

Canil, D., Brearley, M. and Scarfe, C.M., 1987. Petrology of ultramafic xenoliths from Rayfield River, south-central British Columbia. Can. J. Earth Sci., 24 , 1679-1687.

Canil, D. and Scarfe, C., 1989. Origin of phlogopite in mantle xenoliths from Kostal Lake, Wells Gray Park, British Columbia. J. Petrol., 30 (5), 1159-1179.

Canil, D., Virgo, D. and Scarfe, C.M., 1990. Oxidation state of mantle xenoliths from British Columbia, Canada. Contrib. Miner. Petrol., 104 , 453-462.

Carignan, J., Ludden, J. and Francis, D., 1996. On the recent enrichment of a subcontinental lithosphere: a detailed U-Pb study of spinel lherzolite xenoliths, Yukon, Canada. Geochim. Cosmochim. Acta, 60 (21), 4241-4252.

Carlson, R.W. and Irving, A.J., 1994. Depletion and enrichment history of subcontinental lithospheric mantle: an Os, Sr, Nd and Pb isotopic study of ultramafic xenoliths from the northwestern Wyoming Craton. Earth Planet. Sci. Lett., 126 , 457-472.

Chen, C.-Y., Frey, F.A. and Song, Y., 1989. Evolution of the upper mantle beneath southeast Australia: geochemical evidence from peridotite xenoliths in Mount Leura basanite. Earth Planet. Sci. Lett., 93 , 195-209.

Choukroune, P., Ludden, J.N., Chardon, D., Calvert, A.J. and Bouhallier, H., 1997. Archean crustal growth and tectonic processes: a comparison of the superior Province, Canada and the Dharwar craton, India. In: J.-P. Burg and M. Ford (Editor), Orogeny through time. Geological Society Special Publication, 63-98.

Christensen, U., 1995. Effects of phase transitions on mantle convection. Ann. Rev. Earth Planet. Sci., 23 , 65-87.

Clowes, R.M., Cook, F.A. and Ludden, J.N., 1998. Lithoprobe leads to new perspectives on continental evolution. G.S.A. Today, 8 (10), 1-7.

Clowes, R.M., Zeit, C.A., Amor, J.R. and Ellis, R.M., 1995. Lithospheric structure in the southern Canadian Cordillera from a network of seismic refraction lines. Can. J. Earth Sci., 32 , 1485-1513.

Collerson, K.D., Campbell, L.M., Weaver, B.L. and Palcz, Z.A., 1991. Evidence for extreme mantle fractionation in early Archean ultramafic rocks from northern Labrador. Nature, 349 , 209-214.

Creaser, R.A., Erdmer, P., Stevens, R.A. and Grant, S.L., 1997. Tectonic affinity of Nisutlin and Anvil assemblage strata fron the Teslin tectonic zone, northern Canadian Cordillera: Constraints from neodynium isotope and geochemical evidence. Tectonics, 16 (1), 107-121.

Creaser, R.A., Papanastassiou, D.A. and Wasserburg, G.L., 1991. Negative thermal ion mass spectrometry of osmium, rhenium, and iridium. Geochim. Cosmochim. Acta, 55 , 397-401.

Crocket, J.H., Fleet, M.E. and Stone, W.E., 1997. Implications of composition for experimental partioning of platinum-group elements and gold between sulfide and

basalt melt: the significance of nickel content. Geochim. Cosmochim. Acta, 61 (19), 4139-4149.

Cui, Y. and Russel, J.K., 1995. Nd-Sr-Pb isotopic studies of the southern Coast Plutonic Complex, southwestern British Columbia. Geol. Soc. Am. Bull., 107 (2), 127-138.

Daly, R., 1940. Strength and strusture of the Earth. Prentice-Hall, New-York, 434 pp.

Dautria, J.M., Dupuy, C., Takherist, D. and Dostal, J., 1992. Carbonate metasomatism in the lithospheric mantle: peridotitic xenoliths from a melilititic district of the Sahara basin. Contrib. Miner. Petrol., 111 , 37-52.

de Witt, M.J. et al., 1992. Formation fo an archean continent. Nature, 357 , 553-562.

Dick, H.J.B. and Bullen, T., 1984. Chromian spinel as a petrogenetic indicator in abyssal and alpine-type peridotites and spacially associated lavas. Contrib. Miner. Petrol., 86 , 54-76.

Dupuy, C., Dostal, J. and Bodinier, J.L., 1987. Geochemistry of spinel peridotite inclusions in basalts from Sardinia. Min. Mag., 51 , 561-568.

Dupuy, C., Dostal, J., Dautria, J.M. and Girod, M., 1986. Geochemistry of spinel peridotite inclusions in basalts from Hoggar, Algeria. J. Afr. Earth Sci., 5 (3), 209-215.

Eggins, S.M., Rudnick, R.L. and McDonough, W.F., 1998. The composition of peridotites and their minerals: a laser-ablation ICP-MS study. Earth Planet. Sci. Lett., 154 , 53-71.

Eiché, G.E., Francis, D.M. and Ludden, J.N., 1987. Primary alkaline magmas associated with the Quaternary Alligator Lake volkanic complex, Yukon Territory, Canada. Contrib. Miner. Petrol., 95 , 191-201.

Elthon, D., 1992. Chemical trends in abyssal peridotites: refertilisation of depleted suboceanic mantle. J. Geophys. Res., 97 (B6), 9015-9025.

Falloon, T.J., Green, D.H., Hatton, C.J. and Harris, K.L., 1988. Anhydrous partial melting of a fertile and depleted peridotite from 2 to 30 kb and application to basalt petrogenesis. J. Petrol., 29 (6), 1257-1282.

Fiesinger, D.W. and Nicholls, J., 1977. Petrography and petrology of quaternary volcanic rocks, Quesnel Lake region, east-central British Columbia. The Geological Association of Canada(special paper number 16), 25.

Francis, D., 1987. Mantle-melt interaction recorded in spinel lherzolite xenoliths from the Alligator lake volcanic complex, Yukon, Canada. J. Petrol., 28 , 569-597.

Francis, D., 1995. The implications of picritic lavas for the mantle sources of terrestrial volcanism. Lithos, 34 (1), 89-105.

Francis, D. and Ludden, J., 1990. The mantle source for olivine nephelinite, basanite, and alkaline olivine basalt at Fort Selkirk, Yukon, Canada. J. Petrol., 31 (2), 371-400.

Frederiksen, A.W., Bostock, M.G., VanDecar, J.C. and Cassidy, J., 1998. Seismic structure of the upper mantle beneath northern Canadian Cordillera from teleseismic travel-time inversion. Tectonophys., submitted .

Frey, F.A. and Prinz, M., 1978. Ultramafic inclusions from San Carlos, Arizona: petrologic and geochemical data bearing on their petrogenesis. Earth Planet. Sci. Lett., 38 , 129-176.

Friedman, R.M., Mahoney, J.B. and Cui, Y., 1995. Magmatic evolution of the southern Coast Belt: constraints from Nd-Sr isotopic systematics and geochronology of the southern Coast Plutonic Complex. Can. J. Earth Sci., 32 , 1681-1698.

Fujii, T. and Scarfe, C.M., 1982. Petrology of ultramafic nodules from West Kettle River, near Kelowna, Southern British Columbia. Contrib. Miner. Petrol., 80 , 297-306.

Gabrielse, H., Monger, J.W.H., Wheeler, J.O. and Yorath, C.J., 1991. Tectonic framework. In: H. Gabrielse and C.J. Yorath (Editor), Geology of the Cordilleran Orogen in Canada. Geological Survey of Canada, 15-28.

Gabrielse, H. and Yorath, C.J. (Editor), 1991a. Géologie de l'orogène de la Cordillère du Canada. Geology of North America, G-2. Geological Society of America, 915.

Gabrielse, H. and Yorath, C.J., 1991b. Tectonic synthesis. In: H. Gabrielse and C.J. Yorath (Editor), Geology of the Cordilleran Orogen in Canada. Geological Survey of Canada, 677-706.

Galer, S.J. and Goldstein, S.L., 1991. Early mantle differenciation and its thermal consequences. Geochim. Cosmochim. Acta, 55 , 227-239.

Galer, S.J.G. and O'Nions, R.K., 1989. Chemical and isotopic studies of ultramafic inclusions from the San Carlos volcanic field, Arizona: a bearing on their petrogenesis. J. Petrol., 30 (4), 1033-1064.

Galer, S.J.G. and O'Nions, R.R., 1985. Residence time of thorium, uranium and lead in the mantle with implication for mantle convection. Nature, 316 , 778-782.

Gamble, J.A. and Kyle, P.R., 1987. The origins of glass and amphibole in spinel-wehrlite xenoliths from Foster Crater, McMurdo Volcanic Group, Antarctica. J. Petrol., 28 (5), 755-779.

Ghosh, D.K., 1995. Nd-Sr isotopic constraints on the interctions of the Intermontane Superterrane with the western edge of North America in the southern Canadian Cordillera. Can. J. Earth Sci., 32 , 1740-1758.

Goto, A. and Yokoyama, K., 1988. Lherzolite inclusions in olivine nephelinite tuff from Salt Lake Crater, Hawaii. Lithos, 21 , 67-80.

Grand, S.P., 1994. Mantle shear structure beneath the Americas and surrounding oceans. J. Geophys. Res., 99 , 11591-11623.

Green, D.H. and Hibberson, W., 1970. The instability of plagioclase in peridotite at high pressure. Lithos, 3 , 209-221.

Green, T.H., 1994. Experimental studies of trace-element partitioning applicable to igneous petrogenesis - Sedona 16 years later. Chem. Geol., 117 , 1-36.

Griffin, W.L., O'Reilly, S.Y. and Stabel, A., 1988. Mantle metasomatism beneath western Victoria, Australia: II. Isotopic geochemistry of Cr-diopside lherzolites and Al-augite pyroxenites. Geochim. Cosmochim. Acta, 52 , 449-459.

Griffin, W.L., Wass, S.Y. and Hollis, J.D., 1984. Ultramafic xenoliths from Bullenmerri and Gnotuk Maars, Victoria, Australia: petrology of a sub-continental crust-mantle transition. J. Petrol., 25 (1), 53-87.

Hamlyn, P.R. and Keays, R.R., 1986. Sulfur saturation and second-stage melts: application to the Buschveld Platinum metal deposit. Econ. Geol., 81 , 1431-1445.

Handler, M.R., Bennet, V.C. and Esat, T.M., 1997. The Persistence of Off-cratonic Lithospheric Mantle: Os Isotopic Systematics of Variably Metasomatised Southeast Australian Xenoliths. Earth Planet. Sci. Lett., 151 , 61-75.

Hart, S.R. and Zindler, A., 1986. In search of a bulk-earth composition. Chem. Geol., 57 , 247-267.

Hassler, D. and Shimizu, N., 1998. Osmium isotopic evidence for ancient subcontinental lithospheric mantle beneath the Kerguelen island, Southern Indian Ocean. Science, 280 , 418-421.

Hauri, E.H. and Hart, S.R., 1997. Rhenium abundances and systematics in oceanic basalts. Chem. Geol., 139 , 185-205.

Hauri, E.K., Shimizu, N., Dieu, J.J. and Hart, S.R., 1993. Evidence for hotspot-related carbonatite metasomatism in the oceanic upper mantle. Nature, 365 , 221-227.

Hawkesworth, C.J. and Norry, M.J. (Editor), 1983. Continental basalts and mantle xenoliths. Shiva, Cheshire, 272.

Herzberg, C.T., 1993. Lithosphere peridotites of the Kaapvaal craton. Earth Planet. Sci. Lett., 120 , 13-29.

Hirose, K. and Kawamoto, T., 1995. Hydrous partial melting of lherzolite at 1 GPa: the effect of H_2O on the genesis of basaltic magmas. Earth Planet. Sci. Lett., 133 , 463-473.

Hirose, K. and Kushiro, I., 1993. Partial melting of dry peridotites at high pressures: determination of compositions of melts segregated from peridotite using aggregates of diamonds. Earth Planet. Sci. Lett., 114 , 477-489.

Hofmann, A.W., 1988. Chemical differenciation of the Earth: the relationship between mantle, continental crust, and oceanic crust. Earth Planet. Sci. Lett., 90 , 297-314.

Hofmann, A.W., 1997. Mantle geochemistry: the message from oceanic volcanism. Nature, 385 , 219-229.

Hunter, R.H. and Upton, B.G.J., 1987. The British Isles - a Paleozoic mantle sample. In: P.H. Nixon (Editor), Mantle xenoliths. Wiley & sons, 107-118.

Ionov, D.A., Dupuy, C., O'Reilly, S.Y., Kopylova, M.G. and Genshaft, Y.S., 1993. Carbonated peridotite xenoliths from Spitsbergen: implications for trace element signature of mantle carbonate metasomatism. Earth Planet. Sci. Lett., 119 , 283-297.

Ionov, D.A., Hofmann, A.W. and Shimizu, N., 1994. Metasomatism-induced melting in mantle xenoliths from Mongolia. J. Petrol., 35 (3), 753-785.

Ionov, D.A., Prikhod'ko, V.S. and O'Reilly, S.Y., 1995. Peridotite xenoliths in alkali basalts from the Sikhote-Alin, southeastern Siberia, Russia: trace-element signatures of mantle beneath a convergent continental margin. Chem. Geol., 120 , 275-294.

Ionov, D.A. and Wood, B.J., 1992. The oxidation state of subcontinental mantle: oxygen thermobarometry of mantle xenoliths from Central Asia. Contrib. Miner. Petrol., 111 , 179-193.

Irving, A.J., 1980. Petrology and geochemistry of composite ultramafic xenoliths in alkalic basalts and implications for magmatic processes within the mantle. Am. J. Sci., 280-A , 389-426.

Jackson, E.D. and Wright, T.L., 1970. Xenoliths in the Honolulu volcanic series, Hawaii. J. Petrol., 11 (2), 405-430.

Jochum, K.P., McDonough, W.F. and Palme, H., 1989. Compositional constraints on the lithospheric mantle from trace elements in spinel peridotite xenoliths. Nature, 340 , 548-550.

Johnson, K.T.M., Dick, H.J.B. and Shimizu, N., 1990. Melting in the oceanic upper mantle: an ion probe study of diopsides in abyssal peridotites. J. Geophys. Res., 95 (B3), 2661-2678.

Johnston, S.T. et al., 1996. Yellowstone in Yukon: the late Cretaceous Carmacks Group. Geology, 24 (11), 997-1000.

Jordan, T.H., 1988. Structure and formation of the continental tectosphere. J. Petrol., Special Issue , 11-37.

Kelemen, P.B., Dick, H.J.B. and Quick, J.E., 1992. Formation of harzburgite by pervasive melt/rock reaction in the upper mantle. Nature, 358 , 635-641.

Kepezhinskas, P.K., Defant, M.J. and Drummond, M.S., 1995. Na metasomatism in the island-arc mantle by slab melt-peridotite interaction: evidence from mantle xenoliths in the North Kamtchatka Arc. J. Petrol., 36/6 , 1505-1527.

Kepezhinskas, P.K., Taylor, R.N. and Tanaka, H., 1993. Geochemistry of plutonic spinels from the North Kamtchatka Arc: comparisons with spinels from other tectonic settings. Min. Mag., 57 , 575-589.

Lindner, M. et al., 1986. Direct laboratory determination of the ^{187} Re half-life. Nature, 320 , 246-248.

Littlejohn, A.L. and Greenwood, H.J., 1974. Lherzolite nodules in basalts from British Columbia, Canada. Can. J. Earth Sci., 11 , 1288-1308.

Lorand, J.-P., 1989. Abundance and distribution of Cu-Fe-Ni sulfides, sulfur, copper and platinum-group elements in orogenic-type spinel lherzolite massifs of Ariège (northeastern Pyrenees, France). Earth Planet. Sci. Lett., 93 , 50-64.

Lorand, J.P., 1990. Are spinel lherzolite xenoliths representative of the abundance of sulfur in the upper mantle? Geochim. Cosmochim. Acta, 54 , 1487-1492.

Lorand, J.P., 1997. Contents and relative proportions of platinum group elements in upper mantle peridotites: new developments. E.A.G.-Workshop, Mainz,, 47-48.

Maury, R.C., Defant, M.J. and Joron, J.-L., 1992. Metasomatism of the sub-arc mantle inferred from trace elements in Philippine xenoliths. Nature, 360 , 661-663.

McBride, J.S., Lambert, D.D., Greig, A. and Nicholls, I.A., 1996. Multistage evolution of Australian subcontinental mantle: Re-Os isotopic constraints from Victorian mantle xenoliths. Geology, 24 (7), 631-634.

McDonough, W.F., 1990. Constraints on the composition of the continental lithospheric mantle. Earth Planet. Sci. Lett., 1990 , 1-18.

McDonough, W.F. and Frey, F.A., 1989. Rare earth elements in upper mantle rocks. In: B.R. Lipin and G.A. McKay (Editor), Geochemistry and Mineralogy of Rare Earth Elements. Mineralogical Society of America, 99-145.

McIntyre, G.A., Brooks, C., Compston, W. and Turek, A., 1966. The statistical assessment of Rb-Sr isochrons. J. Geophys. Res., 71 , 5459-5468.

McKenzie, D., 1984. The generation and compaction of partially molten rock. J. Petrol., 25 (3), 713-765.

McKenzie, D. and O'Nions, R.K., 1989. Some remarks on the movement of small melt fractions in the mantle. Earth Planet. Sci. Lett., 95 , 53-72.

Meisel, T., Walker, R.J. and Morgan, J.W., 1996. The osmium isotopic composition of the Earth's primitive upper mantle. Nature, 383 , 517-520.

Meissner, R. and Wever, T., 1988. Lithopheric rheology: continental versus oceanic unit. J. Petrol., Special Volume , 53-61.

Menzies, M., 1983. Mantle Ultramafic Xenoliths in Alkaline Magmas: Evidence for Mantle Heterogeneity Modified by Magmatic Activity. In: C.J. Hawkesworth and M.J. Norry (Editor), Continental Basalts and Mantle Xenoliths. Shiva Geology. Shiva Publishing Limited, Cambridge, 272.

Menzies, M.A. and Hawkesworth, C.J. (Editor), 1987. Mantle metasomatism. Academic Press Geology Series. Academic Press Inc., London, 472.

Mercier, J.-C. and Nicolas, A., 1975. Textures and fabrics of upper-mantle peridotites as illustrated by xenoliths from basalts. J. Petrol., 16 (2), 454-487.

Metcalfe, P.M., 1987. Petrogenesis of alkaline lavas from Wells Gray Provincial Park and constraints on the sub-Cordilleran upper mantle. PhD Thesis, University of Alberta.

Mihalynuk, M.G., Nelson, J. and Diakow, L.J., 1994. Cache Creek terrane entrapment: Oroclinal paradox within the Canadian Cordillera. Tectonics, 13 (2), 575-595.

Monger, J.W.H., Price, R.A. and Tempelman-Kluit, D.J., 1982. Tectonic accretion and the origin of the two major metamorphic and plutonic welts in the Canadian Cordillera. Geology, 10 , 70-75.

Morgan, J.W., 1986. Ultramafic xenoliths: clues to Earth's late accretionary history. J. Geophys. Res., 91 , 12375-12387.

Mortensen, J.K., 1992. Pre-mid-mesozoic tectonic evolution of the Yukon-Tanana terrane, Yukon and Alaska. Tectonics, 11 (4), 836-853.

Neal, C.R., 1988. The origin and composition of metasomatic fluids and amphiboles beneath Malaita, Solomon Islands. J. Petrol., 29 (1), 149-179.

Niu, Y. and Hékinian, R., 1997. Basaltic liquids and harzburgitic residues in the Garrett Transform: a case study at fast-spreading ridges. Earth Planet. Sci. Lett., 146 , 243-258.

Niu, Y., Langmuir, C.H. and Kinzler, R.J., 1997. The origin of abyssal peridotites: a new perspective. Earth Planet. Sci. Lett., 152 , 251-265.

Nixon, P.H., 1987. Kimberlitic xenoliths and their cratonic setting. In: P.H. Nixon (Editor), Mantle xenoliths. John Wiley & Sons Ldt, 215-239.

Nixon, P.H., Rogers, N.W., Gibson, I.L. and Grey, A., 1981. Depleted and fertile mantle xenoliths from southern african kimberlites. Ann. Rev. Earth Planet. Sci., 9 , 285-309.

Nowell, G.M. et al., 1998. High precision Hf isotope measurements of MORB and OIB by thermal ionisation mass spectrometry: insights into the depleted mantle. Chem. Geol., 149 , 211-233.

O'Neill, H.S.C., 1981. The transition between spinel lherzolite and garnet lherzolite, and its use as a geobarometer. Contrib. Miner. Petrol., 77 , 185-194.

O'Reilly, S.Y. and Griffin, W.L., 1988. Mantle metasomatism beneath western Victoria, Australia: I. Metasomatic processes in Cr-diopside lherzolites. Geochim. Cosmochim. Acta, 52 , 433-447.

Ozawa, K., 1988. Ultramafic tectonite of the Miyamori ophiolitic complex in the Kitakami Mountains, northeast Japan: hydrous upper mantle in an island arc. Contrib. Miner. Petrol., 99 , 159-175.

Ozawa, K., 1994. Melting and melt segregation in the mantle wedge above a subduction zone: evidence from the chromite-bearing peridotites of the Miyamori ophiolite complex, Northeastern Japan. J. Petrol., 35 (3), 647-678.

Parkinson, I.J., Hawkesworth, C.J. and Cohen, A.S., 1998. Ancient mantle in a modern arc: osmium isotopes in Izu-Bonin-Mariana forearc peridotites. Science, 281 , 2011-2013.

Parkinson, I.J. and Pearce, J.A., 1998. Peridotites from the Izu-Bonin-Mariana forearc (ODP Leg 125): evidence for mantle melting and melt-mantle interaction in a supra-subduction zone setting. J. Petrol., 39 (9), 1577-1618.

Parrish, R.R., 1991. Precambrian basement rocks of the Canadian Cordillera. In: H. Gabrielse and C.J. Yorath (Editor), Geology of the Cordilleran Orogen in Canada. Geological Survey of Canada, 87-96.

Patchett, P.J. and Gehrels, G.E., 1998. Continental influence on Canadian Cordillera Terranes from Nd isotopic study, and significance for crustal growth processes. J. Geol., 106 , 268-280.

Patchett, P.J., Gehrels, G.E. and Isachsen, C.E., 1998b. Nd isotopic characteristics of metamorphic and plutonic rocks of the Coast Mountains near Prince Ruppert, British Columbia. Can. J. Earth Sci., 35, 556-561.

Pearce, J.A., 1983. Role of the sub-continental lithosphere in magma genesis at active continental margins. In: C.J. Hawkesworth and M.J. Norry (Editor), Continental basalts and mantle xenoliths. Shiva, 230-249.

Pearson, D.G. et al., 1994. A Re-Os isotopic and petrological study of Namibian peridotites: contrasting petrogenesis and composition of on- and off-craton lithospheric mantle. Goldschmidt Conference, Edinburgh,, 703-704.

Pearson, D.G., Carlson, R.W., Shirey, S.B., Boyd, F.R. and Nixon, P.H., 1995a. Stabilisation of Archean lithospheric mantle: a Re-Os isotope study of peridotite xenoliths from the Kaapvaal craton. Earth Planet. Sci. Lett., 134 , 341-357.

Pearson, D.G. et al., 1995b. Re-Os, Sm-Nd, and Rb-Sr isotope evidence for thick Archean lithospheric mantle beneath the Siberian craton modified by multistage metasomatism. Geochim. Cosmochim. Acta, 59 (5), 959-977.

Pearson, D.G., Shirey, S.B., Harris, J.W. and Carlson, R.W., 1998. Sulphide inclusions in diamonds from the Koffiefontein kimberlite, S Africa: constraints on diamond ages and mantle Re-Os systematics. Earth Planet. Sci. Lett., 160 , 311-326.

Peslier, A.H., Francis, D. and Ludden, J., 1999. Petrology and trace element characteristics of the lithospheric mantle beneath the Southern Canadian Cordillera. Can. J. Earth Sci., in prep. .

Peslier, A.H., Reisberg, L., Ludden, J. and Francis, D., 1998a. Re-Os systematics in mantle xenoliths: age constraints on the Canadian Cordillera lithosphere. Chem. Geol., in prep .

Peslier, A.H., Reisberg, L., Ludden, J., Francis, D. and Chauvel, C., 1998b. Melting and metasomatism of the lithospheric mantle beneath the Northern Canadian Cordillera: a Re-Os and Lu-Hf study. Earth Planet. Sci. Lett., submitted .

Rampone, E., Bottazi, P. and Ottolini, L., 1991. Complementary Zr-Hf anomalies in orthopyroxene and clinopyroxene in mantle peridotites. Nature, 354 , 518-520.

Reisberg, L. and Lorand, J.-P., 1995. Longevity of sub-continental mantle lithosphere from osmium isotope systematics in orogenic peridotite massifs. Nature, 376 , 159-162.

Reisberg, L.C., Allègre, C.J. and Luck, J.-M., 1991. The Re-Os systematics of the Ronda Ultramafic Complex of southern Spain. Earth Planet. Sci. Lett., 105 , 196-213.

Riddihough, R.P. and Hyndman, R.D., 1991. Modern plate tectonic regime of the continental margin of western Canada. In: H. Gabrielse and C.J. Yorath (Editor), Geology of the Cordilleran Orogen in Canada. Geological Survey of Canada, 435-455.

Righter, K. and Hauri, E.H., 1998. Compatibility of Rhenium in garnet during mantle melting and magma genesis. Science, 280 , 1737-1741.

Ringwood, A.E., 1975. Composition and petrology of the Earth's mantle, 188 pp.

Ringwood, A.E. and Irifune, T., 1988. Nature of the 650-km seismic discontinuity: implications for mantle dynamics and differenciation. Nature, 331 , 131-136.

Roden, M.F., Irving, A.J. and Murthy, V.R., 1988. Isotopic and trace element composition of the upper mantle beneath a young continental rift: results from Kilbourne Hole, New Mexico. Geochim. Cosmochim. Acta, 52 , 461-473.

Ross, G.M., 1991a. Precambrian basemement in the Canadian Cordillera: an introduction. Can. J. Earth Sci., 28 , 1133-1139.

Ross, G.M., 1991b. Precambrian basement in the Canadian Cordillera: an introduction. Can. J. Earth Sci., 28 (8), 1133-1139.

Ross, J.V., 1983. The nature and rheology of the cordilleran upper mantle of British Columbia: inferences from peridotite xenoliths. Tectonophys., 100 , 321-357.

Roy-Barman, M., 1993. Mesure du rapport $^{187}Os/^{186}Os$ dans les basaltes et les péridotites: contribution à la systématique $^{187}Re/^{186}Os$ dans le manteau. PhD Thesis, Paris 7.

Rudnick, R.L., McDonough, W.F. and Chappell, B.W., 1993. Carbonatite metasomatism in the northern Tanzanian mantle: petrographic and geochemical characteristics. Earth Planet. Sci. Lett., 114 , 463-475.

Salters, V.J.M. and Hart, S.R., 1989. The hafnium paradox and the role of garnet in the source of mid-ocean-ridge basalts. Nature, 342 , 420-422.

Salters, V.J.M. and Hart, S.R., 1991. The mantle sources of ocean ridges, islands and arcs: the Hf-isotope connection. Earth Planet. Sci. Lett., 104 , 364-380.

Salters, V.J.M. and Shimizu, N., 1988. World-wide occurence of HFSE-depleted mantle. Geochim. Cosmochim. Acta, 52 , 2177-2182.

Salters, V.J.M. and Zindler, A., 1995. Extreme 176Hf/177Hf in the sub-oceanic mantle. Earth Planet. Sci. Lett., 129 , 13-30.

Samson, S.D., McClelland, W.C., Patchett, P.J., Gehrels, G.E. and Anderson, R.G., 1989. Evidence from neodynium isotopes for mantle contributions to Phanerozoic crustal genesis in the Canadian Cordillera. Nature, 337 , 705-709.

Samson, S.D. and Patchett, P.J., 1991. The Canadian Cordillera as a modern analogue of Proterozoic crustal growth. Austral. J. Earth Sci., 38 , 595-611.

Samson, S.D., Patchett, P.J., McClelland, W.C. and Gehrels, G.E., 1991a. Nd and Sr isotopic constraints on the petrogenesis of the west side of the northern Coast Mountains batholith, Alaskan and Canadian Cordillera. Can. J. Earth Sci., 28 , 939-946.

Samson, S.D., Patchett, P.J., McClelland, W.C. and Gehrels, G.E., 1991b. Nd isotopic characterisation of metamorphic rocks in the Coast Mountains, Alaskan and Canadian Cordillera: ancient crust bounded by juvenile terranes. Tectonics, 10 (4), 770-780.

Schiano, P., Birck, J.-L. and Allègre, C.J., 1997a. Osmium-strontium-neodynium-lead isotopic covariations in mid-ocean ridge basalt glasses and the heterogeneity of the upper mantle. Earth Planet. Sci. Lett., 150 , 363-379.

Schiano, P., Burton, K.W., Birk, J.L. and Allègre, C.J., 1997b. The distribution and behavior of rhenium and osmium among mantle minerals. AGU Fall meeting, San Francisco,EOS, 78 n°46, F812.

Sen, G., 1988. Petrogenesis of spinel lherzolite and pyroxenite suite xenoliths from the Koolau shield, Oahu, Hawaii: implications for petrology of the post-eruptive lithosphere beneath Oahu. Contrib. Miner. Petrol., 100 , 61-91.

Sguigna, A.P., Larabee, A.J. and Waddington, J.C., 1982. The half life of ^{176}Lu by a γ–γ coincidence measurement. Can. J. Phys., 60 , 361-364.

Shaw, C.S.J., Thibault, Y., Edgar, A.D. and Lloyd, F.E., 1998. Mechanisms of orthopyroxene dissolution in silica-undersaturated melts at 1 atmosphere and implications for the origin of silica-rich glass in mantle xenoliths. Contrib. Miner. Petrol., 132 , 354-370.

Shaw, D.M., 1979. Trace element melting models. Phys. Chem. Earth, 11 , 577-586.

Shi, L., Francis, D., Ludden, J., Frederiksen, A. and Bostock, M., 1998. Xenolith evidence for lithospheric melting above anomalously hot mantle under the northern Canadian Cordillera. Contrib. Miner. Petrol., 131 , 39-53.

Shirey, S.B. and Walker, R.J., 1995. Carius tube digestion for low-blank Rhenium-Osnium analysis. Anal. Chem., 67 (13), 2136-2141.

Silver, P.G., 1996. Seismic anisotropy beneath the continents: probing the depths of geology. Ann. Rev. Earth Planet. Sci., 24 , 385-432.

Smoliar, M.I., R.J., W. and Morgan, J.W., 1996. Re-Os ages of Group IIA, IIIA, IVA, and IVB iron meteorites. Science, 271 , 1099-1102.

Snow, J.E. and Reisberg, L., 1995. Os isotopic systematics of the MORB mantle: results from altered abyssal peridotites. Earth Planet. Sci. Lett., 136 , 723-733.

Song, Y. and Frey, F.A., 1989. Geochemistry of peridotite xenoliths in basalt from Hannuoba, Eastern China: implications for subcontinental mantle heterogeneity. Geochim. Cosmochim. Acta, 53 , 97-113.

Souther, J.G., 1991. Volcanic regimes. In: H. Gabrielse and C.J. Yorath (Editor), Geology of the Cordilleran Orogen in Canada. Geological Survey of Canada, 457-490.

Stevens, R.A., Erdmer, P., Creaser, R.A. and Grant, S.L., 1995. Mississippian assembly of the Nitsulin assemblage: evidence from primary contact relationships and Mississippian magmatism in the Teslin tectonic zone, part of the Yukon-Tanana terrane of south-central Yukon. Can. J. Earth Sci., 33 , 103-116.

Stolz, A.J. and Davies, G.R., 1988. Chenical and isotopic evidence from spinel lherzolite xenoliths for episodic metasoamtism of the upper mantle beneath southeast Australia. J. Petrol.(Special Lithosphere), 303-330.

Stosch, H.G., 1982. Rare earth element partitioning between minerals from spinel peridotite xenoliths. Contrib. Miner. Petrol., 78 , 166-174.

Sun, Armstrong and Maxwell, 1991. Proterozoic mantle under Quesnellia: variably reset Rb-Sr mineral isochrons in ultramafic nodules carried up in Cenozoic volcanic vents of the southern Omenica Belt. Can. J. Earth Sci., 28 , 1239-1253.

Sun, M. and Kerrich, R., 1995. Rare earth element and high field strength element characteristics of whole rocks and mineral separates of ultramafic nodules in Cenozoic volcanic vents of southeastern British Columbia, Canada. Geochim. Cosmochim. Acta, 59 (23), 4863-4879.

Sun, S.-S. and McDonough, W.F., 1989. Chemical and isotopic systematics of oceanic basalts: implications for mantle composition and processes. In: A.D. Saunders and M.J. Norry (Editor), Magmatism in the ocean basins. Geological Society Special Publication, 313-345.

Takahashi, E., 1980. Thermal history of lherzolite xenoliths - I. Petrology of lherzolite xenoliths from the Ichinomegata crater, Oga peninsula, northeast Japan. Geochim. Cosmochim. Acta, 44 , 1643-1658.

Takazawa, E., Frey, F.A., Shimizu, N., Obata, M. and Bodinier, J.L., 1992. Geochemical evidence for melt migration and reaction in the upper mantle. Nature, 359 , 55-58.

Tatsumi, Y. and Ishizaka, K., 1982. Origin of high-magnesian andesites in the Setouchi volcanic belt, southwest Japan, I. Petrological and chemical characteristics. Earth Planet. Sci. Lett., 60 , 293-304.

Taylor, S.R. and McLennan, S.M., 1985. The continental crust: its composition and evolution. Blackwell, Oxford.

Titterington, D.M. and Halliday, A.N., 1979. On the fitting of parallel isochrons and the method of maximum likelihood. Chem. Geol., 26 (3-4), 183-195.

Toramaru, A. and Fujii, N., 1986. Connectivity of melt phase in a partially molten peridotite. J. Geophys. Res., 91 (B9), 9239-9252.

Tracy, R.J., 1980. Petrology and genetic significance of an ultramafic xenolith suite from Tahiti. Earth Planet. Sci. Lett., 48 , 80-96.

Ulmer, P., 1989. The dependance of the Fe2+-Mg cation partioning between olivine and basaltic liquid on pressure, temperature and composition. An experimental study to 30 kbars. Contrib. Miner. Petrol., 101 , 261-273.

Umhoefer, P.J., 1987. Northward translation of "Baja British Columbia" along the late cretacious to paleocene margin of Western North America. Tectonics, 6 , 377-394.

Umino, S. and Yoshizawa, E., 1996. Petrology of ultramafic xenoliths from Kishyuku lava, Fukue-jima, southwest Japan. Contrib. Miner. Petrol., 124 , 154-166.

van der Hilst, R., 1995. Complex morphology of subducted lithosphere in the mantle beneath the Tonga trench. Nature, 374 , 154-157.

VanDecar, J.C., James, D.E. and Assumpção, M., 1995. Seismic evidence for a fossil mantle plume beneath South America and implications for plate driving forces. Nature, 378 , 25-31.

Vervoort, J.D., Patchett, P.J., Blichert-Toft, J. and Albarède, F., 1998. Relationships between Lu-Hf and Sm-Nd isotopic systems in the global sedimentary system. Earth Planet. Sci. Lett., in press .

Volkening, J., Walczyk, T. and Heumann, K.G., 1991. Osmium isotope ratio determinations by negative thermal ionization mass spectrometry. Int. J. Mass Spectrom. Ion Phys., 105 , 147-159.

Walker, R.J., Carlson, R.W., Shirey, S.B. and Boyd, F.R., 1989. Os, Sr, Nd, and Pb isotope systematics of southern African peridotite xenoliths: Implications for the chemical evolution of subcontinental mantle. Geochim. Cosmochim. Acta, 53 , 1583-1595.

Weaver, B.L., Wood, D.A., Tarney, J. and Joron, J.L., 1987. Geochemistry of oceanic island basalts from the South Atlantic: Ascension, Bouvet, St Helena, Gough and Tristan de Cunha. In: J.G. Fitton and B.G.J. Upton (Editor), Alkaline Igneous Rocks. Geological Society Special Publication, 253-267.

Wells, P.R.A., 1977. Pyroxene thermometry in simple and complex systems. Contrib. Miner. Petrol., 62 , 129-139.

Widom, E. and Shirey, S.B., 1996. Os isotopic systematics in the Azores: implications for mantle plume sources. Earth Planet. Sci. Lett., 142 , 451-465.

Wilshire, H.G. and Shervais, J.W., 1975. Al-augite and Cr-diopside ultramafic xenoliths in basaltic rocks from western United States. Phys. Chem. Earth, 9 , 257-286.

Wilson, M., 1989. Igneous petrogenesis. A global tectonic approach. Unwin Hyman, London, 466 pp.

Wilson, M.R., Kyser, T.K. and Fagan, R., 1996. Sulfur isotope systematics and platinum group element behavior in REE-enriched metasomatic fluids: A study of mantle xenoliths from Dish Hill, California, USA. Geochim. Cosmochim. Acta, 60 (11), 1933-1942.

Witt-Eickschen, G. and Kramm, U., 1997. Mantle upwelling and metasomatism beneath Central Europe: geochemical and isotopic constraints from mantle xenoliths from the Rhön (Germany). J. Petrol., 38 (4), 479-493.

Wolfe, C.J., Bjarnason, I.T., VanDecar, J.C. and Solomon, S.C., 1997. Seismic structure of the Iceland mantle plume. Nature, 385 , 245-247.

Wood, B.J., Bryndzia, L.T. and Johnson, K.E., 1990. Mantle oxidation state and its relationship to tectonic environment and fluid speciation. Science, 248 , 337-345.

Wood, B.J. and Virgo, D., 1989. Upper mantle oxidation state: ferric iron contents of lherzolite spinels by 57 Mössbauer spectrometry and resultant oxygen fugacities. Geochim. Cosmochim. Acta, 53 , 1277-1291.

Wood, S.A., 1987. Thermodynamic calculations of the volatility of the platinum group elements (PGE): the PGE content of fluids at magmatic temperatures. Geochim. Cosmochim. Acta, 51 , 3041-3050.

Xue, X., Baadsgaard, H., Irving, A. and Scarfe, C., 1990. Geochemical and isotopic characteristics of lithospheric mantle beneath West Kettle River, British Columbia: evidence from ultramafic xenoliths. J. Geophys. Res., 95 (B10), 15879-15891.

York, D., 1969. Least squares fitting of a straight line with correlated errors. Earth Planet. Sci. Lett., 5 , 320-324.

Zangana, N.A., Downes, H., Thirlwall, M.F. and Hegner, E., 1997. Relationship between deformation, equilibration temperatures, REE and radiogenic isotopes in mantle xenoliths (Ray Pic, Massif Central, France): an example of plume-lithosphere interaction? Contrib. Miner. Petrol., 127 , 187-203.

Annexe 1: chimie et techniques analytiques

A1.1 PRÉPARATION DES ÉCHANTILLONS

Chaque échantillon de xénolite est coupé à la scie électrique à roche refroidie à l'eau afin d'éliminer le bord extérieur du xénolite susceptible d'avoir été contaminé par le magma encaissant. L'épaisseur de la partie enlevée est en générale de 1 cm, mais moins si le xénolite est petit (<5 cm de diamètre). Une partie du coeur du xénolite est ensuite prélevée pour la broyer en poudre pour les analyses de roche totale. Le reste est réservé à une lame mince et à des séparations de minéraux. Le broyage de environ 50 g de matériel s'effectue d'abord au marteau, puis dans un broyeur en aluminium (McGill University) ou en agate (CRPG), enfin dans un mortier d'agate.

A1.2 ANALYSE DES ÉLÉMENTS MAJEURS

L'analyse des éléments majeurs a été effectuée à l'Université McGill (Montréal, Canada) par T. Ahmedali sur le spectromètre à fluorescence X (XRF) Philips PW 1400. Avant analyse, la poudre de roche est séchée à 1050°C pendant 12 heures, puis est mélangée à du tétraborate de lithium. La fusion s'effectue dans un creuset de platine et l'échantillon subit une trempe rapide afin d'obtenir un petit disque de verre. La précision analytique pour les éléments majeurs est meilleure que 1%.

A1.3 ANALYSE DES ÉLÈMENTS TRACES

L'analyse des éléments traces a été effectuée au CRPG (Nancy, France) par le personnel du Laboratoire d'Analyse SARM sur une ICP-MS Perkin Elmer SCIEX ELAN 5000. 300 mg de poudre d'échantillon sont mélangés à du métaborate de lithium et fondus dans un four à 980°C. La bille de verre obtenue par trempe est ensuite dissoute dans de l'HNO_3 concentré pendant une nuit. Pour la plupart des échantillons, la solution a été passée sur une résine True Spec afin de concentrer les élèments traces, qui sont en général en faible quantité dans les péridotites. Toutes les 3 à 5 analyses, la mesure d'un blanc est effectuée. Les standards utilisés sont des solutions de basaltes BIR et BR. Les concentrations d'éléments traces sont reproductibles à moins de 2 %.

A1.4 CHIMIE ET ANALYSE RE-OS

La chimie et les analyses isotopiques Re-Os ont été réalisées sous la direction de L. Reisberg au CRPG (Nancy, France), et avec la collaboration de C. Spatz, A.-C. Pierson-Wieckman et B. Jacquier.

A1.4.1 Dissolution des échantillons

La technique de dissolution par attaque acide et Carius tube décrite ici (Shirey and Walker, 1995) a été choisie car elle est la plus efficace pour les roches ultramafiques. Il existe d'autres types d'attaques acides, sans Carius tube, et aussi des dissolutions par fusion. Chacune a ses avantages et inconvénients. Les attaques acides sans Carius tube et à basse température (<150°C) (Walker, 1988; Birck et al., 1997) ont l'avantage d'avoir des blancs très bas, mais leur limitation réside dans le fait que la dissolution de phases comme la chromite et les alliages de Os-Ir se fait mal. Ces phases étant courantes dans les péridotites, cette technique de dissolution n'a pas été retenue. Les techniques de fusion (Hoffman et al., 1978; Morgan and Walker, 1989) ont des blancs totaux de Re trop

importants pour des échantillons contenant moins d'un ppb de Re (comme les péridotites) et posent parfois des problèmes de volatilisation du Re et de l'Os. Elles ont cependant l'avantage de pouvoir dissoudre de grandes quantités d'échantillon (10-100 g). Les péridotites contenant beaucoup d'Os, il n'est cependant pas nécessaire de dissoudre une telle quantité de matériel. Ainsi, la digestion à haute température (200°-260°C) avec des acides oxydants et dans un tube de verre scellé (le Carius tube) a été choisie (Shirey and Walker, 1995). La taille des échantillons dissous par cette méthode ne peut cependant dépasser 10 g.

1.5 g de poudre d'échantillon sont pesés, ainsi que les spikes d'Os et de Re ajoutés ensuite à la poudre. Il suffit en général de 3 gouttes (environ 0.08 g) de spike ^{190}Os 10 ppb et de une goutte (environ 0.025 g) de spike ^{185}Re 15.052 ppb pour les concentrations en Os et Re des péridotites analysées. Ces spikes ont été préparés à partir d'une solution concentrée de spike qui a été diluée: dans du HCl 6N pour le spike d'Os et dans du HNO_3 0.1 N pour le spike de Re.

La première attaque acide se fait dans des béchers de téflon 15 ml avec 4.5 ml d'éthanol, 6 ml d'HCl 12 N et 6 ml d'HF 12N. L'éthanol est versé en premier car il ralentit l'ébullition et ainsi diminue le risque de perdre de l'Os par évaporation. L'éthanol et l'HCL sont des agents réducteurs et servent donc à éviter une perte d'Os qui est un élément volatile en conditions oxydantes. Le bécher est fermé hermétiquement, avec au besoin un fil de téflon sur le pas de vis afin d'éviter toute fuite. Après passage aux ultrasons pour bien mélanger les produits, le tout est laissé dans une étuve à 90°C pendant 12 heures. Le bécher en téflon est ensuite ouvert et mis sur une plaque chauffante à 60°C jusqu'à complète évaporation. Quand il ne reste plus qu'un résidu sec au fond du bécher, 6 ml d'HCl sont rajoutés. Cette étape vise à éliminer toute trace d'HF avant de mettre le mélange dans le Carius tube en verre (l'HF dissout le verre). Après passage aux ultrasons, le bécher fermé est à nouveau mis dans une étuve à 90°C pendant 12 heures, puis ouvert pour laisser évaporer jusqu'au sèchage complet sur une plaque chauffante.

L'échantillon est repris dans 4 ml d'HCl 12N et inséré dans un Carius tube à l'aide d'un entonnoir en verre. Le corps du Carius tube a une longueur de 270 mm, un diamètre intérieur de 11 mm et les parois sont épaisses de 4 mm. Le col plus étroit a une longueur de 50 mm minimum après soudure, un diamètre intérieur de 5 mm et les parois une épaisseur de 2.5 mm. La moindre épaisseur du col par rapport à celle du corps facilite le soudage. La composition du verre est borosilicatée. 2 ml d'HNO_3 12 N sont ensuite rajoutés dans le tube, et l'échantillon se trouve ainsi dissous dans de l'eau régale. Afin de diminuer les risques d'explosion liés à une trop forte pression des gaz à l'intérieur du Carius tube lors de son chauffage en four, l'air en est pompé pendant que la base du Carius tube est refroidie dans un mélange l'azote liquide-éthanol à environ -110°C. Le mélange azote liquide-éthanol est ensuite remplacé par de l'azote liquide pure à environ -190°C, afin d'éviter toute explosion due à l'intéraction entre les vapeurs d'éthanol et la flamme de soudure. La soudure se fait donc avec l'intérieur du tube sous vide et refroidi. Après la fermeture du Carius tube, la partie étroite située en haut de ce dernier est placée dans un petit four à 550°C afin d'éviter que le tube ne casse par distension du verre lors de son refroidissement après la soudure. Le sommet du tube reste dans le petit four pendant une heure, puis est laissé refroidir doucement jusqu'à température ambiante. Le Carius tube est finalement placé dans un four à 230°C pendant 12 heures, où il est inclu dans une gangue de métal inoxidable fermée pour limiter les dangers d'une explosion éventuelle. Il s'agit ici de l'étape susceptible de dissoudre les phases comme la chromite ou le spinelle qui sont très résistantes. Après avoir laissé le four refroidir jusqu'à température ambiante, le tube est retiré de sa gangue de métal et inspecté pour y détecter d'éventuelle phases mal dissoutes comme des petits grains de spinelle noirs. La dissolution totale est réussie dans 90% des cas. Cette procédure résulte donc à l'équilibre complet avec les spikes et à l'oxydation du mélange échantillon-spike en OsO_4.

A1.4.2 Séparation du Re et de l'Os

La technique de séparation du Re et de l'Os utilisée ici est basée sur la volatilité de l'Os en conditions oxydantes et se fait grâce à une distillation (Walker, 1988). D'autres méthodes d'extraction de l'Os ont été développées depuis et sont plus rapides et plus pratiques à mettre en oeuvre. Elles sont basées sur l'extraction de l'Os d'une phase aqueuse à un solvent comme le chloroforme ou le tétrachloride de carbone (Cohen and Waters, 1996), ou encore le liquide bromique (Birck et al., 1997). L'inconvénient principal de ces nouvelles techniques de chimie est que les vapeurs dégagées ou les réactif employés lors de leur application sont dangeureux (CCl_4 et liquide bromique), mais une hotte bien ventilée et une protection avec gants épais et blouse peut y remédier. Par contre la moindre quantité de réactif utilisée par rapport à la technique de distillation contribue à diminuer les blancs. Cette dernière constatation n'est pas capitale pour l'analyse de péridotites qui contiennent beaucoup d'Os (0.05 à 6 ppb d'Os), mais est importante lorsqu'il s'agit d'analyser des basaltes, des sédiments ou des eaux. Les blancs totaux obtenus ici varient de 5 à 7 pg. Nous ne décrirons en détail que la technique qui a été utilisée au cours de cette thèse, c'est à dire la distillation.

Après avoir sorti du four le Carius tube, ce dernier est trempé dans de l'azote liquide et est brisé en haut de sa partie large: un poinçon de verre chauffé à blanc y est appliqué et provoque une fente de tension tout autour du tube, qui peut être ensuite brisé au niveau de la fente avec aisance. Le contenu du tube est ensuite versé dans un grand ballon de distillation avec 40 ml de l'oxydant H_2SO_4 5N. La température du ballon est portée à 105°C, température d'ébullition de l'OsO_4. L'OsO_4 évaporé est récupéré à l'autre extrémité de la distillation dans un petit ballon de verre contenant 6 ml d'NaOH. La procédure totale dure une heure et demie à deux heures. Le Re, resté dans le grand ballon de distillation, est récupéré dans le bécher en téflon de 15 ml du début, rincé entre-temps à l'eau bi-distillée. La solution d'OsO_4 dans du NaOH est distillée une deuxième fois afin de concentrer d'avantage l'Os. A cet effet, en plus de la solution sus-mentionnée, est ajouté dans le grand

ballon de distillation 15 ml d'H_2SO_4 20N et 2 ml d'une solution de Cr^{VI} (dans H_2SO_4 4N), le tout étant extrêmement oxydant et chauffé à plus de 105°C. L'OsO_4 évaporé est une nouvelle fois récupéré, cette fois-ci dans 2 ml d'HBr à l'autre extrémité de la distillation. Cette deuxième distillation dure environ une demi-heure.

A1.4.3 Purification de la solution d'Os et préparation pour l'analyse

Le dernière purification de la solution d'Os se fait à l'aide d'une microdistillation (Roy-Barman, 1993). Quelle que soit la méthode d'extraction de l'Os utilisée, cette technique est encore largement employée pour parfaire la purification de l'Os. Le principe est le même que pour la distillation, c'est à dire mettre la solution d'Os en conditions oxydantes, chauffer pour faire évaporer l'Os et le récupérer dans du HBr.

Après la deuxième partie de la distillation, la solution d'Os est récupérée, transférée dans un bécher de téflon de 5 ml, et mise à évaporation sur une plaque chauffante à 90°C. Lorsque l'échantillon est sec, il est repris dans une ou deux gouttes d'une solution Cr^{VI} (dans H_2SO_4 4N). A l'aide d'une micro-pipette et d'un cathéter, le tout est transféré dans le bouchon d'un bécher conique. Une goutte de HBr est d'autre part déposée au fond du cône. Le cône est ensuite prudemment retourné au dessus du bouchon et vissé à celui-ci, en prenant garde de ne pas laisser tomber la goutte d'HBr sur l'échantillon. Le tout entouré d'une feuille de papier aluminium est laissé sur une plaque chauffante à 80°C pendant trois heures. La goutte d'HBr, dans lequel se trouve maintenant l'Os est ensuite récupérée (toujours en prenant garde de ne pas mélanger la solution de Cr^{VI} avec celle d'HBr!) et transférée dans le couvercle du bécher de 5 ml précédemment utilisé et qui a été rincé entre-temps.

L'Os est déposé sur un filament de Pt ultra-pur pour l'analyse au N-TIMS (spectromètre de masse à thermoionisation à ions négatifs). Le filament de Pt est débarassé d'une possible contamination de matière organique soit en étant chauffé sous

vide dans un banc de dégazage pendant plusieurs heures à environ 1200°C, soit en étant préchauffé à l'air à 1200-1300°C pendant 2 mn. La goutte d'HBr contenant l'Os précédemment obtenue est légèrement mise à évaporation sous une lampe chauffante pour en diminuer la taille, puis déposée à l'aide d'une micro-pipette sur le filament de Pt. Une solution sur-saturée de $Ba(NO_3)_2$ ou du $Ba(OH)_2$ est également déposée sur le filament pour augmenter l'émission d'ions lors du chauffage du filament dans le spectromètre (Walker, 1988; Birck et al., 1997). Le filament est chauffé doucement jusqu'à ce que l'échantillon soit sec.

A1.4.3 Purification de la solution de Re et préparation pour l'analyse

La solution de Re obtenue lors de la première étape de dissolution, est encore purifiée en la passant dans des colonnes chromatographiques anioniques (Morgan and Walker, 1989; Reisberg et al., 1991). A nouveau, d'autres techniques d'extraction du Re existent et sont basées sur des solvents (Walker, 1988; Birck et al., 1997).

La solution de Re est passée sur deux colonnes successives. La résine de la première colonne (1 ml d'AG1X8) est nettoyée par 10 ml d'eau bi-distillée puis mise en condition successivement par 2.5 ml d'HNO_3 0.8 N, 25 ml d'HNO_3 4 N, 5 ml d'H_2SO_4 2.5 N, enfin 2.5 ml d'H_2SO_4 5 N. L'échantillon préalablement centrifugé est versé dans la colonne, puis 2.5 ml d'H_2SO_4 5 N, 2.5 ml d'H_2SO_4 2.5 N, 2.5 ml d'HCl 1 N, 7.5 ml d'HCl 1 N, 2.5 ml d'HNO_3 0.8 N et 4 ml d'HNO_3 4 N. L'élution se fait dans 10 ml d'HNO_3 4 N. La solution d'HNO_3 contenant le Re est mise à évaporation sur une plaque chauffante. L'échantillon est repris dans 2 ml d'HNO_3 0.1 N avant la seconde colonne. Celle-ci est remplie de 0.25 ml de résine rincée par de l'eau distillée et mise en condition par de l'HNO_3 8 N puis 0.1 N, chacun remplissant la colonne tour à tour. Après avoir versé l'échantillon, 2 ml d'HNO_3 0.1 N sont ajoutés quatre fois et l'élution finale se fait dans 5 ml d'HNO_3 8N.

Au début de cette étude, le Re était déposé sur un filament de platine comme l'Os et analysé par N-TIMS. Cependant les blancs obtenus par cette méthode étaient mauvais ainsi que la reprocductibilité. L'analyse par ICP-MS solution s'est avérée plus fiable. Ainsi, les derniers échantillons ayant subi la méthode précédemment décrite ont été évaporés et repris dans 3.7 ml d'HNO_3 0.1 N pour être ensuite analysés par ICP-MS. La plupart des échantillons qui avaient déjà été analysés par N-TIMS ont été refaits par une autre méthode de chimie plus simple (Reisberg et al., 1991) quand il restait de la poudre de roche disponible. 1.5 g de poudre ont été dissous dans 3HF + 1HNO_3 concentrés et laissés dans un four à 140°C pendant trois jours. Le Re a ensuite été extrait dans une colonne à résine anionique (1ml d'AG1X8). Après avoir rincé à l'eau bi-distillée la résine, celle-ci est mise en condition par de l'HNO_3 8 N, puis deux fois 1 ml d'HNO_3 0.8 N. Après avoir versé l'échantillon, puis 4 ml d'HNO_3 8 N, l'élution se fait dans 3 ml d'HNO_3 8 N. Les blancs obtenus à l'ICP-MS tournent autour de 30 pg.

A1.4.4 Analyse de l'Os par N-TIMS

L'analyse des isotopes de l'Os se fait maintenant partout par N-TIMS qui fournit la précision analytique nécessaire (meilleure que ± 0.1% 2σ) pour exploiter pleinement les ressources du système Re-Os (Creaser et al., 1991; Volkening et al., 1991). Les méthodes analytiques utilisées auparavant (SIMS, RIMS, ICP-MS) n'offraient pas une sensibilité suffisante, ni une précision meilleure que 1 à 2 % 2σ. Les analyses de cette thèse ont été effectuées sur un spectromètre de masse Finnigan MAT 262 modifié pour l'analyse en ions négatifs.

L'Os du dépot du filament de Pt est ionisé sous la forme de OsO_3^-. Comme les rapports isotopiques sont mesurés par des rapports d'oxydes par le spectromètre, il est nécessaire de faire une correction dont l'équation est:

$$^{187}Os/^{188}Os = {}^{187}OsO_3/^{188}OsO_3 - 1.6 \times {}^{185}ReO_3/^{188}OsO_3$$

1.6 étant le rapport naturel $^{187}Re/^{185}Re$. Le fractionement de masse du spectromètre est corrigé en fonction du rapport $^{192}Os/^{188}Os$ = 3.08271 (Luck and Allègre, 1983). La plupart des analyses ont été effectuées sur le multiplicateur d'électron, en mode "peak jumping". Cependant, certaines analyses ont été réalisées sur le mode comptage quand le signal était trop faible pour être détecté en mode multiplicateur d'électron. 70 mesures du standard provenant du Lamont Doherty Earth Observatory ont donné des valeurs du rapport $^{187}Os/^{188}Os$ = 0.17391±0.00040 (σ). La précision sur le rapport isotopique est meilleure que ±0.3% (2σ-m).

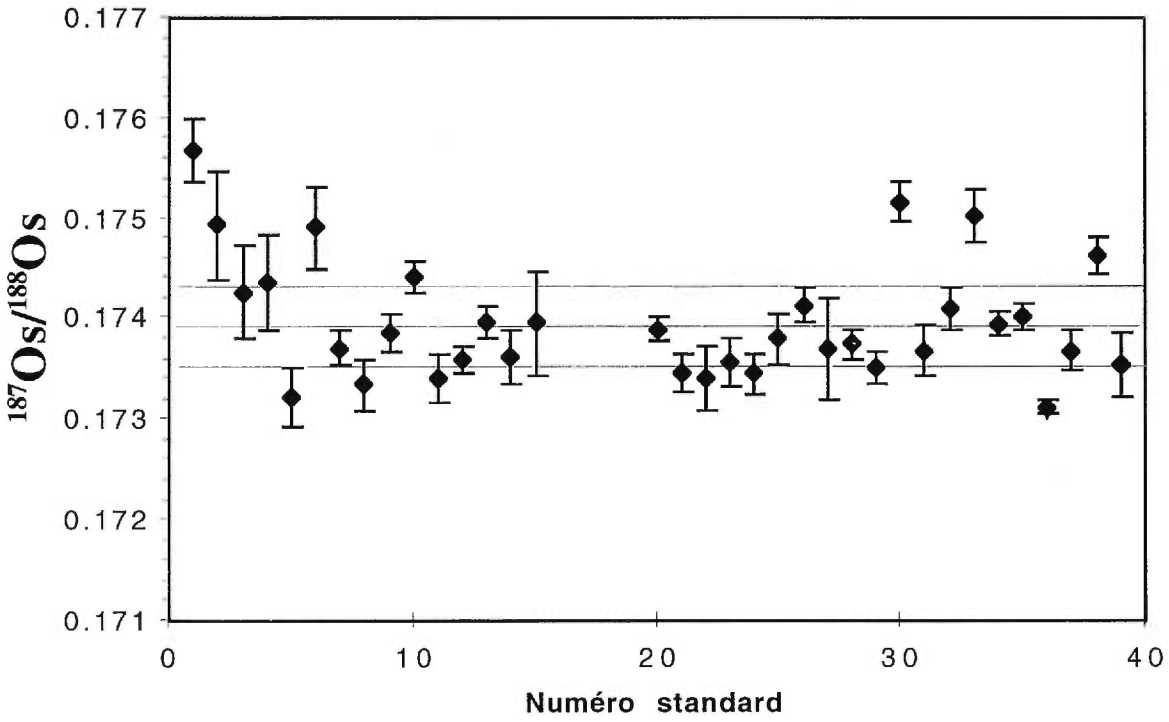

Fig. A: Analyses du rapport $^{187}Os/^{188}Os$ du standard sur l'année 1997

A1.4.4 Analyse du Re par ICP-MS

Les mesures isotopiques du Re ont été effectuées sur l'ICP-MS Elan 6000 du CRPG (Nancy, France), et avec la collaboration de J. Carignan. Cette technique a été décrite entre autres par Richardson et al. (1989). L'échantillon en solution est pulvérisé par le nébuliseur dans une torche à plasma d'argon à 8000°K où il est ionisé. En effet, les problèmes d'efficacité du nébuliseur liés à la présence de solide de la matrice dans la solution sont complètement éliminés par le passage au préalable de l'échantillon dans une colonne anionique. Cette chimie permet également d'éliminer l'Os et le Pt de la solution analysée car certains isotopes de ces éléments sont susceptibles de faire des interférences avec le ^{187}Re. La mesure dure moins d'un quart d'heure pour les 3.7 ml de solution. La précision sur le rapport mesuré est d'environ ±0.2% (2σ-m). 27 mesures d'une même solution standard ont donné $^{187}Re/^{185}Re = 1.7044 \pm 0.0034$ (σ).

A1.5 CHIMIE ET ANALYSE LU-HF

A1.5.1 Chimie

La méthode de chimie employée est celle développée par Blichert-Toft et al. (1997). L'autre méthode existante (Patchett and Tatsumoto, 1980) a l'inconvénient d'utiliser d'énormes quantités d'HF concentré, dans de très grandes colonnes. La chimie a été réalisée à l'Université de Rennes sous la direction de C. Chauvel.

150 mg de Cpx (500 mg pour Opx) sont triés à la main sous la loupe binoculaire et nettoyés à plusieurs reprises dans de l'eau bi-distillée. Un pré-triage a auparavant été réalisé au séparateur magnétique Frantz. Le spike ajouté est enrichi en ^{180}Hf et ^{176}Lu et à 0.0439 nmoles/g d'Hf et 0.1204 nmoles/g de Lu. L'attaque acide se fait d'abord avec 1 ml HNO_3:3 ml HF concentrés dans un savillex de 15 ml fermé laissé sur une plaque chauffante

pendant une nuit à 125°C. Après évaporation à sec, la deuxième attaque se fait à 1ml HNO_3: 3 ml HF: 0.5 ml $HClO_4$ concentrés, le tout étant encore mis plusieurs jours sur une plaque chauffante à 125°C jusqu'à ce que la dissolution soit complète. C'est pendant cette étape que le spike va s'équilibrer pour l'Hf. Après évaporation à sec, l'échantillon est repris dans quelques ml d'HCl 6N pour équilibrer le spike pour le Lu. Après une nuit sur une plaque chauffante bécher fermé, on évapore à sec. Cette dernière procédure (HCl et évaporation) est répétée en tout trois fois. Ensuite, l'HCl est évacué en évaporant, mais pas à sec cette fois-ci, et en ajoutant constamment de l'HF concentré (quelques ml 3 ou 4 fois en tout) au cours de l'évaporation sur plaque chauffante.

La séparation du Lu de l'Hf se fait par précipitation des fluorures (où se concentre le Lu, ainsi que Al, Zr. Ti, Cr,...) et récupération du surnageant d'HF dans lequel l'Hf est soluble. L'étape suivante est répétée trois fois en tout: 1 à 2 ml d'HF concentré sont rajoutés à l'échantillon. Le bécher fermé est passé aux ultrasons puis laissé une nuit (deux heures pour la deuxième fois) sur une plaque chauffante à 100°C. Après centrifugation (10 mn à 4500 tour/min), le surnageant (liquide transparent d'HF où se trouve l'Hf) est pipetté et mis dans un autre bécher en téflon blanc. La solution contenant l'Hf (bécher blanc) est enfin évaporée à sec sur une plaque chauffante à 100°C. 2 ml d'HCl 6N sont ensuite rajoutés dans le bécher blanc contenant l'Hf, puis, quand la dissolution est achevée, 200 µl d'H_2O_2 y sont versés. L'ajout d'H_2O_2 vise à réduire le Cr (de 6+ lors de l'ajout d'$HClO_4$ au début, à 3+ maintenant) avant d'introduire la solution dans la colonne à résine cationique. La solution contenant l'Hf est reprise dans 2 ml d'HF 0.5N, évaporée à sec, puis reprise trois fois dans 3 à 4 ml d'HCl 6N avec une demi journée sur plaque chauffante et évaporation à sec. 2 ml d'HF 0.5M sont encore rajoutés, suivis d'une évaporation à sec (100°C). Enfin, avant de verser la solution d'Hf dans la première colonne, la solution est reprise dans 1 ml de 0.5M HF: 0.5 M HCl, légèrement chauffée pour assurer une bonne dissolution, passée aux ultrasons et centrifugée.

La solution d'Hf est passée sur deux colonnes successives à résine cationique. Il est très important qu'il n'y ait aucun HF dans l'environnement de ces colonnes, en particulier la deuxième. La première colonne a 2 ml de résine AG1-X8 (200-400 mesh). Le conditionement s'y fait avec 0.5M HF: 0.5 M HCl et l'élution dans environ 6 ml d'HCl 6N. Entre les deux colonnes, 5 gouttes d'$HClO_4$ sont rajoutés puis le tout évaporé jusqu'à ce qu'il reste environ 0.5 ml dans le bécher. La même procédure est répétée avec 15 ml, puis 5 ml d'$HClO_4$. Enfin, 300 µl d'HCl 2.5N sont rajoutés à la solution, et juste avant de mettre la solution dans la deuxième colonne, une goutte (30 µl) d'H_2O_2. La deuxième colonne contient 2 ml de résine cationique AG50W-X8 (200-400 mesh), et son conditionnement se fait avec de l'HCl 2,5 N et des traces d'H_2O_2. L'élution se fait dans 5 ml de 2.5 N HCl: 0.3 N HF. La solution récupérée est évaporée à sec. Elle est reprise dans 600 ml d'HNO_3 0.05 N avant l'analyse à l'ICP-MS.

La solution (plutôt une sorte de dépot) contenant le Lu, et qui est toujours dans le bécher 15 ml du début, est reprise deux fois dans 3 à 4 ml d'HCl 6N. Les deux fois, le bécher fermé est laissé une demi journée sur une plaque chauffante, puis la solution est évaporée. 5 ml d'HCl 2 N sont rajoutés et la solution est laissée à reposer 12 heures avant l'introduction dans la colonne (centrifugation auparavant). La colonne contient 2 ml de résine AG50W (200-400 mesh) et est mise en condition par de l'HCl 2 N. Les REE, dont le Lu, sont éluées dans 10 ml d'HCl 6 N. Après évaporation, l'échantillon est nettoyé avec 2 gouttes d'HNO_3 concentré pour éliminer la matière organique.

Une dernière remarque doit concerner le rendement de cette méthode pour des péridotites. En effet cette méthode de chimie marche bien pour la mesure des isotopes de l'Hf dans les basaltes, les météorites ou les sédiments (85% de rendement) (Blichert-Toft et al., 1997), mais beaucoup moins bien pour les roches ultramafiques. Pour les lherzolites analysées dans cette thèse (Chapitre 4), le signal à l'ICP-MS était faible, et même, la plupart des échantillons préparés n'ont pas pu être analysés. Il y a donc certainement perte de l'Hf à une des étapes de la chimie lorsqu'elle est appliquée aux ultramafiques. Ainsi, cette chimie

a été modifiée depuis par J. Blichert-Toft à l'ENS Lyon (France). Le leaching de l'HF (précipitation des fluorures pour séparer Hf et Lu) a été remplacé par une colonne à résine qui permet de séparer l'Hf des éléments majeurs (C. Chauvel, communication personnelle). En effet, il apparaît que c'est à cette étape de la chimie que l'Hf serait perdu dans le précipité au lieu de rester en solution comme pour les roches non-ultramafiques. Ceci expliquerait les mauvais rendements obtenus ici.

A1.5.2 Analyse du Lu et de l'Hf par ICP-MS P54

L'analyse des isotopes de l'Hf et du Lu a été réalisée à l'ENS Lyon (France) sous la direction de P. Telouk et J. Blichert-Toft sur une ICP-MS Plasma 54 de VG Elemental (ICP-MS à secteur magnétique et multi-collection). L'ICP-MS s'est avéré la technique analytique la plus performante pour le Lu-Hf, alliant une meilleure ionisation de l'Hf grâce à la torche à plasma, une meilleure sensibilité, une facilité et rapidité d'analyse et des reproductibilités meilleures que les autres techniques (TIMS, hot-SIMS) (Blichert-Toft et al., 1997). Cette ICP-MS est équipée de 9 cages de Faraday et d'un détecteur multiplicateur Daly à comptage d'ions.

L'aspiration du mélange se fait à l'air libre car les pompes couramment utilisées avec les ICP-MS sont trop rapides (ici flux de 50 µl/mn). Pour la mesure de l'Hf, afin d'augmenter la nébulisation, la solution passe dans un désolvateur à 160°C (MCN 6000) avant d'être pulvérisé dans la torche de plasma d'argon. Tous les trois échantillons, le tube d'aspiration est nettoyé avec de l'alcool isopropylique et entre chaque échantillon avec successivement de l'HF dilué, de l'HNO_3 0.05N et du HNO_3 3%. Les mesures Lu et Hf sont effectuées en multicollection. Une analyse dure en moyenne 20 mn. Le fractionnement de masse de l'Hf est corrigé en fonction du rapport $^{179}Hf/^{177}Hf = 0.7325$. Comme le Lu n'a que deux isotopes, la correction du fractionnement de masse est faite par l'intermédiaire de l'Yb dont le fractionnement de masse est similaire à celui du Lu. Ainsi,

$^{176}Lu/^{175}Lu$ est normalisé à $^{172}Yb/^{171}Yb = 1.5264$. Des mesures répétées du standard d'Hf JMC 475 donnent $^{176}Hf/^{177}Hf = 0.282160 \pm 0.000025$. Les blancs, non spikés, sont mesurés en regardant l'intensité du signal détecté par le Daly et sont d'environ 10^{-15} A. Comme dernière remarque, il est important de ne pas avoir broyé les roches dans du carbure de tungstène, car certains isotopes de ce dernier, ainsi que du Ta, créent des interférences importantes avec l'^{180}Hf.

A1.6 CHIMIE ET ANALYSE SM-ND

La chimie du Sm-Nd a été réalisée à l'Université de Rennes (France) sous la direction de C. Chauvel. Des aliquots pour analyser le Sm-Nd des clinopyroxènes ont été pris de la solution de REE avant que celle-ci ne soit versée dans une colonne cationique pour la séparation du Lu. Il en a été fait de même pour 1.5 à 2 g de poudre de roche totale. Le Nd a ensuite été séparé en passant l'aliquot de solution sur 0.1 ml de résine True Spec (Elution dans de l'HNO_3), puis 2 ml de résine HDEHP (Elution dans de l'HCl) dans des colonnes chromatographiques.

Les rapports isotopiques du Nd ont été mesurés sur le spectromètre à thermoionisation positive Finnigan MAT 262 du CRPG (Nancy, France). Le dépot de l'échantillon est réalisé dans de l'acide phosphorique sur un filament de Re, et l'analyse se fait avec l'assemblage double de filaments de Re et de Ta. Le fractionnement de masse est corrigé par rapport à $^{146}Nd/^{144}Nd = 0.721900$. Les mesures répétées du standard Johnson and Matthey donnent $^{143}Nd/^{144}Nd = 0.511127 \pm 0.000013$. Le Sm de la roche totale a été analysé par ICP-MS solution et la limite de dosabilité est évaluée à 0.005 ppm. La reproductibilité est de ±2 ppm, mesurée sur 3 analyses de deux solutions à 13 ppm et 23 ppm de Sm.

A1.7 BIBLIOGRAPHIE DE L'ANNEXE 1

Birck, J.-L., Roy Barman, M. and Capmas, F., 1997. Re-Os isotopic measurements at the femtomole level in natural samples. Geostandard. Newslett., 20 (1), 19-27.

Blichert-Toft, J., Chauvel, C. and Albarède, F., 1997. Separation of Hf and Lu for high-precision isotope analysis of rock samples by magnetic sector-multiple collector ICP-MS. Contrib. Miner. Petrol., 127, 248-260.

Cohen, A.S. and Waters, F.G., 1996. Separation of osmium from geologocal materials by solvent extraction for analysis by TIMS. Anal. Chem., 332, 269-275.

Creaser, R.A., Papanastassiou, D.A. and Wasserburg, G.L., 1991. Negative thermal ion mass spectrometry of osmium, rhenium, and iridium. Geochim. Cosmochim. Acta, 55, 397-401.

Hoffman, E.L., Naldrett, A.J., Van Loon, J.C., Hancock, R.G.V. and Mason, A., 1978. The determination of all platinum group elements and gold in rocks and ore by neutron activation analysis after preconcentration by a nickel sulfide fire-assay technique of large samples. Anal. Chim. Acta, 102, 157-166.

Luck, J.-M. and Allègre, C.J., 1983. ^{187}Re-^{187}Os systematics in meteorites and cosmochemical consequences. Nature, 302, 130-132.

Morgan, J.W. and Walker, R.J., 1989. Isotopic determinations of rhenium and osmium in meteorites by using fusion, distillation and ion-exchange separations. Anal. Chim. Acta, 222, 291-300.

Patchett, P.J. and Tatsumoto, M., 1980. A routine high-precision method for Lu-Hf isotope geochemistry and chronology. Contrib. Miner. Petrol., 75, 263-267.

Reisberg, L.C., Allègre, C.J. and Luck, J.-M., 1991. The Re-Os systematics of the Ronda Ultramafic Complex of southern Spain. Earth Planet. Sci. Lett., 105, 196-213.

Richardson, J.M., Dickin, A.P. and McNutt, R.H., 1989. Re-Os isotope ratio determinations by ICP-MS: a review of analytical techniques and geological

applications. In: K.E. Jarvis (Editor), Plasma source mass spectrometry. Royal Society of Chemistry, 120-144.

Roy-Barman, M., 1993. Mesure du rapport $^{187}Os/^{186}Os$ dans les basaltes et les péridotites: contribution à la systématique $^{187}Re/^{186}Os$ dans le manteau. PhD Thesis, Paris 7.

Shirey, S.B. and Walker, R.J., 1995. Carius tube digestion for low-blank Rhenium-Osnium analysis. Anal. Chem., 67 (13), 2136-2141.

Volkening, J., Walczyk, T. and Heumann, K.G., 1991. Osmium isotope ratio determinations by negative thermal ionization mass spectrometry. Int. J. Mass Spectrom. Ion Phys., 105, 147-159.

Walker, R.J., 1988. Low-blank chemical separation of rhenium and osmium from gram quantities of silicate rock for measurement by Resonance Ionization Mass Spectrometry. Anal. Chem., 60, 1231-1234.

Annexe 2: planches photographiques

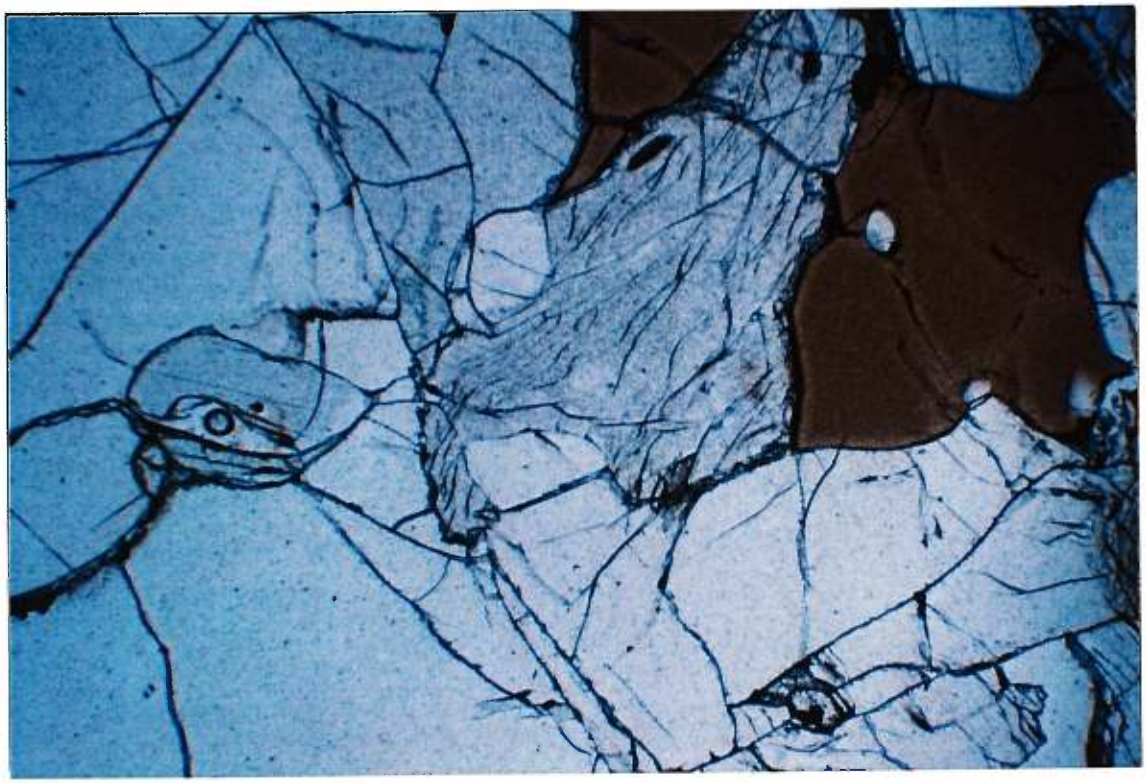

***Photo 1:** Texture protogranulaire: association typique de larges grains de spinelle (brun) avec l'orthopyroxène (gris foncé). Les minéraux clairs sont de l'olivine. Lherzolite BTX-16. Lumière naturelle, largeur du champ: 2.8 x 1.8 mm.*

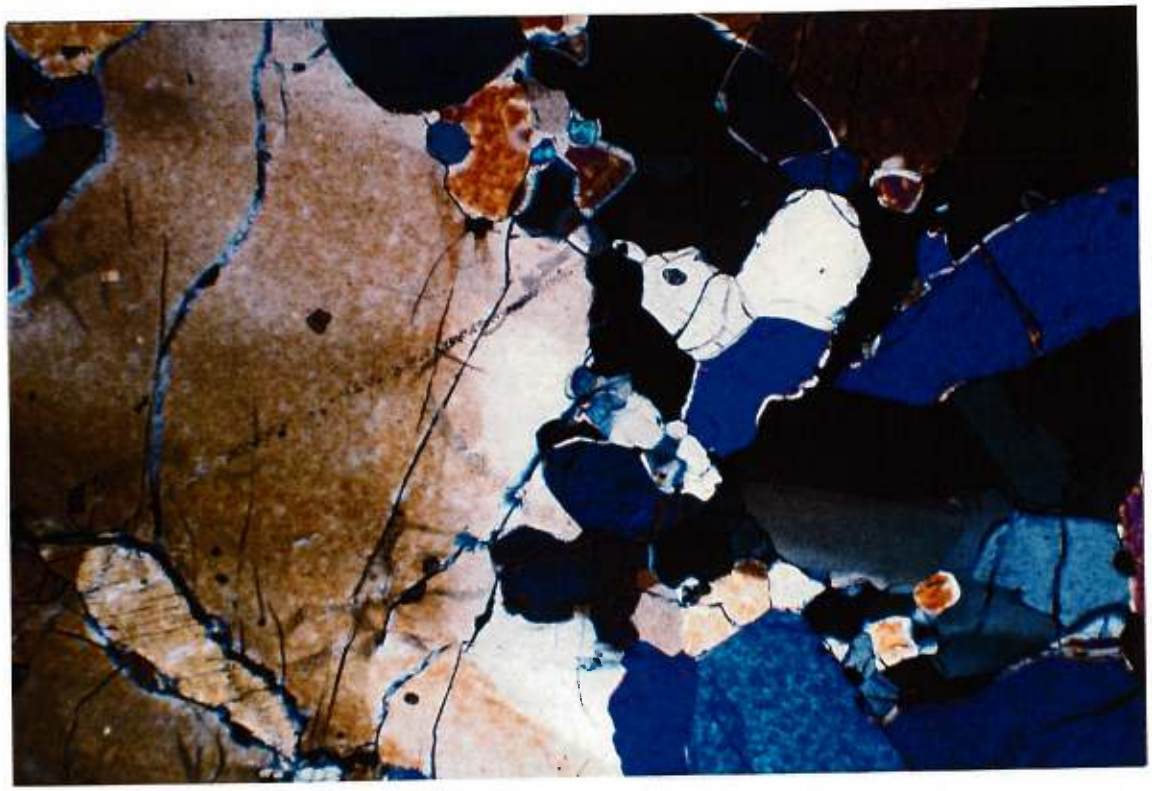

Photo 2: Texture porphyroclastique: porphyroclaste grand et allongé d'olivine et petits grains polygonaux (olivine ici). Dunite KLX-53. Lumière polarisée, largeur du champ: 2.8 x 1.8 mm.

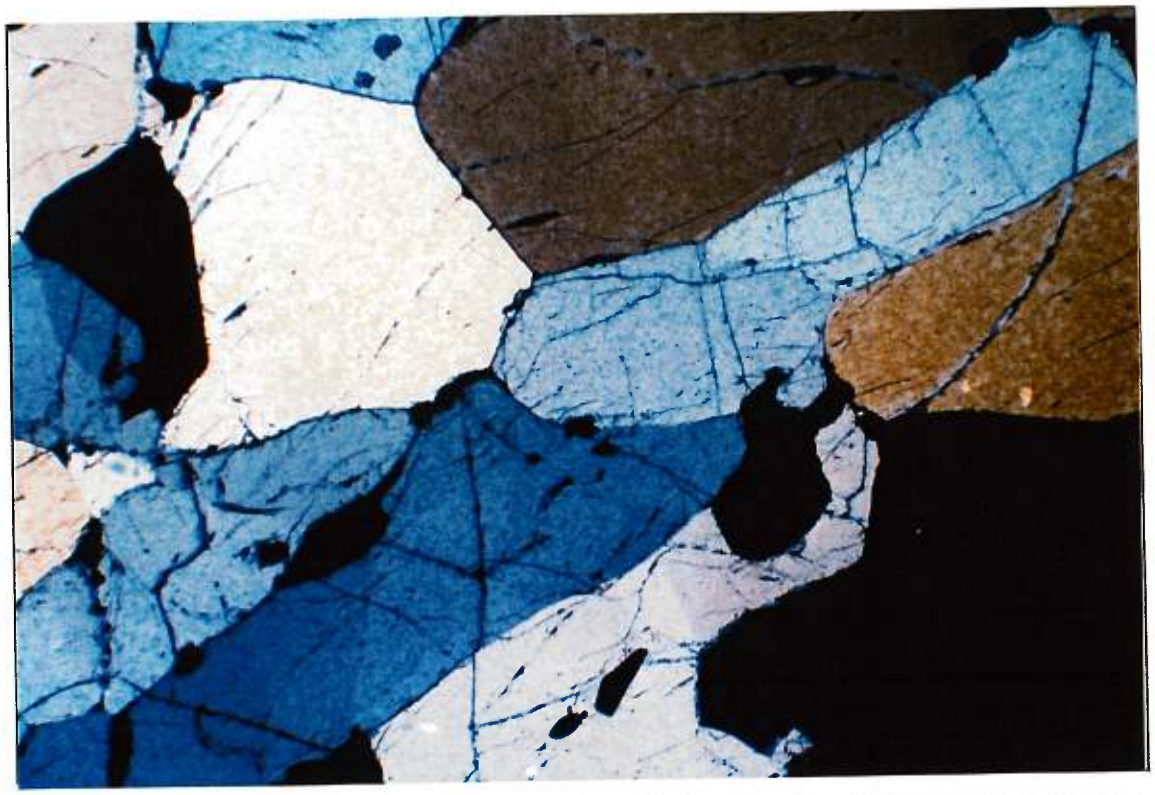

Photo 3: Texture équigranulaire: contacts en ligne droite entre les minéraux et points triples à 120°; spinelles (petits grains noirs sur la photo) petits et de forme arrondies dispersés entre les autres minéraux. Harzburgite KLX-62. Lumière polarisée, largeur du champ: 2.8 x 1.8 mm.

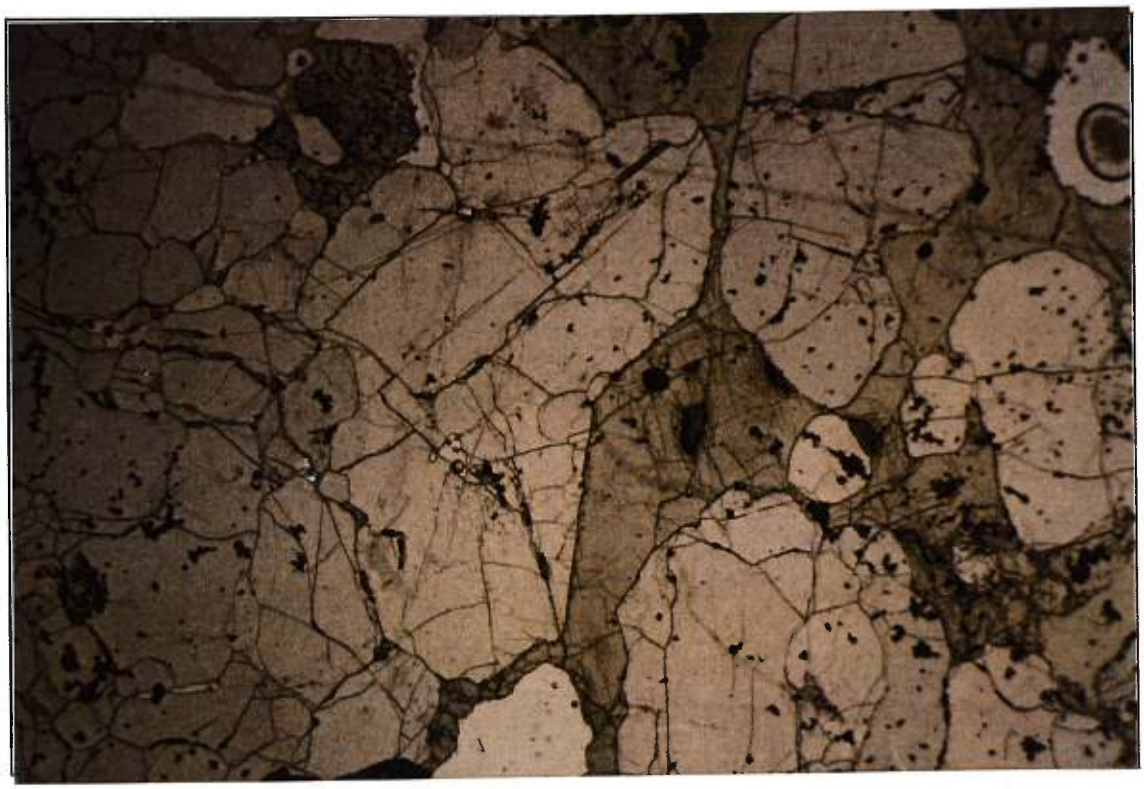

Photo 4: texture poïkiloblastique: grains d'olivine de forme arrondie et en aggrégats entourés de clinopyroxène (augite) poïkiloblastique. Wehrlite KLX-17. Lumière naturelle, largeur du champ: 17 x 9 mm.

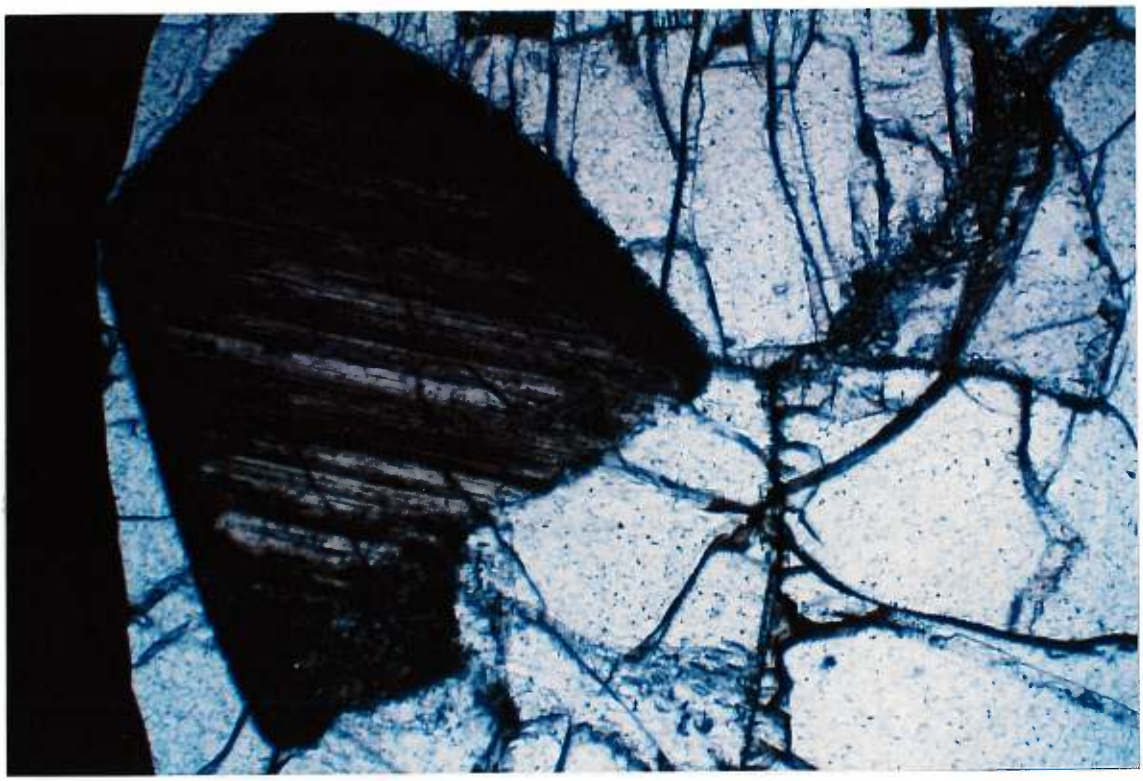

Photo 5: Amphibole pargasitique entourée d'olivines. Lherzolite LPX-11. Lumière naturelle, largeur du champ: 1.35 x 0.9 mm.

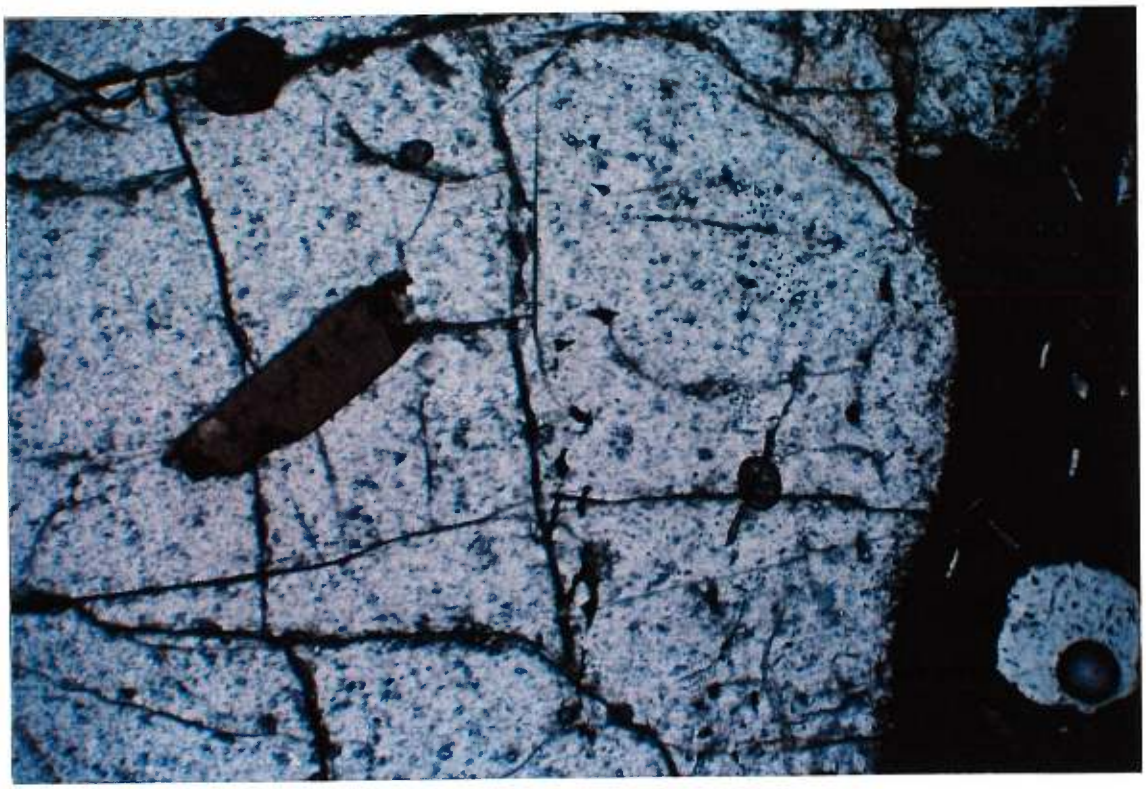

Photo 6: Phlogopite (brune) dans une olivine et contact avec le basalte encaissant (noir). Harzburgite KLX-57. Lumière naturelle, largeur du champ: 1.35 x 0.9 mm.

Annexe 3: Ensemble complet des analyses de roche totale

	KLX-67 Dunite	KLX-59 Dunite	KLX-58 Dunite	KLX-66 Dunite	RRX-19 Harz	RRX-21 Harz	KLX-47 Harz	KLX-62 Harz
Ol	97.04	98.00	97.36	96.12	75.17	78.72	71.13	84.42
Opx	1.34	0.49	0.20	1.12	19.70	16.88	22.86	8.88
Cpx	0.69	0.64	1.35	1.58	3.81	3.10	4.49	5.25
Spi	0.94	0.88	1.09	1.18	1.31	1.30	1.52	1.45
SiO_2	39.890	39.920	39.660	40.090	43.340	42.660	43.730	41.510
TiO_2	0.019	0.017	0.030	0.020	0.010	0.020	0.015	0.041
Al_2O_3	0.300	0.240	0.370	0.410	1.020	0.940	1.260	0.860
FeO_t	10.096	9.628	10.090	8.350	8.420	8.665	7.945	8.359
MnO	0.139	0.136	0.130	0.130	0.130	0.130	0.130	0.126
MgO	47.790	48.370	47.590	48.620	45.000	45.430	44.370	45.920
CaO	0.120	0.110	0.260	0.310	0.750	0.640	0.940	1.090
Na_2O					0.060			0.000
K_2O	0.030	0.000		0.010	0.010	0.010	0.010	0.030
P_2O_5	0.016	0.017	0.040	0.010	0.000	0.000	0.010	0.033
NiO	0.410	0.380	0.380	0.500	0.340	0.320	0.330	0.450
Cr_2O_5	0.382	0.409	0.580	0.900	0.440	0.340	0.399	0.789
Ba (ppm)								34
Co (ppm)	163	146	159	146	123	132	120	139
Sc (ppm)					8.5		30	
LOI								
Total	100.15	100.09	99.13	99.35	99.64	100.03	99.52	100.06
CATION UNITS								
Si	33.000	32.923	32.861	32.961	36.014	35.522	36.521	34.497
Ti	0.012	0.011	0.019	0.012	0.006	0.013	0.009	0.026
Al	0.293	0.233	0.361	0.397	0.999	0.923	1.241	0.843
Fe_t as Fe^{2+}	6.988	6.642	6.992	5.741	5.851	6.037	5.552	5.810
Mn	0.097	0.095	0.091	0.091	0.091	0.092	0.092	0.089
Mg	58.938	59.469	58.784	59.592	55.746	56.394	55.241	56.891
Ca	0.106	0.097	0.231	0.273	0.668	0.571	0.841	0.971
Na	0.000	0.000	0.000	0.000	0.097	0.000	0.000	0.000
K	0.032	0.000	0.000	0.010	0.011	0.011	0.011	0.032
P	0.011	0.012	0.028	0.007	0.000	0.000	0.007	0.023
Ni	0.273	0.252	0.253	0.331	0.227	0.214	0.222	0.301
Cr	0.250	0.267	0.380	0.585	0.289	0.224	0.263	0.518
Total	100	100	100	100	100	100	100	100
O^{2-}	133.28	133.20	133.29	133.47	136.61	136.10	137.29	135.22
Mg#	0.8940	0.8995	0.8937	0.9121	0.9050	0.9033	0.9087	0.9073
T_{Wells}	989.0					874.0		963.0
T_{CaOpx}	985.0					889.1	985.0	999.9

	KLX-57 Harz	KLX-69A Harz	LLX-1 Harz	KLX-37 Lherz	KLX-42 Lherz	KLX-43 Lherz	KLX-44 Lherz	KLX-45 Lherz
Ol	87.43	85.46	76.49	61.64	69.92	58.93	63.98	62.09
Opx	7.49	11.49	18.77	21.49	22.23	23.57	24.98	26.27
Cpx	3.41	1.90	2.70	14.19	6.09	14.65	9.13	9.42
Spi	1.67	1.16	2.04	2.68	1.76	2.86	1.91	2.22
SiO_2	40.630	41.700	42.790	43.560	43.670	43.950	44.580	44.290
TiO_2	0.076	0.020	0.030	0.107	0.020	0.127	0.018	0.020
Al_2O_3	1.170	0.640	1.300	2.770	1.580	3.130	1.780	2.260
FeO_t	9.403	9.250	8.230	9.475	8.251	8.620	8.062	7.693
MnO	0.142	0.140	0.130	0.143	0.131	0.139	0.133	0.130
MgO	45.680	46.390	44.740	39.390	43.630	39.350	42.370	41.720
CaO	0.640	0.380	0.770	2.920	1.280	3.010	1.940	1.970
Na_2O	0.070	0.000	0.020	0.060		0.080	0.000	0.020
K_2O	0.080	0.000	0.070	0.010	0.000	0.010	0.010	0.010
P_2O_5	0.051	0.010	0.010	0.008	0.003	0.009	0.002	0.010
NiO	0.460	0.340	0.340	0.280	0.330	0.270	0.290	0.310
Cr_2O_5	0.802	0.380	0.670	0.426	0.393	0.400	0.439	0.393
Ba (ppm)	63			4				
Co (ppm)	143	133	127	119	131	113	111	119
Sc (ppm)				22		13	15	31
LOI								
Total	100.17	99.25	99.97	100.16	100.13	100.01	100.47	99.24
CATION UNITS								
Si	33.825	34.614	35.718	37.071	36.528	37.354	37.342	37.396
Ti	0.048	0.012	0.019	0.068	0.013	0.081	0.011	0.013
Al	1.148	0.626	1.279	2.779	1.558	3.136	1.758	2.250
Fe_t as Fe^{2+}	6.545	6.421	5.745	6.747	5.771	6.127	5.646	5.430
Mn	0.100	0.098	0.092	0.103	0.093	0.100	0.094	0.093
Mg	56.693	57.406	55.674	49.974	54.406	49.858	52.909	52.513
Ca	0.571	0.338	0.689	2.663	1.147	2.741	1.741	1.782
Na	0.113	0.000	0.032	0.099	0.000	0.132	0.000	0.033
K	0.085	0.000	0.075	0.011	0.000	0.011	0.011	0.011
P	0.036	0.007	0.007	0.006	0.002	0.006	0.001	0.007
Ni	0.308	0.227	0.228	0.192	0.222	0.185	0.195	0.211
Cr	0.528	0.249	0.442	0.287	0.260	0.269	0.290	0.262
Total	100	100	100	100	100	100	100	100
O^{2-}	134.67	135.08	136.56	138.63	137.45	139.08	138.38	138.65
Mg#	0.8965	0.8994	0.9065	0.8810	0.9041	0.8906	0.9036	0.9063
T_{Wells}	983.9		995.0					925.3
T_{CaOpx}	992.5		969.4					927.2

	KLX-46 Lherz	KLX-48 Lherz	KLX-49A Lherz	KLX-52 Lherz	KLX-61 Lherz	KLX-64 Lherz	KLX-69B Lherz	KLX-70 Lherz
Ol	66.32	66.11	56.29	70.27	67.45	63.86	66.95	68.41
Opx	23.85	24.08	25.56	19.71	22.71	22.60	25.23	18.22
Cpx	7.60	7.79	15.25	8.25	7.98	11.45	6.44	11.60
Spi	2.23	2.02	2.89	1.78	1.85	2.09	1.38	1.78
SiO_2	43.820	44.130	44.330	43.560	43.950	44.230	44.420	43.400
TiO_2	0.030	0.040	0.119	0.032	0.009	0.018	0.031	0.146
Al_2O_3	2.240	1.920	3.290	1.640	1.750	2.060	0.990	1.850
FeO_t	8.197	8.089	8.566	8.620	7.972	7.882	8.386	8.665
MnO	0.140	0.130	0.138	0.134	0.128	0.130	0.134	0.139
MgO	42.630	42.840	38.810	43.080	43.000	41.760	43.150	41.650
CaO	1.600	1.650	3.080	1.710	1.670	2.410	1.360	2.280
Na_2O			0.160	0.040	0.020	0.020		0.200
K_2O	0.010	0.010	0.010	0.010	0.000	0.010	0.010	0.020
P_2O_5	0.010	0.010	0.010	0.006	0.002	0.002	0.007	0.021
NiO	0.300	0.320	0.290	0.320	0.320	0.310	0.250	0.310
Cr_2O_5	0.367	0.443	0.438	0.384	0.394	0.427	0.476	0.421
Ba (ppm)		8						
Co (ppm)	117	130	114	115	118	123	118	117
Sc (ppm)	53	36	11	17		13		
LOI								
Total	99.77	99.97	100.13	100.44	100.05	100.08	100.06	100.01
CATION UNITS								
Si	36.738	36.910	37.680	36.436	36.841	37.215	37.290	36.592
Ti	0.019	0.025	0.076	0.020	0.006	0.011	0.020	0.093
Al	2.214	1.893	3.297	1.617	1.730	2.044	0.980	1.839
Fe_t as Fe^{2+}	5.749	5.659	6.092	6.030	5.587	5.545	5.890	6.113
Mn	0.099	0.092	0.099	0.095	0.091	0.093	0.095	0.099
Mg	53.280	53.416	49.177	53.720	53.735	52.381	54.001	52.350
Ca	1.437	1.479	2.805	1.533	1.500	2.173	1.223	2.060
Na	0.000	0.000	0.264	0.065	0.033	0.033	0.000	0.327
K	0.011	0.011	0.011	0.011	0.000	0.011	0.011	0.022
P	0.007	0.007	0.007	0.004	0.001	0.001	0.005	0.015
Ni	0.202	0.215	0.198	0.215	0.216	0.210	0.169	0.210
Cr	0.243	0.293	0.294	0.254	0.261	0.284	0.316	0.281
Total	100	100	100	100	100	100	100	100
O^{2-}	137.99	138.03	139.43	137.36	137.83	138.37	137.96	137.59
Mg#	0.9026	0.9042	0.8898	0.8991	0.9058	0.9043	0.9017	0.8954
T_{Wells}			940.7					982.5
T_{CaOpx}			918.1					944.7

	BTX-9 Lherz	BTX-11 Lherz	BTX-12 Lherz	BTX-13 Lherz	BTX-14 Lherz	BTX-15 Lherz	BTX-16 Lherz	BTX-17 Lherz
Ol	54.69	67.14	60.54	62.14	64.28	61.17	59.58	54.23
Opx	26.04	22.85	27.25	20.12	25.97	23.53	25.71	26.47
Cpx	16.09	8.02	9.61	15.06	7.81	12.84	12.02	16.34
Spi	3.18	1.98	2.60	2.68	1.94	2.45	2.68	2.96
SiO_2	44.500	43.800	44.140	43.690	44.340	44.050	44.320	44.590
TiO_2	0.080	0.050	0.090	0.120	0.030	0.080	0.070	0.110
Al_2O_3	3.680	1.920	2.910	3.130	1.840	2.810	3.050	3.550
FeO_t	8.089	8.035	8.314	8.854	8.107	8.674	8.152	8.170
MnO	0.130	0.130	0.130	0.140	0.130	0.140	0.130	0.130
MgO	38.730	42.750	40.820	39.750	42.420	40.160	40.460	38.430
CaO	3.290	1.660	1.920	3.010	1.650	2.570	2.430	3.250
Na_2O	0.130	0.040	0.130	0.200	0.000	0.170	0.140	0.240
K_2O	0.020	0.030	0.040	0.140	0.010	0.020	0.020	0.020
P_2O_5	0.000	0.010	0.010	0.010	0.000	0.000	0.000	0.010
NiO	0.280	0.330	0.300	0.290	0.310	0.300	0.290	0.270
Cr_2O_5	0.440	0.440	0.400	0.310	0.390	0.290	0.410	0.430
Ba (ppm)				52	21		10	19
Co (ppm)	111	123	109	115	115	112	104	112
Sc (ppm)	15	13	11	15	10		17	14
LOI								
Total	100.22	100.03	100.08	100.59	100.09	100.19	100.34	100.07
CATION UNITS								
Si	37.748	36.751	37.256	36.861	37.260	37.254	37.348	37.907
Ti	0.051	0.032	0.057	0.076	0.019	0.051	0.044	0.070
Al	3.680	1.899	2.896	3.114	1.823	2.802	3.030	3.558
Fe_t as Fe^{2+}	5.739	5.642	5.866	6.244	5.699	6.132	5.743	5.808
Mn	0.093	0.092	0.093	0.100	0.093	0.100	0.093	0.094
Mg	48.977	53.473	51.363	49.996	53.141	50.633	50.828	48.704
Ca	2.990	1.492	1.736	2.721	1.486	2.329	2.194	2.960
Na	0.214	0.065	0.213	0.327	0.000	0.279	0.229	0.396
K	0.022	0.032	0.043	0.151	0.011	0.022	0.022	0.022
P	0.000	0.007	0.007	0.007	0.000	0.000	0.000	0.007
Ni	0.191	0.223	0.204	0.197	0.210	0.204	0.197	0.185
Cr	0.295	0.292	0.267	0.207	0.259	0.194	0.273	0.289
Total	100	100	100	100	100	100	100	100
O^{2-}	139.67	137.84	138.78	138.37	138.32	138.65	138.92	139.70
Mg#	0.8951	0.9046	0.8975	0.8890	0.9031	0.8920	0.8985	0.8934
T_{Wells}							908.3	
T_{CaOpx}							927.2	

	BTX-18 Lherz	BTX-19 Lherz	BTX-21 Lherz	BTX-22 Lherz	BTX-23 Lherz	BTX-24 Lherz	BTX-25 Lherz	BTX-26 Lherz
Ol	56.60	60.77	41.72	44.95	65.78	69.27	64.29	46.44
Opx	27.24	22.10	30.17	30.72	21.34	19.98	24.90	31.50
Cpx	12.94	14.64	23.52	20.66	10.66	8.52	8.43	18.36
Spi	3.22	2.49	4.60	3.67	2.22	2.23	2.38	3.71
SiO_2	44.080	44.140	44.990	45.530	43.720	43.350	43.940	44.960
TiO_2	0.100	0.090	0.150	0.110	0.040	0.070	0.080	0.120
Al_2O_3	3.710	2.930	5.650	4.630	2.140	2.390	2.560	4.560
FeO_t	8.143	8.224	7.145	7.873	8.188	8.692	8.746	7.657
MnO	0.130	0.130	0.120	0.130	0.140	0.130	0.130	0.130
MgO	39.350	40.050	35.050	36.230	41.880	42.620	41.710	36.670
CaO	2.580	2.910	4.650	4.140	2.240	1.710	1.700	3.640
Na_2O	0.170	0.230	0.340	0.280	0.010	0.110	0.100	0.260
K_2O	0.030	0.010	0.020	0.020	0.010	0.010	0.010	0.050
P_2O_5	0.010	0.000	0.000	0.000	0.000	0.010	0.010	0.010
NiO	0.290	0.290	0.240	0.250	0.310	0.310	0.310	0.260
Cr_2O_5	0.540	0.380	0.900	0.400	0.490	0.350	0.370	0.500
Ba (ppm)	40			18				
Co (ppm)	117	114	104	100	119	127	114	102
Sc (ppm)	11	14	17			12		86
LOI								
Total	99.98	100.26	100.02	100.44	100.02	100.67	100.58	99.14
CATION UNITS								
Si	37.385	37.261	38.565	38.817	36.819	36.207	36.861	38.529
Ti	0.064	0.057	0.097	0.071	0.025	0.044	0.050	0.077
Al	3.710	2.916	5.710	4.654	2.125	2.354	2.532	4.607
Fe_t as Fe^{2+}	5.773	5.803	5.118	5.611	5.768	6.070	6.139	5.490
Mn	0.093	0.093	0.087	0.094	0.100	0.092	0.092	0.094
Mg	49.752	50.400	44.790	46.047	52.579	53.068	52.162	46.848
Ca	2.344	2.632	4.271	3.782	2.021	1.530	1.528	3.342
Na	0.280	0.376	0.565	0.463	0.016	0.178	0.163	0.432
K	0.032	0.011	0.022	0.022	0.011	0.011	0.011	0.055
P	0.007	0.000	0.000	0.000	0.000	0.007	0.007	0.007
Ni	0.198	0.197	0.165	0.171	0.210	0.208	0.209	0.179
Cr	0.362	0.254	0.610	0.270	0.326	0.231	0.245	0.339
Total	100	100	100	100	100	100	100	100
O^{2-}	139.34	138.71	141.53	141.11	138.06	137.46	138.22	140.85
Mg#	0.8960	0.8968	0.8974	0.8914	0.9011	0.8974	0.8947	0.8951
T_{Wells}					964.0			978.4
T_{CaOpx}					1271.0			961.3

	BTX-27 Lherz	BTX-28 Lherz	BTX-29 Lherz	BTX-30 Lherz	BTX-31 Lherz	BTX-32 Lherz	BTX-33 Lherz	BTX-34 Lherz
Ol	62.82	52.94	60.20	57.95	59.55	62.35	63.41	57.15
Opx	15.05	27.60	23.85	23.65	23.59	27.16	23.68	23.49
Cpx	19.82	16.00	13.27	15.11	14.21	8.16	10.17	16.68
Spi	2.30	3.46	2.68	3.29	2.65	2.32	2.74	2.68
SiO_2	44.480	43.790	44.070	43.630	44.470	44.170	43.520	44.340
TiO_2	0.130	0.100	0.080	0.170	0.080	0.050	0.100	0.100
Al_2O_3	4.110	2.870	3.010	3.990	3.080	2.250	2.930	3.200
FeO_t	8.233	8.593	8.269	8.359	8.170	8.422	8.449	8.161
MnO	0.140	0.140	0.130	0.140	0.130	0.140	0.140	0.130
MgO	38.180	39.240	40.160	38.850	40.230	41.580	41.040	38.940
CaO	3.200	3.940	2.700	2.960	2.890	1.710	2.070	3.330
Na_2O	0.210	0.300	0.120	0.250	0.160	0.010	0.080	0.230
K_2O	0.020	0.020	0.010	0.140	0.020	0.010	0.030	0.020
P_2O_5	0.020	0.010	0.000	0.010	0.000	0.000	0.010	0.000
NiO	0.270	0.290	0.300	0.290	0.290	0.290	0.300	0.280
Cr_2O_5	0.520	0.210	0.390	0.400	0.370	0.520	0.490	0.370
Ba (ppm)	30							
Co (ppm)	104	110	116	115	106	113	112	115
Sc (ppm)	78	15		18	15	17	11	15
LOI								
Total	99.88	100.42	100.11	100.07	100.75	100.04	100.04	99.97
CATION UNITS								
Si	37.743	37.021	37.265	37.012	37.359	37.269	36.737	37.662
Ti	0.083	0.064	0.051	0.108	0.051	0.032	0.063	0.064
Al	4.112	2.861	3.001	3.991	3.051	2.238	2.916	3.205
Fe_t as Fe^{2+}	5.840	6.073	5.848	5.931	5.740	5.941	5.965	5.796
Mn	0.101	0.100	0.093	0.101	0.093	0.100	0.100	0.094
Mg	48.297	49.455	50.624	49.131	50.383	52.302	51.645	49.308
Ca	2.909	3.569	2.446	2.690	2.601	1.546	1.872	3.031
Na	0.345	0.492	0.197	0.411	0.261	0.016	0.131	0.379
K	0.022	0.022	0.011	0.152	0.021	0.011	0.032	0.022
P	0.014	0.007	0.000	0.007	0.000	0.000	0.007	0.000
Ni	0.184	0.197	0.204	0.198	0.196	0.197	0.204	0.191
Cr	0.349	0.140	0.261	0.268	0.246	0.347	0.327	0.248
Total	100	100	100	100	100	100	100	100
O^{2-}	139.90	138.34	138.84	138.98	138.92	138.58	138.35	139.25
Mg#	0.8921	0.8906	0.8964	0.8923	0.8977	0.8980	0.8965	0.8948
T_{Wells}								
T_{CaOpx}								

	BTX-35 Lherz	BTX-36 Lherz	BTX-37 Lherz	BTX-38 Lherz	BTX-40 Lherz	BTX-44 Lherz	BTX-45 Lherz	LLX-7 Lherz
Ol	57.56	72.17	56.77	60.45	63.45	49.96	60.99	59.48
Opx	26.99	16.88	23.41	27.27	23.69	29.01	20.22	23.36
Cpx	12.68	8.79	17.16	9.38	10.46	17.76	16.39	14.51
Spi	2.78	2.16	2.66	2.91	2.39	3.27	2.40	2.65
SiO_2	44.400	42.640	44.360	43.970	43.810	44.870	44.240	44.000
TiO_2	0.070	0.060	0.130	0.040	0.060	0.140	0.090	0.120
Al_2O_3	3.100	2.280	3.170	3.190	2.640	3.970	2.910	3.050
FeO_t	8.188	8.926	8.260	7.927	8.305	8.107	8.737	8.449
MnO	0.130	0.140	0.130	0.130	0.130	0.140	0.140	0.130
MgO	39.850	42.600	38.710	41.030	41.190	37.330	39.650	39.510
CaO	2.600	1.760	3.420	1.900	2.090	3.540	3.280	2.890
Na_2O	0.090	0.100	0.240	0.090	0.140	0.240	0.240	0.200
K_2O	0.010	0.010	0.020	0.020	0.020	0.100	0.030	0.060
P_2O_5	0.000	0.010	0.010	0.000	0.000	0.010	0.010	0.010
NiO	0.290	0.320	0.290	0.300	0.310	0.270	0.290	0.280
Cr_2O_5	0.380	0.280	0.380	0.550	0.390	0.430	0.220	0.410
Ba (ppm)								21
Co (ppm)	122	116	117	111	116	103	110	107
Sc (ppm)	16	14	12		10			
LOI								
Total	99.98	100.06	100.00	99.97	99.97	99.98	100.77	100.00
CATION UNITS								
Si	37.633	35.818	37.715	37.080	36.962	38.298	37.268	37.325
Ti	0.045	0.038	0.083	0.025	0.038	0.090	0.057	0.077
Al	3.098	2.258	3.178	3.172	2.626	3.995	2.890	3.051
Fe_t as Fe^{2+}	5.805	6.273	5.873	5.593	5.863	5.789	6.157	5.995
Mn	0.093	0.100	0.094	0.093	0.093	0.101	0.100	0.093
Mg	50.353	53.346	49.064	51.582	51.807	47.500	49.793	49.966
Ca	2.361	1.584	3.115	1.717	1.889	3.237	2.960	2.627
Na	0.148	0.163	0.396	0.147	0.229	0.397	0.392	0.329
K	0.011	0.011	0.022	0.022	0.022	0.109	0.032	0.065
P	0.000	0.007	0.007	0.000	0.000	0.007	0.007	0.007
Ni	0.198	0.216	0.198	0.203	0.210	0.185	0.197	0.191
Cr	0.255	0.186	0.255	0.367	0.260	0.290	0.147	0.275
Total	100	100	100	100	100	100	100	100
O^{2-}	139.28	137.00	139.32	138.79	138.32	140.29	138.64	138.88
Mg#	0.8966	0.8948	0.8931	0.9022	0.8983	0.8914	0.8900	0.8929
T_{Wells}								
T_{CaOpx}								

	LLX-11 Lherz	LLX-14 Lherz	KRX-6 Lherz	KRX-8 Lherz	KRX-9 Lherz	KRX-10 Lherz	KRX-11 Lherz	KRX-13 Lherz
Ol	67.51	52.30	49.95	49.13	36.56	51.73	68.15	50.64
Opx	21.84	27.08	29.41	28.33	31.66	26.99	22.32	28.69
Cpx	8.81	17.22	17.16	18.64	27.72	17.77	7.69	17.05
Spi	1.84	3.39	3.48	3.90	4.05	3.51	1.84	3.62
SiO_2	43.640	44.360	44.810	44.690	46.200	44.570	43.820	44.700
TiO_2	0.110	0.140	0.160	0.160	0.210	0.150	0.030	0.160
Al_2O_3	2.050	4.060	4.130	4.770	5.230	4.250	1.810	4.360
FeO_t	8.008	8.377	8.386	8.170	7.405	8.260	8.107	8.485
MnO	0.130	0.140	0.140	0.130	0.130	0.140	0.130	0.140
MgO	42.400	37.590	37.370	37.040	33.600	37.630	43.020	37.460
CaO	1.690	3.440	3.480	3.770	5.540	3.570	1.560	3.430
Na_2O	0.210	0.210	0.160	0.190	0.370	0.210	0.080	0.200
K_2O	0.290	0.110	0.010	0.090	0.050	0.040	0.010	0.020
P_2O_5	0.040	0.010	0.010	0.010	0.010	0.010	0.000	0.010
NiO	0.310	0.270	0.260	0.260	0.210	0.260	0.320	0.260
Cr_2O_5	0.360	0.410	0.390	0.380	0.500	0.410	0.420	0.420
Ba (ppm)	37				58	23		
Co (ppm)	120	102	109	102	88	100	118	96
Sc (ppm)		15	11	12	17	12	10	15
LOI		0.09		0.03	0.02			
Total	100.08	100.10	100.19	100.56	100.28	100.36	100.15	100.54
CATION UNITS								
Si	36.576	37.850	38.227	37.990	39.755	37.886	36.691	37.990
Ti	0.069	0.090	0.103	0.102	0.136	0.096	0.019	0.102
Al	2.026	4.084	4.154	4.781	5.306	4.259	1.787	4.369
Fe_t as Fe^{2+}	5.614	5.980	5.986	5.808	5.332	5.872	5.679	6.034
Mn	0.092	0.101	0.101	0.094	0.095	0.101	0.092	0.101
Mg	52.977	47.814	47.525	46.940	43.103	47.685	53.699	47.462
Ca	1.518	3.145	3.181	3.434	5.108	3.251	1.399	3.123
Na	0.341	0.347	0.265	0.313	0.617	0.346	0.130	0.330
K	0.310	0.120	0.011	0.098	0.055	0.043	0.011	0.022
P	0.028	0.007	0.007	0.007	0.007	0.007	0.000	0.007
Ni	0.209	0.185	0.178	0.178	0.145	0.178	0.216	0.178
Cr	0.239	0.277	0.263	0.255	0.340	0.276	0.278	0.282
Total	100	100	100	100	100	100	100	100
O^{2-}	137.50	139.90	140.41	140.42	142.39	140.07	137.67	140.25
Mg#	0.9042	0.8888	0.8881	0.8899	0.8899	0.8904	0.9044	0.8872
T_{Wells}	984.7						923.5	936.9
T_{CaOpx}	985.0						908.7	918.1

	KRX-14 Lherz	KRX-15 Lherz	KRX-19 Lherz	KRX-20 Lherz	LPX-1 Lherz	LPX-2 Lherz	LPX-3 Lherz	LPX-4 Lherz
Ol	58.35	54.95	61.20	65.51	52.47	60.45	58.79	53.20
Opx	23.37	26.64	18.98	25.65	26.66	23.34	23.72	27.94
Cpx	15.35	15.38	17.19	6.99	17.70	12.98	14.52	15.84
Spi	2.93	3.02	2.63	1.85	3.17	3.22	2.97	3.02
SiO_2	43.870	44.610	43.250	44.390	44.620	43.390	43.740	44.870
TiO_2	0.170	0.110	0.160	0.030	0.150	0.120	0.120	0.140
Al_2O_3	3.450	3.540	3.420	1.630	3.960	3.660	3.390	3.710
FeO_t	8.782	7.999	9.124	8.773	8.422	8.710	8.818	7.927
MnO	0.140	0.130	0.150	0.140	0.150	0.140	0.150	0.130
MgO	38.860	38.980	38.320	42.600	37.610	39.600	39.020	38.590
CaO	3.050	3.120	3.190	1.480	3.470	2.610	2.910	3.150
Na_2O	0.210	0.160	0.490		0.320	0.130	0.160	0.250
K_2O	0.200	0.060	0.180	0.010	0.090	0.040	0.060	0.060
P_2O_5	0.020	0.010	0.020	0.000	0.010	0.010	0.010	0.010
NiO	0.280	0.280	0.280	0.300	0.270	0.290	0.290	0.270
Cr_2O_5	0.360	0.420	0.400	0.450	0.390	0.440	0.390	0.390
Ba (ppm)	32	25		18		24		
Co (ppm)	110	107	110	123	112	116	128	99
Sc (ppm)	18	13	10		18	14	13	16
LOI	0.27		0.39					
Total	100.59	100.26	100.34	100.70	100.35	100.06	99.99	100.34
CATION UNITS								
Si	37.205	37.782	36.828	37.150	37.934	36.796	37.208	37.996
Ti	0.108	0.070	0.102	0.019	0.096	0.077	0.077	0.089
Al	3.450	3.535	3.433	1.608	3.969	3.659	3.400	3.704
Fe_t as Fe^{2+}	6.227	5.666	6.494	6.138	5.986	6.177	6.275	5.616
Mn	0.101	0.093	0.108	0.099	0.108	0.101	0.108	0.093
Mg	49.130	49.216	48.643	53.148	47.667	50.062	49.483	48.716
Ca	2.771	2.831	2.910	1.327	3.161	2.371	2.652	2.858
Na	0.345	0.263	0.809	0.000	0.527	0.214	0.264	0.410
K	0.216	0.065	0.196	0.011	0.098	0.043	0.065	0.065
P	0.014	0.007	0.014	0.000	0.007	0.007	0.007	0.007
Ni	0.191	0.191	0.192	0.202	0.185	0.198	0.198	0.184
Cr	0.241	0.281	0.269	0.298	0.262	0.295	0.262	0.261
Total	100	100	100	100	100	100	100	100
O^{2-}	138.90	139.61	138.30	138.12	139.84	138.73	138.96	139.84
Mg#	0.8875	0.8968	0.8822	0.8965	0.8884	0.8902	0.8875	0.8966
T_{Wells}	957.6							
T_{CaOpx}	936.0							

	LPX-6 Lherz	LPX-7 Lherz	LPX-8 Lherz	LPX-9 Lherz	LPX-11 Lherz	LPX-12 Lherz	LPX-13 Lherz	LPX-14 Lherz
Ol	46.87	53.37	55.34	52.26	54.76	59.36	58.31	52.89
Opx	29.25	26.88	26.14	28.51	25.25	23.07	25.27	26.60
Cpx	20.29	16.44	15.29	16.17	16.67	14.80	13.78	17.43
Spi	3.58	3.32	3.23	3.06	3.31	2.77	2.64	3.08
SiO_2	45.120	44.430	44.270	44.680	44.240	43.900	44.460	44.800
TiO_2	0.170	0.130	0.120	0.140	0.140	0.120	0.120	0.140
Al_2O_3	4.450	3.990	3.720	3.700	3.920	3.250	3.070	3.880
FeO_t	8.062	8.251	8.314	9.097	8.503	8.521	8.413	8.278
MnO	0.140	0.140	0.140	0.150	0.150	0.140	0.140	0.140
MgO	36.390	38.130	38.730	37.470	38.230	39.340	39.730	37.980
CaO	4.060	3.280	3.110	3.190	3.360	2.940	2.770	3.420
Na_2O	0.260	0.220	0.130	0.260	0.180	0.210	0.180	0.330
K_2O	0.150	0.100	0.030	0.110	0.080	0.060	0.030	0.050
P_2O_5	0.000	0.010	0.010	0.010	0.010	0.010	0.010	0.010
NiO	0.250	0.270	0.280	0.270	0.280	0.280	0.280	0.260
Cr_2O_5	0.390	0.430	0.430	0.340	0.400	0.360	0.340	0.410
Ba (ppm)	41							37
Co (ppm)	100	116	108	107	114	111	111	107
Sc (ppm)	16	14	11	13	12	10		15
LOI								
Total	100.30	100.25	100.16	100.38	100.39	100.03	100.44	100.59
CATION UNITS								
Si	38.512	37.740	37.597	38.090	37.557	37.246	37.548	37.949
Ti	0.109	0.083	0.077	0.090	0.089	0.077	0.076	0.089
Al	4.478	3.996	3.725	3.719	3.924	3.251	3.057	3.875
Fe_t as Fe^{2+}	5.753	5.860	5.902	6.488	6.035	6.045	5.940	5.866
Mn	0.101	0.101	0.101	0.108	0.108	0.101	0.100	0.100
Mg	46.304	48.284	49.035	47.620	48.382	49.758	50.021	47.961
Ca	3.713	2.985	2.830	2.914	3.056	2.673	2.506	3.104
Na	0.430	0.362	0.214	0.430	0.296	0.345	0.295	0.542
K	0.163	0.108	0.033	0.120	0.087	0.065	0.032	0.054
P	0.000	0.007	0.007	0.007	0.007	0.007	0.007	0.007
Ni	0.172	0.184	0.191	0.185	0.191	0.191	0.190	0.177
Cr	0.263	0.289	0.289	0.229	0.268	0.241	0.227	0.275
Total	100	100	100	100	100	100	100	100
O^{2-}	140.70	139.74	139.57	139.89	139.56	138.88	139.11	139.83
Mg#	0.8895	0.8918	0.8926	0.8801	0.8891	0.8917	0.8939	0.8910
T_{Wells}					924.1			
T_{CaOpx}					918.1			

	LPX-15 Lherz	LPX-16 Lherz	LPX-17 Lherz	LPX-18 Lherz	LPX-19 Lherz	LPX-24 Lherz	LPX-25 Lherz	LPX-26 Lherz
Ol	59.58	62.12	55.77	64.88	54.69	54.81	51.58	59.28
Opx	23.10	20.87	25.80	18.89	26.42	25.12	27.69	25.46
Cpx	14.43	14.08	15.51	14.11	15.80	17.01	17.59	12.70
Spi	2.89	2.93	2.92	2.12	3.09	3.06	3.14	2.57
SiO_2	43.960	43.190	44.510	43.560	44.460	44.540	44.920	44.460
TiO_2	0.120	0.120	0.130	0.120	0.140	0.150	0.140	0.090
Al_2O_3	3.360	3.360	3.440	3.060	3.660	3.660	3.780	2.920
FeO_t	8.557	9.628	8.467	8.746	8.548	8.314	7.972	8.332
MnO	0.140	0.150	0.140	0.140	0.140	0.140	0.140	0.140
MgO	39.600	39.110	38.840	40.110	38.400	38.450	37.960	40.230
CaO	2.910	2.770	3.130	2.490	3.160	3.430	3.560	2.560
Na_2O	0.160	0.210	0.180	0.610	0.210	0.200	0.190	0.160
K_2O	0.040	0.050	0.010	0.200	0.060	0.070	0.050	0.060
P_2O_5	0.010	0.010	0.010	0.010	0.010	0.010	0.010	0.010
NiO	0.280	0.280	0.280	0.280	0.480	0.270	0.270	0.280
Cr_2O_5	0.350	0.380	0.340	0.290	0.410	0.360	0.360	0.400
Ba (ppm)							19	
Co (ppm)	111	111	110	113	106	102	110	117
Sc (ppm)		15	12		11	12	18	
LOI								
Total	100.40	100.28	100.37	100.55	100.55	100.47	100.20	100.51
CATION UNITS								
Si	37.156	36.695	37.725	36.587	37.683	37.740	38.193	37.453
Ti	0.076	0.077	0.083	0.076	0.089	0.096	0.090	0.057
Al	3.348	3.366	3.438	3.030	3.657	3.656	3.789	2.900
Fe_t as Fe^{2+}	6.051	6.842	6.004	6.146	6.060	5.889	5.667	5.868
Mn	0.100	0.108	0.101	0.100	0.101	0.100	0.101	0.100
Mg	49.897	49.536	49.075	50.223	48.520	48.569	48.115	50.522
Ca	2.635	2.522	2.842	2.241	2.870	3.114	3.243	2.311
Na	0.262	0.346	0.296	0.993	0.345	0.329	0.313	0.261
K	0.043	0.054	0.011	0.214	0.065	0.076	0.054	0.064
P	0.007	0.007	0.007	0.007	0.007	0.007	0.007	0.007
Ni	0.190	0.191	0.191	0.189	0.327	0.184	0.185	0.190
Cr	0.234	0.255	0.228	0.193	0.275	0.241	0.242	0.266
Total	100	100	100	100	100	100	100	100
O^{2-}	138.88	138.39	139.50	137.68	139.55	139.59	140.13	138.94
Mg#	0.8919	0.8786	0.8910	0.8910	0.8890	0.8919	0.8946	0.8959
T_{Wells}		890.4		900.3				
T_{CaOpx}		918.1		918.1				

	LPX-27 Lherz	LPX-28 Lherz	LPX-31 Lherz	LPX-34 Lherz	RRX-5 Lherz	RRX-6 Lherz	RRX-8 Lherz	RRX-9 Lherz
Ol	60.21	60.19	54.91	55.77	62.16	55.73	71.92	60.37
Opx	23.05	22.01	25.18	22.96	24.59	27.50	18.48	24.78
Cpx	13.94	15.18	16.82	18.02	11.02	13.95	7.92	12.12
Spi	2.81	2.62	3.08	3.25	2.23	2.82	1.68	2.74
SiO_2	43.970	43.870	44.510	44.190	44.660	43.390	44.150	44.220
TiO_2	0.110	0.120	0.130	0.150	0.075	0.030	0.089	0.049
Al_2O_3	3.310	3.120	3.680	4.010	3.050	1.430	3.060	2.250
FeO_t	8.422	8.620	8.053	8.296	8.188	8.242	8.674	8.566
MnO	0.140	0.140	0.140	0.140	0.135	0.130	0.134	0.136
MgO	39.860	39.360	38.640	38.310	39.420	43.660	40.310	41.760
CaO	2.770	2.990	3.390	3.580	2.920	1.670	2.480	1.760
Na_2O	0.210	0.250	0.200	0.270	0.030	0.000	0.100	0.090
K_2O	0.060	0.090	0.050	0.070	0.020	0.010	0.040	0.010
P_2O_5	0.010	0.010	0.010	0.010	0.005	0.005	0.003	0.005
NiO	0.280	0.290	0.270	0.270	0.280	0.320	0.290	0.300
Cr_2O_5	0.390	0.350	0.420	0.400	0.394	0.440	0.351	0.437
Ba (ppm)	18	23		20				
Co (ppm)	113	120	114	117	111	115	113	122
Sc (ppm)		13	18		14		21	10
LOI					0.02			
Total	100.42	100.11	100.34	100.57	100.06	100.19	100.60	100.49
CATION UNITS								
Si	37.096	37.189	37.707	37.388	37.913	36.280	37.195	37.125
Ti	0.070	0.077	0.083	0.095	0.048	0.019	0.056	0.031
Al	3.292	3.118	3.676	4.000	3.053	1.410	3.039	2.227
Fe_t as Fe^{2+}	5.941	6.111	5.703	5.873	5.814	5.762	6.109	6.017
Mn	0.100	0.101	0.100	0.100	0.097	0.092	0.096	0.097
Mg	50.132	49.741	48.799	48.321	49.888	54.421	50.627	52.266
Ca	2.504	2.716	3.077	3.245	2.656	1.496	2.239	1.583
Na	0.343	0.411	0.328	0.443	0.049	0.000	0.163	0.146
K	0.065	0.097	0.054	0.076	0.022	0.011	0.043	0.011
P	0.007	0.007	0.007	0.007	0.004	0.004	0.002	0.004
Ni	0.190	0.198	0.184	0.184	0.191	0.215	0.197	0.203
Cr	0.260	0.235	0.281	0.268	0.264	0.291	0.234	0.290
Total	100	100	100	100	100	100	100	100
O^{2-}	138.75	138.70	139.59	139.37	139.59	137.15	138.79	138.34
Mg#	0.8941	0.8906	0.8954	0.8916	0.8956	0.9043	0.8923	0.8968
T_{Wells}								
T_{CaOpx}								

	RRX-10 Lherz	RRX-11 Lherz	RRX-12 Lherz	RRX-14 Lherz	RRX-15 Lherz	RRX-18 Lherz	RRX-22 Lherz	RRX-23 Lherz
Ol	63.64	58.34	62.54	55.10	67.56	53.69	60.10	56.83
Opx	25.52	26.78	23.49	25.01	23.43	26.53	24.97	28.15
Cpx	8.66	12.23	11.62	16.86	7.12	16.56	12.35	12.38
Spi	2.19	2.66	2.35	3.02	1.89	3.22	2.58	2.65
SiO_2	44.610	44.230	44.100	43.870	44.330	44.490	44.370	44.630
TiO_2	0.056	0.055	0.118	0.034	0.070	0.086	0.074	0.033
Al_2O_3	2.870	2.530	3.490	1.750	2.500	3.730	2.820	2.940
FeO_t	7.909	8.179	8.458	8.692	8.395	8.098	8.233	7.918
MnO	0.130	0.132	0.137	0.136	0.140	0.132	0.131	0.132
MgO	40.500	41.220	38.090	42.760	41.070	38.340	40.550	39.980
CaO	2.550	2.390	3.410	1.500	2.200	3.350	2.520	2.540
Na_2O	0.050	0.090	0.140		0.170	0.170	0.120	0.090
K_2O	0.010	0.010	0.010	0.010	0.010	0.010	0.010	0.030
P_2O_5	0.004	0.004	0.004	0.003	0.010	0.003	0.005	0.002
NiO	0.290	0.300	0.280	0.320	0.300	0.270	0.300	0.300
Cr_2O_5	0.438	0.393	0.325	0.350	0.363	0.523	0.491	0.402
Ba (ppm)								
Co (ppm)	117	121	117	124	114	105	115	110
Sc (ppm)	23	10	14	15	57	10		
LOI	0.18	0.02	0.55		0.14	0.12	0.03	0.23
Total	100.43	100.42	100.01	100.31	100.23	100.18	100.52	100.05
CATION UNITS								
Si	37.626	37.181	37.789	36.790	37.272	37.845	37.357	37.837
Ti	0.036	0.035	0.076	0.021	0.044	0.055	0.047	0.021
Al	2.854	2.507	3.526	1.730	2.478	3.741	2.799	2.939
Fe_t as Fe^{2+}	5.579	5.751	6.062	6.095	5.906	5.762	5.795	5.615
Mn	0.093	0.094	0.099	0.097	0.100	0.095	0.093	0.095
Mg	50.924	51.656	48.657	53.458	51.478	48.619	50.896	50.530
Ca	2.304	2.153	3.131	1.348	1.982	3.053	2.273	2.307
Na	0.082	0.147	0.233	0.000	0.277	0.280	0.196	0.148
K	0.011	0.011	0.011	0.011	0.011	0.011	0.011	0.032
P	0.003	0.003	0.003	0.002	0.007	0.002	0.004	0.001
Ni	0.197	0.203	0.193	0.216	0.203	0.185	0.203	0.205
Cr	0.292	0.261	0.220	0.232	0.241	0.351	0.327	0.269
Total	100	100	100	100	100	100	100	100
O^{2-}	139.19	138.53	139.62	137.79	138.54	139.80	138.87	139.37
Mg#	0.9013	0.8998	0.8892	0.8977	0.8971	0.8940	0.8978	0.9000
T_{Wells}	857.1					905.5		
T_{CaOpx}	868.2					936.0		

	SLX-4 Lherz	SLX-5 Lherz	SLX-11 Lherz	SLX-13 Lherz	SLX-16 Lherz	SLX-20 Lherz	SLX-22 Lherz	SLX-26 Lherz
Ol	63.58	48.63	59.74	59.47	64.16	51.74	63.66	56.61
Opx	24.52	29.66	26.26	26.30	24.75	30.19	21.81	24.89
Cpx	9.70	18.10	11.26	11.65	8.63	14.61	12.24	15.50
Spi	2.21	3.61	2.75	2.58	2.45	3.46	2.30	3.00
SiO_2	43.770	44.860	43.980	44.110	43.580	44.360	43.350	44.030
TiO_2	0.053	0.090	0.083	0.099	0.077	0.109	0.082	0.121
Al_2O_3	2.100	4.190	2.950	2.800	2.510	4.060	2.430	3.470
FeO_t	9.358	8.017	8.386	8.845	8.818	8.557	10.105	8.413
MnO	0.155	0.134	0.137	0.145	0.138	0.139	0.173	0.137
MgO	40.780	37.160	40.260	39.910	41.300	37.780	39.520	38.690
CaO	2.030	3.720	2.330	2.390	1.790	2.910	2.430	3.110
Na_2O		0.100	0.040	0.070	0.020	0.180	0.150	0.170
K_2O	0.050	0.080	0.050	0.090	0.040	0.220	0.230	0.130
P_2O_5	0.003	0.003	0.006	0.006	0.006	0.006	0.008	0.005
NiO	0.310	0.270	0.300	0.290	0.310	0.280	0.280	0.290
Cr_2O_5	0.357	0.443	0.386	0.297	0.353	0.445	0.303	0.402
Ba (ppm)				22		46	19	
Co (ppm)	117	95	127	121	117	120	115	101
Sc (ppm)			14			12		15
LOI	0.19	0.2	0.24	0.08	0.12	0.12	0.21	0.15
Total	100.13	100.11	100.03	100.07	99.99	100.07	100.35	100.00
CATION UNITS								
Si	37.153	38.363	37.315	37.448	36.870	37.864	36.911	37.497
Ti	0.034	0.058	0.053	0.063	0.049	0.070	0.053	0.078
Al	2.102	4.225	2.951	2.803	2.504	4.086	2.439	3.484
Fe_t as Fe^{2+}	6.644	5.736	5.953	6.283	6.240	6.110	7.192	5.990
Mn	0.111	0.097	0.098	0.104	0.099	0.100	0.125	0.099
Mg	51.603	47.374	50.923	50.511	52.089	48.074	50.165	49.120
Ca	1.846	3.408	2.118	2.174	1.623	2.661	2.217	2.838
Na	0.000	0.166	0.066	0.115	0.033	0.298	0.248	0.281
K	0.054	0.087	0.054	0.097	0.043	0.240	0.250	0.141
P	0.002	0.002	0.004	0.004	0.004	0.004	0.006	0.004
Ni	0.212	0.186	0.205	0.198	0.211	0.192	0.192	0.199
Cr	0.240	0.299	0.259	0.199	0.236	0.300	0.204	0.270
Total	100	100	100	100	100	100	100	100
O^{2-}	138.33	140.56	138.92	138.91	138.26	139.87	138.05	139.25
Mg#	0.8859	0.8920	0.8953	0.8894	0.8930	0.8872	0.8746	0.8913
T_{Wells}	1038.0							
T_{CaOpx}	1067.5							

	SLX-27 Lherz	SLX-30 Lherz	SLX-31 Lherz	SLX-33 Lherz	SLX-41 Lherz	SLX-44A Lherz	SLX-45 Lherz	SLX-46 Lherz
Ol	72.56	72.88	59.87	54.19	58.95	70.15	50.64	66.74
Opx	20.19	20.03	23.83	27.73	24.75	20.77	25.90	16.48
Cpx	5.73	5.39	13.71	15.25	13.36	7.05	19.75	14.05
Spi	1.52	1.70	2.59	2.83	2.94	2.03	3.71	2.74
SiO_2	43.300	42.910	44.040	44.510	43.910	42.830	44.360	42.560
TiO_2	0.029	0.028	0.086	0.136	0.090	0.095	0.144	0.111
Al_2O_3	1.220	1.360	2.850	3.390	3.200	2.260	4.510	2.980
FeO_t	8.773	10.231	8.395	8.629	8.503	9.079	8.242	9.619
MnO	0.136	0.159	0.137	0.139	0.137	0.138	0.135	0.154
MgO	43.760	42.840	39.850	38.220	39.640	42.200	36.900	39.840
CaO	1.200	1.120	2.770	3.010	2.760	1.310	3.960	2.800
Na_2O			0.140	0.240	0.050	0.200	0.220	0.150
K_2O	0.040	0.030	0.110	0.210	0.110	0.400	0.260	0.170
P_2O_5	0.001	0.003	0.004	0.012	0.005	0.018	0.014	0.012
NiO	0.330	0.300	0.300	0.280	0.300	0.320	0.300	0.290
Cr_2O_5	0.357	0.352	0.462	0.332	0.406	0.269	0.405	0.394
Ba (ppm)			37	42		76	32	47
Co (ppm)	127	125	111	115	116	125	114	123
Sc (ppm)	11			13	15		18	
LOI		0.02	0.21	0.09	0.03	0.11	0.1	0.12
Total	100.03	100.41	100.24	100.12	100.04	100.19	100.42	100.22
CATION UNITS								
Si	36.286	36.105	37.321	37.921	37.265	35.999	37.793	36.133
Ti	0.018	0.018	0.055	0.087	0.057	0.060	0.092	0.071
Al	1.205	1.349	2.848	3.405	3.202	2.240	4.530	2.983
Fe_t as Fe^{2+}	6.146	7.198	5.953	6.149	6.033	6.382	5.871	6.830
Mn	0.097	0.113	0.098	0.100	0.098	0.098	0.097	0.111
Mg	54.668	53.736	50.344	48.542	50.152	52.877	46.866	50.423
Ca	1.077	1.010	2.515	2.748	2.510	1.180	3.615	2.547
Na	0.000	0.000	0.230	0.396	0.082	0.326	0.363	0.247
K	0.043	0.032	0.119	0.228	0.119	0.429	0.283	0.184
P	0.001	0.002	0.003	0.009	0.004	0.013	0.010	0.009
Ni	0.222	0.203	0.204	0.192	0.205	0.216	0.206	0.198
Cr	0.237	0.234	0.310	0.223	0.273	0.179	0.273	0.265
Total	100	100	100	100	100	100	100	100
O^{2-}	137.01	136.90	138.78	139.52	138.97	136.91	139.98	137.63
Mg#	0.8989	0.8819	0.8943	0.8876	0.8926	0.8923	0.8887	0.8807
T_{Wells}		1033.0			1025.2	1043.0		
T_{CaOpx}		1079.8			1041.7	1061.2		

	SLX-48 Lherz	SLX-52 Lherz	SLX-53 Lherz	SLX-14 Opx-poorL	SLX-15 Opx-poorL	SLX-34 Opx-poorL	SLX-50 Opx-poorL	SLX-51 Opx-poorL
Ol	58.05	57.93	61.23	68.06	67.74	73.37	75.46	81.07
Opx	24.45	24.15	24.98	10.51	10.06	9.42	9.95	7.01
Cpx	14.65	15.00	11.37	18.80	19.43	14.93	12.86	10.00
Spi	2.85	2.93	2.41	2.64	2.77	2.28	1.73	1.92
SiO_2	43.830	43.970	43.470	42.230	41.900	41.560	42.330	40.950
TiO_2	0.105	0.109	0.114	0.150	0.170	0.132	0.082	0.109
Al_2O_3	3.310	3.180	2.850	2.810	2.940	2.140	1.710	1.610
FeO_t	8.521	8.377	9.664	10.231	10.213	11.410	9.043	11.104
MnO	0.139	0.137	0.151	0.170	0.160	0.185	0.140	0.176
MgO	38.940	39.180	39.190	38.840	38.390	39.650	42.430	42.250
CaO	2.910	3.100	2.120	3.760	3.870	2.980	2.600	2.060
Na_2O	0.190	0.050	0.310	0.170	0.160	0.120	0.120	0.000
K_2O	0.190	0.160	0.430	0.130	0.180	0.120	0.110	0.100
P_2O_5	0.012	0.008	0.016	0.010	0.010	0.011	0.008	0.021
NiO	0.290	0.280	0.270	0.270	0.280	0.260	0.340	0.280
Cr_2O_5	0.373	0.406	0.325	0.410	0.410	0.429	0.290	0.266
Ba (ppm)			52	24		25		22
Co (ppm)	115	106	113	111	114	131	124	127
Sc (ppm)		12	17	13	13	12		
LOI	0.31	0.2	0.21	0.09	0.44	0.05	0.12	
Total	100.02	100.04	100.16	100.37	100.21	100.28	100.27	100.11
CATION UNITS								
Si	37.343	37.418	37.010	35.992	35.922	35.483	35.569	34.664
Ti	0.067	0.070	0.073	0.096	0.110	0.085	0.052	0.069
Al	3.325	3.191	2.861	2.824	2.972	2.154	1.694	1.607
Fe_t as Fe^{2+}	6.071	5.964	6.878	7.292	7.320	8.147	6.353	7.858
Mn	0.100	0.099	0.109	0.123	0.116	0.134	0.100	0.126
Mg	49.459	49.705	49.741	49.349	49.065	50.466	53.151	53.316
Ca	2.656	2.826	1.934	3.433	3.555	2.726	2.341	1.868
Na	0.314	0.082	0.512	0.281	0.266	0.199	0.195	0.000
K	0.207	0.174	0.467	0.141	0.197	0.131	0.118	0.108
P	0.009	0.006	0.012	0.007	0.007	0.008	0.006	0.015
Ni	0.199	0.192	0.185	0.185	0.193	0.179	0.230	0.191
Cr	0.251	0.273	0.219	0.276	0.278	0.289	0.192	0.178
Total	100	100	100	100	100	100	100	100
O^{2-}	138.95	139.10	138.15	137.44	137.44	136.64	136.42	135.59
Mg#	0.8907	0.8929	0.8785	0.8713	0.8702	0.8610	0.8932	0.8715
T_{Wells}								
T_{CaOpx}								

	SLX-55 Opx-poorL	SLX-56 Opx-poorL	KLX-51 Opx-poorL	KLX-53 Dunite	KLX-65 Dunite	KLX-2 Wehr	KLX-3 Wehr	KLX-4 Wehr
Ol	66.81	61.85	66.13	97.18	96.17	80.80	64.89	57.43
Opx	12.68	17.62	11.19	0.41	0.62	0.70	0.64	0.00
Cpx	17.02	17.40	20.74	1.47	2.14	16.71	32.10	39.67
Spi	3.48	3.13	1.93	0.94	1.07	1.78	2.38	2.90
SiO_2	41.990	43.190	42.640	39.030	39.280	40.640	42.170	42.350
TiO_2	0.119	0.192	0.163	0.037	0.046	0.210	0.310	0.540
Al_2O_3	4.050	3.560	1.580	0.190	0.330	1.490	2.420	3.370
FeO_t	8.485	8.737	12.550	14.410	14.240	13.360	12.440	12.960
MnO	0.137	0.138	0.171	0.179	0.182	0.180	0.180	0.180
MgO	39.730	39.130	36.980	44.360	44.410	39.510	34.560	31.220
CaO	3.370	3.550	4.250	0.280	0.420	3.340	6.400	7.700
Na_2O	0.200	0.110	0.030			0.110	0.210	0.420
K_2O	0.280	0.110	0.010	0.010	0.010	0.020	0.020	0.030
P_2O_5	0.009	0.018	0.015	0.012	0.014	0.020	0.010	0.020
NiO	0.350	0.300	0.240	0.300	0.290	0.180	0.150	0.140
Cr_2O_5	0.510	0.349	0.224	0.049	0.127	0.160	0.260	0.260
Ba (ppm)	21	35	43		18	29		43
Co (ppm)	112	113	147	178	175	161	143	138
Sc (ppm)	10	11	14			14	14	28
LOI	0.17	0.12						
Total	100.28	100.43	100.22	100.27	100.79	100.69	100.50	100.62
CATION UNITS								
Si	35.480	36.608	36.949	33.015	33.070	34.769	36.683	37.247
Ti	0.076	0.122	0.106	0.024	0.029	0.135	0.203	0.357
Al	4.035	3.558	1.614	0.189	0.328	1.503	2.482	3.495
Fe_t as Fe^{2+}	5.999	6.195	9.095	10.194	10.026	9.559	9.050	9.532
Mn	0.098	0.099	0.126	0.128	0.130	0.130	0.133	0.134
Mg	50.046	49.443	47.771	55.939	55.738	50.391	44.817	40.934
Ca	3.051	3.224	3.946	0.254	0.379	3.062	5.965	7.256
Na	0.328	0.181	0.050	0.000	0.000	0.182	0.354	0.716
K	0.302	0.119	0.011	0.011	0.011	0.022	0.022	0.034
P	0.006	0.013	0.011	0.009	0.010	0.014	0.007	0.015
Ni	0.238	0.205	0.167	0.204	0.196	0.124	0.105	0.099
Cr	0.341	0.234	0.153	0.033	0.085	0.108	0.179	0.181
Total	100	100	100	100	100	100	100	100
O^{2-}	137.44	138.50	137.93	133.16	133.31	135.63	138.04	139.09
Mg#	0.8930	0.8887	0.8400	0.8460	0.8480	0.8410	0.8320	0.8110
T_{Wells}								
T_{CaOpx}								

	KLX-5 Wehr	KLX-7 Wehr	KLX-8 Wehr	KLX-9 Wehr	KLX-11 Wehr	KLX-13 Wehr	KLX-14 Wehr	KLX-16 Wehr
Ol	71.04	67.38	40.52	43.95	49.12	33.74	72.04	53.60
Opx	1.41	0.77	0.67	1.00	2.10	0.41	0.24	0.64
Cpx	25.55	29.55	55.26	51.73	45.74	62.14	25.77	42.79
Spi	2.00	2.30	3.56	3.32	3.04	3.71	1.95	2.97
SiO_2	41.750	41.770	44.170	44.010	43.640	45.170	41.520	43.080
TiO_2	0.210	0.310	0.660	0.550	0.480	0.570	0.260	0.490
Al_2O_3	1.740	2.300	4.380	3.850	3.540	4.610	1.950	3.390
FeO_t	13.040	12.850	11.250	11.230	11.640	10.030	12.600	12.080
MnO	0.180	0.180	0.170	0.170	0.170	0.160	0.180	0.180
MgO	36.600	35.000	26.850	28.150	29.890	25.380	36.700	30.840
CaO	5.150	5.820	10.850	10.230	9.060	12.260	5.050	8.440
Na_2O	0.120	0.260	0.430	0.350	0.330	0.480	0.290	0.350
K_2O	0.010	0.030	0.020	0.010	0.030	0.020	0.030	0.040
P_2O_5	0.020	0.020	0.020	0.020	0.020	0.020	0.020	0.020
NiO	0.170	0.190	0.100	0.110	0.110	0.110	0.190	0.140
Cr_2O_5	0.280	0.350	0.240	0.410	0.250	0.480	0.310	0.330
Ba (ppm)	18	25	30	18	53	69	48	38
Co (ppm)	144	138	105	107	129	98	140	121
Sc (ppm)	16	15	32	25	23	29	24	18
LOI								
Total	100.69	100.48	100.38	100.33	100.46	100.40	100.48	100.70
CATION UNITS								
Si	36.079	36.317	39.374	39.104	38.517	40.341	35.842	37.843
Ti	0.136	0.203	0.442	0.368	0.319	0.383	0.169	0.324
Al	1.773	2.358	4.603	4.033	3.684	4.854	1.985	3.511
Fe_t as Fe^{2+}	9.424	9.343	8.387	8.345	8.592	7.491	9.096	8.874
Mn	0.132	0.133	0.128	0.128	0.127	0.121	0.132	0.134
Mg	47.151	45.365	35.681	37.287	39.328	33.791	47.229	40.387
Ca	4.768	5.422	10.363	9.739	8.568	11.731	4.671	7.944
Na	0.201	0.438	0.743	0.603	0.565	0.831	0.485	0.596
K	0.011	0.033	0.023	0.011	0.034	0.023	0.033	0.045
P	0.015	0.015	0.015	0.015	0.015	0.015	0.015	0.015
Ni	0.118	0.133	0.072	0.079	0.078	0.079	0.132	0.099
Cr	0.191	0.241	0.169	0.288	0.174	0.339	0.212	0.229
Total	100	100	100	100	100	100	100	100
O^{2-}	137.11	137.61	141.84	141.35	140.49	142.92	136.87	139.74
Mg#	0.8330	0.8290	0.8100	0.8170	0.8210	0.8190	0.8380	0.8200
T_{Wells}		1037.0			1056.6			
T_{CaOpx}		1028.3			1073.7			

	KLX-17 Wehr	KLX-18 Wehr	KLX-19 Wehr	KLX-20 Wehr	KLX-23 Wehr	KLX-24 Wehr	KLX-25 Wehr	KLX-26 Wehr
Ol	74.72	70.56	70.96	49.43	68.41	73.33	70.43	78.07
Opx	0.72	0.47	0.39	0.32	0.00	0.75	0.52	0.71
Cpx	22.56	26.88	26.51	47.19	28.54	23.86	26.94	19.41
Spi	2.00	2.09	2.13	3.06	3.05	2.06	2.11	1.82
SiO_2	41.140	41.690	41.310	43.480	40.900	41.380	41.550	40.670
TiO_2	0.260	0.260	0.340	0.510	0.480	0.260	0.280	0.230
Al_2O_3	1.790	1.980	2.220	3.570	3.130	1.900	2.020	1.590
FeO_t	13.420	12.750	12.840	11.280	13.620	12.810	13.010	13.390
MnO	0.180	0.180	0.180	0.170	0.180	0.180	0.180	0.180
MgO	37.300	36.310	35.980	29.760	34.420	37.280	35.960	38.230
CaO	4.480	5.360	5.160	9.290	5.840	4.780	5.330	3.820
Na_2O	0.170	0.190	0.300	0.380	0.190	0.140	0.220	0.170
K_2O	0.020	0.010	0.050	0.030	0.020	0.020	0.030	0.030
P_2O_5	0.020	0.010	0.030	0.020	0.020	0.010	0.020	0.020
NiO	0.170	0.160	0.160	0.120	0.160	0.170	0.160	0.170
Cr_2O_5	0.270	0.290	0.240	0.380	0.280	0.220	0.290	0.190
Ba (ppm)	36	23	58	53	41	20	53	
Co (ppm)	141	138	136	121	134	151	138	153
Sc (ppm)	16	15	18	20	15	10	13	18
LOI								
Total	100.69	100.61	100.22	100.24	100.74	100.56	100.49	100.18
CATION UNITS								
Si	35.481	36.047	35.850	38.424	35.620	35.674	36.026	35.113
Ti	0.169	0.169	0.222	0.339	0.314	0.169	0.183	0.149
Al	1.820	2.018	2.271	3.720	3.214	1.931	2.065	1.619
Fe_t as Fe^{2+}	9.679	9.219	9.319	8.336	9.920	9.236	9.434	9.668
Mn	0.131	0.132	0.132	0.127	0.133	0.131	0.132	0.132
Mg	47.957	46.803	46.549	39.207	44.688	47.913	46.481	49.206
Ca	4.140	4.965	4.798	8.796	5.449	4.415	4.951	3.534
Na	0.284	0.319	0.505	0.651	0.321	0.234	0.370	0.285
K	0.022	0.011	0.055	0.034	0.022	0.022	0.033	0.033
P	0.015	0.007	0.022	0.015	0.015	0.007	0.015	0.015
Ni	0.118	0.111	0.112	0.085	0.112	0.118	0.112	0.118
Cr	0.184	0.198	0.165	0.266	0.193	0.150	0.199	0.130
Total	100	100	100	100	100	100	100	100
O^{2-}	136.52	137.17	137.04	140.44	137.49	136.77	137.16	136.00
Mg#	0.8320	0.8350	0.8330	0.8250	0.8180	0.8380	0.8310	0.8360
T_{Wells}								
T_{CaOpx}								

	KLX-27 Wehr	KLX-28 Wehr	KLX-29 Wehr	SLX-7 Wehr	SLX-8 Wehr	SLX-24 Wehr	SLX-38 Wehr	SLX-39 Wehr
Ol	29.21	90.77	70.00	67.64	55.76	52.91	67.57	74.06
Opx	0.02	0.66	0.79	0.32	1.55	2.38	4.84	2.32
Cpx	66.37	6.50	26.93	27.47	38.86	40.44	24.61	21.21
Spi	4.39	2.07	2.28	4.57	3.83	4.26	2.99	2.41
SiO_2	44.970	38.770	41.350	39.000	42.650	42.610	41.560	41.050
TiO_2	0.770	0.140	0.270	1.210	0.313	0.324	0.282	0.178
Al_2O_3	5.670	1.460	2.290	4.940	4.560	5.340	3.420	2.330
FeO_t	10.940	14.680	13.620	14.120	9.040	8.240	10.410	12.090
MnO	0.170	0.190	0.190	0.241	0.166	0.143	0.171	0.193
MgO	23.110	41.590	35.380	32.920	33.600	33.010	37.120	38.070
CaO	12.920	1.280	5.290	5.220	7.770	7.990	4.810	4.230
Na_2O	0.580	0.030	0.240	0.210	0.250	0.340	0.290	0.140
K_2O	0.030	0.020	0.030	0.520	0.070	0.080	0.230	0.040
P_2O_5	0.020	0.020	0.020	0.051	0.017	0.021	0.061	0.065
NiO	0.080	0.230	0.190	0.190	0.230	0.230	0.240	0.230
Cr_2O_5	0.300	0.390	0.200	0.274	0.397	0.356	0.398	0.339
Ba (ppm)	68		31	386	42	44	89	31
Co (ppm)	87	163	143	117	104	105	114	122
Sc (ppm)	40	9	17	12	27	29	14	15
LOI						0.55	0.18	0.06
Total	100.79	100.39	100.57	100.48	100.04	100.12	100.31	100.33
CATION UNITS								
Si	40.403	33.137	35.942	34.241	36.938	36.995	35.655	35.290
Ti	0.520	0.090	0.177	0.799	0.204	0.212	0.182	0.115
Al	6.006	1.471	2.347	5.114	4.656	5.466	3.459	2.362
Fe_t as Fe^{2+}	8.220	10.493	9.901	10.367	6.548	5.983	7.469	8.692
Mn	0.129	0.138	0.140	0.179	0.122	0.105	0.124	0.141
Mg	30.953	52.992	45.845	43.087	43.381	42.725	47.475	48.790
Ca	12.437	1.172	4.927	4.910	7.210	7.432	4.421	3.896
Na	1.010	0.050	0.404	0.357	0.420	0.572	0.482	0.233
K	0.034	0.022	0.033	0.582	0.077	0.089	0.252	0.044
P	0.015	0.014	0.015	0.038	0.012	0.015	0.044	0.047
Ni	0.058	0.158	0.133	0.134	0.160	0.161	0.166	0.159
Cr	0.213	0.264	0.137	0.190	0.272	0.245	0.270	0.230
Total	100	100	100	100	100	100	100	100
O^{2-}	143.53	134.08	137.16	137.28	139.38	139.75	137.40	136.63
Mg#	0.7900	0.8350	0.8220	0.8060	0.8690	0.8770	0.8640	0.8490
T_{Wells}						1028.0		
T_{CaOpx}						1054.8		

	SLX-42 Wehr	SLX-54 Wehr	SLX-44B Pyrox	SLX-10 Pyrox	KLX-49B Pyrox	KLX-72 Pyrox	KLX-74 Pyrox	KLX-71 Pyrox
Ol	69.50	41.66	13.99	20.55	25.55	9.04	2.05	6.17
Opx	2.44	3.92	32.79	33.53	16.06	0.33	1.63	0.18
Cpx	24.84	49.62	47.05	39.59	55.24	85.40	91.53	89.80
Spi	3.22	4.81	6.17	6.33	3.15	5.23	4.78	3.85
SiO_2	40.910	43.770	47.190	45.850	48.110	46.860	48.440	48.910
TiO_2	0.272	0.351	0.270	0.240	0.229	0.944	0.936	0.670
Al_2O_3	3.310	6.110	8.900	8.300	4.510	7.170	6.610	5.130
FeO_t	12.060	7.520	6.074	7.430	5.970	8.458	6.884	6.785
MnO	0.189	0.136	0.118	0.150	0.113	0.152	0.134	0.130
MgO	36.380	30.030	26.220	27.680	28.060	17.820	16.760	18.250
CaO	4.960	9.870	9.080	7.670	11.130	16.510	17.880	17.890
Na_2O	0.110	0.330	0.830	0.560	0.630	0.780	0.830	0.610
K_2O	0.140	0.110	0.130	0.250	0.010	0.020	0.040	0.010
P_2O_5	0.042	0.022	0.007	0.010	0.010	0.020	0.031	0.020
NiO	0.190	0.200	0.170		0.270	0.080	0.060	0.070
Cr_2O_5	0.363	0.320	1.354		0.542	0.389	0.738	0.690
Ba (ppm)	100	35	62		32	68	85	62
Co (ppm)	130	87	67		71	62	44	53
Sc (ppm)	15	32	32		34	47	39	45
LOI	0.14	0.57					0.06	0.04
Total	100.39	100.15	101.00		100.12	100.15	100.17	99.96
CATION UNITS								
Si	35.365	38.329	41.081	40.556	42.079	42.831	44.331	44.693
Ti	0.177	0.231	0.177	0.160	0.151	0.649	0.644	0.460
Al	3.374	6.308	9.135	8.656	4.651	7.727	7.132	5.527
Fe_t as Fe^{2+}	8.719	5.507	4.422	5.496	4.367	6.465	5.269	5.185
Mn	0.138	0.101	0.087	0.112	0.084	0.118	0.104	0.101
Mg	46.884	39.202	34.028	36.500	36.587	24.281	22.866	24.861
Ca	4.594	9.260	8.469	7.269	10.430	16.168	17.532	17.515
Na	0.184	0.560	1.401	0.960	1.068	1.382	1.473	1.081
K	0.154	0.123	0.144	0.282	0.011	0.023	0.047	0.012
P	0.031	0.016	0.005	0.007	0.007	0.015	0.024	0.015
Ni	0.132	0.141	0.119	0.000	0.190	0.059	0.044	0.051
Cr	0.248	0.221	0.932	0.000	0.374	0.281	0.534	0.499
Total	100	100	100	100	100	100	100	100
O^{2-}	137.23	141.51	145.53	144.43	144.21	146.80	148.08	147.64
Mg#	0.8430	0.8770	0.8850	0.8691	0.8934	0.7897	0.8127	0.8274
T_{Wells}								
T_{CaOpx}								

	KLX-1 Pyrox	KLX-35 Pyrox	BTX-4 Pyrox	BTX-6 Pyrox	BTX-7 Pyrox	LLX-15 Pyrox
Ol	0.00	2.35	16.16	0.00	3.82	22.91
Opx	1.55	20.61	45.02	17.66	49.02	14.09
Cpx	95.94	74.93	32.46	73.97	40.86	59.06
Spi	2.21	2.11	6.36	5.17	6.30	3.95
SiO_2	52.410	52.220	47.580	50.490	48.880	46.460
TiO_2	0.207	0.263	0.180	0.340	0.220	0.510
Al_2O_3	2.870	2.790	8.490	7.300	8.620	5.400
FeO_t	4.688	6.245	6.630	6.150	7.320	9.520
MnO	0.148	0.155	0.130	0.150	0.150	0.160
MgO	18.200	21.210	29.290	18.750	25.160	24.080
CaO	19.970	15.550	6.470	14.720	8.080	11.490
Na_2O	0.450	0.470	0.440	0.780	0.560	0.680
K_2O	0.040	0.030	0.040	0.070	0.020	0.110
P_2O_5	0.015	0.022	0.000	0.010	0.000	0.030
NiO	0.050	0.060				0.120
Cr_2O_5	0.825	0.635		0.660		0.310
Ba (ppm)	80	51		39		62
Co (ppm)	40	48		46		91
Sc (ppm)	48	35		41		201
LOI	0.05			0.06		0.6
Total	100.45	100.34	99.25	100.23	99.01	100.23
CATION UNITS						
Si	47.580	47.105	41.417	45.701	43.359	41.728
Ti	0.141	0.178	0.118	0.231	0.147	0.344
Al	3.072	2.967	8.713	7.791	9.015	5.718
Fe_t as Fe^{2+}	3.559	4.711	4.826	4.655	5.430	7.151
Mn	0.114	0.118	0.096	0.115	0.113	0.122
Mg	24.631	28.522	38.009	25.301	33.271	32.241
Ca	19.424	15.029	6.034	14.275	7.679	11.057
Na	0.792	0.822	0.743	1.369	0.963	1.184
K	0.046	0.035	0.044	0.081	0.023	0.126
P	0.012	0.017	0.000	0.008	0.000	0.023
Ni	0.037	0.044	0.000	0.000	0.000	0.087
Cr	0.592	0.453	0.000	0.472	0.000	0.220
Total	100	100	100	100	100	100
O^{2-}	149.15	148.59	145.50	149.35	147.52	144.42
Mg#	0.8737	0.8582	0.8873	0.8446	0.8597	0.8185
T_{Wells}		966.6				
T_{CaOpx}		953.1				